8. POLYMER COMPOSITES R&D

A. Automotive Composites Consortium Focal Project 4 (ACC 007[i])

Principal Investigators: Libby Berger
General Motors Corporation
Research & Development
MC 480-106-710
30500 Mound Road
Warren, MI 48090-9055
(586) 986-1177; fax: (586) 986-1207; e-mail:libby.berger@gm.com

John Jaranson
Ford Motor Company
Vehicle Design R&A
2101 Village Road MD 3137
Dearborn, MI 48121
(313) 390-5842; fax:(313) 337-5581; e-mail: jjaranso@ford.com

Field Project Manager, Composites: C. David Warren
Oak Ridge National Laboratory (ORNL)
P.O. Box 2009, Oak Ridge, TN 37831-8050
(865) 574-9693; fax: (865) 574-0740; e-mail: warrencd@ornl.gov

Technology Development Manager: Joseph Carpenter
(202) 586-1022; fax: (202) 586-1600; e-mail: joseph.carpenter@ee.doe.gov

Field Project Officer: Aaron D. Yocum
(304) 285-4852; fax: (304) 285-4403; e-mail: aaron.yocum@netl.doe.gov

Expert Technical Monitor: Philip S. Sklad
(865) 574-5069; fax: (865) 576-4963; e-mail: skladps@ornl.gov

---

Contractor: U.S. Automotive Materials Partnership (USAMP)
Contract No.: DE-FC-59OR22545 through the DOE National Energy Technology Laboratory

---

Objectives

- Guide, focus, and showcase the technology research of the four Automotive Composites Consortium (ACC) working groups (Materials, Processing, Joining, and Energy Management).
- Design and fabricate structural automotive components with reduced mass and cost, and with equivalent or superior performance to existing components.
- Develop new composite materials and processes for the manufacture of these high-volume components.

Approach

- Design, analyze, and fabricate a structural composite underbody and assemble it into a donor-vehicle structure, focusing on:
  - A 2 ½-minute cycle time (at 100,000 units per annum (upa), 2-shift operation).

  - Methods of joining and assembly of the underbody to the vehicle.
  - Processes for fabricating localized areas of oriented reinforcement within the time window.
- Design, analyze, and fabricate a second-row composite seat (with and without an integrated restraint system (SIR and STD, respectively)) which will combine the functions of a seat and a load floor.

Accomplishments

- Selected glass-fabric sheet molding compound (SMC) with a high-elongation core as our material and process system (MPS) based on mass and cost considerations, demonstrated manufacturing feasibility, and measured initial material properties for this system.
- Developed design methodologies to achieve acceptable performance for Full Frontal, Frontal Offset Deformable Barrier, Side, and Rear Offset Impact, and completed computer-aided engineering (CAE) stiffness, crash-performance, and mass assessments.
- Completed a CAE study on weld-bond modeling and a performance-sensitivity study.
- Completed a technical cost model for the selected MPS.
- Achieved a seat design that meets load requirements for front impact (Federal Motor Vehicle Safety Standard (FMVSS) 2076/210) with a cushion that is 30% lighter and a seat back that is 16% lighter than the comparator average.

Future Direction

- Begin Phase 2, the detailed design of the underbody, including manufacturing and assembly, for the composite underbody.
- Concept development of the weld-bonded joint, including detailed design, analysis, and test validation.
- Further manufacturing demonstration of the selected MPS, with cycle-time analysis, and determination of durability and high strain-rate properties.
- Continued investigation of nondestructive evaluation (NDE) techniques for manufacturing quality and durability.
- Complete additional load-case CAE analysis to confirm composite seat design.
- Complete cost model and analysis of the ACC seat and the Ecole Polytechnic Federale de Lausanne (EPFL) thermoplastic programmable powdered preform process (TPP4) seat.

Introduction

This project encompasses two components, a composite underbody and a lightweight composite seat, with unique goals with respect to vehicle volume per annum (VPA), physical size, materials, and technology development. They both require structural performance with reduced mass and acceptable cost, and with equivalent or superior performance to existing components.

Structural Composite Underbody

The structural composite underbody is targeted to be part of the USAMP Multi-Material Vehicle (MMV) project (see 12.D), and will follow the MMV vehicle technical specifications. The primary research outcomes of this project are:

- A 2 ½-minute cycle time (100,000 upa, 2-shift operation).
- Developing methods of joining and assembly of the underbody to the vehicle.
- Processes for fabricating localized areas of oriented reinforcement within the time window.

Phase 1 of this project was the selection of the materials and processes for the underbody which involves:

- The development of a design concept, including a means of joining and assembly.
- The preliminary design of the concept using three material and process systems,
- The selection of an MPS based on
  - Manufacturing considerations

    - 2 ½ minute cycle time
    - Joining and assembly feasibility
    - Technical feasibility
  - Compatibility with MMV goals
  - Technical cost model analysis

Phase 2 will be full design, incorporating other components of the MMV, based on a Large Rear-Drive Vehicle (LRDV).

Phase 3 will be fabrication of the underbody and assembly to the donor-vehicle structure.

In Phase 1, a preliminary composite underbody design was developed to replace the steel assembly from a production steel LRDV donor vehicle. The preliminary design takes into account three proposed MPS candidates, general vehicle packaging, assembly and joining requirements. The vehicle-level stiffness performance with the composite underbody is required to have equivalent performance to the LRDV, while crash performance is required to meet applicable government and industry requirements.

The deliverable for this phase is the selection of a material and process system, based on a concept design that is suitable for predicting preliminary CAE-based structural performance and mass reduction, conducting technical cost modeling, and further Phase 2 detail design and development.

One concern which has been raised about structural applications of composites is how to ensure quality, both after initial manufacture and through day-to-day durability degradation or low-energy crash events. At what point are they no longer capable of carrying crash loads? This will require development of NDE techniques that are low cost, robust, and easy to use. Examples of techniques which we will be evaluating for further development are thermal wave imaging, embedded microspheres encapsulating a fluorescent die, embedded fiber-optic mesh, and "coin tap" techniques.

Composite Design Concept

Multimatic, the design and analysis supplier for this Phase, examined the benchmark steel vehicle underbody (see Figure 1) to determine the basic construction, attachment requirements, parts count, material selection and gage.

The basic philosophy for designing the preliminary composite design was to:

- Integrate as many components as possible
- Increase section sizes where possible
- Avoid large structural cores
- Consider metallic components for hardpoints and welded attachments
- Optimize material selection based on performance / mass / cost trade-off.

Based on an evaluation of the donor-vehicle design, two composite concepts were proposed for further evaluation (see Figure 2). The first concept was a single-piece molded floor with ribs for maximum manufacturing efficiency, and the second concept was a bonded assembly for maximum structural efficiency.

The team selected the ribbed concept as the primary design direction due to the program cycle time requirements and the desire for minimum cost. The development of this concept is the subject of this report.

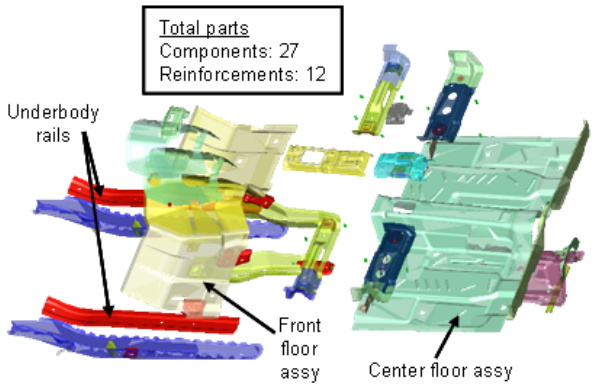

Figure 1. Exploded view of the benchmark steel underbody assembly.

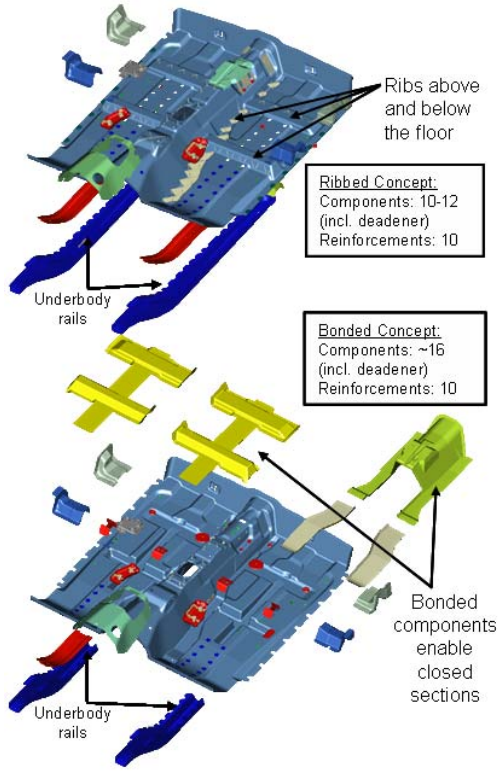

Figure 2. Ribbed and bonded design concepts.

Vehicle Assembly / Joining

Traditional composite structures are often manufactured as bonded assemblies to meet structural requirements. In optimal, lightweight, multi-material designs, structural bonding provides enhanced seam integrity, gap-bridging or tolerance functions and galvanic separation. In the high-volume automotive environment, cycle time, body-shop assembly process compatibility, and structural performance are all key requirements, and welding is a primary joining technique. The combination of welding and bonding, weld-bonding, is currently being implemented in OEM body designs and assembly plants as a means of increasing stiffness, reducing mass, and improving durability. Weld-bonding is currently envisioned as the primary joining process to meet the complex automotive requirements for the composite underbody. Specifically, the concept is either to embed or otherwise attach metallic inserts or doublers to the composite to enable spot welding to the surrounding steel structure as well as to attach the structural underbody rails to the composite floor (see Figure 3). The joints would be bonded prior to spot welding. Not only would this provide compatibility with current body-shop welding processes for installing the underbody itself, but the spot welds would also serve as peel stoppers in the adhesive joints, provide fixturing during adhesive cure, and enhance overall joint durability and robustness.

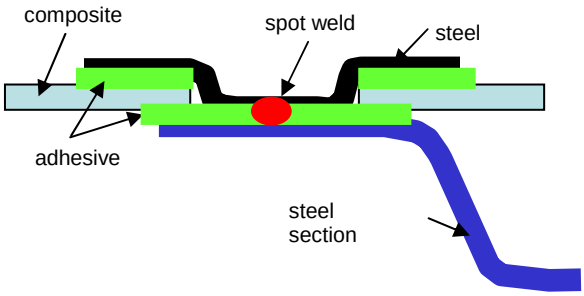

Figure 3. Weld-bonding concept for steel bonded to composite, using a metal doubler.

Computer-Aided Design (CAD) Model

A three-dimensional (3-D) CAD model of the preliminary ribbed design concept was developed to assess structural performance using CAE methods. The model represents the proposed joining concept and component integration. Material thickness and selection are MPS-specific and will be discussed in the following sections.

CAE Performance Assessment

The model was integrated into the full-vehicle noise-vibration-harshness (NVH) (NASTRAN) and crash models (LS-DYNA) for the donor vehicle.

The structural performance of the composite underbody was assessed as an integral part of the full LRDV vehicle. For Phase 1, the following key development load cases were considered:

- Body-in-White (BIW) static torsional and bending stiffness and modal response
- New Car Assessment Program (NCAP) 35-mph Full Frontal Impact
- EuroNCAP/ Insurance Institute for Highway Safety (IIHS) 40-mph Frontal Offset Deformable Barrier (ODB)
- Federal Motor Vehicle Safety Standard (FMVSS) 214 33.5-mph Side Impact
- FMVSS301 50-mph Rear Offset Impact

Material Properties

For the initial design assessments, the ACC-provided surrogate static room-temperature material properties which were used to represent candidate material systems pending the availability of physical test data from molding trials. The primary materials under consideration were fiberglass composites, either randomly oriented or with fabric. Randomly-oriented and fabric-carbon-fiber composites were evaluated to gain insight into maximum potential mass savings. Surrogate material property data were selected based on fiber volumes that could be reasonably achieved for the target MPSs. During the latter stages of Phase 1, the tensile and compressive properties were updated for some candidate materials as preliminary test data became available. Four composite material reinforcement systems were evaluated: (a) random fiberglass with a core, (b) glass fabric, (c) glass fabric with a core, and (d) carbon fiber with a core, where the core is a low-density/high strain-to-failure composite. In these evaluations, processing was not considered.

Global Stiffness Performance

Several vehicle-level stiffness and modal studies were conducted before selecting the ribbed design concept direction. Random fiberglass composite material properties were applied to the geometry of the benchmark steel model to evaluate the effect on the global BIW performance. These studies concluded that global vehicle stiffness is relatively insensitive to the floor stiffness as long as a minimum threshold stiffness is achieved. Assessments of the final four composite material system selections confirmed that the static torsional BIW stiffness increased by up to 4.6%, and the static bending stiffness decreased by up to 2.6% relative to the baseline vehicle. The first bending and torsional modes were within 0.05 Hz of the baseline vehicle.

However, once the first vehicle crash simulations were run, it was found that the requirements to meet crash performance overshadowed the requirements for the vehicle-level stiffness performance. Hence, the effort to develop feasible composite designs to meet crash requirements was prioritized.

Vehicle Crash Performance

Based on the results for the preliminary composite underbody stiffness model and the CAD model for the ribbed composite design concept, an initial LS-DYNA crash model was developed. The composite materials were represented by the MAT58 material model which requires orthotropic stiffness and strength properties, as well as several parameters that govern the post-failure material response. The required parameters were selected based on the surrogate material data, engineering judgment, and several model sensitivity studies. Further material development and test correlation will be needed for the selected materials in Phase 2.

Initial vehicle-level crash simulations indicated that the most severe loading case for the underbody floor structure was the EuroNCAP/IIHS 40-mph Frontal ODB case. The initial studies indicated that the thicknesses required to meet global stiffness were insufficient for maintaining integrity of the structure during crash. To achieve acceptable crash performance, the most mass-effective methods were:

- Optimizing the local material thickness and orientation to keep the strain levels sufficiently low to avoid net section material failure, while allowing localized failure
- Adding a low-density, high strain-to-failure core material such as high-modulus polypropylene (HMPP) to the laminate with a thickness of up to 2.5 mm in strategic regions of the floor
- Allowing the driveshaft to telescope an additional 70 mm
- Reducing the thickness of the carry-over steel underbody rail components
- Reducing the ribbing height and deleting ribbing in some locations.

Using the above methods and an iterative design process, acceptable Frontal ODB crash performance was achieved for the composite under-bodied LRDV with all-composite material systems that were considered. Acceptable performance was defined as the absence of any net section failures, with a small amount of localized material damage deemed acceptable.

Upon meeting the crash performance requirements for the frontal ODB case, the four materials systems were evaluated for all four crash-load cases outlined above. Some additional adjustment to the lay-ups was required to meet the full frontal impact and to account for the as-tested material properties before achieving acceptable performance.

By the end of the Phase 1, a total of 225 crash simulations (165 Frontal ODB, 19 full-frontal, 26 side-impact, and 15 rear-impact crash) and 44 global-stiffness analyses were conducted to arrive at a feasible lower mass solution for each material system design.

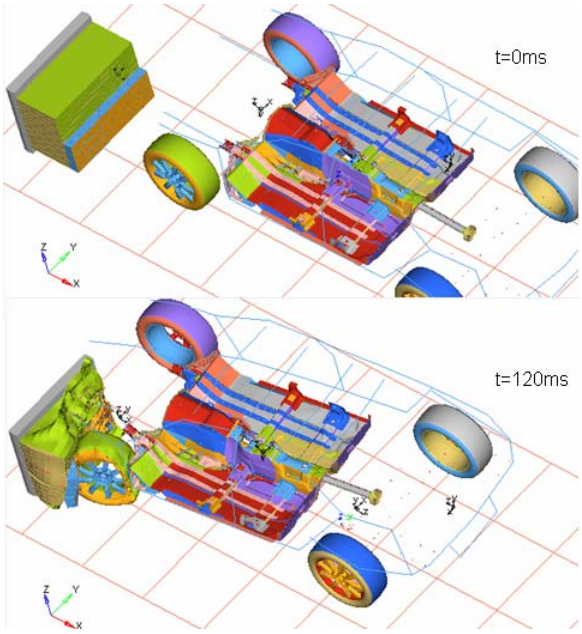

Figure 4. Front OBD – Predicted deformed shape for proposed composite underbody.

A Frontal ODB crash model setup and representative deformations for a fiberglass-fabric composite design are shown in Figure 4. Note that full vehicle crash models were used in the simulations but only the floor structure, wheels, and a wire frame representing the vehicle outline are shown in the figure. As can be seen in the figure, the offset barrier imparts a severe compressive and shearing load in the vehicle which results in local damage and intrusion in the floor structure. A corresponding representative damage plot is shown in Figure 5. The red areas in the damage plot indicate regions of localized material damage due to impact. The crash pulses for the composite underbody designs were found to be compatible with typical occupant restraint systems.

Thickness and Mass

A representative map of the material thicknesses and orientations required to achieve acceptable crash performance for a representative all-fiberglass-fabric underbody design proposal is illustrated in Figure 6. The total material thickness, the core thickness, and fiberglass-fabric composite thicknesses are indicated in the figure. The total material thickness for the final four MPS designs ranges from 1.6 mm to 8.1 mm.
The mass for all the material system designs are compared to the benchmark steel structure mass in Table 1.

Table 1. Representative underbody and mass breakdown.

Trial	Description	Total (Floor & Rails)			Floor Only			Rails Only		
		Mass*	Reduction		Mass	Reduction		Mass	Reduction	
		kg	kg	%	kg	kg	%	kg	kg	%
1098	Baseline steel	68.5	0.0	0%	44.9	0.0	0%	23.6	0.0	0%
1190	Fiberglass random, 2.5mm core, reduced rail thickness, telescoping driveshaft	61.2	-7.3	-11%	39.6	-5.3	-12%	21.6	-2.0	-9%
1175	Fiberglass fabric, reduced rail thickness, telescoping driveshaft	55.9	-12.6	-18%	35.6	-9.3	-21%	20.3	-3.3	-14%
1177	Fiberglass fabric, 1.0mm core, reduced rail thickness, telescoping driveshaft	53.6	-14.9	-22%	33.3	-11.6	-26%	20.3	-3.3	-14%
1188	Carbon fabric, 1.0mm core, reduced rail thickness, telescoping driveshaft	52.0	-16.5	-24%	31.7	-13.2	-29%	20.3	-3.3	-14%
	*Note: includes 14.1 kg of non-composite mass									

The results indicate a total mass reduction potential of 7.3 to 16.5 kg vs. the total 68.5 kg baseline steel structure mass, which includes a secondary 2.0 to 3.3 kg mass reduction as a result of a gage reduction in the carry-over design steel underbody rails. Considering only the floor (not accounting for the reduction in the rails) gives a mass reduction of 5.3 to 13.2 kg, or up to 29%.

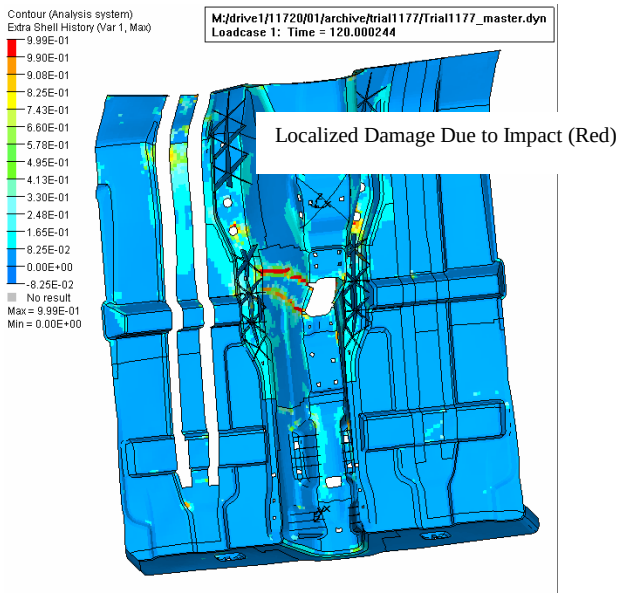

Figure 5. Front ODB – Representative predicted damage contours for proposed composite underbody.

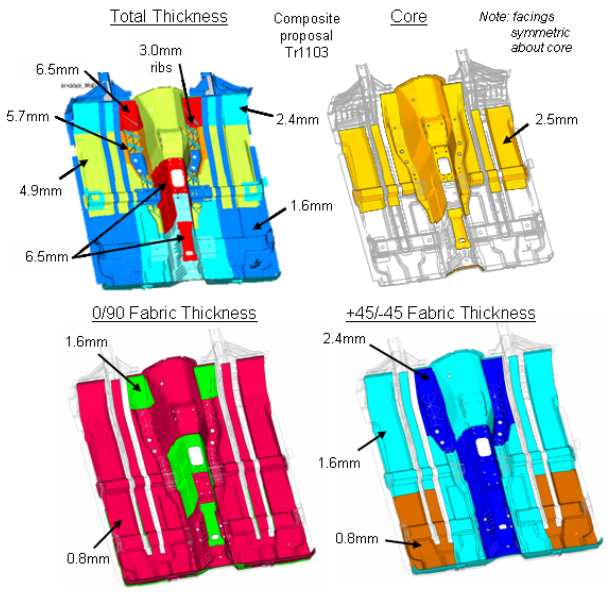

Figure 6. Representative thickness map for composite underbody.

Figure 7 illustrates the predicted mass reduction and compares the four material system designs (white bars) based on meeting the requirements for the four crash cases with revised material properties to the results of the initial predictions based only on the frontal ODB case (shaded bars). As can be seen in the figure, a large range of potential mass reduction is possible depending on the selected material system. The arrows in the figure indicate the change in mass for comparable material system designs.

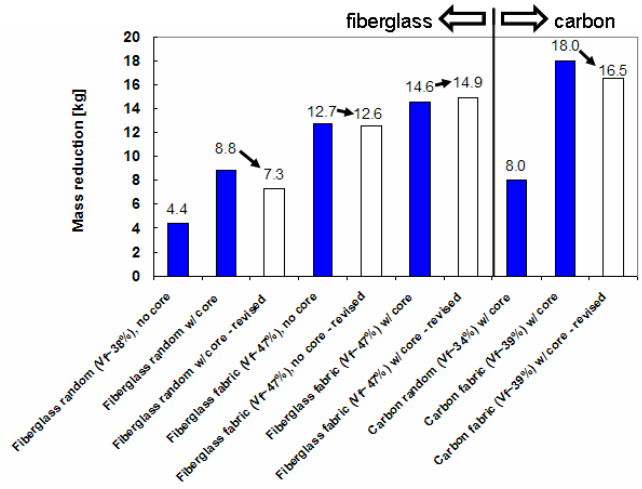

Figure 7. Predicted mass reduction vs. material system.

It is clear from the studies conducted to date, that mass reduction and part thickness are related to the strength of the materials investigated, where higher strength leads to lower mass and part thickness. Although not directly discussed here, materials with higher strength and also higher strain-to-failure properties would further reduce mass and thickness.

Weld-Bond Studies

A weld-bond coupon was designed to evaluate the tensile structural joint performance using several finite-element (FE) modeling methods. The analysis results indicated that physical test data would be required to determine several key modeling parameters. Further, sensitivity studies (see Figure 8) were conducted to establish how various joint and material parameters influence the joint strength. Relative to the nominal configuration, it was found that key joint parameters are the bond-line length, adhesive strength, and metal substrate strength. These results will be used to guide physical testing planned for Phase 2.

Material and Process Systems

Three MPSs have been evaluated for this project, based on manufacturing considerations, ability to deliver mass savings, and cost as predicted by

technical cost modeling. The three MPSs initially selected for evaluation were long-fiber injection (LFI), nylon Direct Long Fiber Thermoplastic (DLFT), and sheet molding compound (SMC). Each of these systems has the potential for a combination of fabric and random fibers, as well as either glass or carbon reinforcement. In the processing trials; however, carbon fiber was not evaluated due to cost targets, a lack of available material, and a lack of dedicated processing equipment.

LFI

The LFI process is currently in production with several relatively large composite components such as heavy truck panels and personal watercraft hulls. The LFI process as developed by Bayer utilizes robotic heads to chop glass into an open mold. As the glass is chopped, it is sprayed with a

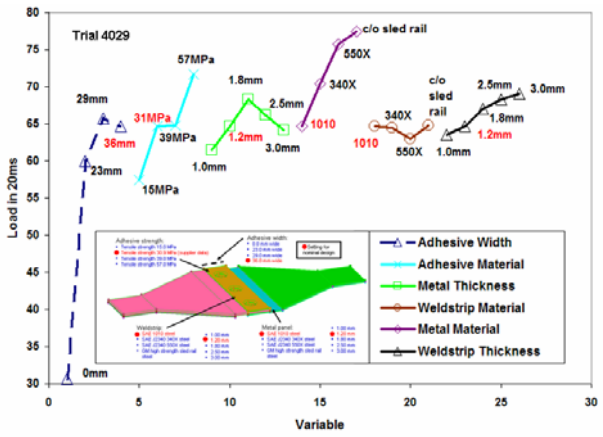

Figure 8. Weld-bond sensitivity study.

urethane resin. Bayer recommended a structural polyurethane (PU) system, Baydur 426, with a chop-and-spray LFI process. The molded samples are made with glass rovings that are dispensed from a reel and cut to any length before processing. PU and glass roving are introduced into the open mold simultaneously, with the chopped glass fiber being externally added to the PU spray jet. The molding is then cured in the closed mold. Bayer has successfully combined chopped LFI with sprayed continuous-filament mats (CFM). Our needs in this project would require replacing this CFM with glass fabric, and combining this with chopped LFI.

Introducing a glass fabric to the process is new, with trials being conducted in June 2007 and again in November 2007, at Bayer's development lab in Pittsburgh. Plaques were successfully molded at glass loading of 45, 50, 55 and 60% glass by weight. Bayer also prepared plaques containing a CFM at 45, 50, 55 and 60% by weight. However, we have been unable to mold with glass fabric.

Benefits for the LFI process:

- Easy mold access to apply local reinforcements
- Low press tonnage, allowing for a large platen size, which can easily accommodate the composite underbody assembly
- Potentially fast cycle time using a carousel and rapid-heating tooling

Concerns for the LFI process:

- Incorporating the fabric, which is needed for acceptable material properties
- Ability of the urethane to withstand temperature requirements of the assembly process
- Lack of existing infrastructure

Nylon DLFT

Nylon DLFT is a derivative of the more traditional polypropylene resin-based DLFT process. In initial trials with Nylon® 6 at 50% glass, significant glass damming in the processing was seen, and the strengths of the tested plaques were very low. Subsequent trials varied the resin and glass formulations with glass volumes ranging from 40-50% by weight. Despite better processing, improved glass flow, the addition of glass fabric and a high modulus polypropylene core, the material strength continues to be very low.

Benefits for the nylon DLFT process:

- Reduced cycle time
- Recyclable

Concerns for the nylon DLFT process:

- Limited mold access to apply local reinforcements

- Material properties- including incorporating the fabric, which is needed for acceptable material properties
- Ability of the nylon to withstand temperature requirements of the assembly process
- Press tonnage
- Capital investment

Due to the nature of the DLFT process, adding glass fabric or a polypropylene core to the charge has proven to be very difficult. The fabric and core must be heated to ensure the nylon DLFT does not cool prior to being compressed in the mold. This requires additional heating elements and increases capital costs as well as complicating the manufacturing process. While the nylon DLFT was processed at 600°F, the polypropylene core had to be processed at 325°F to prevent it from melting. How the two materials interact upon contact when building the charge is still under investigation, but there is concern that the polypropylene core rapidly cools the DLFT while the core is heated past its melting point and loses the strain properties for which it is intended.

SMC

The third MPS system investigated is SMC. Polywheels currently compounds an unsaturated polyester-modified vinyl-ster blend SMC in glass contents ranging from 27% to 55% glass by weight. For this project, additional material strength and strain are required, demanding higher glass content and reinforcement fabrics be added. The glass content of the SMC was increased in increments of 5% until visible non-wetting conditions of the glass occurred at 70%. Further development led to a reduction of the glass content to 57% to improve process capability on the compounding line. Additional material testing is in process to determine if the additional chopped-glass content is beneficial enough to justify the increased complexity involved in compounding a higher glass-content SMC.

Plaque molding trials in April 2007 demonstrated that additional reinforcement via glass fabrics can be incorporated into the SMC, utilizing both a uni-directional glass fabric (FGI W1300) and a bi-directional glass fabric (FGI 1854). These plaques showed a significant improvement in material properties. The bi-directional fabric proved to be the most useful for the underbody in various dynamic-impact scenarios and, therefore, became the primary reinforcement selection. To improve the strain rate of the SMC in order to retain floor integrity during a dynamic impact and to further reduce mass of the system, fabrication of plaques with a highly elastic material sandwiched within the SMC as a thin core was also investigated using a HMPP material as mentioned earlier. In the initial trials, the fabric and core were placed within the charges as dry material. This caused issues with wet-out and trapped air within the plaques, causing blisters and inconsistent material properties.

Subsequent trials in October utilized pre-compounded, bi-directional glass fabric which improved material handling as well as reduced wet-out issues. The core was also pre-compounded for the October trials, but it proved to be less effective—the core became even more difficult to cut, and initial material tests have not shown the increased strain-to-failure performance improvement seen in the earlier trial.

Filling ribs with the high glass-content, chopped-glass SMC has also been successfully demonstrated. Using the bi-directional glass fabric as a base layer and chopped glass to fill the ribs, ribbed plaques consistently filled as long as the ribs were well lubricated. Burn-off tests to determine the glass content in the ribs will be conducted, but evidence while molding suggests that the ribs will be structurally effective with glass reinforcement.

Benefits for the SMC process:

- Best composite material properties among MPSs evaluated
- Relatively easy mold access to apply local reinforcements
- Capable of surviving the elevated temperatures of Electro coat painter operation (ELPO) and paint cure
- Relatively low capital investment, as there is extensive SMC infrastructure within the automotive industry

Concerns for the SMC process:

- Material properties--Can we develop a composite material with enough tensile and shear strength and strain-to-failure performance to meet crash requirements?
- Achieving 2 ½ minute cycle time
- Press tonnage

Material Testing Results

Figures 9 through 11 show examples of the properties of some of the tested materials. The plaque testing has shown that the addition of woven compounded material increases the tensile modulus of the SMC material. Stress and strain values also show a significant increase.

Table 2 shows an evaluation of the possible mass saved for the reinforcement systems in SMC, as compared to the cost. For the glass-fiber materials, the glass fabric with HMPP core saves 14.6 kg, for a cost of $96 per part. The carbon comparisons show a larger mass save of 18.0 kg, but at a cost of $350. Compared to fiberglass, the incremental cost per kg of mass saved of the carbon fiber is about $75, which is considered to be high.

A fabric HMPP material was added to the SMC as a core, to increase elongation to ultimate failure, as well as to increase thickness using a lower density material. The strength properties and elongation of the material increased compared to the SMC. HMPP does have increased elongation properties, which would help to avoid net section failures in the underbody. More development and testing will be done in order to realize the potential mass and elongation benefits of this material in the underbody design. We are currently evaluating issues with the performance of HMPP at high temperatures.

Nylon DLFT material was molded into plaques and tested. The glass content which was easily molded into the DLFT was 40%, compared to the 57% SMC by weight. Increasing the glass content above 40% caused the plaques to have dry fibers. The tests showed a significant decrease in properties compared to the SMC and the SMC with woven glass mats.

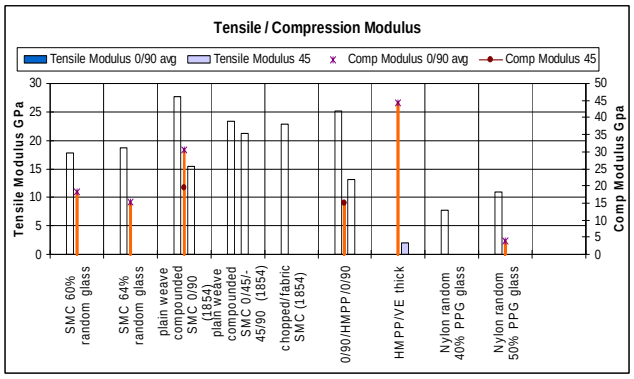

Figure 9. Tension- and compression-modulus values for a range of plaques molded and tested as part of this program.

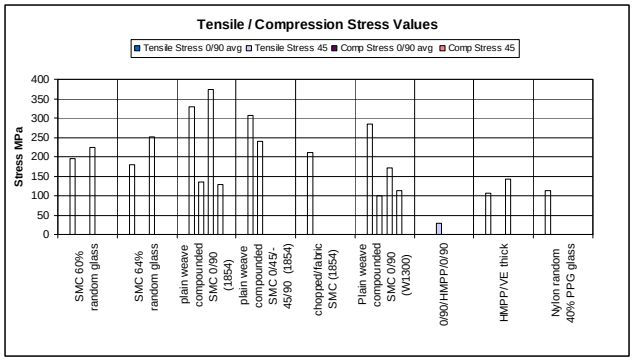

Figure 10. Tension- and compression-strength values for a range of plaques molded and tested as part of this program.

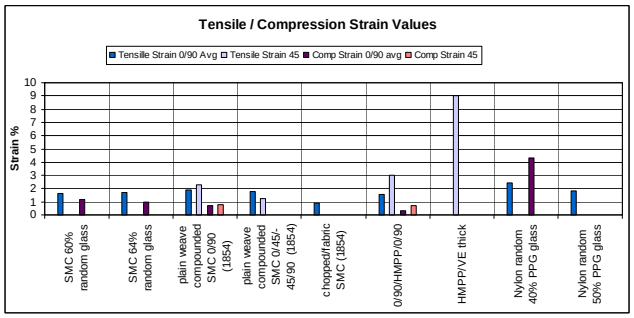

Figure 11. Tension- and compression strain-to-break values for a range of plaques molded and tested as part of this program.

Technical Cost Model

In order to aid in the selection of the MPS, we contracted with IBIS Associates to do a technical cost model for the underbody, comparing the three processes discussed above and incorporating six reinforcement scenarios for each MPS:

- All random fiberglass
- Random fiberglass with HMPP core

- All fiberglass fabric
- Fiberglass fabric with HMPP core
- Random carbon fiber with HMPP core
- Carbon-fiber fabric with HMPP core

This gives a total of eighteen different scenarios. The purpose of this cost model was to compare these systems to each other, not to get an absolute cost for the production of the underbody, nor to compare them to the steel underbody.

Table 2. Mass savings for SMC materials systems and costs/parts from the technical cost model.

		Mass Savings (kg, including rails)	Cost (per part)
Glass	Random no core	4.4	$104
	Random with core	8.8	$97
	Fabric no core	12.7	103
	Fabric with core	14.6	96
Carbon	Random no core		
	Random with core	8.0	368
	Fabric no core	17.6	
	Fabric with core	18.0	350

The result of this study was that the LFI and SMC processes were almost identical in their costs. The DLFT process is more expensive, based on the higher cost of the nylon. However, if a lower-cost nylon can be used (which may be an issue because of temperature requirements), the DLFT is also cost competitive.

IBIS concluded that the competitive position of the target processes will be determined by their respective material performance within each of the component designs. Material requirements will then drive the process rate and investment assumptions outlined in this study. Thus, each scenario's design-material performance will determine its respective mass and part cost.

Selection of MPS

Based on the molding trials, in which SMC is the only one of the processes that successfully incorporated the glass fabric as well as the HMPP core, the material properties, and the technical cost model, we have selected SMC with glass fabric and a HMPP core as our primary MPS. Our future processing, material evaluation, and design efforts will focus on this material. However, both LFI and nylon DLFT show possible unique advantages, so we will continue to follow up on these processes.

Non-Destructive Evaluation (NDE)

The objective of NDE is to evaluate the composite structure during manufacturing operations, final inspection, after durability runs and post-crash analysis. We are currently using NDE techniques to evaluate the panels we have molded as part of the MPS selection process. We have used ultrasound and thermal wave imaging to investigate delamination in the glass SMC/HMPP panels, and have been able to image blisters and delaminations. Plans are underway to use vibro-thermography and pulse-echo ultrasound to evaluate weld-bonded joints, to use fluorescing dye penetrant to investigate damage in panels subjected to impact loads, and to determine the feasibility of conductivity methods for evaluating damaged SMC panels modified to be conductive. NDE surface analysis techniques using optical methods are under investigation for their applicability.

Underbody Summary

Phase 1 of the Composite Underbody Project has been completed, with glass-fabric SMC, and a high-elongation core being selected as our material and process system. A composite underbody design concept was selected based on the potential to reduce cycle time and cost. Studies of global BIW stiffness and crash performance indicated that the dominant design load case was EuroNCAP/IIHS 40-mph Frontal ODB crash. Using this MPS, acceptable crash performance was predicted to occur with only localized material damage and low levels of dash-panel intrusion. A large range of potential mass reduction was predicted when considering all four crash cases, with a minimum reduction of 7.3 kg with random fiberglass and a maximum reduction of 16.5 kg with carbon-fiber-fabric composites. Initial manufacturing feasibility for the glass-fabric SMC system has been demonstrated with good initial material properties, and more extensive molding and testing trials are underway. Phase 2, the detailed design of the underbody, including manufacturing and assembly, is beginning. Investigations into NDE techniques to

determine manufacturing quality and durability are underway.

Lightweight, Low-Cost Composite Seat

The primary objective of the project is to develop materials, processes and designs to yield a light-weight, low-cost composite seat structure. Second-row outboard stand-alone seats are the target applications for the composite-seat project with volumes up to 340,000 upa. Only the back frame, cushion frame, and the pivoting recline/ folding joint will be included in the scope of the effort. The project will investigate predominately glass-fiber-reinforced composites due to cost considerations, but will consider local reinforcement with carbon fiber and other materials including metal reinforcements in order to achieve a 30% weight save versus the components being replaced. Both thermoset- and thermoplastic-matrix material will be included. A design achieving a 50% weight savings utilizing carbon-fiber-reinforced composites is also being developed.

Results from the comparator seat teardowns and testing have been used to develop weight targets for the composite seats. These can be seen in Table 3.

CAE Analysis

Following topology optimization done by Altair Engineering on the available design space for both the seat back and seat pan, initial CAE models of the STD and SIR seat were developed. Linear static analysis was performed initially using the several load cases in order to compare the concept seat to the comparator seats and to provide basic sizing of the sections.

Following that initial FE modeling, a more complex, non-linear model of both the STD and SIR seats was developed. The initial load cases evaluated using these non-linear models have been the FMVSS 207/210 load case for front impact on the SIR seat and a 20-g rear impact for the STD seat. Cargo-retention loading has also been investigated. Several iterations of material and design changes have been performed using these models to date and this work is continuing.

These analyses have resulted in design changes and iterations of both the composite-seat components and the steel hinges and reinforcements. The current seat design meets the 120% loading requirements with only some minor local issues that are being addressed.

Weight Status

The seat design is currently at its 30% target weight for the cushion pan. Additional optimization of the thickness of the seat back is required to meet its weight target. The details of the weight status can also be seen in Table 3 below. The current design of the seat can be seen in Figures 12 and 13 for the standard version of the seat.

Table 3. Composite seat weight status.

Focal Project 4 Composite Seat	Weights (kg)						
	Complete Seat	Riser	Headrest	Soft Trim	Hardware	Cushion Str	Back Str
Comparators							
DCX Stow N Go (non-SIR)	33.02	15.34	0.89	3.59	6.79	4.62	1.79
Ford LR3 (non-SIR)	23.65	8.79	0.63	2.78	3.36	4.28	3.81
GM GMT900 (non-SIR)	22.41	9.29	0.69	3.37	2.29	3.47	3.30
Average (no DCX)	23.03	9.04	0.66	3.08	2.83	3.88	3.56
Targets - 30% Weight Save	**20.46**	**8.80**	**0.63**	**3.00**	**2.83**	2.71	2.49
Current Design Status							
Composite Std Seat	20.52	8.80	0.63	2.78	2.63	2.70	2.98
%Weight Save	11%	3%	5%	10%	7%	30%	16%
Weight Save (kg)	2.5	0.2	0.0	0.3	0.2	1.2	0.6
Composite SIR Seat	22.30	8.80	0.63	2.78	3.59	2.89	3.10

Specifc Gravity Assumptions		
	Steel	7.8
	Carbon/Nylon	1.3

Material Assumptions

The composite seat will be comprised of nylon 6 reinforced with chopped carbon fiber for the bulk of the molded composite part. Local continuous carbon-fiber/nylon 6 inserts will reinforce the edges of the cushion pan and the seat back. These inserts will be symmetrical laminates of 0° and 90° tapes. The location and shape of the inserts is illustrated in Figure 13. The composite parts will be compression molded using DLFT-compounded material. The inserts will be preformed from blanked, pre-laminated sheet stock and heated prior to being placed in the main molding tool. Robotic transfer will be necessary to meet the cycle times for the insert transfer. The process schematic is illustrated in Figure 14.

Figure 12. ACC standard seat design.

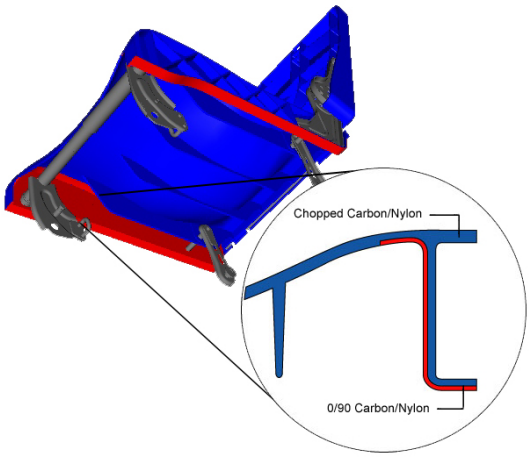

Figure 13. Typical section – cushion.

Cost Modeling

Work continues with EPFL on developing a cost model for the composite seat. EPFL has designed a version of the seat back that utilizes the TPP4 process and materials. This design will be used for comparison to the compression-molded DLFT version of the seat being developed by the ACC. Preliminary estimates show a comparable weight savings using the TPP4 process and materials and there is potential for additional cost savings with the TPP4 seat.

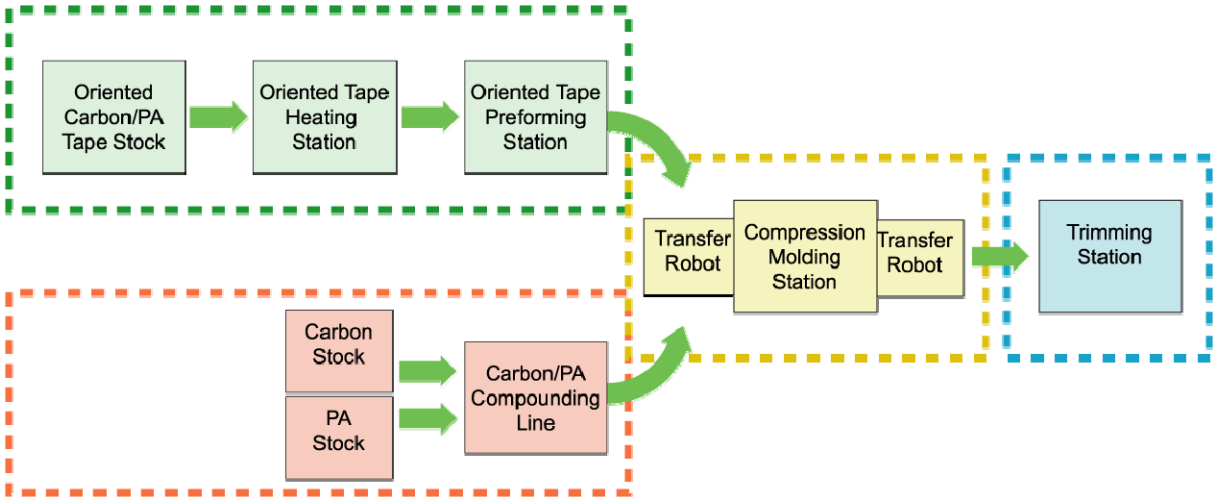

Figure 14. Seat Molding Process Schematic.

Additional trim parts and reinforcements may be necessary for the TPP4 seat and a full cost analysis to get to an equivalent seat in terms of performance and fit and finish needs to be completed. Currently the ACC Seat Team has provided EPFL with cost-model input for the design, materials, and processes for the ACC seat design.

---

[i] Denotes project 007 of the Automotive Composites Consortium (ACC), one of the formal consortia of the United States Council for Automotive Research (USCAR, see www.uscar.org) set up by Chrysler, Ford and General Motors to conduct joint, pre-competitive research and development.

B. Development of Manufacturing Methods for Fiber Preforms (ACC 040[i])

Principal Investigator: Patrick Blanchard
Ford Motor Company, Research and Innovation Center
P.O. Box 2053, MD 3135 RIC, Dearborn, MI 48121-2053
(313) 390-6230; fax: (313) 390-0514; e-mail: pblanch3@ford.com

Principal Investigator: Jeff Dahl
Ford Motor Company, Research and Innovation Center
P.O. Box 2053, MD 3135 RIC, Dearborn, MI 48121-2053
(313) 845-1039; fax: (313) 390-0514; e-mail: jdahl@ford.com

Project Manager: C. David Warren
Oak Ridge National Laboratory (ORNL)
P.O. Box 2009, Oak Ridge, TN 37831-8050
(865) 574-9693; fax: (865) 576-4963; e-mail: warrencd@ornl.gov

Technology Area Development Manager: Joseph A. Carpenter
(202) 586-1022; fax: (202) 586-1600; e-mail: Joseph.Carpenter@ee.doe.gov

Field Project Officer: Aaron D. Yocum
(304) 285-4852; fax: (304) 285-4403; e-mail: aaron.yocum@netl.doe.gov

Expert Technical Monitor: Philip S. Sklad
(865) 574-5069; fax: (865) 576-4963; e-mail: skladps@ornl.gov

---

Contractor: U.S. Automotive Materials Partnership (USAMP)
Contract No.: DE-FC05-95OR22910 through the DOE National Energy Technology Laboratory

---

Objective

- Develop and demonstrate new fiber-preforming processes to decrease cost, increase manufacturing rates and improve reproducibility of large preforms/blanks for composite manufacturing.
- Develop the thermoplastic programmable powdered preform process (TP-P4) concept as a high- volume, composite manufacturing process for thermoplastic composite materials.
- Demonstrate a new method to provide robust corrosion protection for magnesium (Mg) structural members by encapsulating them in polymer.

Approach

- Investigate materials, process equipment, and tooling technology to further reduce the cost and enhance the quality of chopped-fiber preforms.
- Explore the extension of automated-preforming technology to make preforms with a thermoplastic matrix.
- Investigate heating methods for thermoplastic composite blanks manufactured using the TP-P4 process.
- Perform cost analysis of the TP-P4 to determine the economic benefits versus competing process technology.
- Adopting the multi-material approach, use research conducted in the Ultra-Large Casting of Al and Mg (ULC, AMD 406; see 3.C) project as a platform for new research in the Automotive Composites Consortium (ACC). Totally encapsulate Mg structural casting in a polymer to demonstrate robust corrosion prevention while providing more opportunity for parts consolidation. The process of focus will be the Powder Impression Molding (PIM) process, with investigation of other potential encapsulation processes such as Magna Advanced Technologies' Self Aligning and Actuating Mold (SAAM) process (which utilizes low-pressure, compression-molded sheet molding compound (SMC)) and possibly injection molding.

Accomplishments

- Completed processing studies to establish feasibility of the TP-P4 process.
- Finite-element analyses (FEA) of a "shotgun" design and material specifications development have been initiated.

Future Direction

- Extend the capability of TP-P4 deposition equipment to achieve adequate throughput of chopped fiber blanks.
- Continue cost modeling of process concepts to determine business rationale for migration of process technology to original equipment manufacturer (OEM) supply base.
- Perform application studies to expose outstanding processing hurdles that may become obstacles to future technology implementation.
- Perform extended FEA of the shotgun design using multiple materials and reinforcements.
- Investigate other possible materials and processes to lower costs and weight of the component.

Thermoplastic P4 (TP-P4)

Introduction

This work has focused on the development of a thermoplastic-focused derivative of the programmable powdered perform process (P4), TP-P4. This fully-automated deposition process deposits commodity-grade, commingled yarns of polypropylene and glass onto a screen to produce blanks for subsequent compression molding. Previously, experimental studies were performed at the National Composite Center (NCC) in Kettering, Ohio. However, most of the technical development is now being pursued through collaborative use of the P4 cell at ORNL. (See related 8.C.) Extensive experimental investigations have also been conducted in collaboration with the Polymers Laboratory (LTC) at the Swiss Federal Institute of Technology (EPFL) in Switzerland.

During this reporting period, investigations were conducted in the following process areas.

- TP-P4 chopper-gun deposition speeds.
- Preconsolidation and preheating methods for TP-P4 blanks.
- Polymer degradation vs. heating time.
- Hot flow compression molding of TP-P4 blanks.

TP-P4 Chopper-Gun Trials

Previous cost-modeling studies [1,2] performed in 2006 showed that deposition time had an important effect on part cost. A range of values was considered in the cost study, which for one robot ranged from 7.5 kg/min to 12.2 kg/min. For example, comparing the slowest one-cell variant to the fastest two-cell variant, the deposition cell cost/part was decreased from $3.70 to $2.50 per part. Hence, work has focused on the following deposition aspects:

- Improve chopper deposition rates.
- Evaluate a single-motor chopper-gun design for chopping Twintex roving.

Based upon trials at the NCC and ORNL, several factors were found to limit the deposition rates. These included fiber jamming due to fiber fuzz, linear velocity of the fiber rovings and practical limitations on robot acceleration and deceleration. However, modification of the roller pressure, gap and tensioning systems enabled throughput rates of 3200 g/min and 4200 g/min to be achieved for 25-mm and 75-mm long fibers, respectively.

To achieve the higher throughputs needed, the deposition rate of the chopper head needs to be increased and should, hence, be redesigned specifically for Twintex materials. The bounds cost modeled previously were 7.5 kg/min with 11 ends to 12.2 kg/min with 22 ends. Key challenges that remain include reducing downtime due to fiber jamming and improvement in the durability of chopper-gun contact surfaces. As a first step towards this, an alternative glass-fiber chopper head was purchased. Initial trials with this chopper system would suggest that 6 kg/min is feasible with 3 ends of material and without the fiber jamming observed with the current chopper design. A revised design would still be required to incorporate an increase in the number of ends.

Preconsolidation and Preheating Methods

After deposition, a heat-set cycle is used (as in the original P4 process) to partially melt the polypropylene and, hence, stabilize the preform for subsequent handling. Without this step, the preform does not have any mechanical integrity. The heat-set stage consisted of blowing hot air through the preform, which was located between perforated matched tools. The hot-air cycle could also be followed by a cool-air cycle.

The baseline process, as shown in Figure 1, used an additional preconsolidation stage after the deposition process. Studies of the preconsolidation stage have been reported previously. Figure 1 shows that this added an extra $2/part, and a resulting action for this experimental work was to investigate if the preconsolidation stage could be removed, that is, is the heat-setting operation alone sufficient to achieve sufficient mechanical handling integrity of the preformed blank?

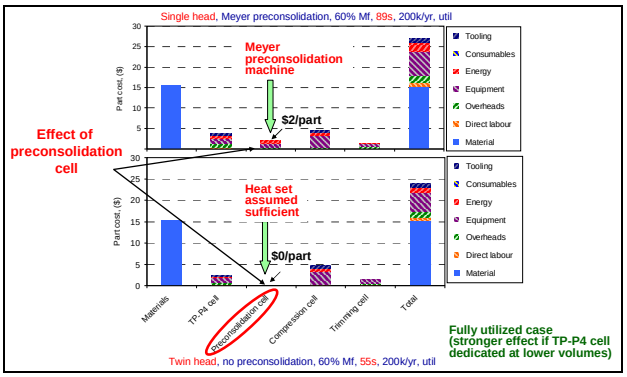

Figure 1. Cost breakdown of TP-P4 process.

The feasibility of eliminating the lamination operation is driven largely by practical limitations of heating thick glass-fiber/polypropylene blanks. The low thermal conductivity often results in surface degradation of the polymer constituent before the blank mid-plane temperature reaches target. This problem is amplified as heat-set blanks are typically over five times the thickness of those laminated. Therefore, heating trials were performed using a forced-hot-air oven to determine whether adequate heating rates could be achieved. A summary of the results is shown in Figure 2.

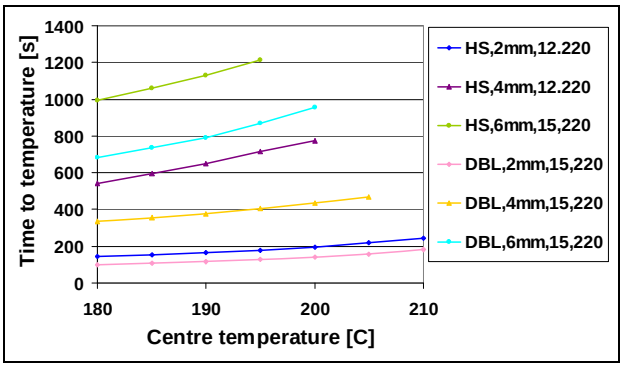

Figure 2. Heating times for heat-set and laminated blanks (of molded thickness 2-6 mm).

Increasing blank thickness resulted in a corresponding increase in heating times. This is most noticeable for heat-set blanks of 6 mm (final molded part thickness). Heating times of over 20 minutes were recorded, with target temperatures above 200°C not possible. Therefore, laminated blanks would be recommended for this thickness. On the contrary, 2-mm blanks showed minor differences in heating times between those that were laminated and those which were heat set. This would suggest that use of 2-mm blanks could eliminate the requirement for the lamination step. However, it should be noted that reducing blank thickness would result in an increase in cycle time for the deposition cell as more blanks would be required for subsequent molding.

Polymer Degradation Studies

In order to determine how temperature and time-at-temperature affected degradation of the TP-P4 polypropylene matrix, measurements of polymer molecular weight were performed. Following deposition of the rovings in the TP-P4 cell, degradation is a function of the subsequent thermal history, including the heat-set phase, the optional double-belt lamination process. Finally, any heating prior to molding will also have an impact. In comparison with heat-set material, double-belt lamination can reduce the heating time needed for the material to reach a temperature suitable for press forming, but also adds an additional thermal process. The study compared degradation of the TP-P4 after compression molding for both heat-set and double-belt laminated material to see the combined degradation effects.

Figure 3 shows a summary chart for polymer molecular weight for a range of heating conditions. 2-mm blanks, whether laminated or heat set, showed few signs of degradation at any temperature. However, increasing thickness to 4 mm and 6 mm showed a significant drop in molecular weight for heat-set samples alone. This reinforces the argument that the lamination process can only be eliminated provided the TP-P4 blank thickness is limited to 2 mm or less.

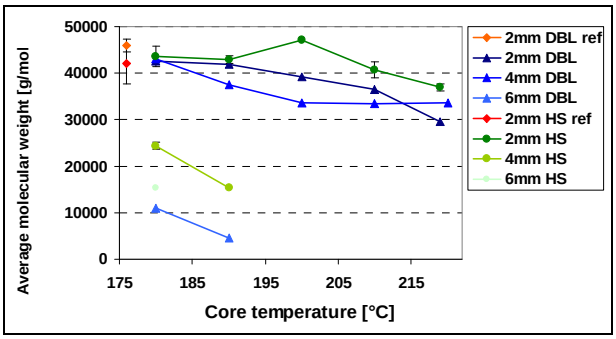

Figure 3. Effect of heating time and target temperature on polymer molecular weight.

Hot Flow Compression Molding

A design-of-experiments approach was used in order to find the necessary press requirements to promote in-plane and out-of-plane flow of TP-P4 blanks. This included the use of a 250-mm x 250-mm, deep-rib tool to establish the appropriate processing parameters. An example of a completely-filled part is seen in Figure 4. Optimum conditions appeared to be a molding pressure of 250 bar, fiber length of 25 mm, and a compression velocity of 100 mm/s. Note that the latter is a 100% increase in compression velocity compared to standard molding presses. This is largely due to the high glass mass fraction of the blank, 60% wt, vs. standard glass-mat thermo-plastic (GMT, 40 wt%). Nevertheless, the TP-P4 blanks were able to flow into the 77-mm ribs which would indicate capability for component geometries featuring similar rib depths.

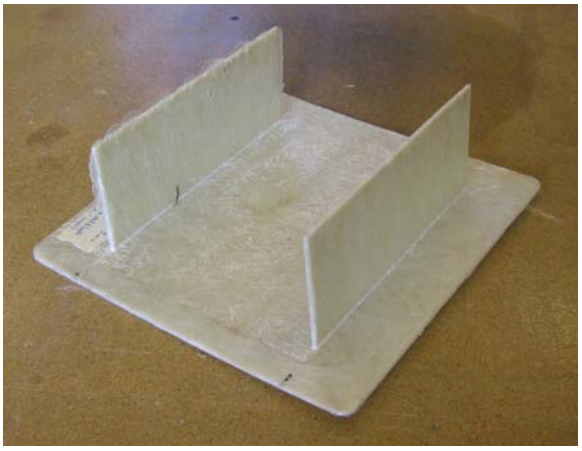

Figure 4. Molded TP-P4 blank using a deep-rib compression-molding tool.

Conclusions and Future Work

Based upon cost and process investigations conducted in 2007, future developments will focus on the development of the high-throughput chopper gun. Once a robust system is in place, a target component will be selected to identify other processing obstacles that may exist.

Powder Impression Molding (PIM)

Introduction

This effort has focused on the development of a fully-encapsulated Mg shotgun utilizing the Powder Impression Molding (PIM) process. The PIM process is based on the licensed technology from 3DM Worldwide and locally at VP Tech in Auburn Hills, MI.

An initial concept was designed based on the USAMP ULC project (AMD 406) in which additional features such as battery tray, washer-fluid reservoir and splash shield were combined into a single molded piece. The shotgun casting consists of a highly-ribbed structure and incorporates hood hinge pivots and front bolster attachments (Figure 5).

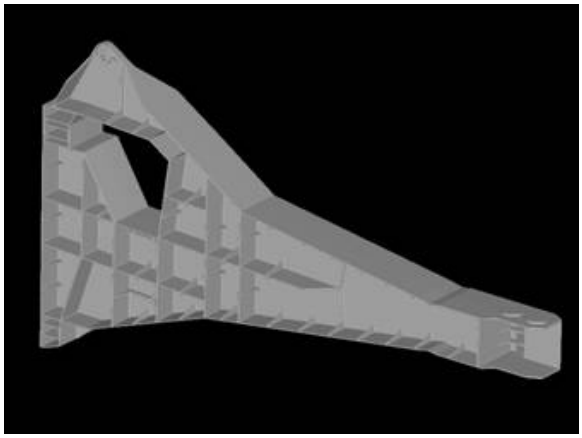

Figure 5. AMD 406 Mg shotgun.

The new process makes use of thermoplastics (primarily polypropylene) to encapsulate a component in foam with a dense (void-free) outer layer. Preliminary investigations were conducted on a cross member to determine the feasibility of the process. The sections that follow describe the results from these studies.

Equipment Capability

The PIM process was developed to manufacture polymer-based composite components by heating a two-piece metal tool and applying powdered polymer material to form a melted skin conforming to the cavity of the mold. The mold halves are brought together after the skins are formed and may include layers of filler or reinforcement materials as well as expandable foam.

Basic Process Principles

The key process parameters are time and mold temperature. The combination of dwell time at a specific mold temperature determines the plastic skin thickness, typically 1 mm or greater. The two mold halves with independently-formed skins are placed together like a sandwich after introducing the desired amount of expandable filler foam material, as well as desired fillers or reinforcements, and held together for a pre-determined time while heated again.

The PIM process is generally carried out at relatively low temperatures, i.e., slightly higher than that of the melting point of the plastic, polymer-based, particulate material being contacted with the heated mold. Because of the low-temperature and low-pressure application, the molds do not degrade as they do in injection molding and thus offer long life cycles. The preferred mold material is aluminum (Al) because of its uniform heat distribution characteristics, machinability and relatively long molding cycle life.

Material

The PIM process was designed to accommodate all thermoplastic materials as long as they can be produced in powder form. The foam is usually of the same material as the skin, except for adding a foaming agent.

Design / Tooling

The process is based upon open cope-and-drag tooling configurations thus allowing for complex shape designs with parting lines. The ability to insert filler material and/or reinforcement materials provides for additional product design flexibility. Size of molds can range from very small geometric objects to large shipping-container mold segments. Tooling material is typically cast or slab Al machined to the desired cavity geometry.

Previous Mg Encapsulation Work

Testing was performed on an encapsulated Mg cross member with favorable results. The Mg cross member was manufactured by machining a billet piece of Mg into a frame cross member typical of those found on frame-based pick-up trucks and sport-utility vehicles (SUVs) (Figure 6). The cross member was encapsulated using the PIM process at VP Tech. Al inserts were molded in place, in lieu of separate isolators to inhibit galvanic corrosion (Figure 7).

The encapsulated cross member was tested according to Ford APG and APGE corrosion test specifications and incurred no detrimental effects. The cross member was also gravelo-meter tested to assess the effects of stone impact, at various temperatures, again incurring no detrimental effects.

Figure 6. Machined Mg cross members.

Figure 7. Encapsulated Mg cross members.

Ongoing Work

A purchase order has been released to Global Tech (licensor of 3DM's PIM technology) to complete deliverables in task 1 (Table 1) of the statement of work. The deliverables include

1) report on previous work completed.
2) completed concept design (Figure 8).
3) comprehensive cost model (Figure 9).

Table 1. Deliverables for Task #1.

Deliverable	Description	Cost ($US)
1	Report on encapsulation work done to date.	35k
2	Complete concept design tailored for the PIM process.	
3	Preliminary cost model based on the PIM process.	
4	FEA analysis of the battery tray area, according to Ford test specs.	9.7k

To date, two of the deliverables have been met (#2 & #3). Red Cedar Technology was consulted regarding finite-element analysis (FEA) of the battery-tray area, to supplement the original deliverables. The FEA concentrates on the battery-tray area to test the feasibility of using the PIM materials without any additional reinforcement except for the designed rib features. A quote was finalized and another purchase order has been released to start the FEA.

Upon completion of the FEA of the battery-tray area, a decision will be made either to proceed to Task #2, fabrication of tooling, or make appropriate design changes involving the possibility of selectively embedding reinforcement in the battery tray.

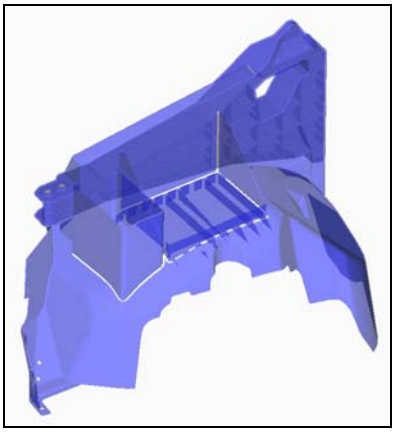

Figure 8. Encapsulated Mg shotgun, showing integrated battery tray, washer-fluid reservoir and splash shield.

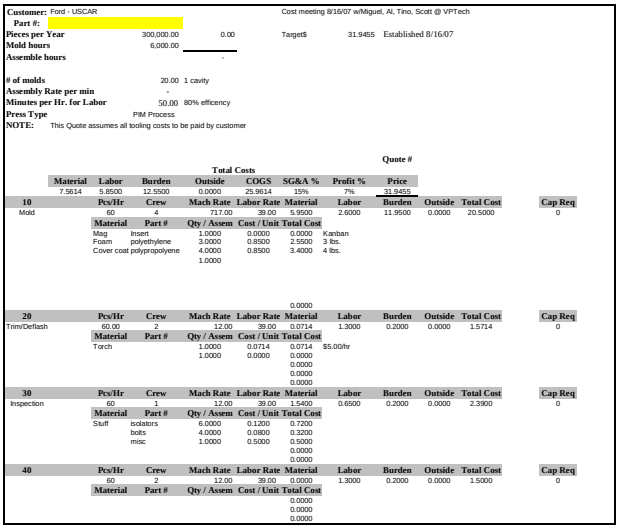

Customer: Ford - USCAR — Cost meeting 8/16/07 w/Miguel, Al, Tino, Scott @ VPTech
Part #:
Pieces per Year 300,000.00 0.00 Target$ 31.9455 Established 8/16/07
Mold hours 6,000.00
Assemble hours -
# of molds 20.00 1 cavity
Assembly Rate per min -
Minutes per Hr. for Labor 50.00 80% efficency
Press Type PIM Process
NOTE: This Quote assumes all tooling costs to be paid by customer

Quote #

Total Costs

Material	Labor	Burden	Outside	COGS	SG&A %	Profit %	Price
7.5614	5.8500	12.5500	0.0000	25.9614	15%	7%	31.9455

	Pcs/Hr	Crew	Mach Rate	Labor Rate	Material	Labor	Burden	Outside	Total Cost	Cap Req
10	60	4	717.00	39.00	5.9500	2.6000	11.9500	0.0000	20.5000	0
Mold										

Material	Part #	Qty / Assem	Cost / Unit	Total Cost	
Mag	Insert	1.0000	0.0000	0.0000	Kanban
Foam	polyethylene	3.0000	0.8500	2.5500	3 lbs.
Cover coat	polypropolyene	4.0000	0.8500	3.4000	4 lbs.
		1.0000			
				0.0000	

	Pcs/Hr	Crew	Mach Rate	Labor Rate	Material	Labor	Burden	Outside	Total Cost	Cap Req
20	60.00	2	12.00	39.00	0.0714	1.3000	0.2000	0.0000	1.5714	0
Trim/Deflash										

Material	Part #	Qty / Assem	Cost / Unit	Total Cost	
Torch		1.0000	0.0714	0.0714	$5.00/hr
		1.0000	0.0000	0.0000	
				0.0000	
				0.0000	
				0.0000	
				0.0000	

	Pcs/Hr	Crew	Mach Rate	Labor Rate	Material	Labor	Burden	Outside	Total Cost	Cap Req
30	60	1	12.00	39.00	1.5400	0.6500	0.2000	0.0000	2.3900	0
Inspection										

Material	Part #	Qty / Assem	Cost / Unit	Total Cost	
Stuff	isolators	6.0000	0.1200	0.7200	
	bolts	4.0000	0.0800	0.3200	
	misc	1.0000	0.5000	0.5000	
				0.0000	
				0.0000	

	Pcs/Hr	Crew	Mach Rate	Labor Rate	Material	Labor	Burden	Outside	Total Cost	Cap Req
40	60	2	12.00	39.00	0.0000	1.3000	0.2000	0.0000	1.5000	0

Material	Part #	Qty / Assem	Cost / Unit	Total Cost
				0.0000
				0.0000
				0.0000

Figure 9. Cost model summary for 300k pieces per year.

Preliminary tests have also been performed on PIM plaques to mimic battery loading at elevated temperatures. Two PIM plaques (nominally 25.4-mm thick) were placed into an oven at 50°C. One plaque was supported by two steel blocks (approximately 25-mm thick) along its length (Figure 10) and the other along its width (Figure 11). A reference measurement was taken near the center of the plaque and approximately

18.6 kg of weight was placed on top of the plaque, relatively centered, to mimic the loading of a typical battery. The oven was then ramped up to 105°C and the maximum deflection of the plaque was recorded over time.

Figure 10. PIM plaque supported along its length (approx. 412.8 mm apart).

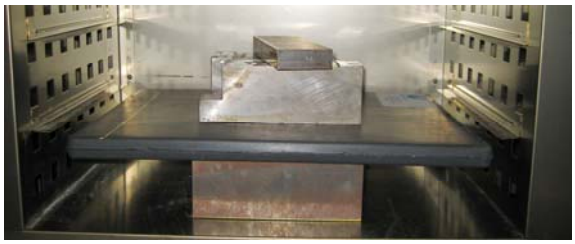

Figure 11. PIM plaque supported along its width (approx. 263.5 mm apart).

Of the plaques tested to date, a maximum deflection of 12.55 mm was observed for the plaque that was supported along its length. For the two plaques that were supported along their widths, a maximum deflection of 2.20 mm was observed (Figure 12).

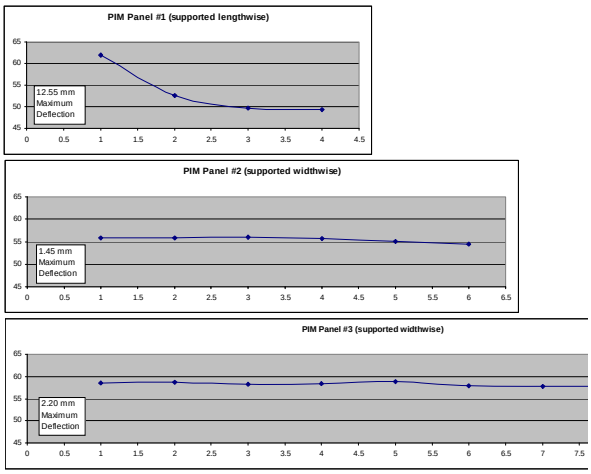

Figure 12. Recorded deflections over time for lengthwise-supported and widthwise-supported PIM plaques. (Same scales utilized.)

Ultimately, the battery tray will have to pass specified durability tests. Red Cedar Tech is currently employing Ford Motor Company specifications for FEA. Further material testing will commence upon receipt of the all deliverables from Task 1 and upon favorable results from the FEA of the battery-tray area.

References

1. M.D. Wakeman, G. Francois, J-A.E. Manson, "USCAR: Cost Modeling of Thermoplastic P4 Process Technology progress report 1", April 2006, EPFL, Lausanne, Switzerland.
2. M.D. Wakeman, G. Francois, J-A.E. Manson, "USCAR: Cost Modeling of Thermoplastic P4 Process Technology progress report 2", September 2006, EPFL, Lausanne, Switzerland

[i] Denotes project 040 of the Automotive Composites Consortium (ACC), one of the formal consortia of the United States Council for Automotive Research (USCAR, www.uscar.org) set up by Chrysler, Ford and General Motors to conduct joint, pre-competitive research and development.

C. Development of Next-Generation Programmable Preforming Process

Principal Investigator: Robert E. Norris, Jr.
Oak Ridge National Laboratory (ORNL)
P.O. Box 2008, Oak Ridge, TN 37831-6053
(865) 576-1179; fax (865)-574-8257; e-mail: norrisrejr@ornl.gov

Field Project Manager, Composites: C. David Warren
ORNL
P.O. Box 2008, Oak Ridge, TN 37831-6065
(865) 574-9693; fax: (865) 576-4963; e-mail: warrencd@ornl.gov

Technology Area Development Manager: Joseph A. Carpenter
(202) 586-1022; fax: (202) 586-1600; e-mail: joseph.carpenter@ee.doe.gov

Expert Technical Monitor: Philip S. Sklad
(865) 574-5069; fax: (865) 574-6098; e-mail: skladps@ornl.gov

---

Contractor: ORNL
Contract No.: DE-AC05-00OR22725

Objectives

- Develop the next-generation of low-cost fiber preforming technologies based on programmable, robotic-controlled, directed-chopped-fiber processes for the application of:
  - low-cost carbon fiber
  - reinforced thermoplastics
  - hybrid glass-carbon
- Develop supporting technologies required to successfully implement the process technology including:
  - preform characterization (e.g., permeability, areal density uniformity)
  - preform process modeling for process-effects analysis
- Conduct parametric process studies to investigate fundamental process effects and establish process-property relationships.
- Conduct requisite molding investigations—experimentally and through modeling—to elucidate relationship between preform characteristics and moldability.

Approach

- Establish a base-research, programmable, robotic preforming system for which advanced capabilities (e.g., new chopper designs) can be developed and evaluated.
- Establish a highly instrumented and controlled, research molding capability to isolate and investigate the effects of process variables on moldability and mechanical properties.
- Develop new severing technology to facilitate the implementation of low-cost carbon-reinforced thermoplastics and hybrid glass-carbon products.
- Benchmark and implement process modeling into experimental work to guide parameter selection and to provide tools for longer-term implementation of preforming and related technologies.

Accomplishments

- Demonstrated successful chopping of small quantities of Direct Re-Enforcement Fabrication Technology (DRIFT) material (reinforcing fibers pre-impregnated with polypropylene) and molded a thin demonstration article.
- Based on the above accomplishment, worked with Polycomp to modify the product form and preformed and molded several 24-in x 24-in panels for demonstration and testing.
- Worked with the Automotive Composites Consortium (ACC) and Ecole Polytechnic Federal de Lausanne (EPFL) to provide a substantial number of panels using TwinTex commingled glass and polypropylene fibers for evaluation of technical and economic feasibility for automotive applications.
- Purchased evaluation quantities of latest commercially-available industrial grades of carbon fiber and initiated experimental work with hybrid blends at various ratios of carbon and glass reinforcement to evaluate potential advantages of combining these materials to achieve performance and/or economic benefits.
- Currently evaluating feasibility of *in-situ* blending reinforcing fiber with thermoplastic matrix fiber at the preforming machine versus buying materials commingled by reinforcement fiber manufacturers such as the TwinTex product. Since the variety of forms of commingled materials is extremely limited, this allows evaluation of materials not available at all in commingled form and in a much broader array of blending alternatives. Although the focus of this approach is to facilitate evaluation of alternative material combinations especially looking at hybrids, *in-situ* blending may prove economically attractive as well.
- Completed integration of injection/compression press and general-purpose mold with associated heating system and instrumentation and initiated molding of test panels.
- Transferred the ACC Wolfangel high-speed prototype chopper to ORNL and initiated modifications to enable control of chopper to simulate robotic preforming operations at speeds exceeding those of the current chopper system.
- Initiated complementary investigation of cutting tribology issues to determine if alternative materials and techniques might improve variations of current severing technologies.
- Continued experimentation to demonstrate feasibility of laser-severing technology concentrating on improved optics to facilitate more focused delivery of the beam energy to the cutting region in order to validate earlier estimated requirements. Initiated effort to model the laser-delivery system and associated energy distribution.
- Previously-developed general modeling approach was modified to improve the flexure model for fiber deformation and to separate modules to improve speed and reduce code size.

Future Direction

- Continue preforming studies with various product forms incorporating reinforcement and thermoplastic matrix materials “co-processed” through the preforming machine including forms with low-cost carbon fiber as available. Near-term focus is hybrid blends of glass and industrial grades of carbon fiber.
- Advance bench-top studies of advanced severing technology to determine technical and economic feasibility of developing new techniques (e.g., laser-severing) or substantially improved equipment (e.g., higher-speed choppers, improved blade materials, etc.) that can be practically adapted and implemented for this application within one to three years.
- Evaluate preform process models relative to physical preform characteristics and expand model capability as resources permit.
- Evaluate programmatic benefits versus costs and risks of refurbishing an existing injection machine or acquiring a rebuilt unit for structural reaction injection molding (SRIM) to complement current focus on other molding technologies and implement if justified. This equipment will be critical for evaluation of any materials in liquid-molding processes and will be useful in evaluating a variety of material forms including hybrid blends, natural-fiber preforms and early evaluation of low cost carbon fiber.

- Continue developing and implementing tools for more effective characterization of process variable and effects on final products. Conduct permeability measurements on preforms made by simulated split-tow products of varying tow-size and construct and test through-thickness permeability rig as funding and other resources permit.

Introduction

Polymer-matrix composite materials offer a number of benefits in lightweighting of automotive and heavy vehicles, including greater stiffness and strength per unit weight than conventional materials, easier formability, less corrosion susceptibility, the ability to tailor properties to specific load requirements, and enhanced noise and vibration damping. However, widespread implementation of carbon-fiber composites, which offer among the greatest mass savings potential, requires lower-cost materials and manufacturing processes than are currently available. Advanced preforming processes offer opportunities to facilitate the widespread use of carbon composites.

Robotic-controlled, programmable, directed-fiber preforming processes have demonstrated exceptional value for rapidly preforming large, glass-reinforced, automotive composite structures. Due to their unique features and flexibility, and to their inherent low scrap rate, they are among the most viable candidate processes for making affordable carbon-fiber preforms for a variety of structural automotive components. The ACC has implemented the Programmable Powdered Preform Process (P4) with glass fibers very successfully in its truck box program—Focal Project 2 (FP2). Prototype B-pillars were also successfully fabricated from both carbon- and glass-fiber reinforcement and tested as part of the ACC's Focal Project 3. Original-equipment manufacturers (OEMs) have transferred the technology to commercial applications such as the General Motors (GM) Silverado pickup box and the Aston Martin Vanquish body-side.

Analyses have indicated a potential for greater than 60% mass savings for a carbon-fiber-intensive body-in-white under the assumption of a thickness design constraint of 1.5 mm. The analyses also indicate the potential of saving an additional 15% if the thickness constraint is reduced to 1 mm. Unfortunately, evidence suggests that 1.5 mm may be a practical limit for liquid molding. However, thermoplastics preforms, in which the matrix and fiber are both deposited in the preforming step, offer a potential path to obtaining thinner sections and, consequently, additional mass savings as well as greater potential for recyclability. Hybrid-fiber preforms that can effectively take advantage of concurrently utilizing carbon and glass fibers offer another potential benefit in terms of economics and property enhancement and may be a good route for actually introducing more carbon fiber at somewhat lower quantities than necessary for all-carbon components in automotive applications.

Preforming Developmental Approach

The objective of this project is to advance directed-fiber preforming processes to effect a further reduction in vehicle mass—relative to conventional glass-fiber composites—while maintaining the economical advantages of net-shape preforming. The project is pursuing three focus areas corresponding to three materials systems: reinforced thermoplastics, carbon fiber, and hybrid glass-carbon fiber. Each focus area consists of four main tasks concentrating on: 1) materials developments, including introduction and evaluation of alternative and/or new fiber product forms and binders; 2) machine developments, particularly new severing technology; 3) process developments, for example, to control areal density uniformity and preform anisotropy; and 4) development of supporting technologies such as modeling and preform characterization techniques. Furthermore, this project will undertake to develop sufficient understanding of fundamental aspects of the process and their effect on preform quality and mechanical properties in the molded part. As such, this project will support, augment, and facilitate the current and future research activities undertaken in related ACC projects.
A research-focused preforming system has been installed in the polymer-composites laboratories at the ORNL to serve as the base for hardware and

associated technology developments. A number of combinations of reinforcing fibers, binders and/or matrix fibers have been obtained to establish materials baselines for comparison with and advancement of previous P4 work conducted by the ACC. This machine is currently being used to build preforms for evaluation utilizing the TwinTex product (glass fiber commingled with thermoplastic fiber to serve as the matrix), glass impregnated with thermoplastic resin utilizing the DRIFT process, and various forms of carbon and glass reinforcement in alternate independent as well as hybrid forms. Although the near-term focus is on demonstrating advances with glass fiber and existing industrial grades of carbon fiber, the longer-term goal is to establish the ground-work for introduction of large-scale implementation of low-cost carbon fiber for significant impact in automotive lightweighting.

Preform Materials and Processing

The ACC Materials and Processing working groups had initiated work with EPFL to study processing effects and material properties of commingled glass and thermoplastic fibers leading to cost-model comparisons of various thermoplastic composite processes. Focus of this work has been on the TwinTex materials produced by Saint-Gobain Vetrotex incorporating glass and polypropylene fibers, while the basic evaluation process can be extended to a variety of materials and processes based on this concept. After up-front trials in preparation, ORNL hosted representatives of EPFL for extensive fabrication of panels supporting the ACC/EPFL-requested experimental matrix. Initial efforts focused on establishing a preferred baseline fabrication process and experiments were conducted to compare temperature data at various locations in order to define data-capture plans.

With support of EPFL and an ACC representative, approximately 200 sample panels were fabricated using various fiber lengths (25-75 mm) and preform thickness (2-4 mm) along with variations in preforming compaction station time (10-60s) and air-temperature variables (180-240^{o}C). Panels were trimmed and shipped to EPFL for molding trials and final analysis. Results so far have helped to establish initial thickness limits for processing at 3 mm without additional heat stabilization modification to the materials. (ORNL and the ACC have separately discussed with Vetrotex adding improved heat-stabilization capability to the TwinTex. ORNL and Vetrotex have tentatively planned specific evaluation trials, but these trials have been on hold pending resolution of the sale of this business unit.) Material properties from the ORNL panels processed by EPFL are competitive with similar materials and, in some cases, significantly improved. Overall economics for this process were shown by EPFL analysis to approach targets as chopping speeds improve, leading to additional near-term focus on demonstrating the technical and economic feasibility of higher-speed chopping processes.

As another portion of the current focus on thermoplastics, ORNL has been working with Polycomp (inventor of DRIFT) and Fiberform (a key licensee) to evaluate the possibility of chopping the DRIFT product form in the ORNL preforming machine as well as providing one route to evaluating the DRIFT material in general. In fiscal year (FY) 2006, Polycomp made sample quantities of glass-impregnated polypropylene using a 2400 tex glass tow which had been processed into a ribbon about 0.2-in wide and .035-in thick. As expected, the ribbon handled more like a solid strip of plastic than a pliable fibrous tow and did not cut as easily as a glass tow. In initial trials, ORNL was able to get some of the material through the chopper, but with only very small amounts cut before beginning to break blades in the chopper.

Polycomp agreed to make some modified samples in FY 2007 in order to get a thinner ribbon using a smaller glass tow size at about 1150 tex, which is essentially the size of glass tow utilized in the current TwinTex product. The samples were actually made at a weight ratio of 65% glass to 35% polypropylene, which yields a product comparable to the 60/40 TwinTex ratio. Polycomp made two variations of these samples – one at about 5/16-inch width and the other at about 3/16-inch width. ORNL was able to cut both tow sizes, having more success with the 5/16-inch width (nominally about .008-in in thickness) than the 3/16-inch width (at about .015-inch thickness). Although there was not enough material for extensive trials, there was enough combined material to conduct several experiments to

establish cutting parameters. The balance of the materials was used to spray up and compact a small amount of material that was subsequently molded in a lab press into a very thin section solely for demonstration purposes.

Based on the success with the small amount of sample materials, ORNL subsequently procured 250 lbs of the DRIFT materials in the 5/16-inch width to do more process development and material evaluation. Initial work established a basic processing envelope including both preforming and molding adequate for being able to fabricate evaluation panels as shown in Figure 1. A panel has been provided to the ACC Materials Group to begin assessing the properties of molded DRIFT materials after preforming. Once initial property data are received in FY 2008, plans are to focus effort on developing more optimum processing techniques taking into account material forms and chopper configurations that might be economically feasible for implementation.

ORNL has initiated a more in-depth study of mechanical chopping in FY 2007 to correlate chopping of various composite material forms versus alternative chopping parameters, configurations, and equipment forms and materials including evaluation of the high-speed Wolfangel chopper recently procured by the ACC. With a better understanding of this background and related equipment experience, we will be able to better address alternative means for processing the DRIFT materials form.

Longer-term, ORNL and Polycomp are continuing the ongoing discussion concerning consideration of putting a prototype DRIFT line at the end of a Low Cost Carbon Fiber pilot line to evaluate and demonstrate technical and economic potential for various automotive applications of the DRIFT process. As improvements are achieved in chopping and molding of the DRIFT material and progress is demonstrated in continuous manufacturing of low-cost carbon fiber, more definitive work plans will be developed for

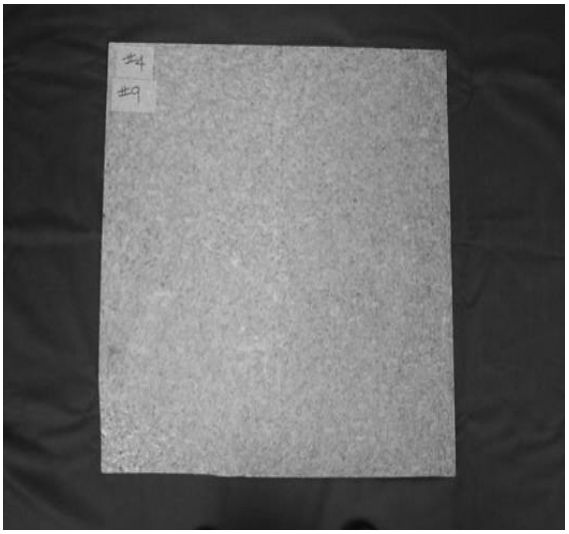

Figure 1. Panel preformed and molded by ORNL from DRIFT.

collaboration in both broad application of DRIFT with carbon fiber as well as more specifically with utilization in performing equipment. Objectives would include optimizing the fiber types, percentages, and types of polymer systems to achieve needed levels of mechanical performance and appearance. Important process characteristics, such as low warpage and reduced material system cost, will be explored. Test specimens and components will both be tested for characterization and durability for use in structural and semi-structural applications.

Since it is believed that hybrid-fiber preforms can effectively take advantage of concurrently utilizing carbon and glass fibers and offer potential benefits in terms of economics and property enhancement, ORNL has obtained standard lower-cost carbon-fiber alternatives from Zoltek and Toho to evaluate in conjunction with glass-fiber reinforcement previous acquired from Owens Corning. ORNL also procured polypropylene fiber to serve as the composite matrix from Fiber Science to use in initial trials to evaluate and demonstrate *in-situ* blending at the preforming machine. Due to current product availability typically only in very small tow sizes and desire to enhance intermixing of fibers and maintain capability to adjust the mix ratios to a large degree, the polypropylene was combined by the vendor to a larger tow size that was still about $1/6^{th}$ the size of the smaller glass and carbon tows on hand. Currently, the only packaging found

immediately available was outside pull for this product. These limitations necessitated use of a multiple-position creel to facilitate processing and mitigate entanglement (Figure 2). Further combining of packages at ORNL also served to minimize spatial requirements as more polypropylene is added to the blend ratios. During the initial preparation for the hybrid experiments, a limited amount of time was spent evaluating

Figure 2. Multi-package creel for *in-situ* blending experiments.

potential for use of the high-speed photographic equipment from the nearby Test Machine for Automotive Crashworthiness test system. (See 12.B) It appears this equipment will be beneficial in evaluating degree of intermixing in at least the glass and carbon or carbon and polypropylene mixtures, although it may be difficult to distinguish polypropylene from glass without additional study.

Although the initial work is utilizing polypropylene for demonstration purposes, the concept should also be applicable for other thermoplastic materials including polyethylene terepthalate (PET), nylon, and others. It is believed that regardless of whether the *in-situ* blending proves adequate for high-quality thermoplastic matrix parts, the technology being developed could prove advantageous in blending glass and carbon reinforcement to a level adequate for utilization of hybrid reinforcement and may be a good route for actually introducing more carbon fiber at somewhat lower quantities than necessary for all-carbon components in automotive applications.

Establishment of Molding Capability for Composites Evaluation

Key to being able to demonstrate the advances achieved in preforming technology is the ability to demonstrate that these advances translate into improvements in actual representative composites. The best way to effect this demonstration is through adequate evaluation of the preform itself as well as full consolidation of the preform and resin in a composite in the manner in which this would be accomplished in actual composite manufacturing.

Previously, ORNL staff worked with members of the ACC's Processing Group to quantify process-equipment requirements so that an appropriately-equipped research press and general-purpose research mold could be procured and installed at ORNL to support programmatic needs. The intelligent-leveling press was specified to accommodate various molds and molding processes and to be instrumented above routine standards in order to provide more process details in experimental research. Nominal pressing capacity is 750 tons. The general purpose plaque mold is specified for instrumented experiments using SRIM, compression molding of reinforced thermoplastics, and sheet molding compound (SMC) processes. This equipment will allow ORNL to demonstrate preform advances while further investigating advances in the various molding processes themselves.

In order to complete capability for basic molding operations, a dual-zone Sterling heat-transfer system was procured and installed at ORNL. Due to the differences in mass of the sections, dual-zone heating is necessary to be able to balance the temperature of the top and bottom sections of the mold to achieve uniform temperatures and is also useful in controlling the mold clearances and shear edges as the sections slide together and separate in operation. Also during this period, mold instrumentation was completed and integrated into the press data-acquisition system. In order to conduct initial materials evaluation experiments and establish detailed requirements

for more optimum charge heating and transfer of the charge to the press, a screen and aluminum (Al) plate are being used in various configurations in molding experiments. Currently, an existing laboratory oven is being utilized for charge heating, but the oven is not designed for rapid material insertion, charge heating, and material removal and is located further away from the press than would be optimally employed for routine manufacturing operations, especially when molding relatively-thin sections that would rapidly dissipate heat. The Al plate is used to convey the charge from the oven to the press and has raised sections on three sides for rigidity and to somewhat impede air flow across the charge surface while allowing ease of transfer of the charge from the fourth side. The screen is used to allow air flow across the surface of the charge and, when employed on the top surface of the charge, can be used to mitigate "lofting" of the preform while heating. Initial experiments do indicate that the plate helps to retain enough heat during transfer to still have flow in the molding operation, but more experimentation in FY 2008 will help to define adequacy of this approach versus utility and requirements for a dedicated oven in close proximity to the press and mold.

Although originally a portion of the press and mold procurement process, procurement of an SRIM machine was deferred due to higher than expected bid costs during the formal procurement period and somewhat less recent focus on development and demonstration of the SRIM process. Programmatic benefits for utilizing an existing, older-model SRIM machine having capacities close to those identified as targets for the procurement process are being evaluated versus costs and risks for possible refurbishment and/or upgrade of this machine or trade-in for a rebuilt unit with capabilities comparable to the targeted parameters. In current planning, it is thought that this equipment will be critical for evaluation of any materials in liquid-molding processes since this capability is being down-scoped at other program facilities and will be very useful in evaluating a variety of material forms including hybrid blends, natural-fiber preforms, and early evaluation of low-cost carbon fiber. This decision has been deferred again until budget and program direction are better defined.

Fiber-Severing Technology

Due to significant differences in the physical properties of various reinforcement fibers as well as their available product forms, chopping technology that has been successful for glass-fibers systems has demonstrated less-satisfactory results for the carbon-fiber products that are currently available. It is expected that similar results will occur for reinforced thermoplastics and hybrid glass-carbon products. Accordingly, consideration is given in this project to identifying alternative severing technology. A literature and patent search was previously undertaken to assess promising technologies for bench-top investigation. Possibilities identified include mechanical-based, laser-based, CO_2 pellet, liquid nitrogen, water-jet, and ultrasonic. Based on the information available in the literature and consideration of project-team experience in related activities, laser-based choppers appeared to offer the most promise for development and eventual deployment.

Calculations based on the enthalpy of vaporization of carbon indicated that a neodymium: yttrium-aluminum-garnet (YAG) laser system should be able to comfortably deliver the energy required to sever a large carbon-fiber tow (roughly 50,000 filaments) at about 1,000 cuts per second, which would represent a tow traveling at close to the maximum velocity as would be encountered in the ORNL chopper and chopped at a rate sufficient to yield a 0.5-inch cut length. However, in initial experiments at or close to these conditions, we were unsuccessful in getting the necessary power delivered into the entire fiber bundle to effect severing. It appeared that the surface of the outer fiber was ionizing and preventing further energy deposition and penetration into the bundle. In follow-up work conducted using a continuous-wave CO_2 laser as well as an excimer laser and a more tunable (and slower pulse-rate) neodymium: YAG laser, severing of carbon fiber was demonstrated, although none were accomplished at the rates representative of the most aggressive cases thought possible with the original neodymium: YAG laser.

During FY 2007, work was continued with various smaller cross-sectional tow sizes and the

more tunable neodymium: YAG laser. New optic configurations were introduced and evaluated with each iteration targeting a more compact and "efficient" energy-deposition line. A recently-evaluated aspheric lens clearly reduced the spherical aberrations noticed in prior attempts to form a much better line-focus. However, the performance of this configuration in actual cutting was less successful than expected. Essentially, those conditions that produced cuts in the original configuration were now only producing partial cuts. Taking a closer look at several burn patterns as a function of energy and working distance, it was noticed that, at higher energies, the line was much broader than had been hoped and the line was very sensitive to working distance because the numerical aperture (NA) of the new design was much larger than the original configuration (depth of focus is inversely proportional to NA). In terms of cutting, the first observation says that, despite what the simulation showed, the new optics were still not getting all the photons into the smallest possible line. This is most likely due to the fact that the real collimated beam departs significantly from the beam profile assumed in most ray tracers. The second observation is that this system develops a tight focus over a very narrow range of displacements which, in this case, is unfortunately corresponding to some fraction of the thickness of the fiber bundle.

Subsequent work compared the newer beam-line to the former utilizing systematic burns repeated with swapped optics. This repeated experimentation did not illuminate any specific new issues that had been overlooked in introducing the new optics. Since it is still believed that the key immediate issue remains the delivery optics, effort was initiated late in FY 2007 to identify capability to more effectively model optics configurations during FY 2008 to determine what is really practical in terms of the desired processing speeds and physical limitation likely to exist in a production environment. If it appears success can be achieved with improved optics alone or in combination with other alternative systems, these results will be utilized to define the more detailed laser-parameter and control requirements in order to be able cleanly sever a moving carbon-fiber tow at the speeds required for utilization in the P4 system. Initial work will continue to be done in static tests to determine beam width, power levels versus time, and other necessary information before moving to low-speed tests and then tests at speeds more representative of actual fiber deposition rates. With the concept demonstrated, plans would then be to scale up the hardware for on-machine experimentation and demonstration. In addition to severing carbon fiber, future work will address other reinforcing fibers, as well as fibers used as binders, and blends of reinforcing and binder fibers.

As previously mentioned, ORNL has initiated a more detailed study of mechanical chopping for various materials forms and techniques along with the above plans to continue evaluation of the potential for laser-severing. It also had been mentioned earlier that effort is underway to more fully evaluate the Wolfangel chopper at ORNL and to evaluate modifications to the chopper equipment including cutting wheels and blades for both units. Near-term plans for the Wolfangel chopper include very extensive cutting of a large amount of TwinTex material up to a simulated work-week to establish speed and durability of the chopper in its current configuration, as well as potential for scale-up to even higher speeds that may be required for process economics. These trials should afford a good opportunity to evaluate several blade options and possibly other options as well as establishing solid data for the baseline configuration. Effort has been initiated to characterize the metallurgy of the current cutting blade materials and identify candidate replacement materials, coatings, surface treatments, or cutter designs. Initial work has shown that the commercially-available blades currently supplied by Aplicator may be supplied with edge chips (Figure 3) at sizes on the order of fiber diameter, which at a minimum could lead to incomplete fiber cutting.

Sources for other commercial blades and coatings are being surveyed and samples of the most promising materials are being obtained for further evaluation. Current alternatives include the low-temperature carburization process developed by Swagelok (this recently won the 2006 ASM engineering materials award) and the C3I coating

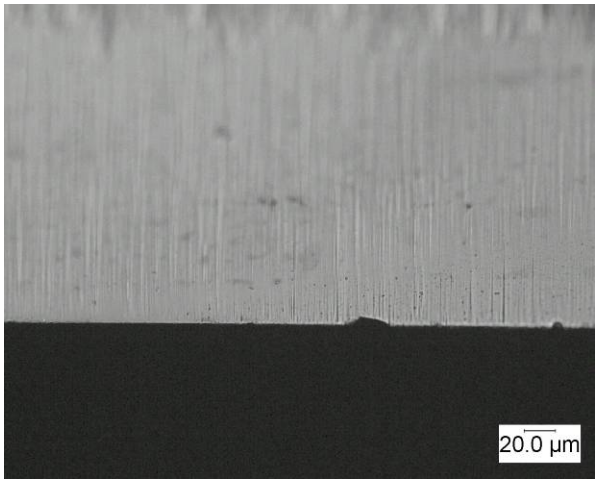

Figure 3. Commercially-supplied blade with edge chip.

process (this won a 2006 R&D 100 award). Both can be used on the existing material. Tungsten carbide blades have also been obtained. Based on test data and other input, recommendations will be developed for enhancing the durability of cutter assemblies. This may include changing to more durable materials, changing the surface finish, changing design of the cutters or holders, and applying coatings or surface treatments to existing or alternative materials.

With a better understanding of chopping mechanics and developing experience with varying blade designs, blade materials, and cutting mechanisms, we will be able to better address a variety of cutting issues associated with carbon fibers specifically as well as with other materials and material blends including somewhat unique products such as the DRIFT materials.

Modeling of Fiber Deposition

A C-based program continues to be developed to analyze the effect of process variables on preform characteristics. The program can be used to evaluate preforms in terms of measures such as fiber run length, fiber connectivity, distribution of voids, etc. When correlated with permeability data and areal density measurements, the program will provide an understanding of the effect of process variables on resulting preforms and their "moldability."

Advancements to the program have included continued enhancement of the previously-developed general modeling approach by addition or improvement of many of the capabilities such that it can simulate a variety of fiber-deposition patterns, orientations, fiber types, layers, network densities, and thicknesses. The program models statistical material properties such as distribution of contacts, voids, segment lengths, fiber undulation, layers, etc. in a full three-dimensional fiber network structure.

A very-much-improved flexure model for fiber deformation has been completed and integrated into the Simulator code. Although not quite as fast as earlier deflection models employed, the new one produces much more realistic fiber conformations than any of the earlier versions and can be extended to include physical effects that would have been impossible for earlier versions to handle.

The full Simulator code has been divided into two separate, stand-alone systems. The first of these eliminates the Void Search and Void Analysis routines, but includes all functions required for managing lay-up growth and for performing various analyses of a completed lay-up. Upon completion of a lay-up, all data relevant to a user-selected "sampling slice" are written to files for further analysis and for support of the now stand-alone Void Analysis code. Several factors motivated the decision to partition the code. Code size was certainly one of these. More important, however, was the desire to be able to develop and store a lay-up upon which a variety of Void Search and Void Analysis experiments could be performed.

The stand-alone Void Search module resulting from the division noted above has been very much refined relative to earlier versions and is now both considerably faster and much more accurate in its delineation of the Void spaces in a lay-up. Void Analysis capabilities are likewise enhanced. For instance, using the stand-alone Void code, the same lay-up (as represented by the data stored with the intermediate "sample slice" file noted above) can be searched many times for Voids, each time using a different probe sphere size. Extraction of information relevant to resin flow, etc. is thus considerably simplified.

Near-term plans include the development of capability to simulate fiber lay-ups made of multiple fiber types deposited concurrently, with emphasis on on-line and off-line commingling for different deposition scenarios. Plans also include development of methods for evaluation of manufacturing feasibility of the above lay-ups. Work is underway to improve availability of the code for more wide-spread evaluation, likely on a work-station platform.

Summary and Conclusions

This project is continuing to build on past development and application of directed-fiber preforming processes, namely, those of the baseline P4, to extend the process to new material systems. Developments are expected to facilitate the use of lower-cost carbon fiber, reinforced thermoplastics, and glass-carbon hybrid materials as effectively as is the current state-of-the-art with glass. Utilizing these materials is expected to lead to further reductions in vehicle mass in a more cost-competitive scenario than is currently possible.

A research-focused preforming system installed in the polymer-composites laboratories at ORNL is currently being used to build preforms for evaluation utilizing various forms of glass fiber commingled with thermoplastic fiber to serve as the composite matrix and glass fiber pre-impregnated with thermoplastic resin utilizing the DRIFT process. Evaluation of a large number of ORNL-fabricated preforms from off-the-shelf commingled TwinTex by EPFL and the ACC has been both technically and economically encouraging, while data have not yet been received on the DRIFT forms. With the acquisition of polypropylene fiber and establishment of means to combine a number of tows *in-situ*, the focus is being expanded to include evaluation of current commercially-available industrial grades of carbon fiber and hybrid blends of carbon fiber and glass fiber along with various blends of thermoplastic fiber.

Also during FY 2007, a heat-transfer system for the complementary advanced research press and general purpose plaque mold was procured, installed, and integrated with instrumentation providing the requisite equipment necessary to demonstrate the advances achieved in preforming technology through composite manufacturing. Use of this system is expanding in evaluating DRIFT and hybrid material variations produced in preforming experiments.

Severing investigations are being conducted in two areas looking at both mechanical-chopping and laser-severing alternatives. The mechanical investigations are looking at blade materials and coatings to also include various cutter configurations. In laser-severing, the optics delivery system is being modeled to determine if there is a practical route to effective laser-energy deposition applicable to this project's requirements.

Modeling of the fiber-deposition process continues through the development of an in-house code. Work is underway to incorporate capability to simulate lay-ups made with multiple fiber types and to provide availability of at least a portion of the model to operate on a more accessible work-station platform.

Collectively, the technologies under development in this project will advance low-cost processing on two fronts. First, it will provide the opportunity to employ additional materials in the net-shape preforming process, which is expected to lead to additional mass reduction and/or better performance. Second, it will provide the requisite tools to evaluate the effect of process parameters on the utility and performance of preforms and molded parts.

D. Low-Cost Carbon-Fiber Composites for Lightweight Vehicle Parts

Principal Investigator: Mark A. Janney
Materials Innovation Technologies, LLC
320 Rutledge Road, Fletcher, NC 28732
(828) 651-9646; fax 828-651-9648; e-mail: mjanney@emergingmit.com

Technology Area Development Manager: Joseph A. Carpenter
(202) 586-1022; fax: (202) 586-1600; e-mail: joseph.carpenter@ee.doe.gov

Contractor: Materials Innovation Technologies, LLC
Contract No.: DE-FG02-05ER84327 (Small Business Innovative Research (SBIR) and Small Business Technology Transfer (STTR) Program

Objectives

- Develop at pilot-scale the Three Dimensional Engineered Preform (3-DEP) process, a slurry-based, low-cost, high-volume production process for making net-shape, carbon-fiber preforms for use in polymer-composite automobile parts.
- Optimize 3-DEP tooling development and evaluate how it influences fiber placement in the preform.
- Optimize carbon-fiber slurry development and determine how it affects preform properties.
- Develop process capabilities to include material handling, preform molding, preform drying, and reducing preform variability.
- Demonstrate the utility of 3-DEP preforms to make an in-production, thermoset composite, automotive component using production tooling (Corvette wheelhouse support).
- Build a process cost model for composites made using 3-DEP preforms.
- Write training and quality manuals.

Approach

- Investigate effects of processing parameters on properties of flat-plate parts and Corvette wheelhouse-support parts in the 3-DEP machine.
- Examine effects of (1) fiber flow within the tank and (2) 3-DEP forming-head motion to produce uniform preforms.
- Demonstrate ability to control part weight during a 3-DEP production run.
- Demonstrate ability to control within-part areal weight distribution (i.e., fiber areal density).
- Collaborate with a current Tier 1 automotive supplier to demonstrate the applicability of 3-DEP preforms in an existing production process.

Accomplishments

- Made 14 x 14-inch flat preforms in 1/4-inch, 1/2-inch, and 1-inch chopped carbon fiber with part-to-part coefficient of variation (COV) between 1 and 4%.
- Made complex shape preforms (Corvette wheelhouse support) in 1-inch carbon fiber with part-to-part COV of 2-4%.
- Made both flat preforms and Corvette preforms having within-part COVs $\leq$ 3.5 %.
- Demonstrated that carbon-fiber Corvette preforms could be molded into composite parts on production molding equipment using a standard production polyester resin.
- Demonstrated that plaques molded from 3-DEP flat preforms had mechanical properties acceptable for automotive semi-structural applications.
- Demonstrated the ability to make molded plaques with fiber loadings up to 30 vol %.

- Demonstrated that 3-DEP works well with reclaimed/recycled carbon fiber.

Future Direction

- Develop preforming technology to achieve higher fiber loading (>50 vol %) in molded composites.
- Extend the capability of the technology to make large parts up to 6 feet x 6 feet (e.g., hood inners, trunk liners).
- Combine 3-DEP preforms with continuous-fiber face sheets to make true structural composites.
- Identify opportunities within the automotive, industrial, and aerospace communities to commercialize the 3-DEP technology.
- Expand our forming capabilities to other fiber-reinforced composites including fiberglass, aramid, natural fibers, and hybrids of these.

Introduction

This work is being conducted under an SBIR Phase II project. The goal of the project is to develop at pilot-scale a potentially low-cost, high-volume production process for making net-shape, carbon-fiber composites for use in polymer-composite automobile parts. The main technical focus of the project is making components and optimizing their manufacture using the 3-DEP fiber-forming process. 3-DEP is an advanced slurry molding process which produces a homogeneous fiber distribution within parts, and consistent part weight and dimensions from part-to-part. Making a consistent preform is key to making consistent parts. A more detailed account of the 3-DEP process, including a short video, can be found at http://www.emergingmit.com/Presentations.html.

The overall objective of the project is to complete the development of the technology started in the Phase I SBIR project by focusing on a complex-shaped component that will be commercially viable. The part chosen for the Phase II project is the front wheelhouse lower support for the Corvette, Figure 1.

This part is currently manufactured by our partner in the project, the Molded Fiber Glass Companies (MFG) of Ashtabula, Ohio. MFG has been supplying Corvette with fiberglass-reinforced polymer parts since the car was introduced in 1953. MFG currently manufactures ~60,000 of the front wheelhouse lower supports per year in fiberglass. The average thickness of these parts is 2.5-3 mm; the glass fiber content is 24% by volume and the part weighs about 0.75 lb. It is about 12 inches wide by 4 inches tall.

Figure 1. Corvette wheelhouse lower support demonstration part molded at MFG using a carbon-fiber preform made by the 3-DEP process.

The front wheelhouse lower support was chosen as a demonstration part because:

a). It is a very complex shape with multiple curvatures, deep draws, nearly-vertical walls, and sharp-edge and corner features. It is one of the most challenging parts MFG molds by the preform process. If this part can be produced using preforms made by the 3-DEP process, then there are a number of related automotive parts (e.g., hoods, trunks, floors, doors) that can also be readily produced.

b). It is currently made in commercial quantities (60,000 per year) in fiberglass giving a body of production and technical data to which we can compare our new process.

c). It is a structural part but not a safety-critical one. Also, it does not require a "Class-A" surface finish (such as an exterior body panel

would require), which would add another level of difficulty to its production.

d). The impregnation/compression molding tool is available at MFG, eliminating an expensive capital expenditure for new tooling.

At the completion of Phase II, we will have a process producing trial parts for evaluation by an automobile manufacturer, General Motors (GM).

Specifically, the technical objectives of our Phase II project are to:

1). Develop at pilot-scale the 3-DEP process, a slurry-based, low-cost, high-volume production process for making net-shape, carbon-fiber preforms for use in polymer-composite automobile parts.

2). Optimize 3-DEP tooling development and how it influences fiber placement in the preform.

3). Optimize carbon-fiber slurry development and how it affects preform properties.

4). Develop process capabilities to include material handling, preform molding, preform drying, and reducing preform variability.

5). Demonstrate the utility of 3-DEP preforms to make a thermoset composite, in-production automotive component using production tooling (Corvette wheelhouse support).

6). Build a process cost model for composites made using 3-DEP preforms.

7). Write training and quality manuals for the 3-DEP process.

Progress to date has been excellent. We have conducted twelve runs of carbon-fiber preforms. The tests comprised between 16 and 40 parts each; we ran 14 x 14-inch flat plaques and the Corvette wheelhouse part. The part-to-part COV was between 0.8 % and 4.9 % depending on the part being formed, the mass of the part, and the fiber length. The within-part COV for flat plaques in 1-inch-long carbon fiber was $\leq$ 3.5%. This is considered good repeatability by automotive standards.

We have made substantial modifications to the 3-DEP lab-scale machine that should allow us to achieve forming consistency from part to part and within-part that are acceptable to the automotive community. We have also demonstrated the ability to make preform molds that will produce good quality parts in a cost-effective manner. Twenty-five carbon-fiber preforms of the Corvette lower wheelhouse support and twelve 14 x 14 inch flat preforms were sent to MFG in 2007 for molding in polyester. Preliminary molding trials have been favorable.

Task 1 - Design and Construction of the Forming Tool and Vacuum Box

Our objective is to design a low-cost tooling system for the wet-forming and drying operations, Figure 2.

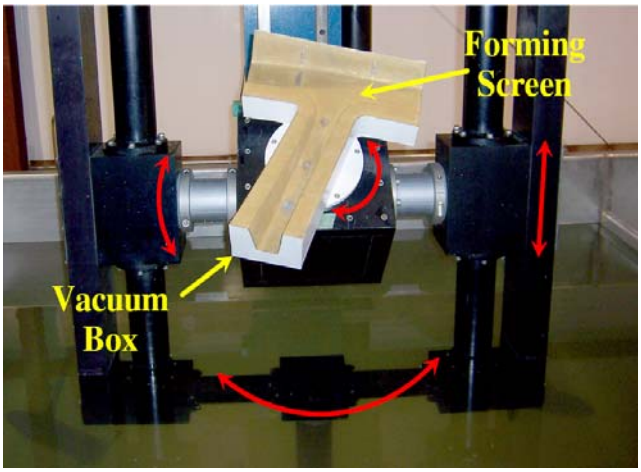

Figure 2. 3-DEP forming head with B-pillar forming tool.

We have considered three approaches:

- An all stainless steel or brass, heavy production tooling system.
  This approach was the lowest risk, but highest cost. The risk was low because it employs technology that has been used for more than 30 years in the speaker-cone industry. The cost is high because it requires complex sheet-metal forming processing to form the perforated stainless steel sheet into the complex shape of the demonstration part, the Corvette wheelhouse support.

- A low-cost, composite prototype tooling system.
  This approach has the advantage that a tool can be formed directly from an existing part. The tool was made in just a few days, rather than the several weeks required for the

stainless-steel tool. The trade-off was that the tool is not as robust as an all-metal tool.

- A semi-composite tools design that is more robust but yet low in cost.
  This approach delivered a combination of properties of the metal and composite tools. It was manufactured fairly quickly, like the composite tool, but was nearly as robust as the stainless-steel tool. This is the approach we think will be most valuable as production tooling as we go forward with the 3-DEP commercialization process.

We have shown proof of concept on all three tooling systems and now have moved on to study how the fibers form against these tools as they are deposited from the suspension.

Task 2 - Fiber and Suspension Issues

A new computer-programmable agitation system has been designed and built for the gimbaled molding machine. This new agitator system allows us to make changes during the formation cycle, which is reducing some of the variations we had previously seen in the suspension. The new agitation system is also a much more robust design that will be suitable for use in the next-generation preforming machine. Our current, lab-scale machine has a suspension tank with a 2000 gallon capacity. The next-generation machine will have a suspension tank capacity of about 50,000 gallons.

Task 3 - Motion Program for Vacuum Forming Parts

We have conducted numerous trials to determine what the capability of the 3-DEP machine is relative to making 14 x 14-inch flat plaques and the Corvette lower wheelhouse support part in carbon fiber. We have used 1-inch, 1/2-inch and 1/4-inch-long fibers in our studies. The binder fibers, which bind the carbon fiber together in the dry state, are either cotton linter or acrylic fiber, which have found extensive use in the speaker-cone industry.

Figures 3-5 show overviews of the Corvette wheelhouse support preform in 1-inch and ¼ -inch carbon fiber along with a set of 25 1-inch carbon-

Figure 3. Top and bottom view of Corvette lower wheelhouse support preform in 1-inch chopped carbon fiber. As-formed, no trimming was done.

fiber preforms that were sent to MFG for initial compression molding trials using their production equipment. The dried preforms are quite robust. The parts shown in Figure 5 were shipped by ground transport to MFG for molding and all parts survived the trip intact and ready to be molded.

A close-up of the fibers in a preform is given in Figure 6. This shows that the architecture of the carbon-fiber preforms is a combination of individual fibers and some fiber bundles. We have

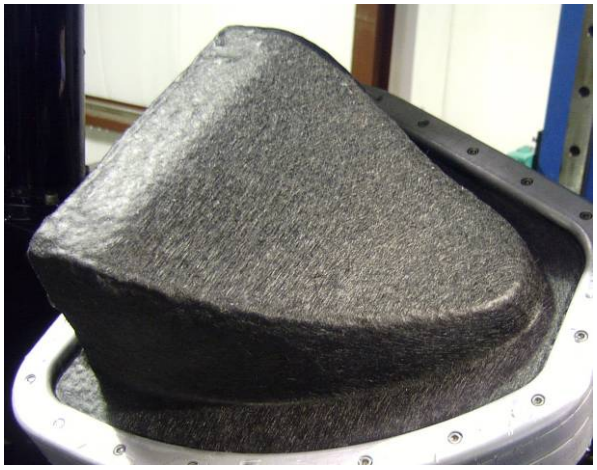

Figure 4. Corvette lower wheelhouse support; ¼- inch chopped carbon fiber; part still mounted on the forming tool. Note improved surface finish of 1/4-inch compared with 1-inch chopped fiber in Figure 3.

Figure 5. Corvette wheelhouse support preforms were shipped to MFG for molding in polyester.

not measured the orientation distribution of the fibers in the preforms (it was not a defined task in this project); however, the distribution appears to be fairly random based on observations of many different areas in numerous preforms.

Machine Variables

We have identified forty-two variables in this new wet-molded preforming process and now have computer-programmable control of twenty-two of them with the remaining twenty manually controllable.

By proper selection of machine variables, we have been able to fine-tune our preforming process.

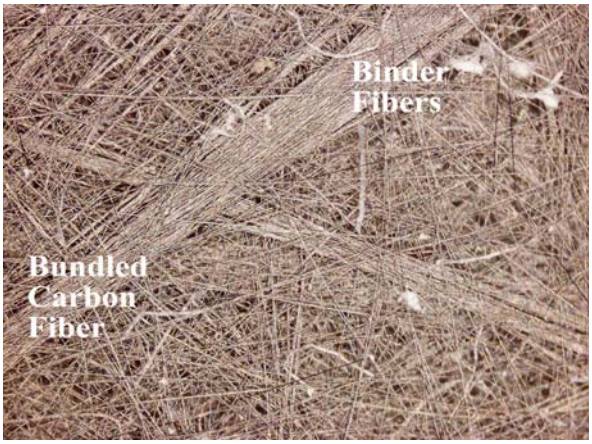

Figure 6. Photomicrograph (20X original magnification) of carbon-fiber preform showing individual carbon fibers, some bundled carbon fibers, and binder fibers.

Figure 7 shows run charts for the Corvette part and for 14 x 14-inch flat plaques from our initial trials in April 2007 and for trials in June 2007.

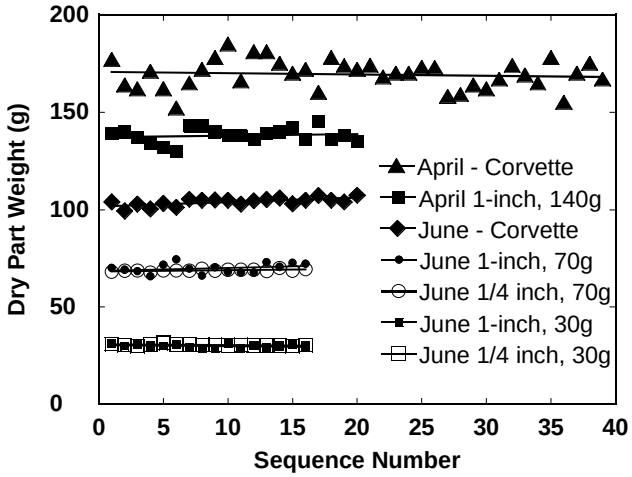

Figure 7. Control charts (part weight vs. sequence number) for 3-DEP preforms (flat and Corvette) made from 1/4- and 1-inch carbon fiber. Similar results were obtained for 1/2-inch carbon fiber.

Table 1 summarizes the mean part weight and part-to-part COV for each run. The April Corvette parts exhibited a very respectable COV of 4.4%; engineers at GM informed us that a COV <10% would be acceptable. The April flat preforms exhibit a good COV (2.7%) but show evidence of "chasing weight" during the run, which necessitated making manual adjustments to the machine settings (at part 7 and part 13). In contrast, the Corvette parts made in June (after running several 3-DEP experiments to optimize

uniformity of the Corvette preform) show extremely good part-to-part COV (2%). The flat plaque COVs for short (1/4-inch) fibers were even smaller, ~ 1%.

Table 1. Summary Data for 3-DEP Parts.

Part	Fiber Length (inch)	Part Mass Mean (g)	Part Mass COV (%)	Number of Parts
April 2007 Corvette	**1**	**169**	**4.4**	**40**
Flat plaque	**1**	**138**	**2.7**	**20**
June 2007 Corvette	**1**	**104**	**2.0**	**20**
Flat plaque	**1**	**69.5**	**3.5**	**16**
Flat plaque	**1**	**49.1**	**4.9**	**16**
Flat plaque	**1**	**29.9**	**3.3**	**16**
Flat plaque	**0.25**	**68.8**	**0.8**	**16**
Flat plaque	**0.25**	**50.3**	**0.9**	**16**
Flat plaque	**0.25**	**30.6**	**1.3**	**16**

In addition to the part-to-part variation, we are also interested in within-part variability of the basis weight. Figure 8 shows a Corvette preform and a flat preform that were sampled for basis-weight variation using a 3-inch diameter punch. The basis weights for the two preforms were similar (852 vs. 857 g/m^2). The within-part basis-weight COVs were also similar at 3.5 and 3.6 %. What this means is that the uniformity of a preform manufactured by the 3-DEP process is not sensitive to the part geometry. This is a very exciting result given the complex geometry of the Corvette wheelhouse support.

Finally, it should be noted that forming time for parts using the 3-DEP process is not a function of the geometric complexity of the part. The Corvette part and the flat preform shown in Figure 8 were made in a similar amount of time.

Task 4 - Drying the Preform

We are starting to investigate combining the step of "de-watering" the preform with the step of transferring the preform to a separate drying station. ("Dewatering" the preform is the initial drying step and uses a high volumetric flow of air through the preform to reduce the water content from 30 wt % to about 10 wt %.) The transfer system design draws the remaining molding water from the preform as it transfers the preform to the drying station where the remaining moisture can be driven away with heat and possibly pressure.

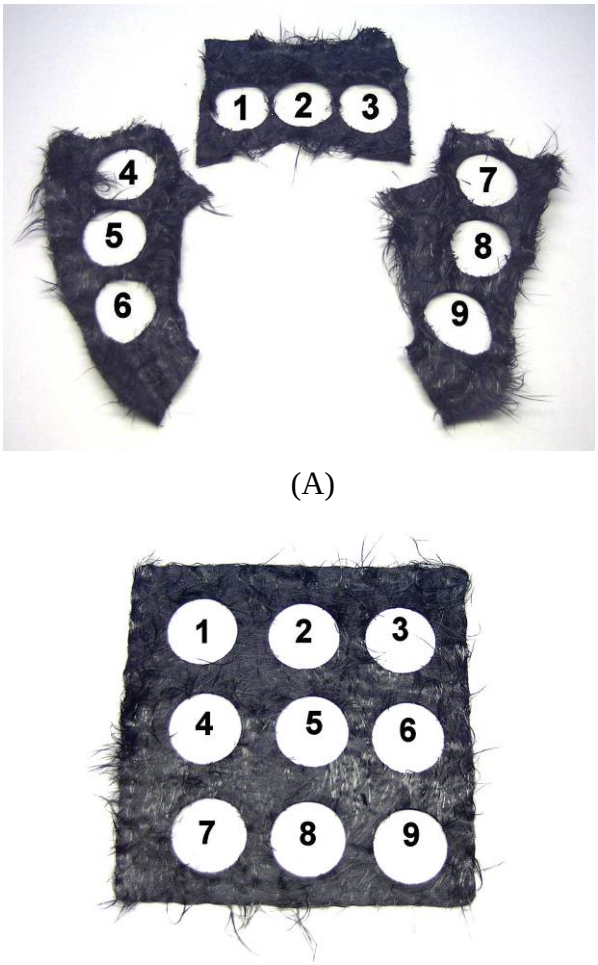

Figure 8. Basis-weight sampling using a 3-inch diameter punch was conducted on a flattened Corvette preform (A) and a flat preform (B).

The design goal is to minimize the number of tools required in the preform drying operation to support a three-minute production cycle.

Task 5 - Fiber and Suspension Issues

All of our work to date has been conducted using ¼-, ½-, and 1-inch polyacrylonitrile (PAN)-derived carbon fibers with cotton linter or acrylic fiber as the binder fiber. We are starting to look at a variety of additional binder fibers to help increase dry strength.

Figure 9 shows three flat-plaques that were made using ¼, ½ and 1 inch fibers. Clearly, the ¼-inch fiber creates the most loft and the1-inch fiber creates the least. It is believed that similar changes in loft can be affected by the proper selection of binder fiber.

Task 6 - Properties of Molded Flat Plaques

We have collected some preliminary physical property data for flat plaques, Table 2. The plaques were molded at MFG using 1-inch carbon-fiber flat preforms and an unfilled production polyester resin. The strength and stiffness were reasonable given the low fiber content of the plaques (17 vol %).

Task 7 - Reclaimed Carbon-Fiber Processing

The following task is not a part of the DOE SBIR Phase II project. It is included because of the wide interest in how one might use reclaimed carbon fiber.

There is a strong interest in the reclamation of carbon fibers from retired aircraft and other carbon fiber-intensive products. In the reclamation process, used composite materials are roughly chopped and processed to free the fibers from the epoxy matrix using thermal or chemical processes. After the fibers have been freed from the matrix, the resulting product has been shown to have individual fiber properties very close to those of the virgin material.

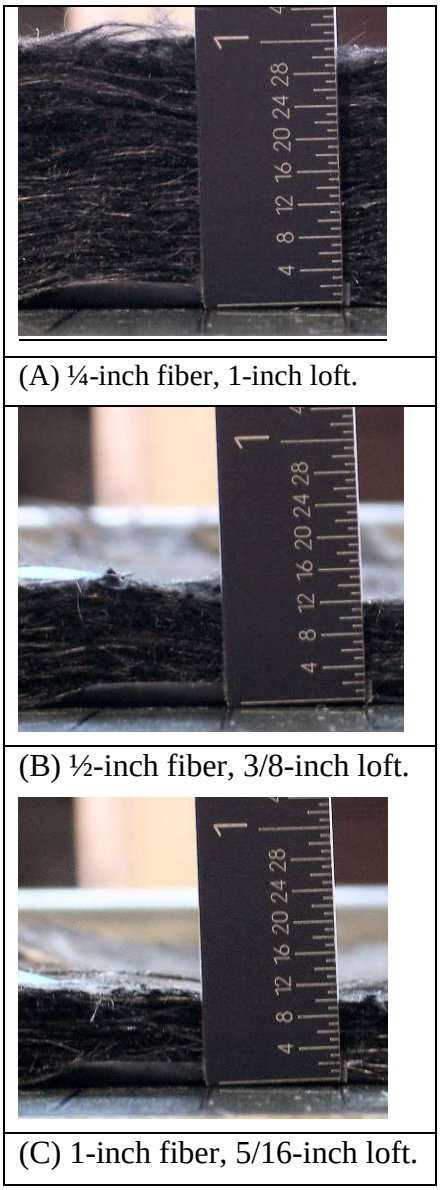

(A) ¼-inch fiber, 1-inch loft.

(B) ½-inch fiber, 3/8-inch loft.

(C) 1-inch fiber, 5/16-inch loft.

Figure 9. Preform loft decreased as fiber length was increased from ¼-inch to 1 inch. Side view of dry preforms.

Table 2. Mechanical properties of flat test panel fabricated at MFG, 17 vol % fiber, polyester resin.

Property	ASTM Method	N	Mean	Unit	COV (%)
Tensile Strength	**D-638**	**6**	**156 23**	**MPa kpsi**	**12.8**
Tensile Modulus	**D-638**	**6**	**16.8 2.4**	**GPa Mpsi**	**9.1**
Flexural Strength	**D-790**	**6**	**264 38**	**MPa kpsi**	**9.1**
Flexural Modulus	**D-790**	**6**	**13.3 1.9**	**GPa Mpsi**	**14.7**
Un-notched Izod	**D-4812**	**6**	**370**	**J/m**	**24.3**
Density	**D-792**	**5**	**1.29**	**g/cm3**	**1.6**
Water Absorption	**D-570**	**5**	**0.72**	**wt %**	**8.3**

The reclaimed carbon fibers were supplied to MIT-LLC by Boeing Corp. The material was taken from an F-18 stabilator. The composite material had been roughly chopped before the fiber-reclaiming process was applied. It contained a large quantity of impurities (metal particles, wire, support structures, aluminum honeycomb materials). The carbon fiber was variable in type, length and configuration. Unidirectional fiber, woven carbon fabric, and lose carbon fibers were present. The fibers ranged in length from <1" to >4." After inspection of the pyrolyzed fiber, it was determined that it needed to be thoroughly cleaned prior to use in the 3-DEP process.

The cleaned and length-reduced fibers were used in the 3-DEP process to evaluate the potential of the process to manufacture useful preforms. In the process, standard machine settings and fiber loading rates were used. No issues were found in dispersing the fibers in the system on in generating a uniform suspension. Six flat-panel preforms and six Corvette wheelhouse fiber preforms were manufactured from the reclaimed fibers; panels were also formed from virgin fiber. Figures 10a and 10b show Corvette wheelhouse preforms manufactured from recycled and virgin chopped carbon fibers. The shorter average fiber length in the reclaimed fiber accounts for the smaller amount of "fuzz" around the edges of the reclaimed preform (cf., Figures 3 and 4) as compared with the virgin fiber preform.

Figure 10a. Corvette preform from reclaimed carbon fiber.

Figure 10b. Corvette preform from virgin carbon fiber.

The Corvette wheelhouse parts were successfully molded with polyester resin at MFG. To make a composite part, the top and bottom of a preform were coated with unfilled polyester resin. The part was then placed on the bottom tool, the mold was closed, and the part was densified and cured. No issues were encountered in molding parts by this method. The preforms showed excellent resin penetration during molding and the product showed excellent stiffness after molding.

Summary and Conclusions

The key to the 3-DEP process is the ability to handle chopped-fiber reinforcements in a high-volume, cost-effective process while enhancing the quality and the functionality of the component. Typical forming times are 1 to 2 minutes. Neither the time required to make a preform, nor the

uniformity of fiber distribution with a preform, are sensitive to the geometric complexity of a part.

This has significant implications for making composite parts for automotive applications since those parts often contain deep draws, narrow channels, combined vertical and horizontal surfaces, sharp corners and edges, etc. Uniformity of parts is high; COVs of part-to-part weight and weight distribution a part are ~3%. Preforms are truly net-shape with almost no scrap.

The 3-DEP process brings to materials forming an exciting, innovative way to make composites. 3-DEP has the potential to radically change the way preforms and the composites made from them of are fabricated and used.

Presentations/Publications/Patents

1. Mark A. Janney, "Forming Natural Fiber Composites by the 3-DEP Process: An Initial Study," presented at the Automotive Composites Consortium Annual Meeting, September 25, 2007, Dearborn, MI.
2. M. Janney, E. Geiger, Jr., and N. Baitcher, "Fabrication of Chopped Fiber Preforms by the 3-DEP Process," Proceedings of COMPOSITES & POLYCON 2007, ACMA, October 17-19, 2007, Tampa, FL.
3. Mark A. Janney and David P. Haack, "Fabrication of Net-Shape, Chopped Fiber Preforms by the 3-DEP Process," presented at Carbon Fiber 2007, December 5-7, 2007, Washington, D.C. Online at http://www.emergingmit.com/Presentations.html.

E. High-Volume Processing of Composites (ACC 115[i])

Principal Investigator: Gerard Olszewski
Chrysler LLC, Materials Engineering
CIMS 429-50-00, 2301 Featherstone Road, Auburn Hills, MI 48326
(248) 512-8531; fax (248) 512-7915; e-mail: go5@chrysler.com

Technology Area Development Manager: Joseph A. Carpenter
(202) 586-1022; fax: (202) 586-1600; e-mail: joseph.carpenter@ee.doe.gov

Field Project Officer: Aaron D. Yocum
(304) 285-4852; fax: (304) 285-4403; e-mail: aaron.yocum@netl.doe.gov

Expert Technical Monitor: Philip S. Sklad
(865) 574-5069; fax: (865) 576-4963; e-mail: skladps@ornl.gov

---

Contractor: United Sates Automotive Materials Partnership (USAMP)
Contract No.: DE-FC-59OR22545 through the DOE National Energy Technology Laboratory

---

Objective

- Develop and demonstrate high-volume manufacturing (molding) processes to produce lightweight composite automotive components.
- Expand the scope of the Automotive Composites Consortium (ACC) composite projects into the thermoplastic and natural-fiber areas.
- Develop, build, and demonstrate an economical, lab-scale, automated fiber-retting process and apparatus suitable to bast-based fibers including hemp, kenaf, and flax.
- Develop, build, and demonstrate a lab-scale, natural-fiber preform and compression-molding process, and produce panels to develop a mechanical and thermal natural-fiber polymer-composite database.

Approach

- Develop and study high-volume composite manufacturing processes within approved research programs.
- Work with a Tier 1 automotive composites supplier to investigate and develop an improved carbon-fiber sheet molding compound (SMC) material amenable to cost-effective, high-volume applications.
- Acquire tooling necessary for the support of the ACC 115 research programs.
- Continue development of a tool to quantify the severity of bondline read-through (BLRT).
- Conduct several lab-scale process trials of fiber preparation-retting processes enabling the development of the most appropriate process and instrumentation.
- Develop, design and construct a lab-scale, non-aqueous, fiber-preform manufacture apparatus.
- Conduct full mechanical, thermal, and environmental characterization of natural-fiber-reinforced panels.

Accomplishments

- Provided process support for Automotive Composites Consortium Focal Project 4 (ACC 007, see 8.A).
- Proposed upgrading an existing SMC compounder at a Tier 1 supplier, Continental Structural Plastics (CSP), to acquire carbon-fiber capability. Secured DOE and ACC funding to accomplish that. Purchase orders are being issued.

- Injection-molding and compression-molding plaque tools completed and starting work on thermoplastic and thermoset characterization database and supporting Development of Manufacturing Methods for Fiber Preforms (ACC 040, see 8.B) and ACC 007 investigations.
- Continued work on BLRT by the molding, bonding, and analysis of plaques to develop base-line measurement of bondline read-through.
- Initiated efforts with Pacific Northwest National Laboratory (PNNL, viz., James Holbery, Kevin Simmons, Dan Howe) for retting, preforming, and manufacture of natural-fiber-reinforced composites (See 8.F).

Future Direction

- High-volume processing of lightweight structural thermoplastic composites.
- Oak Ridge National Laboratory (ORNL will continue researching optimization of the Direct Reinforced Fabrication Technology (DRIFT®) material-processing envelope.
- Carbon-fiber SMC materials for structural automotive applications:
- Continue working with fiber and resin suppliers through the Tier 1 supplier (CSP) to develop a superior material with improved manufacturability within cost and supply constraints.
- Demonstrate material on potential applications.
- Natural-fiber reinforcements and soy-based polymers:
- Optimize fiber surface treatments and polymer systems to minimize the moisture absorption of natural-fiber composite systems.
- Characterization results will be used to refine testing methods for determining durability properties of natural fiber composite systems.
- Provide process support to ACC 007.
- Utilize the injection- and compression-molding plaque tools to manufacture composite plaques for material characterization and development of a thermoplastic reference database.

Introduction

The purpose of this project is to develop the high-volume, composite-molding technologies germane to automotive production. The direction of the project ACC 115 is to collaborate with suppliers to develop low-cost, high-volume molding processes compatible with the material- property and processing requirements of the automotive industry.

Five processing investigations are under way: 1.) DRIFT®, a patented pultrusion process, is being studied for its ability to support the project objectives and its compatibility. This work is being conducted at ORNL; 2) BLRT, continued with studies of plaques molded with specific bond-area variations to assess the ability of the ONDULO system to identify and quantify the surface distortions; 3) A program has been initiated to upgrade an existing SMC compounder at a Tier 1 supplier to produce carbon-fiber-SMC compounding capability; 4) The creation and use of specialized tools for both injection and compression molding, highly instrumented and capable of producing test specimens of advanced composites; and, finally, 5) To develop a critical capability in the area of natural-fiber retting, preform and composite manufacture to enable the large-scale insertion of natural-fiber reinforcement into the automotive industry.

DRIFT®

As part of the current focus on thermoplastics, ORNL has been working with PolyComp (inventor of DRIFT®) and Fiberform (a key licensee) to evaluate possibility of chopping the DRIFT® product form in the ORNL preforming machine as one means of evaluating the DRIFT® material in general. In fiscal year (FY) 2006, PolyComp made sample quantities of glass-impregnated polypropylene using a 2400 tex glass tow which had been processed into a ribbon about 0.2-inch wide and 0.035-in thick. As expected, the ribbon handled more like a solid strip of plastic than a pliable fibrous tow and did not cut as easily as a glass tow. In initial trials, ORNL was able to get some of the material through the chopper,

but with only very small amounts cut before beginning to break blades in the chopper.

PolyComp agreed to make some modified samples in FY 2007 in order to get a thinner ribbon using a smaller glass tow size at about 1150 tex, which is essentially the size of glass tow utilized in the current TWINTEX® product. The samples were actually made at a weight ratio of 65% glass to 35% polypropylene, which yields a product comparable to the 60/40 TWINTEX® ratio. PolyComp made two variations of these samples – one at about 5/16-inch width and the other at about 3/16-inch width. ORNL was able to cut both tow sizes, having more success with the 5/16-inch width (nominally about .008-inch thick) than the 3/16-inch width (at about .015-inch thick). Although there was not enough material for extensive trials, there was enough combined material to conduct several experiments to establish cutting parameters. The balance of the materials was used to spray-up and compact a small amount of material that was subsequently molded into a very thin section solely for demonstration purposes in a lab press.

Based on the success with the small amount of sample materials, ORNL subsequently procured 250 lbs of the DRIFT® materials in the 5/16-inch width to do more process development and material evaluation. (See 8.C) Initial work established a basic processing envelope, including both preforming and molding, adequate for being able to fabricate evaluation panels. A panel has been provided to the ACC Materials Group to begin assessing the properties of molded DRIFT® materials after preforming. Once initial property data are received in FY 2008, plans are to focus effort on developing more optimum processing techniques taking into account material forms and chopper configurations that might be economically feasible for implementation.

Bondline Read-Through

Phase 1

Development of a tool to quantify the severity of BLRT continued. In FY 2006, the Joining team manufactured seventy-two panels that exhibited varying levels of BLRT. Thirty-six panels from this set and twelve white-painted panels from a previous Ford study were imaged using the ONDULO technology this year.

The BLRT "signatures" seen in the ONDULO images demonstrated that the source of the variation seen in the jury visual assessment may simply have been a result of differing perceptions of the relative severity of the different "types" of read-through by different jurors. The team also found that severity rankings based on visual assessments of filtered ONDULO curvature maps are unreliable. Consequently, the team determined that panel severity must be judged via visual assessment of the panels.

Visuol Technologies generated numerous algorithm candidates to quantify the severity of the defects. A critical step in post-processing of the curvature data is the selection of the type and wavelength of the filter. Once the data are filtered, pixels with small curvature amplitude are removed from the curvature map. The remaining pixels are then aggregated into continuous "identified defects." Finally, defects with a small average curvature are deleted. The severity of each remaining defect is quantified by multiplying the square of the average amplitude times the size of the defect. The severity scores for all the defects on a panel are added to generate a final overall severity rating. This algorithm was found to correlate well to visual assessment of the panels.

Since the team is interested in understanding the relationship between adhesive geometry and BLRT severity, the team made two panels using drops of adhesive. When those panels were imaged, one curvature map clearly showed oval defects. Further refinement of the algorithm was required to achieve a set of parameters that are applicable to both continuous beads as well as drops. The team also manufactured and painted a set of twelve panels bonded with drops of adhesive. These panels were made using the same conditions as the painted panels made with continuous beads. Unfortunately, the BLRT visible on these panels was less severe than on the equivalent continuous bead panels, so these were not particularly useful in the algorithm development.

The ACC Joining Working Group purchased an ONDULO system for our use this year. Four members of the team have been trained to use the system. Learning to use the system has given the team a much better understanding of the potential sources of variation in the data. Two gage repeatability and reproducibility tools for the system will be completed in FY 2008. The first will evaluate the repeatability and reproducibility of the measurements when the system is not moved between measurements. The second will evaluate the repeatability and reproducibility of the measurements when the system is moved between measurements.

Phase 2

To conclusively determine what factors contribute to BLRT, the manufacturing process used to build prototype assemblies must eliminate as many sources of manufacturing noise as possible. Consequently, several pieces of equipment were built to mold the panels that will be used in this work and to facilitate the bonding operation. A compression-molding tool for molding inner panels was completed by JATCO Machine & Tool Co., Inc. in early FY 2007.

A matched metal bonding fixture, small bonding press, and small cooling fixture were built by R/PC Alliance. The bonding fixture and press will be used to control the stress created between the panels, the bondline thickness, and the panel heating conditions during bonding. The cooling fixture will be used to create a repeatable amount of warpage in the inner panels. The "outer panels" in these assemblies are flat plaques. Some of the outer panels in the first experiment will be steel panels, so the team obtained twenty-five 24"x24" sheets of electrogalvanized, bake-hardened 210 steel from Mittal Steel. These sheets were then e-coated by Ford Motor Company in preparation for bonding. The SMC outer panels will be molded using the existing ACC compression-molding plaque tool. Many other groups within the ACC also used this tool this year. Since the tool was not designed to produce Class "A" panels, the other groups used this tool first. It was then sent back to the tool shop to have the top surface brought up to a Class "A" finish. This has delayed completion of the first experiment until the first quarter of FY 2008.

Tooling

More trials were held at Husky in Novi, MI for the injection-molding tool. The intent of the trials was to see the effect of various gating scenarios on glass-reinforced polypropylene (PP) material. The material for this trial was a Ticona Celstran PP-GF40-03 which is a 40% long-glass-filled PP. The new gate configurations included an insert to shut off the edge gate for a truly balanced center fill. Parts were made at thicknesses of 3.0 mm and 5.0 mm. All previous tool problems that were fixed from the trial in Mexico were validated. During this trial, a liquid-crystal polymer was molded at the 2.0-mm thickness to see if the tool was indeed capable of making parts this thin. The parts were filled from the center gate only at a mold temperature of 190°F which is the maximum Husky will go with the rubber hoses on their machine. The parts were full shots and measurements were taken to confirm that 2.0 mm is possible.

Further improvements/refinements to the tool ancillaries are necessary. These include a trim fixture for edge de-gating, a set of tools for thickness changes and parts measurement and a tool case to ship everything in. As part of this, a data acquisition system (DAS) is currently being specified. This will include everything to take data from the tool sensors and thermocouples and from the injection-molding machine. This DAS will coordinate all molding data in a manner that aligns to Materials Property Database for direct insertion.

Once everything is purchased, fixed and proven-out, a trial will be run for PNNL with long-fiber materials for the long-fiber prediction-modeling project (See 8.J).

The compression tool was also used at various molding trials at Polywheels, Bayer Material Science and Meridian. Polywheels molded both SMC and nylon 6. The nylon was processed with glass on their direct long fiber thermoplastic (DLFT) line. Various reinforcement mats, both glass and thermoplastic, were compounded/ molded with these materials in different configurations/lay-ups. Bayer molded plaques using the Kraus-Maffei Long Fiber Injection - Polyurethane (LFI-PUR) system along with the Hennecke Composite Spray Molding (CSM)

system. The plaques were glass-mat reinforced with Bayer Baydur 426 polyurethane.

Meridian molded class "A" panels for the BLRT experiments for the Joining Group.

Carbon-Fiber SMC

The objectives of this work are to develop high-performance, cost-effective, carbon-fiber-SMC materials and associated processing techniques for high-volume automotive components. The technical emphasis is to optimize properties, improve consistency of the properties, and to optimize the manufacturability of the compound. The project assumptions are that the material could be used for all current structural and Class-A SMC applications, that the current SMC compounding, molding processes and equipment can be utilized, and that the thickness of the new materials will be in the range of 1.0 to 3.0 mm. In addition to the technical issues and constraints, business challenges have been addressed by working with CSP to leverage their production knowledge of what it takes to develop a marketable system. Zoltek, a low-cost carbon-fiber manufacturer, has agreed to work with CSP, supplying appropriate carbon fibers and developmental sizing systems suitable for automotive resin systems.

Upgrading the CSP SMC compounder to provide carbon-fiber-compounding capability was proposed, justified, and approved. DOE and ACC funding was secured to initiate the effort and the purchase orders are being generated.

Conclusions

ACC 115 explores different approaches to the high-volume processing of composites. Five processing programs are in progress, each with the objective of researching ways to save weight in automobiles, at the volumes unique to the industry. Carbon-fiber-SMC research is progressing slowly against constraints of cost and supply. DRIFT® work continues; basic characterization is in progress and applications will be considered. Acquisition of new equipment specifically owned by ACC will speed research by eliminating time needed to move tools between suppliers, and will also provide the benefit of reducing variation in the test results. The natural-fiber efforts, begun on July 1, 2007, are underway with the initial focus on developing a fiber-preparation/ mechanical retting process for industrial scale. At this time, PNNL has investigated several concepts and will be finalizing the design in the next quarter. In parallel, fiber-structure analysis and composite processing has begun, green fiber has been contracted to be planted and harvested for this project in Mississippi, and relationships have been developed with the following partners:

- Ashland Chemical
- AOC resins
- TimTek Inc.
- Material Innovation Technologies
- Kengro, Inc.
- Stemergy, Inc.
- Mississippi State University

[i] Denotes project 115 of the Automotive Composites Consortium (ACC), one of the formal consortia of the United States Council for Automotive Research (USCAR) set up by Chrysler, Ford and General Motors to conduct joint, pre-competitive research and development.

F. Natural-Fiber Composite Retting, Preform, Manufacture and Molding (RPM2)

Principal Investigators: James Holbery, Kevin Simmons, Dan Howe
Pacific Northwest National Laboratory (PNNL)
P.O. Box 999
Richland, Washington 99354
(509) 375-3686; fax: (509) 375-2379; e-mail: james.holbery@pnl.gov

Technology Area Development Manager: Joseph A. Carpenter
(202) 586-1022; fax: (202) 586-1600; e-mail: joseph.carpenter@ee.doe.gov

Contractor: PNNL
Contract No.: Prime Contract No. DE-AC06-76RLO 1830

Objective:

- To develop, build, and demonstrate an economical, lab-scale, automated fiber retting process and apparatus suitable to bast-based fibers including hemp, kenaf, and flax;
- To develop and demonstrate a thermoset polymer preform compression molding process and produce panels to develop a mechanical and thermal natural-fiber polymer-composite database.

Approach:

- Explore existing and new fiber-preparation approaches including decordication techniques, high-speed fiber separation, steam explosion, chemical treatment, and modified extrusion methods.
- Develop the fundamental understanding of bast-fiber structure that will provide direction for fiber separation.
- Conduct several lab-scale process trials of fiber preparation-retting processes enabling the development of the most appropriate process and instrumentation.
- Develop a non-aqueous natural-fiber preforming process capable of integrating surface modification and hybrid fiber, preform geometries.
- Design and construct a lab-scale, non-aqueous, fiber preform manufacturing apparatus.
- Explore alternative material forms including, sheet-molding compounds (SMCs) from natural-fiber and hybrid reinforcements.
- Conduct full mechanical, thermal, and environmental characterization of manufactured panels.

Accomplishments:

- Conducted fiber structural tests on kenaf and hemp samples.
- Explored chemical methods to break down pectin bonding – work currently underway.
- Conducted preliminary fiber surface analysis.
- Conducted fiber calandering on kenaf fibers; subsequently molded panels of clean fiber.
- Established relationships with U.S. kenaf farm, Kengro Inc.; planted, harvested, and delivered one ton of green kenaf.
- Investigated several forms of decordication-fiber preparation including previously-developed systems derived from the wood products and cotton industries.

- Developed three designs that integrate existing processes – now exploring small-scale decordication and fiber-preparation tests to determine validity of the methods.
- Initiated research to develop a fundamental understanding of bast-fiber structure that will provide direction for fiber separation.
- Developed relationships with resin suppliers including AOC, Reichold, and Ashland Chemical; with processing companies including Material Innovat ion Technologies, TimTek, Inc., and Canadian hemp supplier, Stemergy.

Future Direction:

- To build a small-scale bast-fiber processing cell to conduct accelerated fiber separation techniques.
- Explore further environmentally-friendly fiber-retting technologies.
- Integrate fiber-decordication, fiber-separation, and fiber-preparation-retting techniques into a lab-scale fiber-preparation unit.
- Deliver process and lab-scale unit to our customer in FY 2008.
- Explore non-aqueous, natural-fiber preforming processes capable of scaling to industrial volumes.
- Develop natural-fiber SMC and hybrid-fiber architectures; produce panels and characterize in mechanical, thermal, and environmental tests.

Introduction

The objective of this project is to develop a critical capability in the area of natural-fiber retting, preform manufacture, and composite manufacture to enable the large-scale insertion of natural-fiber reinforcement into the automotive industry. The benefits of natural-fiber-reinforced composites are well known, including lightweight, energy savings, cost reduction, carbon capture, recycling, and the environmental benefits from using renewable resources. However, several technical milestones must be met before the full confidence of the engineering, manufacturing, and commercial sectors will embrace natural-fiber reinforcement as a viable replacement for glass fiber. In the proposed research and development effort, three critical barriers restricting natural-fiber usage in automotive manufacture are addressed: (1) to develop an inexpensive, rapid, and environmentally-friendly mechanical process to remove natural fibers from plant stalks; (2) to develop a rapid, cost-effective method to create natural-fiber preforms suitable for infusion of a thermoset polymer matrix; and (3) to develop a natural-fiber polymer-composite molding process adaptable to hybrid fiber composites and ester, soy, and urethane resin.

(A parallel, complementary effort is covered in Report 8.G.)

Natural fibers can be harvested annually, or for kenaf, jute, and hemp, may be planted and harvested two to three times annually. Kenaf, cultivated in the U.S. for a variety of uses, including oil-spill absorbent, can grow to a height of four meters in four months, and can yield two or three harvests a year. Jute, grown in China, India, and Bangladesh, can be grown in four to six months. Agronomically, jute and kenaf have advantages because of their resistance to climatic extremes, pests, and diseases.

Once bast fiber is harvested, it must go through a process to separate the fiber from the woody stem by removing the non-fibrous cementing materials that hold the fibers together, without damaging the fiber cellulose. It is advantageous to use retted fibers in polymer-composite applications, as it has been shown that unretted fiber tissue may change, or degrade, over a time scale of months or years after it has been embedded in a polymer resin, seriously affecting the useful life of the composite.

Essentially, retting is a process to moisten or soak the fiber to soften and separate the fibers by partial rotting and can take up to two weeks or longer. The following retting processes are the most

prominent in use today, and each has certain advantages and disadvantages:

- Dew retting occurs when the stalks are left in the field so that rain, dew, or irrigation is used to keep the stems moist. This may take up to 6 weeks and produces a coarse fiber with a light brown color.

- Water retting occurs when stems are bundled and then submerged in water so that bacteria break down pectin. This takes 7-10 days and produces a quality fiber.

- Warm-water retting occurs when bundles are soaked for 24 hours after which the water is replaced. Heat is then applied to warm the batch for the next two or three days. This results in a uniform, clean fiber.

- Chemical retting occurs when chemicals (usually alkali solutions) are used to dissolve the pectin, allowing the components to be separated from the decorticated stalk. This shortens the time to as little as 48 hours, though it affects several fiber properties including a loss in tenacity, color, and luster, as compared to the bacterially-retted fibers.

Once retted fiber has been produced, the fibers can be modified by a variety of physical and chemical methods, to correct fiber deficiencies; fibers can be treated to promote bonding and adhesion, dimensional stability, and thermoplasticity. Surface modification of natural fibers can be employed to optimize properties of the fiber-matrix interface and integrated within the fiber preform manufacturing process, to produce a preform that may be stored for long periods of time before composite manufacture without a loss of properties, or more importantly, excessive moisture uptake with compromised composite interfacial properties.

When considering natural fibers as engineering materials, several factors must be considered, particularly, their hygroscopic nature. Physical and chemical methods have been used to optimize the interfacial characteristics and improve the properties of natural-fiber polymer composites, although high moisture absorption and low microbial resistance are disadvantages, compounded by the fact that their hydrophilic behavior adversely affects the properties of the fibers and their composites. One outcome is that lignocellulosic-based fibers change dimensions with changing moisture content because the cell-wall polymers contain hydroxyl and other oxygen-containing groups that attract moisture through hydrogen bonding. High water and moisture absorption of the fiber causes swelling and a plasticizing effect, resulting in dimensional instability and poor mechanical properties.

A primary consideration in bonding cellulose-based fibers to a surface polymer is the moisture present in the fiber during the reaction. It is costly to dry natural fibers to less than 2-3 percent moisture, but the -OH group in water is more reactive than the -OH group available in the lignocellulosic components, rendering hydrolysis faster than substitution. The most favorable condition for surface reaction is one that requires a trace of moisture and the rate of hydrolysis that is relatively slow. Three factors determine the rate at which moisture is removed from lignocellulosic materials: temperature, relative humidity, and air velocity. The ability to control and minimize energy input during this process is one opportunity foreseen within processing natural-fiber materials. The ability to eliminate water absorption during service of natural-fiber-based composite components is an enabling technology within automotive natural-fiber-reinforced hardware development; this is particularly true where a Class A finish is required.

Fiber Preparation - Retting

PNNL began this effort by contacting Kengro, Inc. in Charleston, MS to contract 0.5 acres (approximately 1500 lbs.) of kenaf to be grown and cut green, to be used in developing the fiber-preparation process. Fiber was planted in mid-July, and cut on November 7, 2007. PNNL personnel traveled to MS in July, 2007, to meet with Kengro, the USDA-ARS cotton research facility in Stoneville, MS, and Mississippi State University (MSST). In addition, to begin the research effort the following fibers were procured for research purposes: (1) fresh-water-retted kenaf from Bangladesh; (2) un-retted fiber from Kafus, Inc., Raymondville, TX; (3) industrial hemp from Stemergy, Ontario, Canada; and (4) chemically-

modified kenaf from Prof. Brian Baldwin, Agriculture Department, MSST.

PNNL personnel have thus far investigated the following processing approaches:

- Decordication (removal of kenaf core) using parallel rollers, both at MSST (Prof. Dan Seale's laboratory with a patented process from TimTek Corporation) and at PNNL with parallel rolling device. Progress has been made; we have just received fiber and are working on techniques to rapidly achieve decordication.

- Chemical retting: PNNL has developed a process to achieve kenaf chemical retting. This includes using a combination of sodium hydroxide and hydrochloric acid treatments; we are now attempting to develop a continuous flow process that utilizes near 100% of the constituents.

- Water retting: PNNL is exploring a combination warm water-steam retting approach, which shows promise.

- PNNL has produced a lab-scale carding roller to align bast fiber for preform or SMC manufacture. The simple design allows fiber to be processed in very small quantities, removing the fiber fines and unwanted core from the fiber (Figure 1).

Figure 1. Manually-operated fiber carding device (top), fiber fines and unwanted remnants removed from the process (bottom).

Bast-Fiber Structure

The structure of several bast fibers has been explored to determine the composition and to assist future process development. This is important because process changes affect fiber structure, which in turn affects fiber behavior, and most importantly for this effort, the separation of fiber from core, and fiber-fiber interaction, enabling fiber separation for follow on steps (i.e., preform manufacture).

Three techniques have been undertaken: fiber structure analysis, using TAPPI (previously "the Technical Association of the Pulp and Paper Industry, now just "TAPPI") specification 222 and others, to determine cellulose, hemi-cellulose, lignin, and extractive content, Fourier transform infrared (FTIR) analysis and x-ray photoelectron spectroscopy (XPS) analysis. Fiber structure analysis results for two trial runs each of MS kenaf (Kengro, Inc.), hemp (Stemergy, Ontario, Canada), TX kenaf (Raymondville, TX), and water-retted kenaf (Golden Tiger Fiber, Bangladesh) have been run. The cellulose and hemi-cellulose are still being analyzed. Results for the lignin content indicate that, surprisingly, water-retted kenaf contains the highest total (Table 1). This is a very curious result, as neither the MS nor TX kenaf had been processed.

The results of the extractive, ash, and lignin content (cellulose and hemi-cellulose will be completed as soon as the high-performance liquid chromatograph (HPLC) at PNNL is operational – within two weeks) indicate distinct differences in the fiber structures.

Table 1. Results of two samples each of lignin content from MS kenaf (Kengro, Inc.), hemp (Stemergy, Ontario, Canada), TX kenaf (Raymondville, TX), and water-retted kenaf (Golden Tiger Fiber, Bangladesh).

Type	Dry Wt. Total 1	Dry Wt. Total 2	Avg. Dry Wt.	Sample (ex free, dry basis)	%lignin
MS Kenaf	34.4852	34.4857	34.4855	0.1882	6.88%
MS Kenaf	35.7119	35.7104	35.7112	0.1896	8.62%
Hemp	35.8981	35.8995	35.8988	0.1939	7.68%
Hemp	34.4496	34.4534	34.4515	0.1904	8.56%
TX Kenaf	35.8253	35.8219	35.8236	0.1903	9.51%
TX Kenaf	35.7241	35.7235	35.7238	0.1899	7.21%
Water Ret Kenaf	37.7416	37.7407	37.7412	0.1893	13.39%
Water Ret Kenaf	34.1437	34.1445	34.1441	0.1904	11.40%

Table 2 shows the averaged data of two samples each that have been tested and characterized. Note that the water-retted fiber has no extractives; this is a critical finding, as the extractives can cause long-term degradation to fiber-polymer interfacial bonding. Also, note the lignin content of the water-retted fiber; this can be important for many reasons, including extraction for process fuel, which can be of economic benefit. Ash content, usually due to the quality of the soil, is highest in Texas kenaf, which could be due to a high mineral content.

Table 2. Results of extractive, ash, and lignin content of MS kenaf (Kengro, Inc.), hemp (Stemergy, Ontario, Canada), TX kenaf (Raymondville, TX), and water-retted kenaf (Golden Tiger Fiber, Bangladesh). Note cellulose and hemi-cellulose data still under analysis.

Type	Avg. % Extractive	Avg. % Ash	Avg. % Lignin	Total
MS Kenaf	0.1467%	1.39%	7.75%	9.2883%
Ontario Hemp	0.5921%	2.42%	8.12%	11.1387%
TX Kenaf	0.2716%	4.35%	8.36%	12.9874%
Water Ret Kenaf	0	1.24%	12.39%	13.6327%

XPS has been conducted on several samples to obtain binding energies of different fiber structures. Figure 2 provides a comparison of hemp, chemically-retted kenaf, unretted kenaf, and water-retted kenaf.

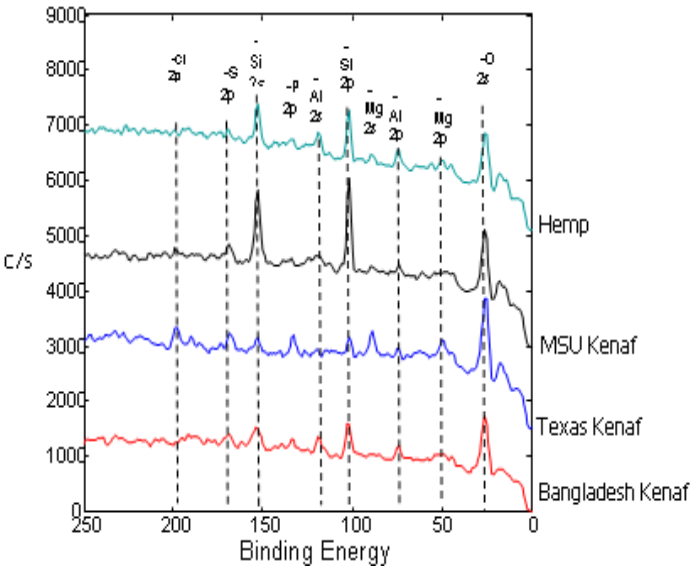

Figure 2. Wide-scan XPS spectra 0-1350 eV comparison of hemp (top), chemically-retted kenaf (second from top), Texas kenaf –unretted (second from bottom), and water-retted kenaf (bottom).

The plot in Figure 2 does not provide a great deal of information. Further analysis of 0-250 eV in Figure 3 indicates Si, Mg, Al, and P peaks that vary with fiber type. A full analysis of the XPS data is presented in Table 3 below.

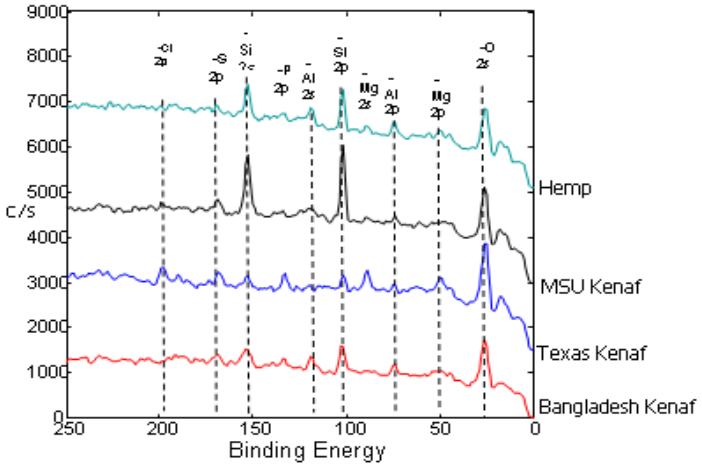

Figure 3. XPS spectra 0-250 eV comparison of hemp (top - Stemergy, Ontario, Canada), chemically-retted kenaf (second from top; - MS), kenaf –unretted (second from bottom – Raymondville, TX), and water-retted kenaf (bottom - Golden Tiger Fiber, Bangladesh). Note Si peaks in the hemp and chemically-retted fibers at 153 eV.

FTIR analysis has been initiated on the fibers, but at this time, the data are inconclusive. For example, Figure 4 illustrates plots of the fiber and their spectral differences. While distinct bond differences exist, particularly at wave numbers 1300-1800, PNNL is now using a software package to analyze the data further.

Scanning electron microscopy (SEM) has been employed to characterize the fiber surface of several fibers.

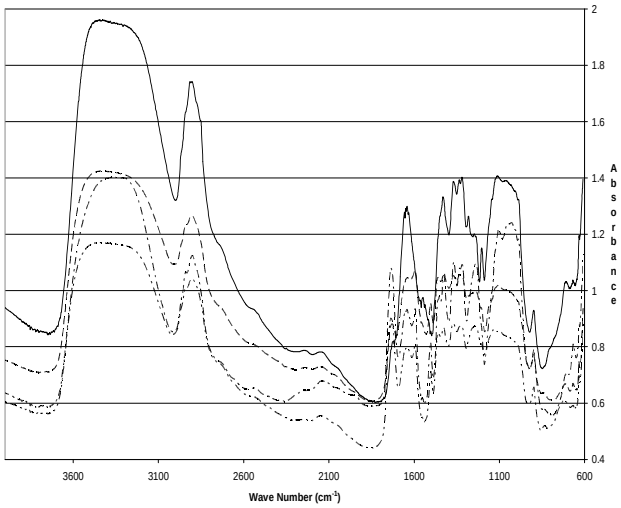

Figure 4. FTIR plot of fiber surfaces. Straight line is hemp, long-short-short long is chemically-treated MS kenaf, long-long is Texas kenaf, and long-short-long is water-retted kenaf from Golden Tiger, Bangladesh.

Table 3. Atomic concentrations from the wide-scan XPS spectra. This provides a baseline understanding for further process development and fiber modification.

File name	Sample description	C1s	N1s	O1s	Mg1s	Al2p	Si2p	P2p	S2p	Cl2p	Ca2p
09190701.spe	59755-4-B1 XPS fibers	67.7	2.3	28.4	0.0	0.3	0.6	0.1	0.1	0.0	0.5
09190705.spe	59755-4-B1 XPS fibers	67.5	2.8	28.0	0.2	0.2	0.6	0.1	0.1	0.0	0.5
Average of both data sets	**Kenaf – Golden Tiger, Bangledesh Enzyme Field Retted**	67.6	2.6	28.2	0.1	0.3	0.6	0.1	0.1	0.0	0.5
09190702.spe	59755-4-B2 XPS fibers	67.7	3.4	27.0	0.3	0.2	0.3	0.1	0.1	0.1	0.9
09190706.spe	59755-4-B2 XPS fibers	68.5	2.9	27.1	0.2	0.0	0.2	0.1	0.1	0.1	0.8
Average of both data sets	**Kenaf – Kafus, Raymondville, TX**	68.1	3.1	27.0	0.2	0.1	0.2	0.1	0.1	0.1	0.9
09190703.spe	59755-4-B3 XPS fibers	75.9	1.0	21.4	0.0	0.1	1.2	0.0	0.1	0.0	0.3
09190707.spe	59755-4-B3 XPS fibers	83.9	0.8	13.5	0.0	0.1	1.2	0.0	0.1	0.0	0.3
Average of both data sets	**Kenaf – MS \ Chemically Retted**	79.9	0.9	17.4	0.0	0.1	**1.2**	0.0	0.1	0.0	0.3
09190704.spe	59755-4-B4 XPS fibers	73.9	2.1	22.4	0.1	0.3	0.8	0.1	0.1	0.0	0.4
09190708.spe	59755-4-B4 XPS fibers	72.7	2.1	24.0	0.1	0.2	0.5	0.1	0.0	0.0	0.4
Average of both data sets	**Hemp-Stemergy, Ontario, Canada**	73.3	2.1	23.2	0.1	0.2	**0.6**	0.1	0.0	0.0	0.4

The images at 10,000x are not all that different, as shown in Figure 5.

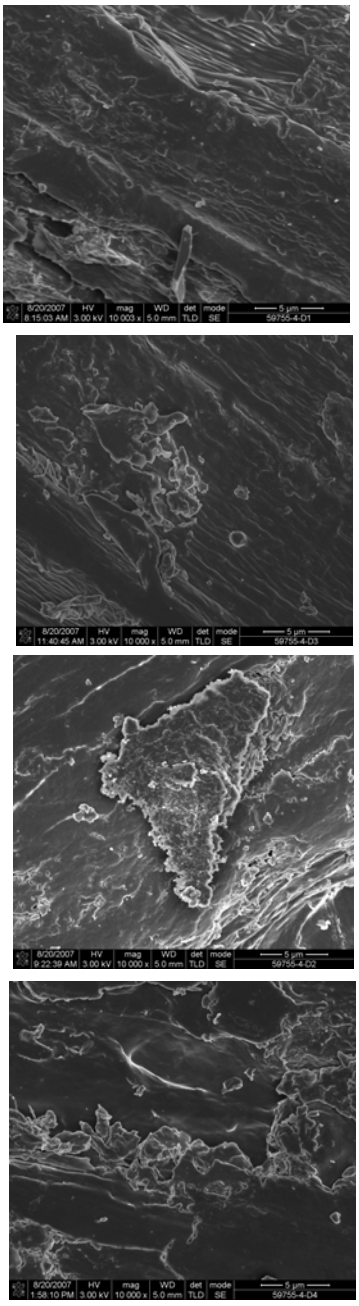

Figure 5. SEM image (10,000x) of fiber surface of fiber surface of water-retted fiber (top - Golden Tiger, Bangladesh), unretted fiber (2nd - Texas kenaf), chemically-retted fiber (3d - MS kenaf), and hemp (4th - Stemergy, Ontario Canada).

However, at 25,000x, distinct differences appear, particularly the surface of the chemically-retted fiber (Figure 6).

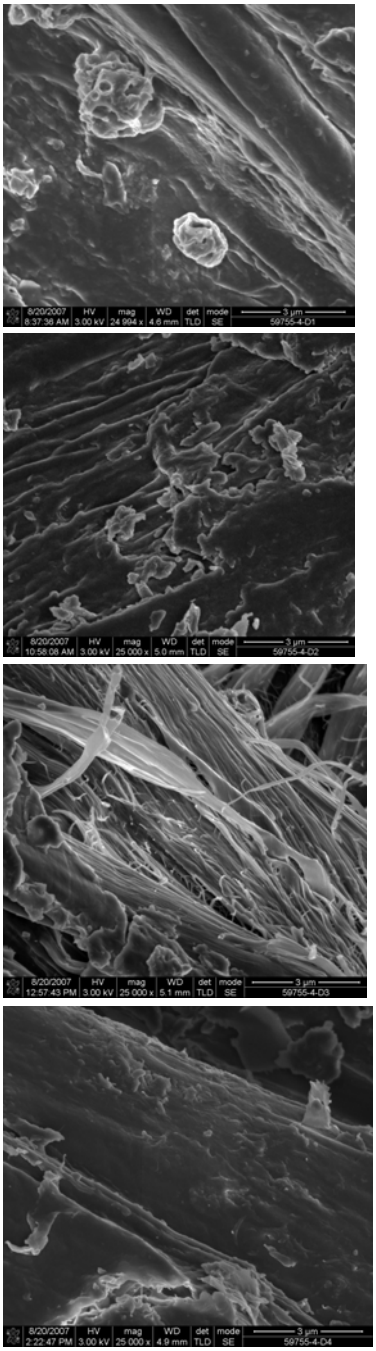

Figure 6. SEM image (25,000x) of fiber surface of fiber surface of water-retted fiber (top - Golden Tiger, Bangladesh), unretted fiber (2nd - Texas kenaf), chemically-retted fiber (3rd - MS kenaf), and hemp (4th - Stemergy, Ontario Canada).

Preform Processing

The goal of this task is to develop a preforming process to produce natural-fiber-reinforced preforms of a variety of geometries without an

aqueous solution. This task will begin in the second year of the project and has not been undertaken.

Composite Manufacture & Characterization

This task has begun, as it is believed that the program must produce and test full-scale test coupons, as the program progresses, to determine the effectiveness of the fiber-preparation processes. Using the carding machine described previously, PNNL has molded several panels from kenaf preforms (Figure 7).

Figure 7. Preform prior to molding with polyester resin, preform in the press (middle) and after molding (bottom).

As we begin to produce fibers emanating from the processes we are developing, full characterization will take place using PNNL personnel and outside vendors, as necessary. We will focus on mechanical, thermal, and environmental properties. These tests are outlined in the following paragraphs. A schedule is not presented at this time. While this task is to be the focus of year 3 of the project, it will be ongoing with full completion and focus in year 3.

Mechanical Properties

Tensile properties will be tested per American Society for Testing and Materials (ASTM) D 3039, and flexural properties per ASTM D 790. Compression testing will be conducted on composites per ASTM D 695. In addition, short-beam shear will be tested to determine the interlaminar bonding of the composite per ASTM D 2344.

Moisture Absorption

Treated and untreated samples will be characterized for moisture absorption per ASTM D 5229M. Samples first dried by heating will be weighed (W1) and then soaked in a bath of deionized water, at room temperature, for a prescribed time (W2). Water absorption (WA) will be determined by the following:

$$\mathrm{WA}(\%) = \left(\frac{W_2 - W_1}{W_1} \right) \bullet 100$$

Thickness swelling (TS) will be calculated on the fibers as follows:

$$TS(\%) = \frac{(t_c - t_o)}{t_o} \bullet 100$$

where t_c is the thickness of the sample after immersion and t_o is the thickness of the sample before immersion.

PNNL has constructed a special accelerated moisture-uptake system capable of infusing composites with moisture at 60°C and 85% relative humidity (RH) at pressures up to 10 bar. This has proven to be a successful process for accelerating long-term moisture-uptake testing on carbon epoxy composites; it may be utilized as needed in this program (Figure 8).

Figure 8. Picture of the PNNL accelerated composite moisture-uptake experimental set-up consisting of two pressure vessels, data logger, etc.

TGA/DSC Characterization

Thermogravimetric analyses (TGA) and differential scanning calorimetry (DSC) are useful methods to determine the glass transition, extent of cure, moisture uptake, and thermal stability of virgin fibers, treated fibers, and polymer fiber composites. Our intent will be to utilize TGA and DSC to measure the properties of the composites, and to probe the process parameters, to achieve an optimum process for both the polyester and virgin fibers.

DMA Testing

Dynamic mechanical analysis (DMA) will be utilized to measure the viscoelastic response of selected composites.

Conclusions

This program, begun on July 1, 2007, is underway with the initial focus on developing a fiber-preparation mechanical-retting process for industrial scale. At this time, PNNL has investigated several concepts and will be finalizing the design in the next quarter. In parallel, fiber-structure analysis and composite processing has begun, green fiber has been contracted to be planted and harvested for this project in Mississippi, and relationships have been developed with the following partners:

- Ashland Chemical
- AOC resins
- TimTek Inc.
- Material Innovation Technologies.
- Kengro, Inc.
- Stemergy, Inc.
- Mississippi State University

Presentations/Publications/Patents

1. Presentation to the Auto Composite Consortium, Sept. 26, 2007, Detroit MI.
2. Presentation to Mississippi State University, July 15, 2007, Starkville MS.

G. Natural-Fiber Composites for Structural Component Design

Jilei Zhang: Co-Principal Investigator
Associate Professor, FWRC – Forest Products
Franklin Center, Rm 113
Mississippi State University (MSST)
Mississippi State, MS 39762
(662) 325-9413; fax: 662-325-8126; email: jzhang@cfr.msstate.edu

Yibin Anna Xue: Co-Principal Investigator
Assistant Research Professor, Center for Advanced Vehicular Systems (CAVS)
MSST
Mississippi State, MS 39762-5405
(662) 325-5450; fax: (662) 325-5433; e-mail: axue@cavs.msstate.edu

R. Daniel Seale
College of Forest Resources
MSST
Mississippi State, MS 39762
662-325-3072; fax: 662-325-8126; email: dseale@cfr.msstate.edu

Sheldon Q. Shi, Co-Principal Investigator
Assistant Professor, FWRC – Forest Products
Franklin Center, Rm 222
MSST
Mississippi State, MS 39762
662-325-3110; fax: 662-325-8126; e-mail: sshi@cfr.msstate.edu

Thomas Lacy
316C Walker Engineering Building
P. O. Box A
Mississippi State, MS 39762
(662) 325-2754; e-mail: lacy@ae.msstate.edu

Steven Elder: Co-Principal Investigator
Associate Professor, Ag & Bio Engineering
Ag & Bio Engineering Bldg, Rm 214
MSST
Mississippi State, MS 39762
(662) 325-9107; e-mail: selder@abe.msstate.edu

L. Catherine Brinson
Department of Materials Science and Engineering
Northwestern University
2220 Campus Drive, Evanston, IL 60208-3108;
(847) 491-3537; fax: (847) 491-7820; e-mail: cbrinson@northwestern.edu

Ray Boeman
Oak Ridge National Laboratory (ORNL)
P.O. Box 2008, MS-6472
Oak Ridge, TN 37831-6472
(865) 946-1203; fax: (865) 946-1214; e-mail: boemanrg@ornl.gov

Cliff Eberle
ORNL
P.O. Box 2008,
Oak Ridge, TN 37831-6053
(865) 574-0302; fax: (865) 574-8257; e-mail: eberlecc@ornl.gov

C. David Warren
ORNL
P.O. Box 2008
Oak Ridge, TN 37831-6065
(865) 574-9693; fax: (865) 574-6098; e-mail: warrencd@ornl.gov

Technology Area Development Manager: Joseph A. Carpenter
(202) 586-1022; fax: (202) 586-1600; e-mail: joseph.carpenter@ee.doe.gov

Expert Technical Monitor: Philip S. Sklad
(865) 574-5069; fax: (865) 574-6098; e-mail: skladps@ornl.gov

---

Contractor: MSST
Contract No.: 4000054701

Objective

- Obtain material data of several biomaterials (e.g., kenaf) to study microstructural characteristics, fabrication methods (i.e., retting, formatting), and mechanical properties (i.e., polymer resin/fiber compatibility) for use in automotive structural design.

Approach

- For automotive exterior applications, natural-fiber-reinforced, polymer-based composites are developed according to the following steps: 1) evaluating current fiber-retting technologies and recommending solutions aimed at cost reduction of fiber-retting process; 2) evaluating two-dimensional (2D) fiber-mat format and other fiber-feeding systems with the aim of developing a natural-fiber format and formatting method for ready feeding into a sheet molding compound (SMC) line; 3) enhancing composite mechanical properties through dispersing nano-phase additives, improving interfacial bond strength, and developing mechanical models.

Accomplishments

Fabrication methods:

- A new chemical-retting technique was developed with the aim of improvement of fiber quality and cost reduction of the fiber-retting process.

Micro-structural characteristics and mechanical properties:

- An inorganic nano-particle impregnation technique was developed with the aim of reducing defects in the natural-fiber polymer-composite processing and enhancing mechanical properties through filling voids on fiber-cell-wall structures and surface modification.
- Tensile behaviors of different kenaf-bast-fiber forms (yarns, slivers and bundles) were measured. Effects of kenaf-fiber orientation on mechanical properties of kenaf-fiber/polymer composites and effects of weight fraction of kenaf fibers in the polypropylene (PP) matrix on thermal properties of the composite, and interaction between the fibers and PP matrix, were experimentally investigated and analyzed.

- A simple, rate-dependent model was proposed for kenaf fibers. Effects of moisture content, fiber volume fraction, and distribution pattern on the elastic modulus of woodfiber-reinforced composites were simulated and quantified using micromechanical approaches.

Future Direction

- Fabrication methods - Continue the current effort of evaluation of retting technologies with the aim of recommending a cost-effective retting process. Develop a natural-fiber format and formatting method for ready feeding to a SMC process.
- Mechanical properties and enhancement - Continue the research efforts to understand and improve interfacial bonding between natural fiber and polymer matrix and study processing and environmental variables (such as moisture and heat) effects on composite properties through conducting experimental and simulation work. Disperse nano-phase additives into traditional natural-fiber/polymer-based composites with the aim to improve material properties.

Statistical Evaluations of Tensile Properties of Kenaf Fibers and Composites

Team Members: Yibin Xue, Yicheng Du, Steve Elder, Devin Sham, Mark Horstemeyer, Jilei Zhang

Introduction

Plant-bast fibers such as kenaf, hemp, and flax have low density and high specific strength and are of utmost interest in applications striving for lightweight and high strength. Bast-fiber-reinforced, polymer-based composites have been developed successfully as of automotive interior panels. The quality of fibers, the formats of fibers and the interfacial bonding with polymer matrices are extremely important for advanced applications that require high strength such as automotive sub-structural exterior components.

Since the 1990s, various aspects related to kenaf-fiber production, fabrication, and composites have been investigated at MSST. These are cultural and biological factors, harvesting and processing, chemical and physical properties, woven and non-woven products, pulp and paper products, and composites [1]. Injection-molded, 40 wt% kenaf-fiber and PP composites were found to have comparable tensile moduli to the glass-fiber-reinforced PP (8.3 MPa vs. 9 MPa) [2]. Due to the lower density of kenaf fibers, the specific tensile modulus is greater than glass-fiber composites by a ratio of 7.8:7.3. To the writers' best knowledge, no systematic evaluations and fabrications have been conducted to explore advanced applications of kenaf-fiber-reinforced plastic composites in the US research community until now. Currently, we are seeking implementation of kenaf-fiber-reinforced plastic composites for automobile exterior components or semi-structural applications. *Understanding the fundamental mechanical properties of kenaf-fiber bundles, which is in a natural form of kenaf, as composites is necessary before they can be processed with plastics.* Kenaf-bast-fiber bundles (KBFBs) are composed of many semi-unidirectionally-aligned kenaf fibers of length from 1.6 to 5 mm and diameter range from 16 to 23 micrometers (μm) and are bonded with lignin and pectin [3]. In this report, the KBFB test samples were selected to be at least four times the maximum length of a single kenaf fiber. The tensile behaviors of KBFBs were evaluated at two loading rates. Kenaf-bundle-reinforced epoxy in sliver and yarn forms were also evaluated in a similar approach.

Experimental

Materials

Two forms of kenaf-fiber-related products were evaluated: KBFBs obtained directly from kenaf stems, as shown in Figure 1, and kenaf-bast-fiber, unidirectionally-reinforced epoxy strands (sliver and yarn), as shown in Figure 2. Both KBFB sliver and yarn are composed of 50 weight percent of KBFB and 50 weight percent epoxy, in which the strands were twisted with KBFBs along the fiber longitudinal direction. The yarns have a spiraling angle of 20° while slivers have a very small spiraling angle of 8°.

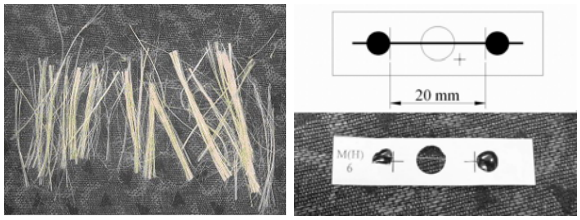

a) b)

Figure 1. KBFBs cut from the kenaf plant stem a) and the dimension of KBFB samples and test frame b).

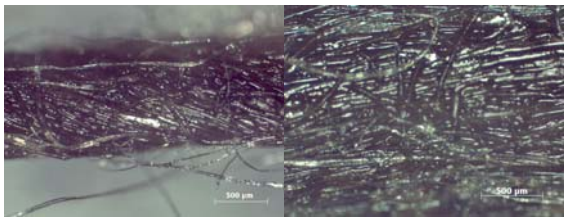

a) b)

Figure 2. Optical micrographs of KBFB-reinforced epoxy strands: a) yarns and b) slivers.

The cross-sectional area of the sliver was about six times larger than the cross-sectional area of the yarn. Both kenaf fibers and composite strands were conditioned in an environment with an ambient temperature of 23ºC and a relative humidity of 30-40% for over 48 hours prior to tests. The moisture content (MC) of the KBFB was around 8.5% based on this conditioning.

Test Setup and Sample Preparations

Uniaxial-tension properties of KBFB were evaluated according to ASTM Standard C 1557 – 03 for a standard test method for tensile strength and Young's modulus of fibers [4]. KBFBs were extracted from three locations along the full plant-size fiber bundles. Top and bottom KBFBs were taken from within 10 cm at both ends; middle KBFBs were from right at the middle of the kenaf stalk. KBFBs were cut to 30 mm in length with the top and bottom KBFBs having 30 replicates, respectively, and the middle KBFB having 45 replicates. Observed under an optical microscope, all short KBFB samples have no obvious defects. Figure 1 shows KBFBs as-cut and KBFBs mounted on a paper card as a frame for the grip and test assembly. Yarns and slivers were cut to 70 mm in length and their optical micrographs are shown in Figure 2.

The cross-section of the KBFBs was assumed to be elliptical in shape with the area of the cross-section, A, calculated using, $A = \pi ab/4$, where a and b are the diameters along the major and minor axes of the ellipse, respectively. The major and minor diameters of KBFBs and yarn were measured directly from optical images obtained using an optical microscope (Nikon Eclipse E 600). A fast-cure epoxy was used to bond the KBFB to the paper card.

Tests for KBFBs were performed on a stepper-motor-driven micromechanical testing system (Model: Mach-1 V500cs). The instrument has a maximum loading capacity of 10 N and a precision of 0.1 gram (g.) Precision of displacement control is about 0.5 µm. Displacement-controlled loading was applied at a speed of 25 µm/s, which is equivalent to a strain rate of 0.0125/s when the nominal length of the specimens is 20 mm. A lower loading-rate condition was applied to specimens from the middle part of the plant at a loading speed of 2.5 µm/s (0.00125/s). Specimens were gripped at the paper tabs. After being mounted on the grips, the tabs were disconnected using scissors. A 0.5-g preload was applied to avoid slack in the fiber. The tests were conducted under displacement control. Both forces and displacements were recorded at the frequency of 20 Hz. Stress was calculated using load and the averaged cross-sectional area. Strain was calculated using displacement and the nominal gauge length. The slope of the best-fit line through a subjectively-chosen linear portion of the stress-strain curve was considered to be the Young's modulus.

The cross-section of the yarns was measured in the same manner as the KBFBs. Compared to KBFBs and yarns; a sliver has a relatively larger, flat cross-sectional area. Therefore, the area of sliver was considered to be rectangular and the width and thickness were measured using a caliper. Both slivers and yarns were tested on an Instron (Model 1011) universal testing machine. A 500-N load cell was used. Nominal gauge length was about 50 mm. Only one loading rate was applied to yarns. Load for slivers was applied at three different speeds: 3 mm/min (equivalent strain rate at 0.001/s), 15 mm/min (0.005/s), and 60 mm/min (0.02/s). The accuracy of load and displacement was approximately 0.5% of indicated values.

Mechanisms of tensile failure were evaluated by examining the fracture surface of the samples using a field-emission gun scanning electron microscope (FEG-SEM) with the fracture surface sputter-coated with gold.

Results and Discussions

Tensile Properties of KBFBs from Different Locations Along the Kenaf Stalk--Test Results

Figure 3 shows randomly-selected stress-strain curves of KBFBs from three different parts of the kenaf stalk. The scatter in measurements is significant due to the large variation of natural-fiber constituents and distribution, such as the scatter in the diameter and length of a single kenaf fiber.

Table 1 lists the Young's modulus, tensile strength, and failure strain of KBFBs obtained from the tests shown in Figure 3. KBFBs from the middle of the plant had the highest Young's moduli and higher tensile strengths compared to those from the other two parts along the stem. The fiber length, in general, is shorter at the bottom of the stalk and longer at the top of the plant, and the increase in fiber length from the bottom to the top plant was not linear but S-shaped [5]. This might contribute to the bottom KBFBs having the lower Young's moduli and tensile strengths.

Table 1. Mean comparisons of KBFBs' Young's moduli, tensile strengths, and failure strains obtained from three different parts along the stem under uniaxial tension at the loading rate of 0.0125/s.

	Young's Modulus(GPa)			Tensile Strength (MPa)			Failure Strain (%)		
	Mean	Std Dev	COV(%)	Mean	Std Dev	COV(%)	Mean	Std Dev	COV(%)
Top	13.05 (B)	4.78	36.6	199.45 (A, B)	109.26	54.8	1.80 (A)	1.04	57.8
Middle	20.19 (A)	6.50	32.2	260.87 (A)	151.47	58.1	1.57 (A)	1.07	68.1
Bottom	12.81 (B)	3.94	30.8	156.36 (B)	73.06	46.7	1.59 (A)	1.20	75.9

Note: Values with the same capital letter are not statistically significant at 5-percent significance level. COV = coefficient of variance.

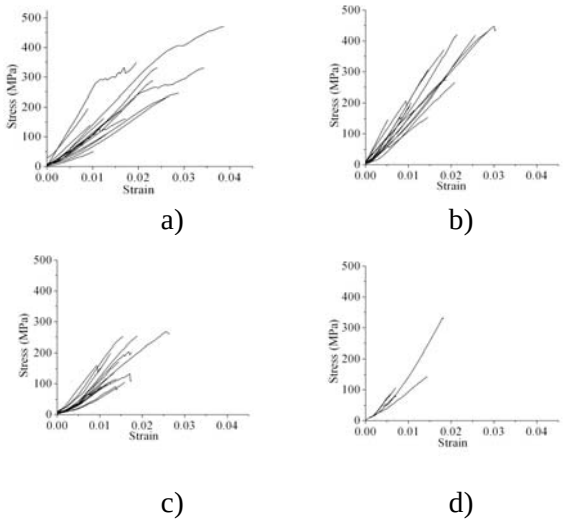

Figure 3 Stress-strain plot of top, middle, and bottom KBFBs at the loading rate of $0.0125s^{-1}$ at: a) top, b) middle, and c) bottom of the kenaf plant, respectively, and d) at the loading rate of $0.00125s^{-1}$ on the middle section of kenaf plant only.

In optical observations, KBFBs from the top appear slim, soft, full of branches, and uniform in area; middle KBFBs, to the contrary, were uniform and branchless. This might be the reason why the top KBFBs did not have the higher tensile properties.

Statistical Distribution of Tensile Properties

Figure 4 presents histograms of the tensile strength and failure strain of KBFBs from three different parts of the kenaf stalk. Most of them showed a right-skewness. Kohji Suzuki et al. [6] found that, at the same loading rate, the distribution of tensile strength was well described by the two-parameter Weibull distribution. Weibull-distribution parameters were calculated and statistical evaluations of the tensile properties of KBFBs are presented in Table 2. The accuracy of this set of Weibull evaluations is limited by a small sample size, as illustrated in histograms of the distributions shown in Figure 4. The mean and COV of tensile strength are similar to those obtained by assuming a normal distribution. Meanwhile, the histogram of failure-strain distributions also shows a right-skewness and does not obey normal distributions.

Table 2. Weibull measures of KBFBs' tensile strengths obtained from three different parts along the stem under uniaxial tension at the loading rate of 0.0125/s.

		Top	Middle	Bottom
		Tensile Strength	Tensile Strength	Tensile Strength
		MPa	MPa	MPa
Parameter Estimates	λ	1.993	1.763	2.334
	κ	226.182	292.330	176.670
Mean		200.46	260.24	156.54
Std Dev		105.10	152.42	71.24
COV (%)		52.4	58.6	45.5

Failure Mechanisms

The SEM micrographs display two possible failure modes in the KBFBs, as shown in Figure 5: fiber pullout from the bundle (a and c) and fiber fracture (b and d). Accompanying fiber pullout from the bundle, a large region of fiber separation exists at the interfaces. On the possibly broken-fiber section, there is only a slight hint of fibrous debonding. Figure 5(a) also shows a coexistence of debonding and fiber failure.

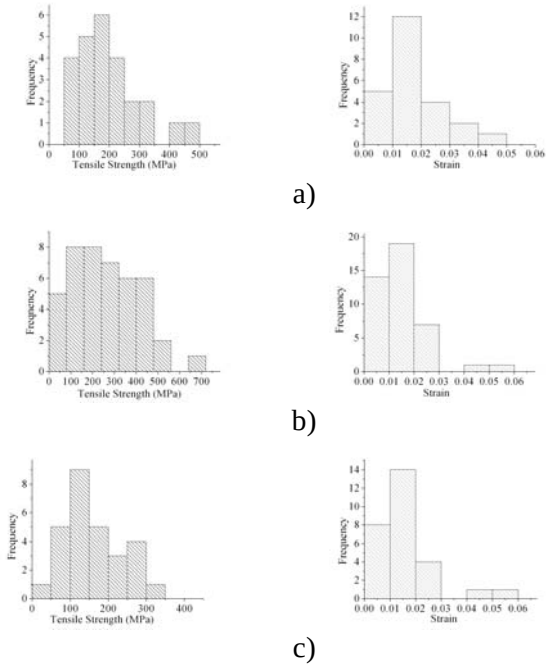

Figure 4. Histograms of failure strain and tensile strength for KBFBs from three different parts along the stalk (0.0125/s): a) top, b) middle, and c) bottom of the kenaf plant.

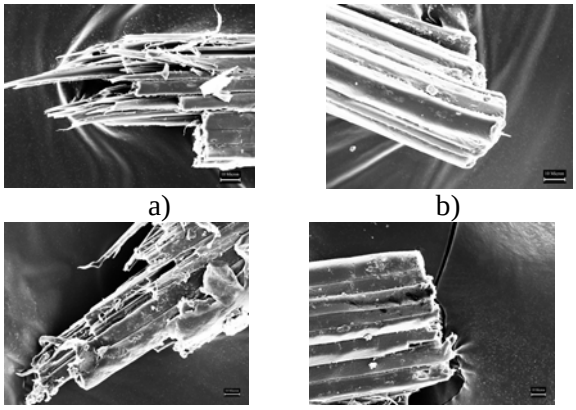

Figure 5. SEM micrographs of fracture surfaces of KBFBs.

Tensile Properties of Kenaf-Reinforced Epoxy

Test Results

Figure 6 shows typical stress-strain curves of yarns and slivers under uniaxial tension. It should be noted that a flat region appeared in the stress-strain curve where stress had no significant increase when strain increased.

For yarns, the flat regions appeared when the stress went up to around 100 MPa; for slivers, flat regions were found when the stress was just about 20 MPa. This probably was ascribed to the earlier failure of a weak region in the composites. Young's moduli were presented for the two regions before and after the appearance of the flat region: 1st stage, the modulus calculated from the linear region on the stress-strain curve before the flat region occurred; 2nd stage, modulus obtained after the flat region occurred.

Table 3 summarizes the test results for both yarns and slivers. Yarns demonstrated higher Young's moduli and tensile strengths than slivers. However, they are both relatively low when compared to KBFBs (sliver is about 1/3 and yarn is about 0.8 of that of KBFB). Meanwhile, the variations of yarns and slivers were both lower than those of KBFBs with respect to Young's modulus and tensile strength.

Table 3. Summary table of Young's moduli and tensile strengths of epoxy-reinforced kenaf, performed at three different test strain rates.

Sliver (0.001/s)				
	Young's Modulus (GPa)		Tensile Strength	Maximum Strain
	1st Stage	2nd Stage	(MPa)	(%)
Mean	4.47	4.5	115	3.46
Std Dev	0.84	0.66	26.98	0.94
COV (%)	19	15	23	27
Sliver (0.005/s)				
	Young's Modulus (GPa)		Tensile Strength	Maximum Strain
	1st Stage	2nd Stage	(MPa)	(%)
Mean	5.59	5.12	103.9	2.28
Std Dev	1.48	0.49	16.3	0.25
COV (%)	26	10	16	11
Sliver (0.02/s)				
	Young's Modulus (GPa)		Tensile Strength	Maximum Strain
	1st Stage	2nd Stage	(MPa)	(%)
Mean	3.7	5.2	98.7	2.82
Std Dev	0.74	0.38	5.98	0.35
COV (%)	20	7	6	12
Yarn (0.001/s)				
	Young's Modulus (GPa)		Tensile Strength	Maximum Strain
	1st Stage	2nd Stage	(MPa)	(%)
Mean	10.69	8.37	249.5	3.45
Std Dev	2.68	1.25	39.75	0.37
COV (%)	25	15	16	11

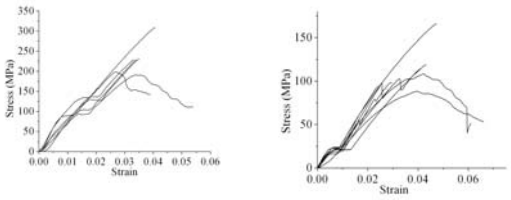

a) b)

Figure 6. Stress-strain plots for slivers and yarns under displacement-control uniaxial tension with a strain rate of 0.001/s: a) sliver and b) on yarn.

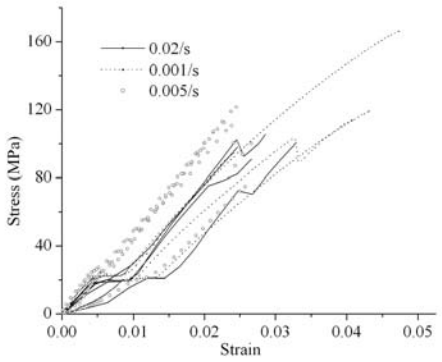

Figure 7. Stress-strain curves of kenaf slivers under displacement-controlled uniaxial loading at the strain rate of 0.001, 0.005, and 0.02/s.

When the loading rate increases, slivers demonstrated a slightly different tensile behavior, as shown in Figure 7. The sliver had relatively lower failure strength at a higher strain rate while the flat region occurred at almost the same stress level. A larger sample set will be evaluated for statistical analysis of the rate-dependent properties of slivers.

Modeling of Rate-Dependent Tensile Behavior

A standard linear model for viscoelastic behavior of solid materials, which effectively combines the Maxwell Model, $\dot{\varepsilon} = \frac{\sigma}{\eta} + \frac{\dot{\sigma}}{E}$, and a Hookean spring in parallel, is used in this study. This model can also be treated as a modification of the Kevin-Voigt model of Newtonian damper and Hookean elastic spring in parallel,

$\sigma = E\varepsilon + \eta\dot{\varepsilon}$, i.e.,

$$\sigma = \sigma^e + \sigma^v = E_\infty \varepsilon + \eta\dot{\alpha} \qquad (1a)$$

$$\sigma = \sigma^e + \sigma^v = E_\infty \varepsilon + E(\varepsilon - \alpha) \qquad (1b)$$

where the total stress is decomposed into an elastic and a viscous component that are determined using an elastic spring constant, E_∞ and a linear viscosity constant, η, which can be extended to an internal state variable shown in Equation (1a) [7]. (See "Nom-enclature" at the end of theis section to identify other symbols.) The viscous stress can also be represented as an inelastic strain in the dashpot, at the extended time interval (-∞,T] shown in Equation (1b). However, the time dependence of inelastic strain in Equation

(1) makes it almost impossible to be directly quantified using tensile tests. For the purpose of demonstrating the loading-rate dependency of the material, a simplification has been proposed by assuming a rate-dependent elastic behavior of the tensile modulus in a form of

$$E = E_0\left(1+\lambda_1 \ln\frac{\dot{\varepsilon}}{\dot{\varepsilon}_0}\right), \qquad (2a)$$

which is also applied to the proportional stress, or "yield strength," or flow stress, when considering viscoplasticity or nonlinear viscoelasticity,

$$\sigma_Y = \sigma_{Y0}\left(1+\lambda_2 \ln\frac{\dot{\varepsilon}}{\dot{\varepsilon}_0}\right) \qquad (2b)$$

where, E_0, σ_{Y0} and $\dot{\varepsilon}_0$ can be treated as reference tensile modulus, reference yield strength, and reference strain rate, respectively. Two parameters, $\lambda_{1,2}$, in Equation (2) are similar to other strain-rate dependent coefficients, which can be obtained using experimental results in Table 3 as

$$\lambda_{1,2} \propto \frac{\partial\left(E,\sigma_y\right)}{\partial \ln \dot{\varepsilon}}. \qquad (3)$$

It should be noted that Equation (2b) and subsequent strain-rate dependent coefficients in Equation (3) may depend on the flow rules introduced to evaluate the nonlinear viscous behaviors of materials. Figure 8 shows the experimental data and model correlations of strain-rate dependency of tensile modulus and "yield" strength of KBFB-epoxy slivers with the loading strain rate ranging from 0.001 to 0.02. It is interesting that the yield strength of the sliver decreases as the loading strain rate increases, which is different from most observations of other short-fiber-reinforced composites.

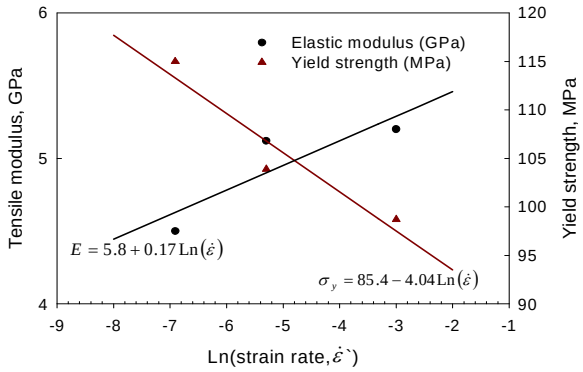

Figure 8. The experimental data and model correlations of strain-rate dependency of tensile modulus and "yield" strength of KBFB-epoxy slivers.

References

1. Kenaf Properties, processing and products, ed. By Terry Sellers, Jr., Nancy A. Reichert, Mississippi State University, 1999.
2. R. M. Roger, A. Sanadi, R. Jacobson, D. Caulfield, Properties of Kenaf/Polypropylene Composites, In: Kenaf Properties, processing and products, ed. By Terry Sellers, Jr., Nancy A. Reichert, Mississippi State University, pp. 381-92, 1999.
3. M. J. Kocurek et al. Secondary Fibers and Nonwood Pulping, The Pulp and Paper Manufacture Series, Vol. 3, 1987.
4. American Society for Testing and Materials. 2003. Standard Test Method for Tensile Strength and Young's Modulus of Fibers. ASTM C 1557-03. ASTM, West Conshohocken, PA.
5. James S. Han et al. Validity of plant fiber length measurement – a review of fiber length measurement based on kenaf as a model, Kenaf properties, In: Processing and products, pp.149 – 167, 1999.
6. Kohji Suzuki, Isao Kimpara, Hiroshi Saito, Kunio funami, Cross-sectional area measurement and monofilament strength test of kenaf bast fibers, Journal of the Society of Materials Science, Japan. Vol. 54, No. 8, pp. 887-894, 2005.
7. J. C. Simo and TJR Hughes, Computational Inelasticity, Interdisciplinary Applied Mathematics, Mechanics, and Materials, Springer, 1997.

Acknowledgement

The authors would like to express appreciation for the support of the U.S. Department of Energy and the Center for Advanced Vehicular Systems at Mississippi State University. We would also express special thanks to Mr. David Baker for his support on micrographs using scanning electron microscope. We would also express special gratitude to Mr. Hugh McKee, the president of Bast Fibers LLC, for his consistent support on Kenaf bast fiber and composites.

Presentations/Publications/Patents

1. Publications - Xue Y., Y. Du, S. Elder, K. Wang, and J. Zhang. 2007. Multiscale Experiments and Modeling of Kenaf Fiber Bundles and Composites. Submitted for publication in the Composites Part B: engineering.
2. Presentation - Xue, Y., Y. Du, S. Elder, D. Sham, M. Horstemeyer, and J. Zhang. Statistical tensile properties of Kenaf fibers and its composites. The 9th International Conference on Wood & Biofiber Plastic Composites, May 21-23, 2007, Madison, WI.

Nomenclature

$\dot{\varepsilon}$	=	Strain Rate
$\dot{\varepsilon}_0$	=	Reference Strain Rate
σ	=	Total Stress
$\dot{\sigma}$	=	Stress Rate
η	=	Linear Viscosity Constant
$-\infty$	=	Extended Time Interval
E'	=	Storage Modulus
σ^e	=	Elastic Component
σ^v	=	Viscous Component
E_∞	=	Elastic Spring Constant
E	=	Tensile Modulus
E_0	=	Reference Tensile Modulus
σ_Y	=	Yield Strength
σ_{Y0}	=	Reference Yield Strength
$\lambda_{1,2}$	=	Strain-rate Dependent Coefficients

Chemical Retting for Stem-Length Natural Bast Fibers: Fiber Characteristics

Team Members: Sangyeob Lee, Sheldon Q. Shi, and Mark F. Horstemeyer

Introduction

Kenaf is a seasonal fiber crop, grown in large amounts every year in the United States. In Mississippi, for example, kenaf fiber production is about 3,600 tons per year (Columbus 2006). Kenaf-bast fiber is an excellent cellulose resource for fiber-based products such as newsprint, bond paper, and corrugated liner board. Extracting the kenaf fibers has less environmental impact because less chemical is required for the process than for wood sources. Short-bast-fiber retting has been developed for the pulp-and-paper applications (Ramaswamy et al. 1994, Hesch 2002, Kawahara et al. 2005). A limited number of studies have been conducted to generate long bast fibers used in the natural-fiber polymer composite (NPC) area. Other limited uses of the kenaf bast fibers include automobile dashboards, carpet padding, corrugated medium, and textiles (Ramaswamy et al. 1995, Webber et al. 2002).

The overall objectives of this study are threefold: investigate a chemical-retting technique, characterize fiber properties, and develop inorganic nanoparticle impregnation technology to produce natural-fiber cell-wall structures. *We focus on investigating a chemical-retting technique first*, followed by developing inorganic nanoparticle impregnation technology for the micropore cellular structure of natural fibers using the ionic salts for making NPC. We also examine the framework of compatible nanoparticle loading and nanoparticle sizes as a function of increased attraction force at the fiber and polyolefin interphase.

Experimental

Materials

For the retting study, kenaf stems (*Hibiscus cannabinus*, L.) were harvested from MSST north farm in January 2007 (Courtesy of Dr. Dan Seale). Bast and core were separated and bast was cut into 5.1-cm lengths from the top, middle and

bottom sections of the stems. The bast was conditioned in an environment with an ambient temperature of 22ºC and a relative humidity of 50% until the MC reached an equilibrium of 8%. Retting chemicals sodium hydroxide (NaOH), hydrogen peroxide (H_2O_2) and acetic acid (CH_3COOH) were purchased from Fisher Scientific, Inc.

Chemical Retting of Kenaf Stem

Table 4 shows the chemical-retting conditions used in this study. Top and bottom sections were taken from within 10 cm at both ends; the middle section was removed from the exact middle of the kenaf stalk. Each section was cut into 25.4-mm lengths and 30 grams of samples were weighed out. Each section was pre-soaked in 80°C water for 24 hours. The pre-soaked kenaf sections were washed and dewatered by gravity. The dewatered sections were retted with 1%, 5%, and 8% sodium hydroxide for an hour at 60 °C. Washed chemically-retted kenaf bundles were neutralized with 5% acetic acid. The excessive chemicals were washed out and the kenaf fiber bundles were dried by air. The dried fiber bundles were characterized using field-emission scanning electron microscopy (FESEM: JSM-6500F) for surface morphology and atomic force microscopy (AFM- Nanoscope IIIa from Digital Instruments) for the surface roughness. Kenaf single fibers were also prepared using a fiber-maceration method (H_2O_2) to address single-fiber dimensions in each section using an image-analysis system (Spot Insight camera and UTHSCSA Image tool Ver. 3.0).

Table 4. Conditions for Chemical Retting

Kenaf Stem	51 mm Length
Sample Collect Location	Top, Middle and Bottom
Pre-soaking	H_2O
Pre-soaking Temperature & Time	80°C for 24 hours
Kenaf/H_2O Ratios for Pre-soaking	1:20
NaOH Concentration	1%, 5% and 8%
Liquid Ratios (Kenaf: NaOH)	1:30
Reagent Chemicals	Acetic Acid (CH_3COOH)
Reaction Temp.	60°C
Reaction Time	1 Hour

Results and Discussions

Characteristics of Chemically-Retted Kenaf-Fiber Bundles

Table 5 shows the chemical composition of kenaf harvested from the MSST north farm. Chemically-retted bast fibers have three principal chemical components such as α-cellulose (46%), hemicelluloses (30%), and lignin (19%) with minor components (5 to 6%) called fats, waxes, inorganic matter, nitrogenous matter, and pigments. The lignin and the hemicelluloses can be almost completely removed by dilute alkali. Due to the chemical treatment, the α-cellulose remained as a final insoluble residue in a fiber form. The chemical compositions of hemicellulose and lignin, compared with published values, were slightly lower and resulted in decreased α-cellulose contents. However, the cellulose content is still equal or higher than fiber sources coming from wood materials. Bast fibers contain a higher cellulose content which contributes to their strength properties. The fibers also have less lignin to support their structural stand. Therefore, the fibers should require fewer chemicals to separate fiber bundles or single fibers. The hemicellulose and lignin contents relate directly to the void spaces of the cell-wall structure and lower amorphous regions. All percentages refer to the weight fraction of oven-dried initial samples.

Table 6 shows fiber dimension and surface roughness of chemically-retted kenaf-fiber bundles as an addition to the single-fiber characteristics. The highest yield was obtained from the top section of the kenaf stem and this section provided longer and more slender fibers than fibers extracted from other sections. Fiber dimensions of stem bast fibers contributed to extreme aspect ratios (length to width). Increased sodium hydroxide contents from 1 to 8% altered fiber surfaces. Sampling locations in the kenaf stem also dictate the smoothness of the surface of chemically-retted fibers. The top section produced rough surfaces of bast fibers, caused by remaining hemicellulose and lignin. Due to the relatively high cellulose contents, the mechanical and physical properties of the kenaf fibers are higher than or equal to those of wood fibers. The cell-wall structure of kenaf-fibers is similar to that of the wood fibers.

Table 5. Chemical Composition of Kenaf- Bast Fibers Harvested from MSST North Farm.

Characteristics	
Moisture content (wt. %)	7.40
Ash (wt. %)*	5.07
Klason Lignin (wt. %)**	19.10
Holocellulose (wt. %)***	75.83
α- cellulose****	45.95
Hemicellulose (by subtraction)	29.88

* TAPPI standard 211-om93 (TAPPI 1993).
** Institute of paper chemistry, Appleton, Wisconsin 428, 1951.
*** Wise, L.E., M. Murphy, and A.A. D'Addieco, Paper Trade J. 122(2):35 (1946).
**** Zellcheming Merkblatt IV/29A

Figure 9 shows topographical and morphological images of fibers treated with different chemical concentrations. The scanning electron microscopy (SEM) images show the changes of surface morphology through sodium hydroxide extraction at different levels of chemical concentrations. A higher chemical concentration provides a smoother fiber surface with less deposited materials on the surface of natural fibers. Bacterially-retted fiber shows similar surface roughness and deposited-material conditions somewhere between 1% and 5% diluted sodium hydroxide levels. This result indicates that a smooth surface was produced under the 8% concentration and may provide a better opportunity for the inorganic nano-particle impregnation method to produce porous structures of natural fibers.

Table 6. Physical Characteristics of Chemically- Retted Kenaf Fiber Bundles.

	Fiber Yield	Length*	Diameter*	Root Mean Squire (RMS) Surface Roughness					
				1% NaOH		5% NaOH		8% NaOH	
	(%)	(mm)	(μm)	2.5 μ Scan	1 μ Scan	2.5 μ Scan	1 μ Scan	2.5 μ Scan	1 μ Scan
Top	73 (2.0)	2.72 (0.50)	12.6 (2.1)	159.8 (69.7)	78.4 (36.5)	77.1 (15.8)	44.7 (15.3)	73.4 (18.3)	35.4 (16.5)
Middle	66.3 (2.3)	2.49 (0.42)	14.1 (1.9)	117.3 (32.9)	70.3 (28.6)	86.3 (25.1)	43.8 (18.9)	55.2 (17.8)	29.6 (13.7)
Bottom	59.4 (1.7)	2.57 (0.31)	13.6 (1.5)	99.1 (35.1)	45.5 (23.9)	68.8 (12.1)	36.7 (18.4)	66.9 (19.2)	38.6 (18.4)

*= Measurement from single fibers (Averages of 25 Single Fibers), ()= Standard Deviation

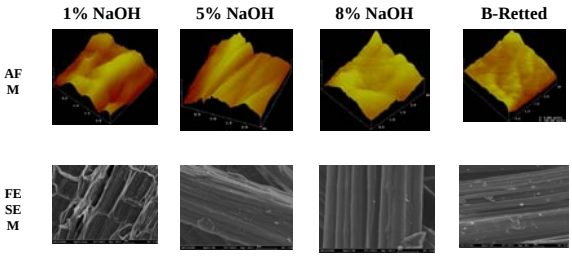

Figure 9. Surface topography and morphology of chemically-retted kenaf-fiber bundles with 1%, 5% and 8% sodium hydroxide concentrations at middle sections. Bacterially-retted images (right) are used for comparison.

Conclusions

Chemically-retted kenaf-bast fibers and their characteristics were evaluated to explore practical applications of such methods to the compressed polymer composite. Relatively higher α-cellulose content (45.95%) was obtained from the kenaf harvested from the MSST north farm. The physical appearance of chemically-retted fiber bundles was quantified as follows: an average 2.6 mm in fiber length and 13.3 μm in diameter with 66% fiber yield. Sodium hydroxide concentrations at 5 to 8% provided smoother surfaces and less deposited materials compared with the 1% NaOH extraction and bacterially-retted fibers. This result was also confirmed by the surface topography and morphology. Uniform root mean square (RMS) roughness and clean surface were obtained from increased NaOH concentration.

References

1. Columbus, E.P. 2006. Telecommunication. (Dec. 14. 2006).
2. Hesch, R. 2002. Device and method for producing a fiber composite. US Pat. 6,460,224. (Oct. 8, 2002).
3. Kawahara, Y., T. Keiichi, R. Endo, M. Shioya, Y. Sugimura, T. Furusawa. 2005. Chemically retted kenaf fibers. Sen'i Gakkaishi, 61(4):115-117.
4. Ramaswamy, G.N., C.G. Ruff, and C.R. Boyd. 1994. Effect of bacterial and chemical retting on kenaf fiber quality. Textile Res. J. 64(5):305-308.
5. Ramaswamy, G.N., and S. Craft. 1995. Uniformity and softness of kenaf fibers for textile products. Textile Res. J. 65(12):765-770.
6. Technical Association of Pulp and Paper Industry (TAPPI). 1993. Ash in wood, pulp, paper and paperboard: combustion at 525°C, TAPPI T 211 om-93. TAPPI Press, Atlanta, GA.
7. Webber, C.L., V.K. Bledsoe, R.E. Bledsoe. 2002. Kenaf production: fiber, feed, and seed. J. Janick and A. Whipkey. Eds. ASHS Press, Alexandria, VA.

Acknowledgement

The authors would like to express appreciation for the support of the US Department of Energy and the Center for Advanced Vehicular Systems at Mississippi State University. We would also express special thanks to Dr. Leslie H. Groom and Dr. Thomas Elder, USDA-Forest Service Southern Research Station, Pineville, LA for Instrumental Support. The authors would like to thank Dr. El Barbary M. Hassan, Bio-oil Group, Forest Products Dept, Starkville, MS for Instrumental Support.

Presentations/Publications/Patents

1. Publication - Lee, S., S.Q. Shi, and M. Horstemeyer. 2007. Morphology and mechanical properties of chemical retted natural bast fibers. ***Paper in preparation.***
2. Publication - S.Q. Shi, S. Lee and M. Horstemeyer. 2007. Natural Fiber Retting and Inorganic Nanoparticle Impregnation Treatment for Natural Fiber/Polymer Composites. 22nd Annual American Society for Composites. University of Washington, Seattle, WA.
3. Presentation - Kenaf Bast Fiber Retting and Inorganic Nanoparticle Impregnation Treatment for Natural Fiber/Polymer Composites. 22nd Annual American Society for Composites Tech. Conf. Univ. of Washington Seattle, Washington, USA. Sept. 17–19, 2007.
4. Presentation - Chemical retting for stem-length natural bast fibers: fiber morphology and mechanical properties. 61st International Convention, Forest Products Society, Knoxville, Tennessee, USA. June 10-13, 2007.

Multifunctional Nanoparticles at the Hydrophilic and Hydrophobic Interface

Team Members: Sangyeob Lee, Sheldon Q. Shi, and H. Michael Barnes

Introduction

The cell-wall structure of natural fibers contains many micropores. One of the events occurring in fiber processing is that lignin and hemicellulose of natural fibers are usually removed during chemical treatments or pulping, which creates additional micropores (Allan et al. 1992a). The presence of these micropores in the cell wall could cause manufacturing defects in composites, such as interfacial failure and air pockets. To reduce the air-pocket defect, one can incorporate a vacuum-assist system in the natural-fiber polymer-composite (NPC) processing to reduce air bubbles to some extent. Another effective way is to introduce nano-particles into the micropores of the fiber cell-wall structure through an impregnation process to fill those voids.

Compatibility between the hydrophilic natural fibers and the hydrophobic polyolefins has been a major issue for the NPC (Lee 2002, Ma *et al.* 2005). Lee *et al.* (2006) indicated that the deposited nano-scale particles on a natural-fiber surface may serve as heterogeneous nucleation sites to initiate crystalline orientation of a molten-polymer matrix. These results suggested that nanoparticles might control the heterogeneous nucleation of a semicrystalline polymer on the natural-fiber surface. The natural fiber itself

cannot initiate nuclei due to extremely unbalanced free energy between the cellulosic fibers and molten polyolefin matrices (Mullin 1993, Gasser *et al*. 2001, Lee *et al*. 2006). Therefore, the nanoparticle impregnation would not only fill the micropores of the fiber-cell-wall structure by minimizing air-bubble defects of the NPC, but would also introduce nanoparticles onto the fiber surfaces to serve as attraction-force manipulators to polymer matrices for improving the compatibility between fiber and polymer interfaces.

Calcium carbonate is a versatile additive for use in the pulp/paper and plastic industries for elastomeric applications to obtain a hydrophobic surface-coating (Khrenov *et al.* 2005). It has a regular and controlled crystalline shape (orthorhombic) and a 0.05 to 2.5-µm particle size (Allan and Carroll 1994, Kuang *et al.* 2002, Yan *et al.* 2005). A smaller particle size can be obtained from ionic-salt impregnation to build a crystal form of calcium carbonate (Choi 1995). Chemical-impregnation technology has well been developed and applied in pulp-and-paper and surface-coating industries (Allan *et al.* 1991, Allan *et al.* 1992a and 1992b, Lee *et al.* 1999, Koepenick 2000, Lork 2004, Kuusipalo *et al.* 2005). However, in the pulp-and-paper applications, the amount of inorganic-compound loading is limited to 7% due to the concerns of surface-printing ability and paper strength (Kocman and Bruno 1995, Li *et al.* 2002, Perng and Wang 2004, Kralj *et al.* 2004, Frederick *et al.* 2004, Sancaktar and Walker 2004, Yan *et al.* 2005). For NPC applications, the amount of inorganic nanoparticle loading in the natural fibers could be increased, thus improving the attractive forces in the composites. The nanoparticle sizes and their distribution presented in the impregnated natural fibers may have a significant impact on the NPC properties. It has been shown that the inorganic nanoparticle size can be controlled by the reaction time and the ionic salt ratio (Choi 1995, Gasser *et al.* 2001).

The objective of this present study is to develop inorganic nanoparticle impregnation techniques for the natural-fiber cell-wall structures in order to reduce the NPC processing defects and enhance the mechanical properties.

Experimental

Materials

In the inorganic nanoparticle impregnation experiments, Kraft wood-pulp fibers (southern pine-*Pinus* spp.) were obtained from a local pulp company. They were collected from a bleached pulp stream and kept in a wet condition (150% MC) to obtain optimum nano-void openings. The fibers were stored at a temperature of 4ºC until ready for further experiments. Primary (Na_2CO_3) and secondary ionic ($CaCl_2$) salts were purchased from Fisher Scientific Inc.

Experimental Procedures

Figure 10 shows a simplified flow chart for the inorganic nanoparticle impregnation using two steps of the ionic-salt treatment under heat and pressurized-chamber conditions. Micropore impregnation of ionic salts was effected with never-dried Kraft pulp fibers in a pressurized reactor. The primary salt, Na_2CO_3, and secondary ionic salt, $CaCl_2$, were impregnated into micropores of the natural-fiber cell wall consecutively to obtain nanoparticles (< 100 nm). The nanoparticle sizes were controlled by the reaction time and molar fraction of ionic salts. The chemical reaction is described as follows:

$$CaCl_2 \cdot H_2O + Na_2CO_3 \xrightarrow{H_2O} CaCO_3 + 2NaCl + 2H_2O$$

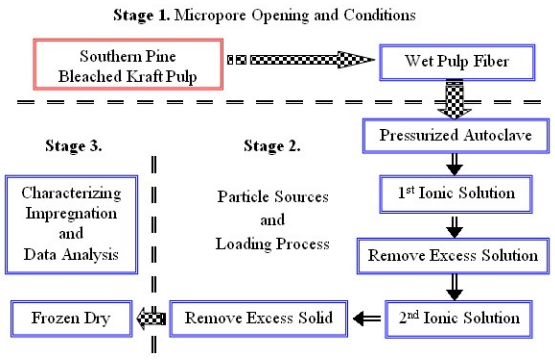

Figure 10. Inorganic nanoparticle impregnation using two steps of the ionic salt treatment under heated and pressurized chamber conditions.

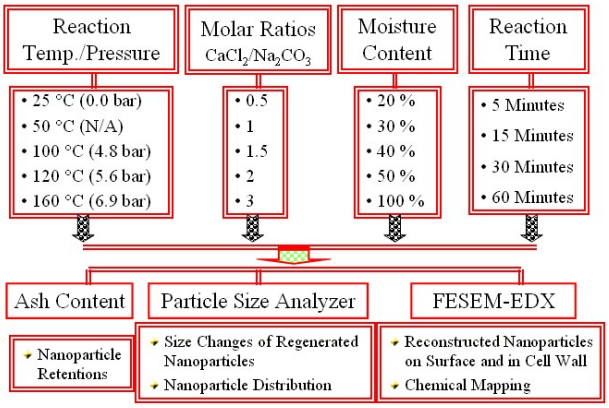

Figure 11. Experimental variables for the inorganic nanoparticle impregnation into the cell-wall structure of natural fibers.

For this study, parameters (Figure 11) were selected to optimize inorganic nanoparticle loading into the porous structures of natural fibers. The parameters investigated included reaction temperature, molar ratios of two ionic salts, moisture content of natural fibers, and reaction time. The experimental process was to optimize the process to get the best impregnation conditions. The MCs (oven-dry-basis (ODB)) of 20, 30, 40, 50, 100% and molar ratio of 1 were chosen to see the effect of MC. From the result, 20% and 30% MC were selected. Molar ratios of 0.5, 1, 1.5, 2, and 3 with the two MCs were evaluated by ash contents of pulp fibers impregnated with $CaCO_3$. After the previous steps, reaction temperature and time factors were recorded without Kraft pulp with primary (Na_2CO_3) and secondary ionic salt ($CaCl_2$). Temperatures of 25, 50, 100, 120 and 160°C were evaluated with a fixed molar ratio of 1 and MC of 30%. The effect was evaluated with particle size analysis and SEM to address how the temperatures influence the nanoparticle formation and sizes. Two molar ratios, 0.5 and 1, MC of 30%, and a temperature of 25°C were selected to evaluate reaction times of 5, 15, 30 and 60 minutes between primary and secondary ionic salts after the primary ionic salt was diluted for 15 minutes. The selected parameters such as molar ratio of 1, MC of 30%, temperatures of 25 and 160°C, and reaction time of 15 minutes were directly applied to impregnate nanoparticles into the cell wall structure of kenaf fibers. SEM-energy dispersive x-ray (EDX) was used to evaluate the Ca++ ion mapping and chemical-element analysis.

A 1-L pressurized reactor (Parr Instrumental Co.) with Model 4843 controller was employed to affect the inorganic-nanoparticle-impregnation process. In a typical experiment, bleached commercial pulp fibers (0.5% ash content, 91% MC (ODB)) were introduced into the pressure vessel along with the primary ionic solution. The vessel was sealed and pressurized to the level shown in Figure 11 for the reaction temperature used. The solution was constantly stirred at 100 rpm. Pressure was maintained for 15 minutes followed by venting to atmospheric pressure and removal of the reacted fiber. After washing out the excess primary solution, the fiber was reintroduced into the reaction vessel with the secondary ionic salt and the process was repeated. The inorganic-nanoparticle-impregnated fibers were dried and evaluated in terms of nanoparticle-size distribution, surface morphology, and chemical loading of the inner cell-wall structure of the natural fibers. The treated fibers were freeze-dried under vacuum for 12 hours and stored in a vacuum desiccator. A muffle furnace was used to measure ash contents (T 211 om-93) for each treatment condition.

A particle size analyzer (Microtrac UPA 250) with Microtrac V.9.1.17 software was used to determine inorganic-nanoparticle growth and distribution. The micro- to nano-scales of particles were detected by a dynamic-light-scattering detector (0.003 to 6.541 micron capability) for 180 seconds. Nanoparticle samples were treated with sonic waves for three minutes to increase the detector sensitivity. Deionized water was used as a carrier. The morphology and chemical-mapping analysis using field-emission scanning electron microscopy (FESEM: JSM-6500F and EDX: Oxford Instruments INCA Energy with X-ray Elemental Analysis) were used to investigate the inorganic nanoparticle distribution in the cell wall and surface morphology. Mounted fibers were coated with an approximately 15-nm thin gold layer using an ion sputter. Images were generated at 5 kV and 10,000x.

Results and Discussion

Effect of Reaction Temperature

Figure 12 shows the effect of reaction temperature on the inorganic nanoparticle formation and growth in the reaction chamber. The nanoparticle sizes were from 138 nm to 2,000 nm. The crystal size was decreased with an increased reaction time. Also, the longer the reaction time, the more uniform the particle size distribution is. Nano-scale crystal formation on the surface of micro-scale inorganic particles was observed at a relatively lower temperature under 50°C. When the reaction temperature reached 160°C, the reaction-chamber pressure was 6.9 bar; the pressure might play a role in inorganic-nanoparticle formation and growth during the reaction of two ionic salts.

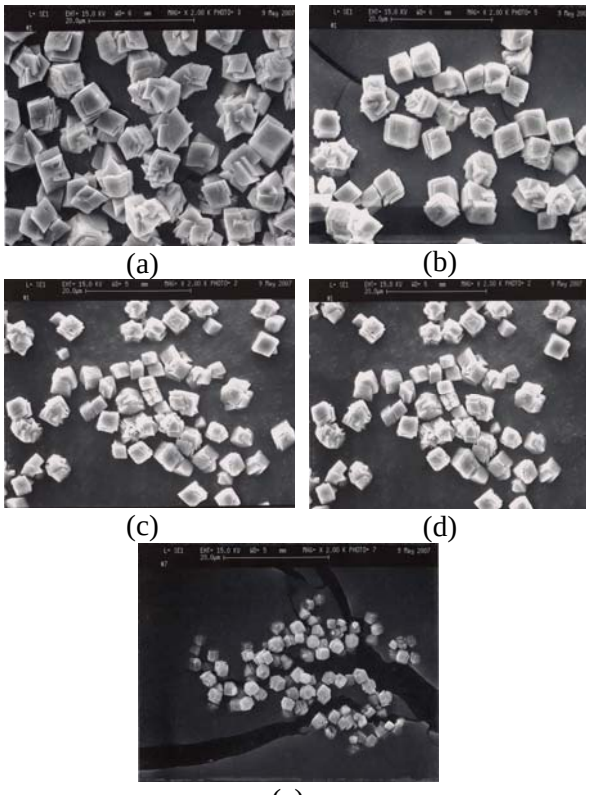

Figure 12. Inorganic-nanoparticle formation and growth of consecutively-reacted ionic salts with reaction time applied in the reaction chamber at 2000 x. (a) 25 °C, (b) 50 °C, (c) 100 °C, (d) 120 °C, and (e) 160 °C.

The optimum reaction time was 15 minutes after the secondary ionic salt was introduced into the reaction chamber. The reaction time was evaluated at a temperature of 25 °C with two types of molar ratios of sodium carbonate and calcium chloride. The longer reaction time contributed to the growth of $CaCO_3$ crystal structures. The molar ratios of $CaCl_2/Na_2CO_3$ of 1 and 2 provided relatively low average particle size. The ratio 2 showed a wide distribution from 45 nm to 6 µm, while the ratio 1 showed a relatively uniform distribution.

Moisture Content of Kraft Pulp

Figure 13 shows the effect of fiber MC on the nanoparticle loading for the fiber-cell-wall impregnation. It shows that the fiber-saturation point (FSP) of the bleached Kraft fibers at about 30% MC is a critical point to impregnate the fillers into their cell-wall structure. When the MC is less than FSP (i.e., MC<30%), cellular structures of natural-fiber cell wall may play an important role. It also influences the dispersing characteristics of ionic salts into the porous structure of the cell wall. Below FSP, the microfibrils are closer and fewer micropores are available to be impregnated with inorganic fillers (Choi 1995, Kocman and Bruno 1996). It should also be noted that the dry fibers are not compatible with the impregnation of inorganic compounds due to the collapsing cellular structure of fiber cell walls. It is difficult to recover their structure with swelling agents (Allan 1992, Choi 1995). In this impregnation study, we targeted 10 to 15 % inorganic nanoparticle loading in order to keep both the fiber strength properties and the void-filling requirement. Since the inorganic nanoparticle loading is higher than the target (10 to 15%), all of the wet-fiber conditions can be acceptable for the nanoparticle loading, except that the MC remains below FSP.

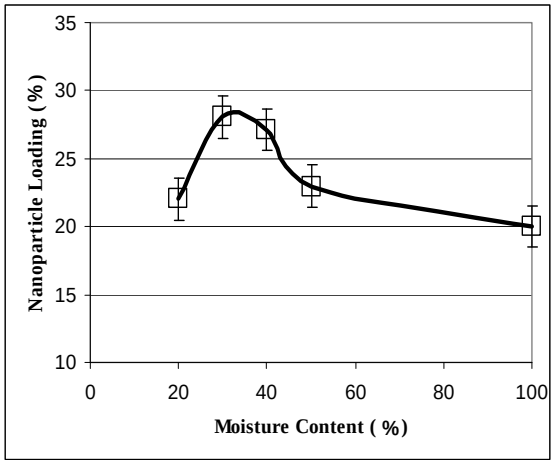

Figure 13. Moisture contents of Kraft fiber on a wood cell wall loaded with $CaCO_3$ particles.

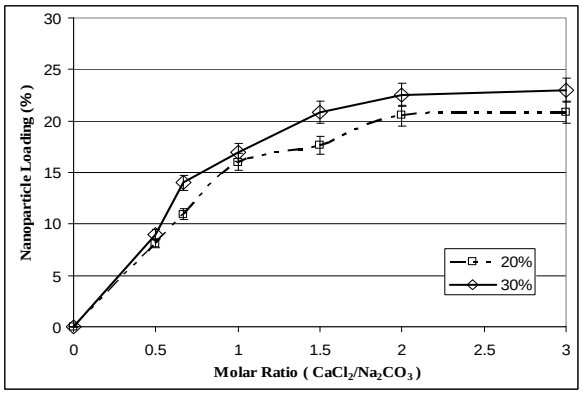

Figure 14. The effects of molar ratios of calcium chloride and sodium carbonate on cell-wall loading (CWL) of wood fibers at 25ºC for 30 minutes.

Effect of Molar Ratios of Ionic Salts

Figure 14 shows that the increase of concentration of calcium chloride ($CaCl_2$) and a greater molar ratio (calcium chloride to sodium carbonate =$CaCl_2/Na_2CO_3$) level will increase the precipitation level of calcium carbonate ($CaCO_3$). Additional findings suggest that longer reaction times and higher ionic-salt ratios will result in a large $CaCO_3$ crystal structure (up to > 1 µm in diameter). The desirable particle sizes for the nanoparticle impregnation are in the range of 10 nm up to 200 nm. This can be achieved by controlling the reaction time and calcium chloride contents in the ionic-salt ratio. The effect of molar ratios ($CaCl_2/Na_2CO_3$ =1) of ionic salts addressed 16 % to 17% cell-wall loading (CWL) capability.

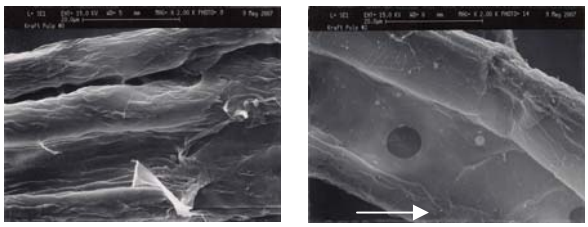

(a) (b)

Figure 15. Surface nanoparticles formed by excessive ionic salts. (a) before ionic treatment and (b) after ionic treatment.

Reconstructed Nanoparticles and $CaCO_3$ Precipitation

Figures 15 and 16 show the FESEM images and the EDX analysis before and after inorganic-nanoparticle impregnation. The morphological images show that the deposited materials remain on the surface. The deposited materials may consist of lignin and hemicellulose materials as well as the particles from natural fiber itself. The bright particles shown in Figure 15 (b) indicate that the inorganic crystal is formed on the surface and grown with excessive ionic salts. The residual ionic salts generally allow forming larger crystals of the calcium carbonate than the crystals formed in the inner cell wall. Because the largest voids are generally around 1,000 Å, the inorganic nanoparticles loaded inner cell wall may be less than the largest voids. The evidence of calcium carbonate impregnation as a filler of the nano-scale porous structure in the natural-fiber cell wall is shown in Figure 16. The dots (Figure 16 (a)) indicate Ca^{++} ion distribution inner cell- wall structures. The dots also indicate that impregnated inorganic nanoparticles ($CaCO_3$) are uniformly distributed through the natural-fiber cell wall. The EDX analysis (Figure 16 (b)) shows higher quantities of Ca^{++} ions with residual sodium and chloride ions.

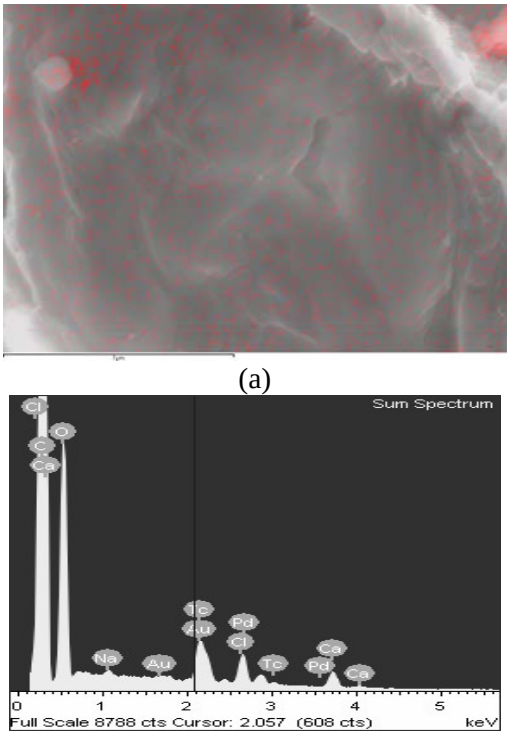

Figure 16. Chemical mapping of Ca^{++} ion in cross-section using SEM-EDX in the cell-wall structure of natural fibers. (a) Ca^{++} ion mapping, and (b) chemical-element analysis.

Conclusions

Through the impregnation process developed in this study, inorganic nanoparticles were observed in the micropore structure of the cell wall. These nanoparticles may serve as void fillers and potentially provide nucleation sites for the semi-crystalline polymers. The longer the reaction time, the smaller the reconstructed nanoparticle size and the more uniform is the nanoparticle size distribution. Parameters for the inorganic nanoparticle impregnation using ionic salts to the natural-fiber cell-wall structures were evaluated to optimize the attraction force at the fiber and polyolefin interphase. The inorganic nanoparticle precipitation increases with the increase of $CaCl_2/Na_2CO_3$ molar ratio. To reach an optimal loading condition, the process should keep the reaction time shorter, the reaction temperatures higher (120 to 160°C) with applied pressure, the reconstructed nanoparticle size smaller, and the nanoparticle distribution uniform. An optimum MC for the inorganic nanoparticle loading is at FSP, about 30% . Under the optimum conditions, Ca^{++} ions were observed in the cell wall of the fiber cross-section. During the course of developing impregnation processes, inorganic nanoparticles were observed in the micropore structure of the cell wall. These nanoparticles may serve as void fillers in the micropores of the natural fibers and potentially provide nuclear sites for semi-crystalline polymers.

References

1. Allan, G.G., Y.C. Ko, and P. Ritzenthaler. 1991. The microporosity of pulp. Tappi J. 74(3): 205.
2. Allan, G.G. 1992. Cell wall loading of never-dried pulp fibers. U.S. pat. 5,096,539 (Mar. 17, 1992).
3. Allan, G.G., A.R. Negri, and P. Ritzenthaler. 1992a. The microporosity of pulp; the properties of paper made from pulp fibers internally filled with calcium carbonate. Tappi J. 75(3):239-244.
4. Allan, G.G., J.P. Carroll, A.R. Negri, M. Raghuraman, P. Ritzenthaler, and A. Yahiaoui. 1992b. The microporosity of pulp; the precipitation of inorganic fillers within the micropores of the cell wall. Tappi J. 75(1):175-178.
5. Allan, G.G. and J.P. Carroll. 1994. Composition and methods for filling dried cellulosic fibers with an inorganic filler. U.S. pat. 5,275,699 (Jan. 4, 1994).
6. Choi Y.D. 1995. Impregnation behavior of $CaCO_3$, KCl and K_2SO_4 into micropore of pulp fiber. MS thesis, Yeungnam Univ., Kyungsan, Korea. 41p.
7. Frederick, W.J., B. Shi, D.D. Euhus, and R.W. Rousseau. 2004. Crystallization and control of sodium salt scales in black liquor concentrators. Tappi J. 3(6):7-13.
8. Gasser, U., E.R. Weeks, A. Schofield, P.N. Pusey, and D.A. Weitz1. 2001. Real-space imaging of nucleation and growth in colloidal crystallization. Science. 292:258-262.
9. Khrenov, V., M. Klapper, M. Koch, and K. Müllen. 2005. Surface functionalized ZnO particles designed for the use in transparent nanocomposites. Macromol. Chem. Phys. 206(1):95–101.
10. Kocman, V. and P. Bruno. 1995. Accurate determination of six common fillers in fine papers, newsprint, and recycled stock by X-

ray fluorescence spectrometry. Tappi J. 78(4): 129-134.

11. Kocman, V. and P.J. Bruno. 1996. Thermal stability of paper fillers: A strong case for a low temperature paper ashing. Tappi J. 79(3): 303-306.
12. Koepenick M. 2000. Nanoparticle prospects and perspectives. TAPPI J. 83(5): 45-47.
13. Kralj, D., J. Kontrec, L. Brečević, G. Falini, and V. Nöthig-Laslo. 2004. Effect of inorganic anions on the morphology and structure of magnesium calcite. Chem. Eur. J. 10:1647-1656.
14. Kuang, D., A. Xu, Y. Fang, H. Ou, and H. Liu. 2002. Preparation of inorganic salts ($CaCO_3$, $BaCO_3$, $CaSO_4$) nanowires in the Triton X-100/cyclohexane/water reverse micelles. J. Crystal Growth 244:379–383.
15. Kuusipalo, J., M. Kaunisto, A. Laine, and M. Kellomäki. 2005. Chitosan as a coating additive in paper and paperboard. Tappi J. 4(8):17-21.
16. Lee, S.Y., J. Lee, and S. Yang. 1999. Preparation of silica-based hybrid materials coated on polypropylene film. J. Materi. Sci. 34:1233-1241.
17. Lee, S.Y. 2002. Transcrystallization behavior and interfacial strength of a semicrystalline polymer combined with thermomechanical pulp (TMP) fiber. M.S. Thesis. Univ. of Idaho, Moscow, ID. 72 p.
18. Lee, S.Y., T.F. Shupe, L.H. Groom, and C.Y. Hse. 2006. Heterogeneous nucleation of a semicrystalline polymer on fiber surfaces. In: Recent developments in the particleboard, fiberboard, and molded wood products industry. Shupe, T.F. ed. Forest Products Society. Madison, WI. pp. 99-105.
19. Li, L., A. Collis, and R. Pelton. 2002. A new analysis of filler effects on paper strength. JPPS. 28(8):267-273.
20. Lork, A. 2004. Silicone resin emulsion coatings: the strength profile of the silicone resin network in paint microstructures. Surface Coatings Inter. Part B: Coatings Transa. 87(B1):1–6.
21. Ma, C., M. Rong, M. Zhang, and K. Friedrich. 2005. Irradiation-induced surface graft polymerization onto calcium carbonate nanoparticles and its toughening effects on polypropylene composites. Polym. Engin. Sci. 45(4):529-538.
22. Mullin, J.W. 1993. Crystallization, 3rd Edit. Butterworth-Heinemann Ltd. Oxford, England. 527p.
23. Perng, Y. and E. Wang. 2004. Development of a functional filler: swelling sericite. Tappi J. 3(6):26-31.
24. Sancaktar, E., and E. Walker. 2004. Effects of calcium carbonate, talc, mica, and glass-fiber fillers on the ultrasonic weld strength of polypropylene. J. Appli. Polym. Sci. 94:1986–1998.
25. Yan, Z., Q. Liu, Y. Deng, and A. Ragauskas. 2005. Improvement of paper strength with starch modified clay. J. Appl. Polym. Sci. 97: 44–50.

Acknowledgement

The authors would like to express appreciation for the support of the US Department of Energy and the Center for Advanced Vehicular Systems at Mississippi State University. The authors would like to thank Dr. James Rawlins and his research group, Thames-Rawlins Polymer Research, Shelby Freland Thames Polymer Science Research Center, University of Southern Mississippi, Hattiesburg, MS for instrumental support.

Presentations/Publications/Patents

1. Publication - Lee, S**.,** S.Q. Shi, and H.M. Barnes. 2007. Inorganic nanoparticle impregnation into micropore cellular structure as void filler and interfacial compatibilizer. ***Paper in preparation.***
2. Publication - Lee, S., S.Q. Shi, and H.M. Barnes. 2007. Multifunctional Nanoparticles at the Hydrophilic and Hydrophobic Interface. In Advanced Biomass Science and Technology for Bio-Based Products. International Rattan and Bamboo Center, Beijing, China. ***In press.***
3. Publication - S.Q. Shi, S. Lee and M. Horstemeyer. 2007. Natural Fiber Retting and Inorganic Nanoparticle Impregnation Treatment for Natural Fiber/Polymer Composites. 22nd Annual American Society for Composites. University of Washington, Seattle, WA..

4. Presentation - Kenaf Bast Fiber Retting and Inorganic Nanoparticle Impregnation Treatment for Natural Fiber/Polymer Composites. 22nd Annual American Society for Composites Tech. Conf. Univ. of Washington Seattle, Washington, USA. Sept. 17–19, 2007.
5. Presentation - Inorganic nanoparticle impregnation into micropore cellular structure: void filler and interfacial compatibilizer. 2007 Intern. Conf. on Nanotechnology for the Forest Products Industry. Knoxville, Tennessee, USA. June 13–15, 2007.
6. Presentation - Multifunctional Nanoparticles at the Hydrophilic and Hydrophobic Interface. Advanced Biomass Science and Technology for Bio-Based Products. International Rattan and Bamboo Center. Beijing, China. May 23–25, 2007.

Unidirectional Natural-Fiber Polyolefin Laminates: Thermal and Mechanical Properties

Team Members: Sangyeob Lee, Sheldon Q. Shi, and Yibin Xue

Introduction

Natural-fiber (mainly woodfiber) polyolefin composites (NPC) have been a natural choice for both non-structural and structural applications such as decking, doors, window frames, flooring, fencing, walls, furniture, automobiles and electronic products (Clemons 2002, Serizawa *et al.* 2006). However, due to their shorter fiber length, their reinforcement potential is limited in terms of the strength properties of the composites (Feng *et al.* 2001, Arzondo *et al.* 2004, Bledzki *et al.* 2004, Serizawa *et al.* 2006). Increasing the length of the natural fiber is one of the alternatives to improve natural-fiber reinforcement. Agricultural bast fibers from jute, hemp, sisal and kenaf can be good candidates because of relatively high cellulose content and enhanced fiber properties (Karnani *et al.* 1997, Rana *et al.* 1998, Eichhorn *et al.* 2001, Sanadi *et al.* 2002, Joseph *et al.* 1993, 2003, Tajvidi *et al.* 2005). Long kenaf (*Hibiscus cannabinus* L.) bast-fiber bundles are traditionally used to make ropes, mats, carpets, paper, and other products (Sellers and Reichert 1999). In recent years, there has been an increasing interest in finding new applications of natural bast fibers in making fiber-reinforced polymer composites for automobile parts to replace synthetic fibers made of glass and carbon.

The objectives of this study are threefold: evaluate kenaf-bast-fiber characteristics, investigate the effect of fiber orientation on the mechanical properties of laminates, and address the thermal and interfacial characteristics at the kenaf fiber and polymer interface.

Materials and Experimental Procedures

Materials

For this study, stem-length kenaf fibers (*Hibiscus cannabinus*, L.) were obtained from an international trading company in February 2007. The fibers were bacterially-retted, stem-length kenaf fibers. The bast was conditioned in an environment with an ambient temperature of 22ºC and a relative humidity of 50% until the MC reached an equilibrium of 8%. The stem-length fibers were macerated to evaluate single-fiber characteristics. For the kenaf maceration, hydrogen peroxide (H_2O_2) was purchased from Fisher Scientific Inc. Polypropylene film (CO-EX), as a polymer matrix, was provided from Plastic Suppliers, Inc. Dallas, TX.

Laminate Fabrication

Figure 17 shows the fabrication procedure of kenaf and polypropylene (PP) film laminates for this study. Stem-length, bacterially-retted fibers were cut into 7-inch lengths and combed to separate the kenaf fibers into separate fiber bundles. A total of thirteen layers (six layers of kenaf fiber and seven layers of PP films) of laminates were fabricated to evaluate the effect of fiber orientation angles (0°, 45° and 90°) and material formulations (kenaf/PP= 30/70, 40/60 and 50/50). A laboratory hot press (6 × 6-inches) was used to press the laminates under 100 psi at 200 °C for 2½-minutes pressing time. The compressed laminates were cooled down at a rate of $25°C \cdot min^{-1}$ as a super-cooling condition. The compressed samples were stored at an ambient temperature of 22ºC for 24 hours before cutting samples for mechanical tests. The kenaf-fiber bundles were also cut into 2-inch lengths of each

top, middle, and bottom to characterize fiber properties such as single-fiber length, diameter, surface topography and surface roughness.

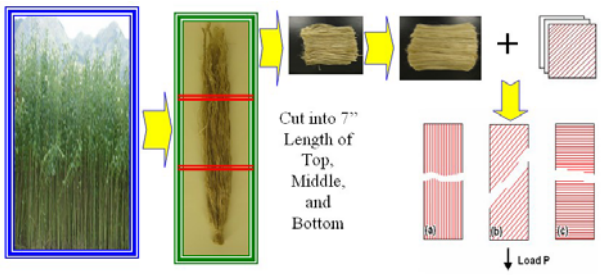

Figure 17. Thirteen layers of laminate fabrication to evaluate the effect of oriented angles.

Instruments and Data Collection

The fiber-bundle strength tests were carried out to address the strength properties at the top, middle and bottom using Mach1V500 (CS instrument Inc.). Loading capacity for this tester was 0-10 N with precision of 0.1 g at 0.5-µm displacement. Before and after the test, the fiber-bundle images were generated using Spot Insight Camera (Advanced V 4.6, Diagnostic Instrument Inc.) as an image-capture system and UTHSCSA Image Tool® V.3.0 for image analysis. Using the image analysis, fiber length and diameters of bast-fibers data were collected to characterize regional differences of kenaf fibers from the top, middle, and bottom sections.

An AFM (Nanoscope IIIa -Digital Instruments) and an SEM (Zeiss SupraTM 40 – Gemini®) were used for the surface topography and morphology of top, middle and bottom bast fibers. The AFM used the tapping mode and two scanning areas, 2.5 × 2.5 µm and 1× 1 µm, to evaluate topographical and RMS surface roughness differences at the top, middle, and bottom section of whole-length bast-fiber bundles. An environmental SEM was also used to address morphological characteristics of the fracture surfaces at 100 and 500 magnifications at 15 kV.

Mechanical test data for kenaf fiber and PP film laminates were evaluated by an Instron 5869 with 5 kN load cell. The cross-head speed was 0.25 in.·min.$^{-1}$ for tensile strength and 0.125 in.·min.$^{-1}$ flexural (modulus of elasticity, MOE, and modulus of rupture, MOR) tests based on ASTM D638-03. Laminate failure was also observed in samples made from fiber-orientation angles of 0°, 45°, 90° and random.

Thermal analysis was carried out by using a thermogravimetric analyzer - differential scanning calorimeter (TGA-DSC) 150 (Setsys Evolution 1750 TGA-DSC) with Fourier transform infrared (FTIR) and gas chromatograph-mass spectrometer (GC-MS, Setaram Instrumentation). The experiment followed standard procedures of ASTM E793-01 and E794-01. Thermal characteristics such as peak, onset temperature, and heat flow were collected with 5°C·min^{-1} heating and cooling rate from -25 to 200°C and 200 to 50°C, respectively

Results

Results are briefly displayed here. Detailed discussion will be furnished in the next report.

Table 7. Kenaf-fiber bundles and single-fiber properties.

	Young's Modulus* (GPa)	Tensile Strength* (MPa)	Length*** (mm)	Diameter*** (µm)	Surface Roughness (RMS)	
					2.5 µ Scan	1 µ Scan
Top	12.1 (2.0)**	0.20 (0.05)	2.50 (0.72)	12.0 (1.5)	119.5 (114.1)	47.5 (29.9)
Middle	18.5 (3.4)	0.26 (0.10)	2.62 (0.58)	11.7 (1.3)	57.5 (19.1)	30.9 (15.8)
Bottom	13.5 (3.0)	0.17 (0.41)	2.79 (0.52)	12.3 (1.1)	54.6 (25.2)	26.1 (11.5)

* = Averages of 25 fiber bundles.
** = Standard deviation.
*** = Measurement from single fibers.
RMS = Root mean square.

Fiber strength and physical properties are fundamental elements to predict and design composite properties. Table 7 shows the mechanical strength, surface roughness and fiber dimensions of the bacterially-retted, stem-length kenaf fibers. The fibers were from the top (2 inch from top), middle and bottom (2 inch from bottom) of the stem-length kenaf fibers. The highest Young's moduli and higher tensile strengths were obtained from fiber bundles from middle fibers compared to those from the other two sections. However, fiber-bundle strength may not be appropriate to address or design the final polymer-composite properties. Both fiber length and diameters were close to published values and the collected data were under the variation ranges, while mean fiber lengths were increased from top

to bottom section. The surface roughness of the bundle fibers showed smother surface of fibers from the top to bottom section. In general, the bottom section of kenaf stems contained higher lignin content to support stem structure. In contrast, top fibers contained juvenile fibers with lower fiber length. Therefore, fiber bundles from the middle section might have the better Young's modulus and tensile strength.

Figure 18 shows morphological and topographical images at top, middle and bottom sections of kenaf bast fiber bundles generated by stem-length bacterial retting. The SEM images were generated with 100x magnification and showed a general appearance of surfaces with relative smoothness. The images also showed deposited particles on the surface of the bacterially-retted kenaf fibers regardless of the fiber sections. The deposited materials might be fractures of the kenaf fibers generated during the retting process. The topographic images also showed similar appearances of surfaces due to the different Z height of the surface. The high Z height from the middle section was 190 nm and represented as the smoothest surface. However, surface roughness analysis on each scan area showed the differences were under variation ranges of sample measurements while the Table 7 showed a trend of the reduced mean surface roughness from the top to bottom section.

Effects of Fiber Orientation and Material Types on the Mechanical Properties

Figure 19 shows that MOE increased as the kenaf-fiber contents in the laminates increased when the fibers were highly oriented to fiber direction. In contrast, the 40% the kenaf-fiber content provided higher strength than its other mixing formulations. Modulus and strength decreased as the fiber angle increased. The 45^{o} and 90^{o} angles of fiber orientation provided a lesser contribution to the flexural modulus and strength of kenaf-fibers/PP film laminates regardless of fiber amounts in the laminate system. The fiber-orientation angles played an important role on the mechanical-property enhancement. The strength of kenaf fibers contributed to an enhanced strength of the natural-fiber-reinforced composites. This result also can be explained by less matrix and lack of interfacial compatibility between surface of natural kenaf fibers and the polyolefin matrix.

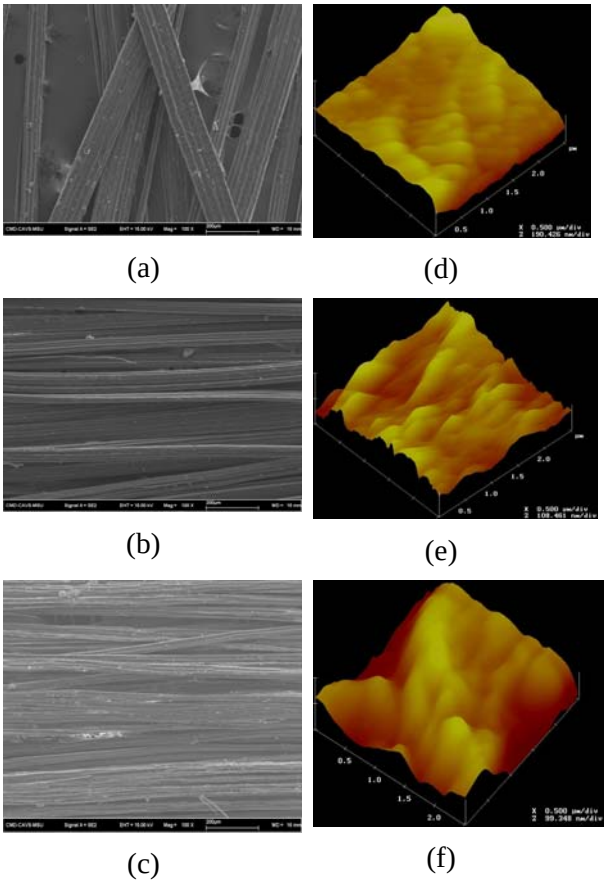

Figure 18. Morphological (a= Top, b= Middle, and c= Bottom) and topographical (d= Top, e= Middle, and f= Bottom) images of kenaf bast-fiber bundles produced by bacterial retting.

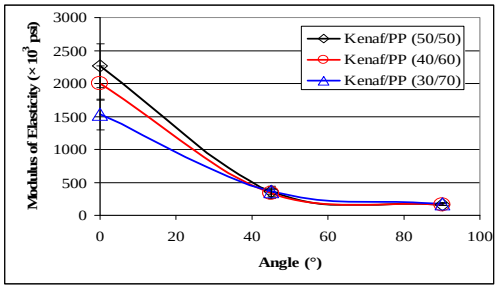

(a)

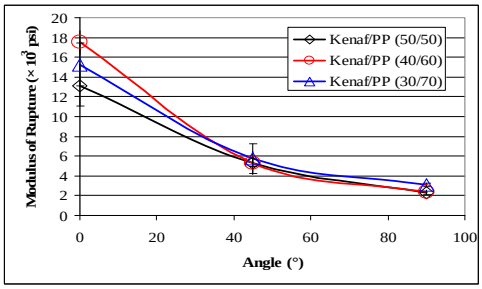

(b)

Figure 19. Flexural modulus and strength of kenaf fiber and PP laminates as function of the different fiber orientation with three different kenaf and PP formulations. (a= Modulus of Elasticity, b= Modulus of Rupture).

Figure 20 shows flexural modulus and strength of kenaf fiber and polypropylene laminates as functions of fabrication types. The different fiber orientation data were collected with 40% kenaf-reinforced PP film laminates. Pure PP matrix, wood flour and 90° fiber orientation showed a poor performance on the mechanical properties. Sheet molding compound (SMC) contained 25% fiberglass provided by Meridian Automotive Systems Inc. Even though the matrix was polypropylene, randomly-oriented kenaf-fiber reinforcement provided an equal or higher enhancement of NPC compared to fiberglass reinforcement in polyvinyl ester resin. The differences between the two matrices were behaviors during the mechanical failure of composites. SMC products showed linear behavior to failure, while NPC behavior was linear to curvilinear during the mechanical test.

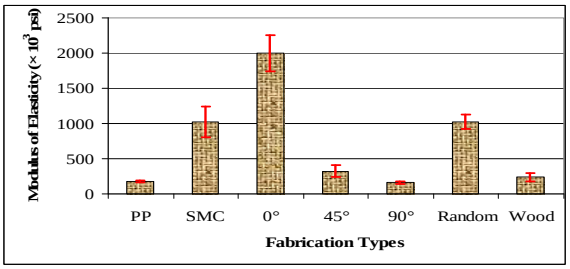

(a)

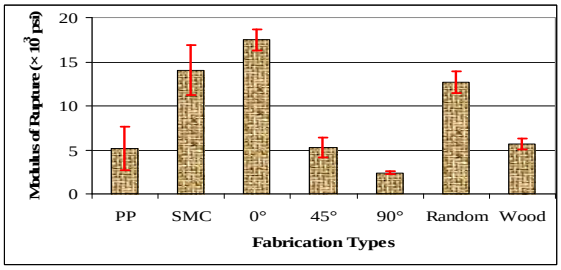

(b)

Figure 20. Flexural modulus and strength of kenaf fiber and PP laminates as function of the different fiber orientation with three different kenaf and PP formulations. (a= Modulus of Elasticity, b= Modulus of Rupture).

Figure 21 shows tensile strength of kenaf fiber and PP film laminates. The results of NPCs were obtained with composites fabricated with 40% kenaf fibers and 60% PP film. The tensile strength properties showed similar trends compared to flexural modulus and strength. The highest tensile strength was obtained with the 50% kenaf content in the polymer composite system with 0° fiber orientation. From the mechanical test results, it is encouraging to see that the randomly-oriented kenaf-fiber reinforcement has potential to provide equivalent properties to the fiberglass/polyvinyl ester composites with the current lab compression-molding process.

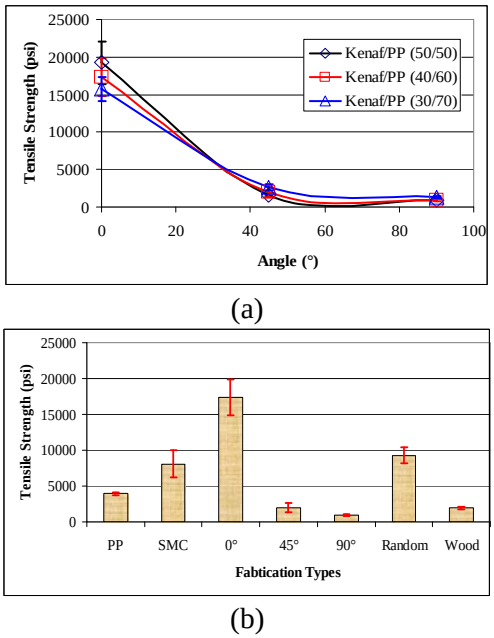

Figure 21. Tensile strength of kenaf fiber and polypropylene laminates. (a= tensile strength at the different fiber orientation, b= comparisons between fabrication types --- fiber and matrix ratio = 40% kenaf/60% PP).

Thermal Properties of kenaf/PP Formulations

Thermal characteristics of the prepared kenaf and PP formulations were evaluated by TGA-DSC. Results are summarized in Table 8. Polymer melting and maximum crystallization points with the addition of kenaf fibers initiated earlier than the pure PP formulation. Increased crystallization peak temperatures were observed when the fibers were incorporated in the polymer matrices. This increment could be more sensible when the fibers are chemically and physically modified. Thus, the fiber reinforcement influenced thermal histories of the PP polymer such as increased heat flow and delayed polymer relaxation. The thermal property changes resulted in higher enthalpy in both melting and crystallization. The increased heat of fusion and earlier induction of PP crystallization can be explained by the increased nucleation ability and crystallinity of the polymer matrices on the surface of retted kenaf fibers.

Table 8. Thermal characteristics of kenaf fiber and polypropylene formulations.

	Heating			Cooling		
	Onset Temp.	Peak Temp.	Enthalpy	Onset Temp.	Peak Temp.	Enthalpy
	°C	°C	µV·s/mg	°C	°C	µV·s/mg
PP only	153.0	166.3	24.5	122.3	116.9	25.5
Kenaf/PP (50/50)	154.9	165.3	37.9	127.1	120.9	42.2
Kenaf/PP (40/60)	154.2	165.0	37.7	126.7	120.0	35.2
Kenaf/PP (30/70)	153.1	164.9	53.1	127.1	120.5	57.9

Fractural Morphology at the Interface

A SEM examination of fracture surfaces at the thermoplastic and kenaf fiber interface is shown in Figure 22. The figure clearly shows that there was relatively uniform fiber distribution in the PP matrix and polymer melt flow among the reinforced kenaf fibers. As the fiber content increases, the concentration of fibers is also increased. The figure also suggested that the fracture process appeared to have been dominated by a shear failure mode. Here, a considerable number of fibers and matrix exposure without bonding are in evidence to indicate a poor interaction between both materials. Fracture surfaces of the kenaf-fiber/polypropylene composites revealed inter-laminar crack propagation at the hydrophobic and hydrophilic interface. The kenaf fibers oriented along the fiber direction (Figure 22 (a)) were pulled out from the brittle matrix.

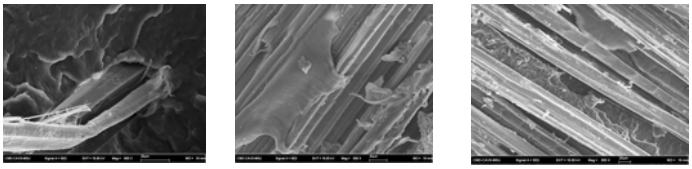

(a) (b) (c)

Figure 22. Fractural morphology of kenaf bast fibers and polypropylene laminates. (fiber orientation angles of a= 0°, b= 45°, and c= 90°).

The other two orientations clearly showed interfacial failure and separation at the interface. The fiber bundles oriented as 45° angles were covered by the molten PP polymer matrix, and failure occurred at the interface with stretched matrix under shear loads. Most failure at the interface and matrix itself were observed with the fiber oriented perpendicular to the fiber direction. Therefore, fracture macrographs indicated a weak interaction and incompatibility at the fibers and PP matrix interface.

Conclusions

This study investigated the effect of fiber orientation on the mechanical properties of laminates, kenaf-bast-fiber characteristics, and thermal/interfacial characteristics at the kenaf-fiber and polymer interface. Fibers from the middle section of the kenaf stem showed relatively smooth surfaces and strengths comparable to those of fibers from other sections. The mechanical properties (MOE, MOR and tensile strength (TS)) were increased as the fiber orientation angle decreased. Randomly-oriented kenaf-fiber reinforcement provided equal (random fiber orientation) or better (0° fiber orientation) property enhancement to fiberglass reinforcement into polyvinyl ester resin. Thermal properties were also altered with the presence of different weight fractions of kenaf fibers in the PP matrix. Fracture macrographs indicated a week interaction between the fibers and PP matrix.

References

1. Arzondo, L.M., A. Vazquez, J.M. Carella, and J.M. Pastor. 2004. A low-cost, low-fiber-breakage, injection molding process for long sisal fiber reinforced polypropylene. Polym Eng Sci 44(9):1766-1772.
2. Bledzki, A.K., H.P. Fink, and K. Specht. 2004. Unidirectional hemp and flax EP- and PP-composites: influence of defined fiber treatments. J. Appl. Polym. Sci. 93(5):2150-2156.
3. Clemons, C. 2002. Wood plastic composites in the Unite States; the interfacing of two industries Forest Products J. 52(6):10-18.
4. Eichhorn, S.J., C.A. Baillie, N. Zafeiropoulos, L.Y. Mwaikambo, M.P. Ansell, A. Dufresne, K. M. Entwistle, P.J. Herrera-Franco, G.C. Escamilla, L. Groom, M. Hughes, C. Hill, T.G. Rials, and P.M. Wild. 2001. Review current international research into cellulosic fibres and composites, J. Mater. Sci. 36:2107–2131.
5. Feng, B., D.M. Cao, W.J. Meng, J. Xu, R.C. Tittsworth, L.E. Rehn, P.M. Baldo, and G.L. Doll. 2001. Characterization of microstructure and mechanical behavior of sputter deposited Ti-containing amorphous carbon coatings. Surface Coatings Tech. 148(2-3):153-162.
6. Joseph, K., S. Thomas, C. Pavithran, and M. Brahmakumar. 1993. Tensile properties of short sisal fiber-reinforced polyethylene composites. J. Appl. Polym. Sci. 47:1731-1739.
7. Joseph, P.V., K. Joseph, S. Thomas, C.K.S. Pillai, V.S. Prasad, G. Groeninckx, and M. Sarkissova. 2003. The thermal and crystallisation studies of short sisal fibre reinforced polypropylene composites. Composites: Part A. 34:253–266.
8. Karnani, R., M. Krishnan, R. Narayan. 1997. Biofiber-reinforced polypropylene composites. Polym. Engin. Sci. 37(2):476-483.
9. Rana, A.K., A. Mandal, B.C. Mitra, R. Jacobson, R. Rowell, and A.N. Banerjee. 1998. Short jute fiber-reinforced

polypropylene composites: effect of compatibilizer. J. Appl. Polym. Sci. 69:329-338.
10. Sellers, T. and N.A. Reichert. 1999. Kenaf Properties, Processing and Products. Mississippi State University, Ag & Bio Engineering, Starkville. 532 p.
11. Sanadi, A.R., J.F. Hunt, D.F. Caulfield, G. Kovacsvolgyi, and B. Destree. 2002. High fiber-low matrix composites: kenaf fiber/polypropylene. In: 6th Intern. Conf. on woodfiber-plastic composites. Madison, Wisconsin. pp.121-124.
12. Serizawa, S., K. Inoue, M. Iji. 2006. Kenaf-fiber-reinforced poly (lactic acid) used for electronic products. J. Appl. Polym. Sci. 100:618–624.
13. Tajvidi, M., R.H. Falk, and J.C. Hermanson. 2005. Time-temperature superposition principle applied to a kenaf-fiber/high-density polyethylene composite. J. Appl. Polym. Sci. 97:1995-2004.

Acknowledgement

The authors would like to thank Dr. Leslie H. Groom and Dr. Thomas Elder, USDA-Forest Service Southern Research Station, Pineville, LA for Instrumental Support.

Presentations/Publications/Patents

1. Publication - Lee, S., S.Q. Shi, and Y. Xue. 2007. Thermal and mechanical properties of unidirectional natural fiber-polyolefin laminates. ***Paper in preparation.***
2. Presentation - Unidirectional natural fiber-polyolefin laminates: thermal and mechanical properties. 61st International Convention, Forest Products Society, Knoxville, Tennessee, USA. June 10-13, 2007.
3. Presentation - Unidirectional natural fiber-polyolefin laminates: thermal and mechanical properties. 9th International Conference on Wood and Biofiber Plastic Composites. Monona Terrace Community and Convention Center. Madison,Wisconsin, USA. May 21-23, 2007.

Micromechanical Simulation on Hygro-Mechanical Properties of Woodfiber-Reinforced Plastic Composites

Team Members: Kungpeng Wang, Yibin Xue, Hongwu Zhang, Mark Horstemeyer

Introduction

Woodfiber-reinforced composites (WRCs) have received considerable attention in the forest-product industry for engineering applications like automotive panels. They show many potential merits such as increased durability of woods, low maintenance during service, low cost, and ease of fabrication using traditional plastic/composite processing techniques (Rowell et al. 1998, Rowell 1998). To assess its potential as an engineering structure, a better understanding of the mechanical performance of woodfiber-reinforced composites is vital. Woodfiber, as a kind of natural material, is sensitive to changes of environment such as moisture; therefore, understanding the influence of MC on woodfiber composites is critical. The aim of this work is to predict the elastic properties of woodfiber-reinforced composites using micromechanical approaches in which fiber volume fraction (FVF), fiber distribution, and MC are incorporated.

Micromechanical simulations can be used to obtain an overall behavior of woodfiber composites when the properties of constituents are known (woodfiber and matrix). Typical simulations are conducted based on a representative volume element (RVE) or a unit cell (Aboudi 1991, Nemat-Nasser and Hori 1993). Some empirical and semi-analytical methods have been developed to predict the effective material properties of composites (Xue et al. 2007), and were applied to specific cases. Knowing the limit of analytical methods and the recent advances of computational efficiency, numerical methods such as finite-element modeling (FEM) have been utilized to predict the mechanical performance of composites.

In the micromechanical approach to predict the effective elastic properties of woodfiber-reinforced composites, one of the key issues is the selection of a proper size of RVE necessary to

capture all prominent features of the entire composite of interest. Drugan and Willis (Drugan and Willis 1996) stated that the minimum size of a RVE is the smallest volume element of the composite that is at least twice the diameter of the reinforcement. They also indicated that the maximum error is about five percent in elastic constants obtained from this minimum RVE size.

The mechanical response of a composite material can be effectively simulated by applying periodic boundary conditions to a single RVE (Segurado and Llorca 2002). When periodic boundary conditions are applied to a macroscopic composite, deformation within each RVE is identical and deformation along each RVE boundary/edge is compatible.

In the present research work, woodfiber-reinforced composite is considered as a short-fiber composite. In order to investigate the mechanical performance of woodfiber composites, two three-dimensional micromechanical models with imposed periodic boundary conditions are established: 1) using single-fiber RVE to predict the effective elastic properties of composites and the effect of moisture content (MC) and 2) using two-fiber RVE to calculate the influence of the woodfiber arrangement on the effective material properties of composites.

Woodfiber-Reinforced Composite

Generally, woodfiber-reinforced composite is composed of cellulose-like fibers of wood, bamboo or straw and plastics such as a high-density polyethylene (HDPE) or polyvinylchloride (PVC). The effective properties of woodfiber composite can be expressed as linear-elastic orthotropic, assuming homogeneity in the medium,

$$\bar{\sigma}_{ij} = D_{ijkl}\bar{\varepsilon}_{kl} \quad (4)$$

in which the volume average of the local or microscopic stress σ_{ij} and strain ε_{ij} can be expressed as

$$\bar{\sigma}_{ij} = \frac{1}{V}\int_{\Omega}\sigma_{ij}d\Omega, \quad \bar{\varepsilon}_{ij} = \frac{1}{V}\int_{\Omega}\varepsilon_{ij}d\Omega \quad (5)$$

where Ω denotes the domain of the RVE and V is the volume of RVE. The superscript bar denotes the volume average of a quantity, e.g., macroscopic or effective quantity.

Material Properties of Constituents of Woodfiber-Reinforced Composite

Elastic Properties of Woodfiber

It is well known that woodfiber is, in general, elastic and orthotropic in the longitudinal, radial and tangential directions of wood and has nine independent elastic constants, which can be denoted as elastic moduli (E_L, E_R, E_T), shear moduli (G_L, G_R, G_T) and Poisson's ratios (ν_{LR}, ν_{LT} and ν_{RT}), in which *L* denotes the longitudinal direction parallel to the fibers, *T* means tangential to the growth rings in the cut section and *R*, radial, perpendicular to the growth rings in the cross-section. Woodfiber, hydrophilic in nature, is prompted to absorb and desorb water when the environmental moisture contents (MCs) change. The elastic properties of wood are affected adversely by MC. In this research, Sikta spruce is chosen as the woodfiber whose properties are shown as a function of moisture contents in Table 9.

Table 9. The material properties of Skita spruce at various moisture content (Carrington 1922).

MC (%)	1	5	10	15
E_L (MPa)	13556.0	13591.0	13282.0	12742.0
E_R (MPa)	822.6	832.2	743.6	605.3
E_T (MPa)	504.7	463.8	411.0	344.5
G_{LR} (MPa)	699.7	734.7	706.9	655.3
G_{LT} (MPa)	614.2	613.0	575.4	514.9
G_{RT} (MPa)	23.8	22.7	20.8	18.7
ν_{LR}	0.363	0.355	0.344	0.329
ν_{LT}	0.507	0.517	0.558	0.616
ν_{RT}	0.501	0.483	0.516	0.574

It is worth noting that, for simplicity, the influence of the growth ring's direction is neglected. The local cylindrical coordinates of woodfiber, T, R and L, convert to the global coordinates, 1, 2 and 3 in the present work.

Material Properties of Matrix

HDPE, of relatively high strength and easy machinability, is used as the matrix. HDPE is considered to be isotropic. The elastic properties of HDPE are Young's modulus, $E = 641\text{MPa}$, and Poisson's ratio, $\nu = 0.41$ (Li 2001).

In the woodfiber-reinforced composites evaluated, the orthotropic fibers are embedded unidirectionally in an isotropic matrix. The resulting composite is also an orthotropic material, whose properties can be calculated by the method as described in the next section.

Numerical Solution with FEM

Representative Volume Element (RVE)

One of the most powerful tools used to speed up the modeling process, both the composite discretization and the computer simulation of composites in real conditions, is the homogenization method (Aboudi 1991, Nemat-Nasser and Hori 1993). The main idea of the method is to find a globally-homogeneous medium equivalent to the original composite, where the strain energy stored in both systems is approximately the same. In general, the object under consideration is regarded as a large-scale/macroscopic structure. The common approach to modeling the macroscopic properties of three-dimensional (3D) woodfiber-reinforced composites is to create a RVE that captures the major features of the underlying microstructure. Woodfiber composite can be considered as a short-fiber composite, which is composed of short fragments of woodfibers and a polymer-matrix material. Schematic views of unidirectional-woodfiber composite (a) and the RVE (b), that is selected as the simplest form of (a), are illustrated in Figure 23.

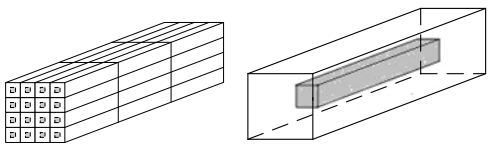

(a) (b)

Figure 23. (a)The microstructure of periodic woodfiber-reinforced composite; (b) A RVE for (a), where □ - matrix, ▨ - woodfiber.

In this work, a static analysis of periodic structures with perfectly-bonded condition between woodfibers and matrix is performed. Assuming symmetric boundary conditions exist, a regular woodfiber-reinforced composite will be analyzed by using a RVE approach, imposed with periodic boundary conditions.

Periodic Boundary Condition

Composite materials can be represented as an array of periodic RVEs, which are the smallest volume that contains sufficient information of geometrical and material parameters at the microscopic level. To obtain the effective properties of composites, periodic boundary conditions must be applied to the RVE to ensure that deformation-compatible results and that stress and strain are correctly computed. Thus, displacements that need to be applied to a uniform strain field in a corresponding homogeneous composite are given by the equation below (Suquet 1987)

$$u_i = \varepsilon_{ij}^0 x_j \qquad i, j = 1,2,3 \tag{6}$$

where u_i is the prescribed displacement at some large distance, x_j is a position vector from a reference point to a point on the boundary, and ε_{ij}^0 is the applied average strain in the composite array.

Finite-Element Modeling

In this work, all calculations were conducted using the ABAQUS FEM package. To obtain homogenized effective properties, the periodic boundary conditions, Equation (6), were applied to all the six faces of the RVE by coupling opposite nodes on opposite boundaries. To utilize these periodic boundary conditions by ABAQUS FEM, meshes on the opposite boundary surfaces must be the same. On each nodal pair, a constraint condition (periodic boundary condition) was imposed on its displacements. Because numerous constraints should be applied on the opposite boundary surfaces, it was very difficult to implement constraints in ABAQUS manually. A FORTRAN program, which generated all required constraint conditions automatically, was developed. Element C3D8R in ABAQUS was used.

Numerical Results and Discussion

Effect of Fiber Volume Fraction (FVF) on the Effective Elastic Properties of Composites

Primary interest to material designers and engineers is the effect of FVF on the effective material properties. To investigate that, a RVE, as shown in Figure 24, was developed, which includes a single woodfiber of an elongated cubic shape, $f_1 \times f_2 \times f_3 = 1 \times 1 \times 10\,\mathrm{mm}^3$ and the RVE size is $L_1 \times L_2 \times L_3 = (f_1 + 2d) \times (f_2 + 2d) \times (f_3 + 2d)$ in which *d* can be considered as a parameter to determine the FVF. Table 10 gives the relation between FVF and *d*. The material properties of woodfiber were chosen at 5% MC as shown in Table 9. Appling the periodic boundary conditions stated previously, the effective material moduli of the RVE could be obtained, as illustrated in Figure 25 (a-c), in which the effective material properties of composites at 0% and 100% FVF correspond to the material properties of HDPE and woodfiber, respectively.

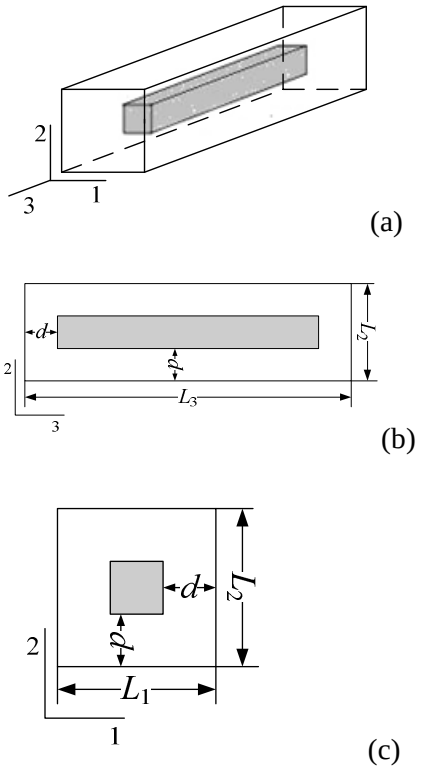

Figure 24. (a) The sketch of RVE for predicting the effective material properties of woodfiber composite; (b) The projection at Plane 2-3; (c) The projection at Plane 1-3.

Table 10. The relation between fiber volume fraction and *d*.

d (mm)	FVF (%)
1.0	9.26
0.5	22.73
0.2	49.06
0.1	68.08
0.0	100.00

With the increase of FVF, the effective material properties of woodfiber-reinforced composites trend to the material properties of woodfiber. It clearly shows the effect of the change in FVF on the effective material properties of composites, and woodfiber as an inclusion changes the properties of composites greatly.

The approach used in this work has been used successfully in (Berger et al. 2005) for predicting the effective material properties of long-fiber, unidirectional composite. Because the aspect ratio of woodfiber is relatively high, we expect the material properties of this composite to be similar to the properties of long-fiber composites. The material properties of a long-fiber composite, made of the same matrix and woodfiber, are illustrated in Figure 25 to validate this approach. It shows good agreements between the analytical long-fiber properties and the finite element analysis (FEA) simulation results. Therefore, the approach presented is suitable for predicting the material properties of short-fiber composites, i.e., woodfiber-reinforced composites.

Effect of Moisture Content on the Effective Elastic Properties of Composites

Woodfiber is sensitive to the variation of MC. The changes of effective elastic coefficients of woodfiber-reinforced composites by MC are calculated in this section. Since FVFs in the range of 50% to 70% are of great interest to the composite designers, the same RVE with d=0.2 mm (FVF=49.06%), as used in the previous section, was chosen for investigating the influence of moisture content. Due to hydrophobicity of the matrix, HDPE, the elastic properties of HDPE are assumed not to be affected by its MC. Since the woodfibers are surrounded with the matrix, HDPE, its MC would not go beyond its FSP. Therefore, only Fick's-law diffusion was

considered in the moisture-diffusion study. The elastic properties of woodfiber at 1%, 5%, 10% and 15% MC, as listed in Table 9, were used in this present research. Following the method described previously above, the effective elastic moduli of woodfiber-reinforced composite, as a function of MC, were obtained and shown in Figure 26 (a-c).

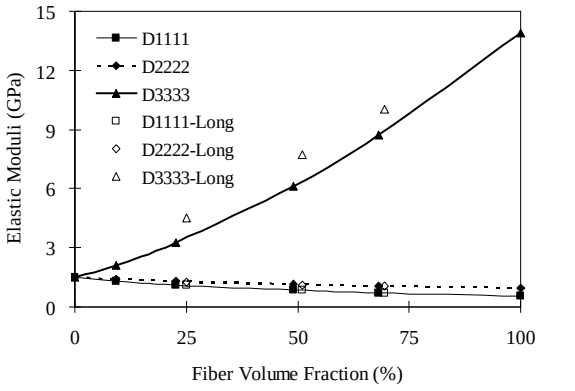

(a)

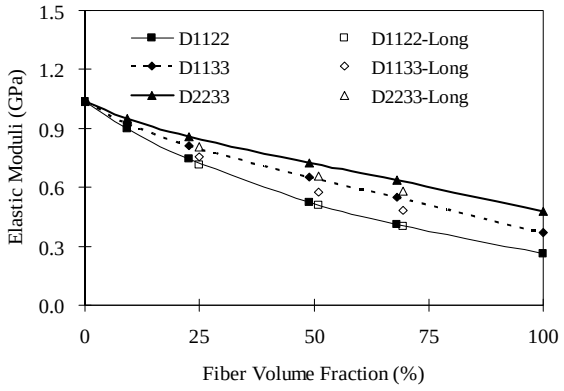

(b)

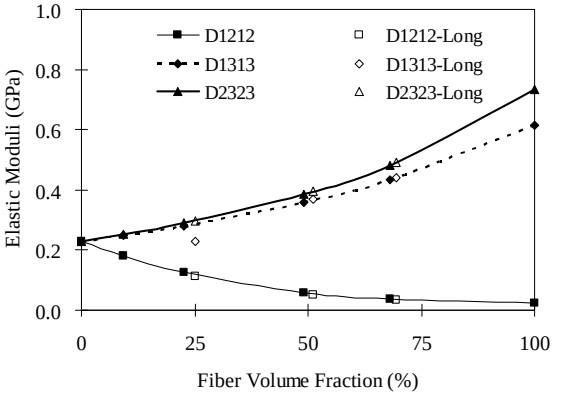

(c)

Figure 25. Effective material moduli of WPCs as a function of FVF.

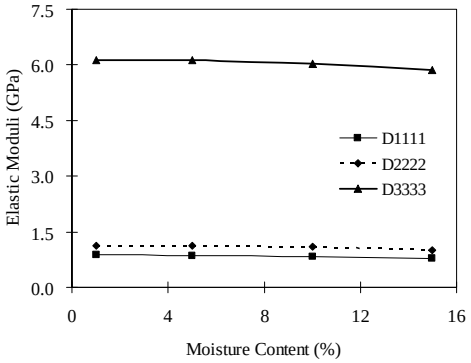

(a)

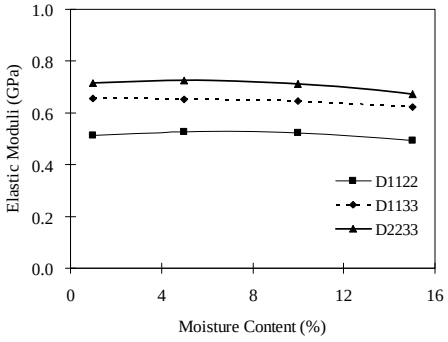

(b)

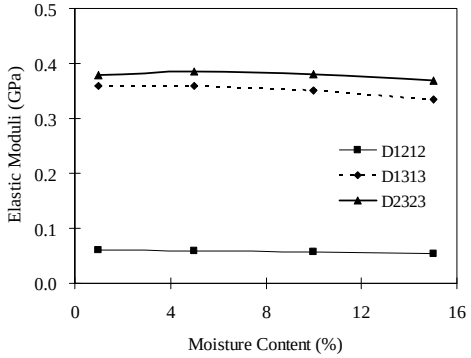

(c)

Figure 26. Effective material moduli of a WPC with 50 % fiber volume fraction as a function of moisture content.

As shown in Figure 26, the strength of woodfiber-reinforced composite is weakened slightly with the increase of woodfiber MC; the woodfiber-reinforced composites are relatively insensitive to moisture.

Effect of Woodfiber Arrangement on the Effective Elastic Properties of Composites

Woodfiber-reinforced composite, as one kind of short-fiber-reinforced composite, could have complex interactions between fibers. The effect of woodfiber arrangement on the effective material properties of composites is very important to the composite designer. In the past, most common models used were with square fiber arrangement, hexagonal fiber arrangement and random fiber distributions. In this work, an offset model was proposed based on the model with square fiber arrangement, as shown in Figure 23 (a). As shown in Figure 27 (a), the RVE included two complete fibers paralleled along the direction of the 2-axis in the Cartesian coordinate. The offsets might occur in the longitudinal direction (the 3-direction) or transverse direction (the 1-direction) as illustrated in Figure 27 (b-c). The material properties of matrix and woodfiber given previously above were used here. The RVE size was defined by three constants: $L_1 = f_1 + 2d$, $L_2 = 2L_1$, and $L_3 = f_3 + 2d$, in which *d* is a parameter to control FVF. To express the influence of fiber offsets clearly, relations between the deviation of effective moduli and the offset ratio were obtained, in which the offset ratio was defined as the ratio between the offset quantity, W_3 or W_1, and a length of composite RVE, L_3 or L_1, and the deviation of effective moduli were normalized with respect with the quantities of the zero offset. In this section, d=0.2 mm (FVF=49.06%).

Figure 28 and Figure 29 (a-c) illustrate the effective material properties of composites as a function of transverse and longitudinal offsets. The influence of offset on material properties of composites, no matter whether it is in transverse or longitudinal direction, is within 15%. Because the aspect ratio of woodfiber is fixed, the influence of longitudinal offset is relatively smaller than the effect of transverse offset on the effective material properties of woodfiber-reinforced composites.

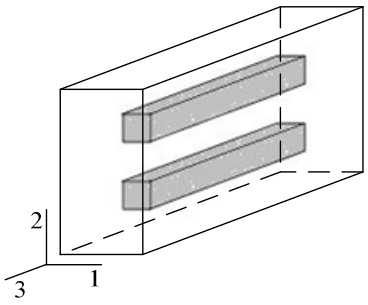

(a)

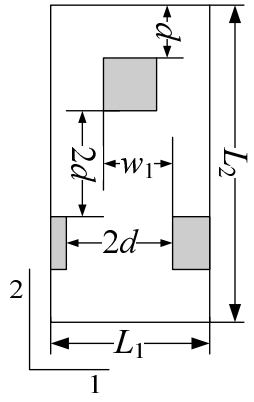

(b)

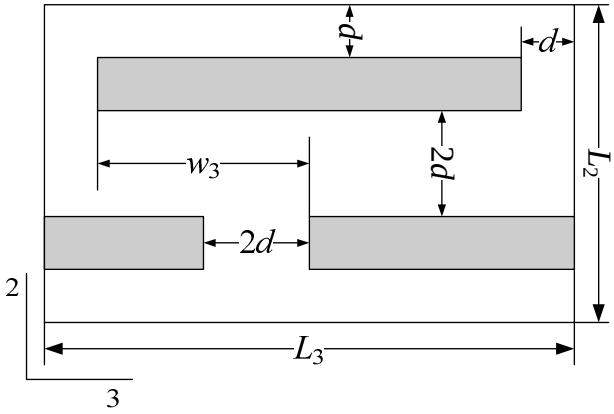

(c)

Figure 27. (a) A sketch of RVE for evaluating the influence of woodfiber arrangement. (b) The projection at Plane 1-2. (c) The projection at Plane 2-3.

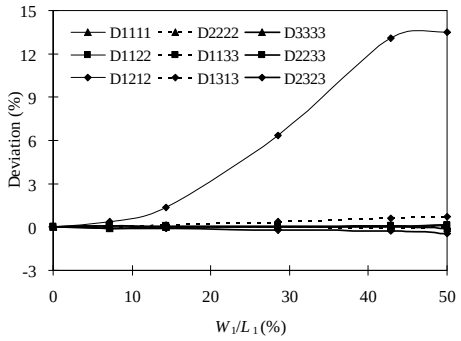

Figure 28. The deviation of effective material moduli of a WPC with 50 % FVF as a result of the fiber offset along the transverse direction. There is almost no significant dependency except D_{1212}.

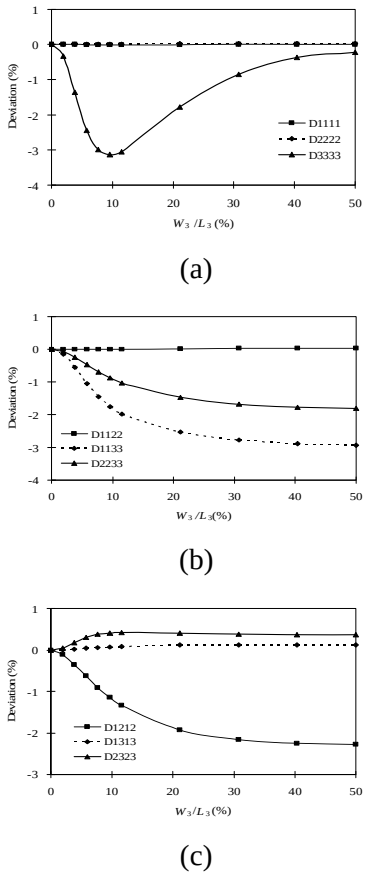

Figure 29. The deviation of effective material moduli of a WPC with 50 % fiber volume fraction as a result of the fiber offset along the longitudinal direction, which demonstrated significant dependency on the fiber offset distance.

Conclusions

A numerical approach for predicting the effective elastic properties of unidirectional woodfiber-reinforced composites has been developed using micromechanical simulations. The effective orthotropic coefficients of woodfiber composites were calculated by imposing periodic boundary conditions on a RVE. It is observed that FVF affects the effective material properties of woodfiber-reinforced composites strongly, while the effect of moisture content has slight impact on the effective properties of woodfiber composites. In the short-woodfiber-reinforced plastic composite, the interactions between fibers are more complex than long-fiber composites. The woodfiber arrangement will affect the effective properties of woodfiber composites: when the aspect ratio of woodfiber is relatively large, the influence of transverse offset on the effective elastic properties of composites is relatively larger than the longitudinal offset.

References

1. Aboudi, J. 1991. Mechanics of Composite Materials. A Unified Micromechanical Approach. Elsevier Science Publishers. Amsterdam.
2. Berger, H., Kari, S., and Gabbert, U. 2005. An analytical and numerical approach for calculating effective material coefficients of piezoelectric fiber composites. International Journal of Solids and Structures. 42(21-22): 5692-5714.
3. Carrington, H. 1922. The elastic constants of spruce as affected by moisture content. Aeron. J. 26:462-471.
4. Drugan, W., and J. Willis. 1996. A micro mechanics-based non local constitutive equation and estimates of representative volume element size for elastic composites. Journal of the Mechanics and Physics of Solids. 44: 497-524.
5. Li, R. 2001. Effect of flake distribution on elastic properties of flake composites. Journal of Composite Materials. 35: 1529-52
6. Nemat-Nasser, S., and M. Hori. 1993. Micromechanics: Overall Properties of Heterogeneous Materials. Elsevier Science Publishers. Amsterdam.

7. Rowell, R.M., D.F. Caulfield, and G. Chen. 1998. Recent advances in agro-fiber/thermoplastic composites. *In*: Proceedings of the second international symposium on natural polymers and composites, Atibaia, Brazil. pp. 11–20.
8. (not called) Rowell, R.M. 1998. Economic opportunities in natural fiber–thermoplastic composites. *In*:. Science and technology of polymers and advanced materials. Plenum Publishing Corp., New York. pp. 869–72.
9. Segurado, J., and J. Llorca. 2002. A numerical approximation to the elastic properties of sphere-reinforced composites. Journal of the Mechanics and Physics of Solids. 50:2107-2121.
10. Suquet, P. 1987. *In*: Homogenisation Techniques for Composite Media. Springer-Verlag. Berlin. pp. 194-275.
11. Xue, Y., Veazie, D.R., Glinsey, C., Horstemeyer, M.F., Rowell, R.M. 2007, Environmental Effects on the Mechanical and Thermomechanical Properties of Aspen Fiber-Polypropylene Composites, Composites B: Engineering, 38:152-58.

Acknowledgement

The Mississippi State University authors would like to express appreciation for the support of the US Department of Energy and the Center for Advanced Vehicular Systems at Mississippi State University.

Presentations/Publications/Patents

1. Presentation - X Kungpeng Wang, Yibin Xue, Hongwu Zhang, and Mark Horstemeyer. Micromechanical Simulation on Hygro-Mechanical Properties of Woodfiber-Reinforced Plastic Composites. The 9th International Conference on Wood & Biofiber Plastic Composites, May 21-23, 2007, Madison, WI.

H. Interphase Analysis and Control in Fiber Reinforced Thermoplastic Composites

Principal Investigator: Jon J. Kellar
Department of Materials and Metallurgical Engineering
South Dakota School of Mines and Technology
501 E. St. Joseph Street
Rapid City, SD 57701-3901
605-394-2343, 605-394-3369, jon.kellar@sdsmt.edu

Technology Area Development Manager: Joseph A. Carpenter
(202) 586-1022; fax: (202) 586-1600; e-mail: joseph.carpenter@ee.doe.gov

Field Project Officer: Aaron D. Yocum
(304) 285-4852; fax: (304) 285-4403; e-mail: aaron.yocum@netl.doe.gov

Expert Technical Monitor: Philip S. Sklad
(865) 574-5069; fax: (865) 576-4963; e-mail: skladps@ornl.gov

---

Contractor: South Dakota School of Mines and Technology
Contract No.: DE-FG02-04ER46117

Objectives

- Develop the science underlying the formation and effects of transcrystalline regions in carbon fiber reinforced thermoplastic matrix composite systems.
- Exploit the understanding developed from the research described above to allow controlled tailoring of the interphase transcrystallinity for specific applications.
- Analyze processing parameters in new thermoplastic matrix composite technologies, specifically the DRIFT (**D**irect **Rei**nforcement **F**abrication **T**echnology, Southern Research Institute/University of Alabama-Birmingham) and the P4 (**P**rogrammable **P**owered **P**reform **P**rocess, Department of Energy (DOE)/Oak Ridge National Laboratories (ORNL)) processes.
- Generate composites with tailored interphases for specific applications of laminates produced by the DRIFT and P4 processes in the FreedomCAR and other DOE initiatives in lighter weight vehicles.

Approach

- Choose matrix materials relevant to the FreedomCAR and DOE automotive lightweight materials initiatives.
- Characterize the chosen matrix materials with respect to mechanical properties and crystallinity.
- Determine the thermodynamic and practical adhesion between the chosen matrix materials and carbon fibers. The carbon fibers will be both sized and unsized.
- Identify and control the presence and size of transcrystalline regions in the matrix material adjacent the carbon fibers.
- Manufacture laminates using the DRIFT and P4 processes having controlled transcrystalline regions.
- Perform mechanical testing, including tensile testing, impact testing and indentation testing of the laminates having controlled interphases.

Accomplishments

- Finalized design and build of a compact, laboratory-scale DRIFT machine.
- Completed an operator's manual for the DRIFT machine.
- Conducted preliminary testing with the DRIFT machine for the following fiber/matrix systems: E-glass/polypropylene (PP), Kevlar®/nylon, pitch/PP, PAN/PP.
- Batch samples (pitch/PP, PAN/PP) for detailed analysis were produced.
- Samples were examined using optical and scanning electron microscopy (SEM).
- SDSM&T research team held two Access Grid meetings with Mr. Robert Norris from ORNL.

Future Direction

- Manufacture tape laminates with fibers other than unidirectional carbon fibers. This will include Kevlar® and glass fibers and multi-directional fabrics.
- Manufacture tapes suitable for use, after further preparation, in the P4 process at ORNL.
- Optimize the manufacture of composite tapes with PAN carbon fibers in a manner to improve fiber dispersion.

Introduction

Over the past decade considerable effort has been expended to develop a new generation of vehicles that are lighter and more fuel-efficient than today's vehicles. In addition, these vehicles should retain crashworthiness and be of relatively low cost. Targets include reduction in overall weight of approximately 40%, primarily achieved through lighter body and chassis materials. Polymer matrix composites (PMCs) have reached this target with a potential weight savings of 70%. At the current time, PMC technology has, in general, been deemed too costly, as carbon fiber based PMCs can cost ten times as much as steel parts. Some of this increased cost is due to the high price of carbon fibers and some due to limitations in the manufacturing process. Many of the problems in the manufacturing process are caused or exacerbated by lack of fundamental scientific knowledge of the interactions between the fibers and matrix materials.

This research is of significance to the DOE Automotive Lightweighting Materials Program in that it will help develop the necessary science base to allow more complete exploitation of PMCs having thermoplastic matrices. Traditionally, these materials have trailed the use of PMCs having thermosetting matrices, because of processability issues stemming from the low viscosity and wetting of the thermoplastic matrix material. In addition, thermoplastic matrices are generally less strong and less stiff than thermoset matrices. This liability is further compounded by the fact that most fiber reinforcements associated with thermoplastic matrix PMCs are of fairly short length, mainly because of the processing limitations mentioned earlier. This latter aspect is relevant because short fiber reinforcements do not carry load as well as long or continuous fiber reinforcements. From the automotive perspective, short fiber reinforced PMCs are therefore most utilized in non-structural components. Further comparisons between thermoplastic and thermoset matrix PMCs are warranted here to highlight the focus of this research project, namely the role of the interface / interphase region between the fiber and the matrix.

The development of the interphase in thermoplastic PMCs is quite different from that of thermosetting matrices, which tend to be amorphous in nature. Rather, in thermoplastic PMCs, the interphase development is generally due to nucleation and growth of crystallites from the fiber surface rather than actual chemical reactions within the interphase. The interphases formed in these systems are termed transcrystalline regions, reflecting their dependence upon the thermoplastic crystallinity. There has been much speculation in the literature as to the cause for the formation of the transcrystalline region and its role in bulk composite properties. Several conclusions can be reached. First, the transcrystalline region can grow in size to tens of microns, depending upon such parameters as fiber type, morphology and fiber surface treatments such as sizings. Second, the transcrystalline region can significantly affect properties such as the strength and impact

resistance. Also, in some cases different types of transcrystalline interphases may be formed. For instance, both α and β transcrystalline regions were produced around natural fibers in polypropylene matrix composites. These regions could be altered by inclusion of maleic anhydride in the polypropylene or on the fiber.

With respect to these novel processing routes, two examples are of particular interest to this research. The first is a low-cost process to produce continuous reinforcing fibers with thermoplastic matrices, called the **D**irect **Rei**nforcement **F**abrication **T**echnology (DRIFT) developed by the Southern Research Institute (SRI) and now located at the University of Alabama-Birmingham (UAB). PMCs produced by this continuous fiber technology could serve as metal-replacements in structural applications, specifically for the automotive industry. Keys to optimal utilization of the DRIFT process are fiber wetting, and ultimately adhesion, of the thermoplastic matrix. Traditionally, sizings are applied to the fibers to help prevent abrasive damage, and assist with lubrication. A major component of the sizing is a coupling agent that aids in wetting, adhesion and hydrothermal stability of the composite. Research conducted in this program will utilize thermoplastic matrix PMCs produced by UAB or in-house using the DRIFT process. The second novel processing route of interest is the **P**rogrammable **P**owered **P**reform **P**rocess (P4). While the P4 technology does allow control over fiber length, its main potential benefit is its ability to circumvent previous PMC process limitations through robotic control. To our knowledge, no fundamental analysis of PMC interphases formed by the P4 technology has been undertaken.

This research program builds upon a multi-disciplinary effort with a strong background in interphase analysis and control in thermosetting PMC systems, and applies this experience to new thermoplastic matrix PMC systems critical to the future success of the Lightweight Materials Program. The research investigates model systems deemed of interest by members of the Automotive Composites Consortium (ACC) as well as samples at the forefront of PMC process development (DRIFT and P4 technologies). Finally, the research investigates, based upon the fundamental understanding of the interphases created during the fabrication of thermoplastic PMCs, the role the interphase play in key bulk properties of interest to the automotive industry.

Project Deliverables

This research will provide a better understanding of the science, particularly with respect to adhesion, of thermoplastic matrices with fiber reinforcements. The adhesion data will be used to identify processing parameters for thermoplastic matrix composites to tailor transcrystalline interphase formation. Transcrystalline interphases are often quite large (>10 microns) and can be stronger and stiffer than the matrix material or tougher and with greater work of fracture than the matrix. In addition, this work will produce composite samples using new processing technologies and the scientific knowledge gained with respect to adhesion and interphase formation. These test protocols are important to possible end uses for the tailored PMCs in automotive applications.

Accomplishments

Research accomplishments during the past year occurred primarily in the effect of transcrystallinity on composite performance area; specifically, the manufacture and testing of specimens using a custom designed mini-DRIFT machine. Progress in this area is described below.

Research on the effect of transcrystallinity on composite performance has centered on developing a miniature DRIFT machine. The goal of this mini-DRIFT research was to develop a system for producing lab-scale thermoplastic composite prepreg samples using the DRIFT process. The DRIFT process is a procedure for making continuous-fiber prepreg materials. In the process a continuous-fiber reinforcement material is drawn through a molten resin after being heated beyond the temperature of the resin. While in the resin, a shear is applied to the reinforcement material leaving substantially no voids in the prepreg material (Patent Number: 5,911,932). One of the goals of this aspect of this research is to control and monitor operating parameters and their effects on fiber wetting and material properties. The parameters to be

controlled include: fiber draw speed, fiber tension, fiber preheat temperature, resin temperature, and prepreg cooling. Two primary areas with respect to the mini-DRIFT machine were completed. One area investigated was the manufacture of the mini-DRIFT machine and the second area investigated was assessment of the product quality of the mini-DRIFT manufactured composite materials.

Mini-DRIFT Manufacture

There were three primary goals identified for this phase of the work:

1. Make the DRIFT process less "art" and more "science".
2. Make the machine of smaller scale for research purposes.
3. Allow for system adjustability for experimentation.

These goals resulted in a set of requirements for the mini-DRIFT machine. These requirements were:

1. System variables should be accurately monitored and controlled.
2. Based on available lab space, the machine should have a footprint of approximately 4 feet by 8 feet.
3. Allow for up to 20K fiber tows.
4. The machine should have the ability to heat the fibers up to ~450 ºC.
5. Allow for system flexibility and adjustment through replaceable die heads, moveable/ replaceable shear pins, and sufficient temperature operating range.

The design and manufacturing of the mini-DRIFT machine culminated in early 2008. There were five primary components to the design:

1. Extruder
2. Impregnation Tool/Tool Heating
3. Fiber Puller/Fiber Feed
4. Fiber Heating
5. Chiller

The design process for these components is described in detail in the Master of Science thesis of Mr. R.D. McGlothlen (see Reference 1). The extruder chosen was one already located at the site where the mini-DRIFT machine would be located. This extruder was a Haake PolyLab extruder as shown in Figure 1. This extruder has a maximum operating temperature of 450 ºC and maximum through- put of 5 kg/hr. Both of these meet or exceed the requirements for the DRIFT design.

The impregnation tool was designed after visiting an operating DRIFT machine at the University of Alabama-Birmingham and was made to fit the Haake extruder. Figure 2 show the impregnation tool with front face removed. The pins over which the fibers travel are adjustable to accommodate different fiber types. The tool is able to be completely taken apart for cleaning and for use of different fiber entrance and exit plates for tows of differing sizes. In addition, the tool was designed with a cartridge heating system using four heaters with temperature feedback provided by a thermocouple inserted into the center of the tool. This design feature allows the tool to be kept at the processing temperature of the molten thermoplastic material dispensed into the tool from the extruder.

The third portion of the mini-DRIFT machine is the fiber puller and feed assembly. The fiber puller chosen is shown in Figure 3 and consists mainly of pulling the fibers through two motorized, rubber-surfaced drums. The drums have an aluminum core coated in 60A durometer polyurethane. The coating provides a firm grip on the material being processed, but prevents the material from being damaged. One drum was fixed in position and the other was attached to an adjustable lever arm to allow for adjustment of the gripping force on the fibers. The stationary wheel was attached to a keyed shaft driven by a motor through a belt and pulley system to reduce the motor speed. The motor was controlled by a Genesis variable-frequency-drive, which allowed accurate control of the motor speed. The frame for the puller was constructed of 2 in. x 2 in. x 1/8 in. angle iron and bolted to the top of the steel cart on which the mini-DRIFT machine was mounted to keep from moving. The puller speed can be varied between 0.55 and 33 m/minute.
A brake system for the fiber feeding was also needed. The final brake design can accommodate fibers on any size spool. The final design involved

attaching an adjustable magnetic brake to the end of a keyed shaft. The magnetic brake unit purchased was Precision Tork™ model MC5 capable of being adjusted from 0-25 in.-lb of torque. The actual force applied by the brake unit depends on the radius of the fiber spool. With the goal of great flexibility, the brake unit was modified to accept fibers regardless of their storage system. The system was retrofitted with drums similar to the puller unit and an adjustable upper arm. Fibers were routed to the drums through a system of guides. The guide configuration used depended on the dispensing system of the fibers and was left to the discretion of the researcher. The frame for the unit was also constructed from 2 in. x 2 in. x 1/8 in. angle iron and bolted to the lower shelf of one of the carts to conserve space and to minimize fiber exposure. Fibers were routed through the system through a series of guides. Figure 4 shows the final brake design.

The next portion of the system to be designed was the fiber heating section. This variable is one of the key to the DRIFT process. The final design consisted of a tube furnace that allowed the fibers to be heated as they passed through the furnace to the opening of the impregnation tool. A Lindberg Mini-Mite tube furnace was purchased for this task and can be seen in Figure 5. The furnace has a single heating zone with a maximum operating temperature of 1100 °C and a single set point digital controller. An 18 in. long by 1 in. outer diameter alumina process-tube was placed inside the furnace. The length of the tube purchased was chosen so that the tube could extend beyond the furnace and be butted up to the impregnation tool to insulate the fibers as they passed from the furnace to the impregnation tool. The fiber guide system for the machine ensured that the fibers do not touch the walls of the process tube.

The final portion of the mini-DRIFT machine to be designed was the chiller system. The chiller system chosen is shown in Figure 6. The chiller uses two stainless steel drums with water circulating internally acting as a coolant. Water is passed through the drums through swivel joints on the ends of either drum. The drums are supported by bearings bolted to adjustable platforms, allowing the configuration of the drums to be changed for routing purposes. The system was initially cooled using only tap water. The system could also utilize a re-circulating water cooler for greater system control, although that was not done here

Figure 7 shows the assembled system used for assessment of product quality. This system meets all the requirements specified earlier.

Figure 1. Haake PolyLab extruder.

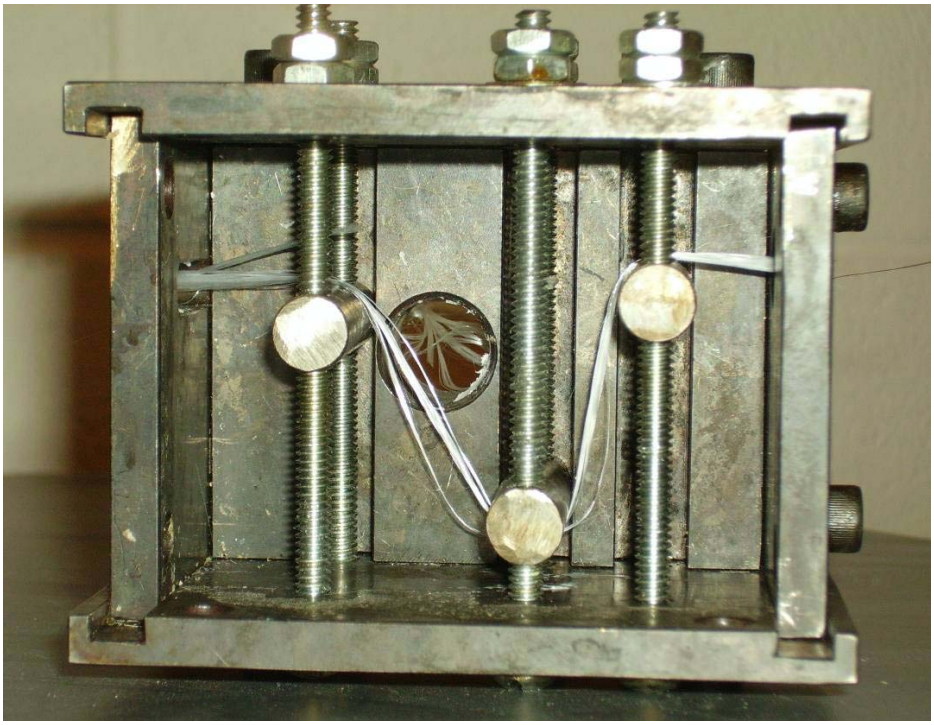

Figure 2. Impregnation tool with side plate removed showing fiber routing.

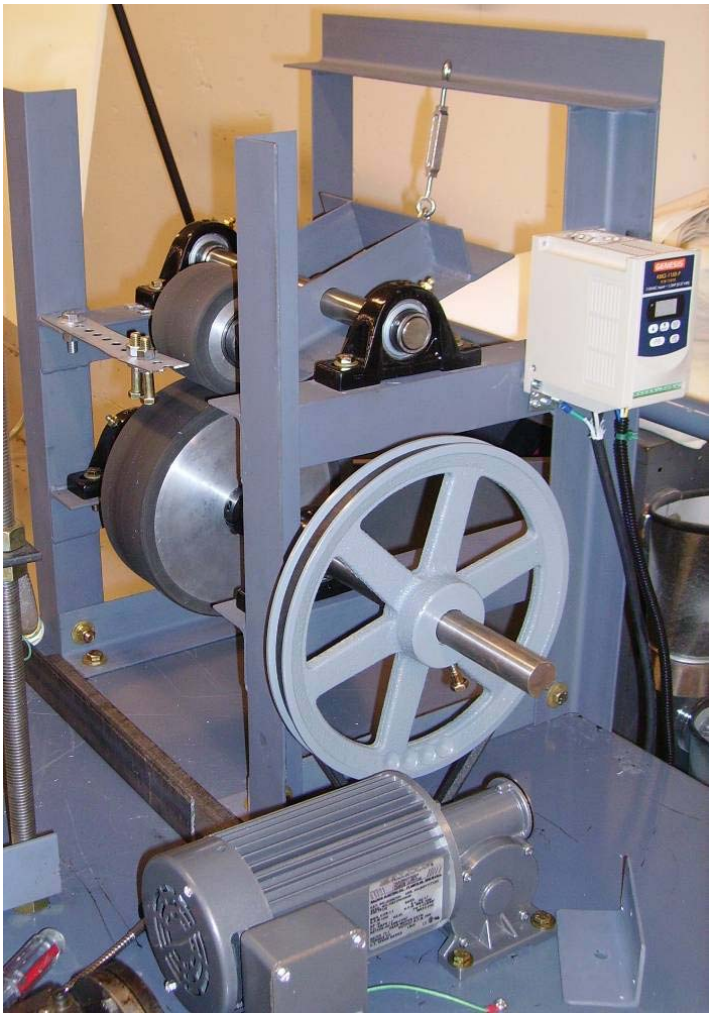

Figure 3. Completed puller system.

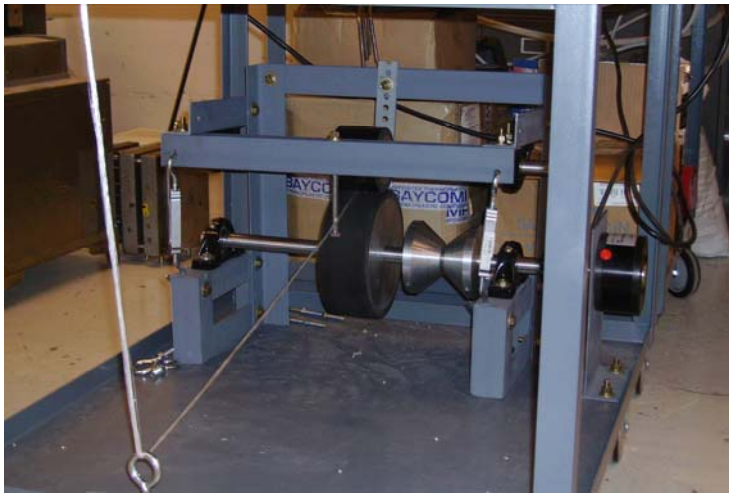

Figure 4. Final brake design.

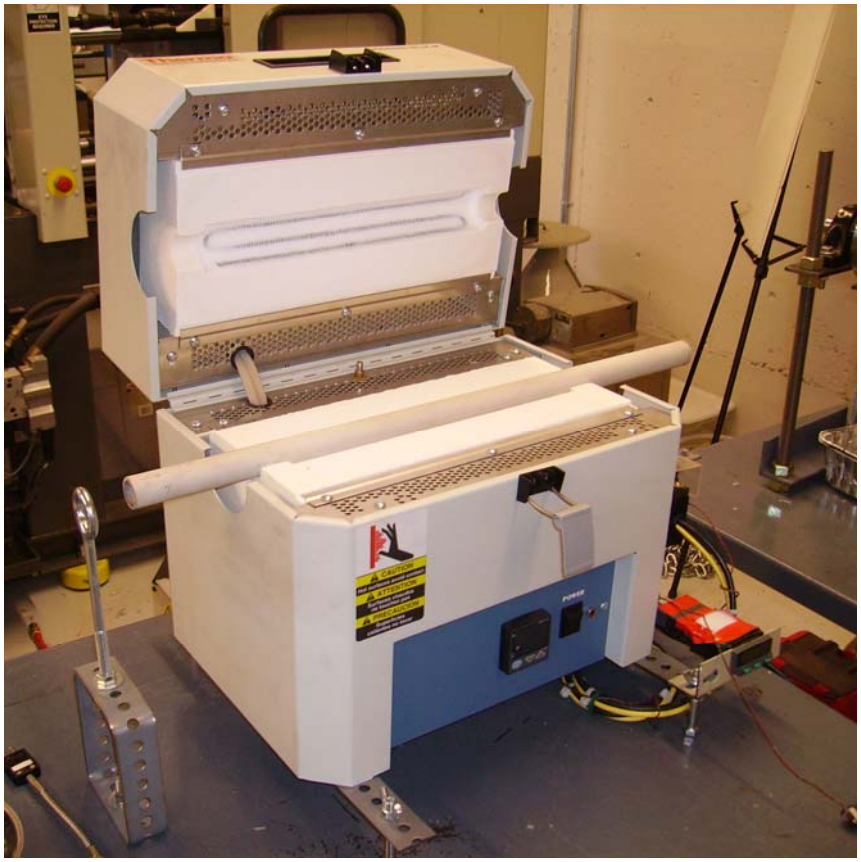

Figure 5. Tube furnace with its top open showing the process tube.

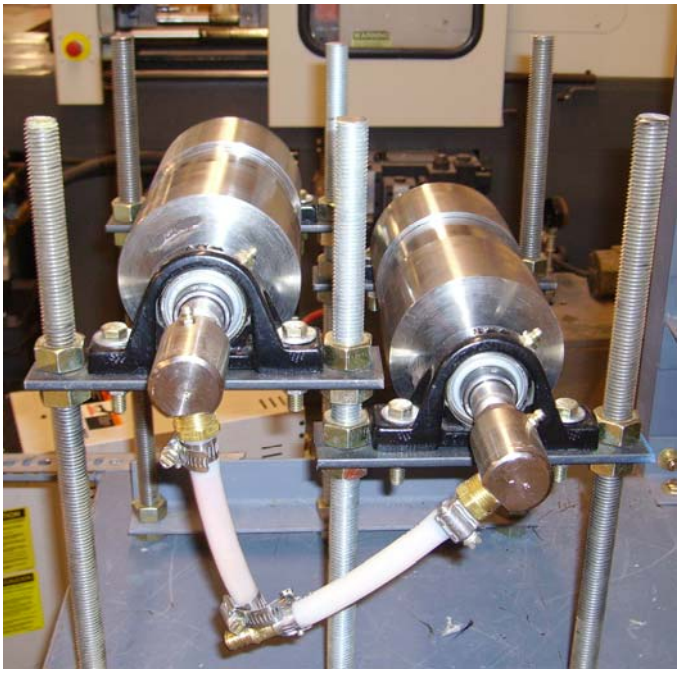

Figure 6. Chiller system.

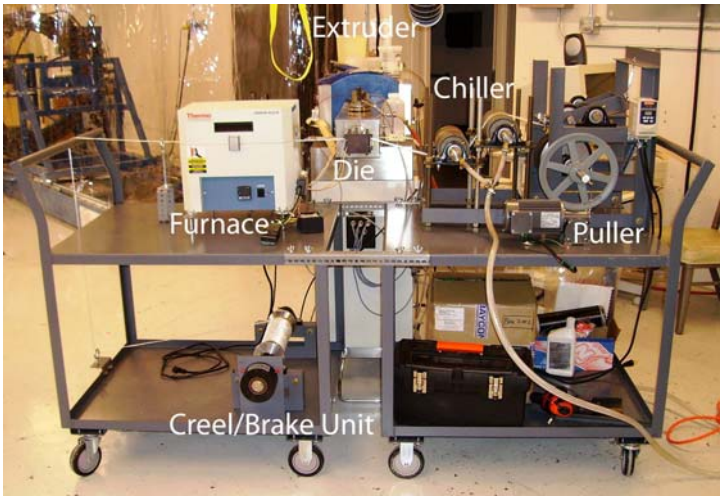

Figure 7. Completed miniature DRIFT system.

Assessment of Product Quality

The product quality of tapes manufactured by the mini-DRIFT machine described previously was accomplished by two primary methods, tensile testing of the tapes produced and microscopic analysis of the materials. In microscopic analysis, fiber dispersion was examined through both optical and scanning electron microscopic (SEM) techniques, while wetting was primarily examined by SEM. Composite samples were made with polypropylene as the polymer matrix. Both pitch and PAN carbon fibers were used as reinforcement. Tensile testing and microscopic examination of these two composites systems were then compared to each other. In addition, the effect of fiber preheat temperature was also examined.

Tensile Testing

Tapes were manufactured using both PAN and pitch-based carbon fiber reinforcement in polypropylene matrix, and mechanical performance assessed by tensile testing. Tensile tests were conducted following the guidelines set forth in ASTM D 3039/ ASTM D 3039M with the exception that the samples produced did not meet dimensional tolerance requirements. As such, the measurement and calculation methods used came from the standard. Figure 8 shows a stress-strain curve resulting from tensile testing. From this data, the modulus of elasticity, the maximum tensile strength, the elongation at break and the modulus of resilience were determined as per ASTM D3039M. The stress-strain curve in Figure 8 shows that the composite is brittle, as little deviation from linearity is observed. At least five samples were tested for every fiber/matrix and processing temperature combination to help to understand the variability of the manufacturing process. The results are shown in Figures 9-12. In general, the PAN-fiber composites showed better properties, as expected. There does not to be a large difference in the properties of either composite system as the fiber pre-heat temperature increased. The mean behavior at room temperature is often slightly less than the properties found when the fibers are preheated, but this was within the 10-15% variation between samples. Complete description and results of all testing are given in Reference 1.

The tensile strength was examined further by comparing the measured value to the value calculated from the rule of mixtures. At all fiber preheating temperatures and fiber types, the measured strength was 66-75% of the theoretical value. This decrease is likely due to damage to the fibers during processing. However, little of this decrease is due to preheating the fiber.

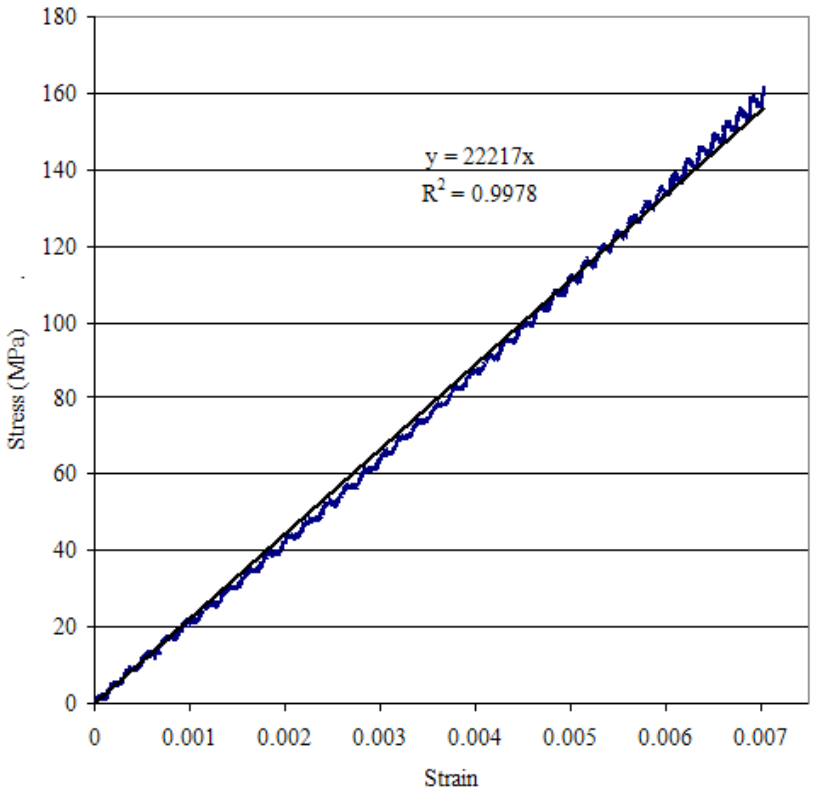

Figure 8. Example pitch 225 °C sample stress-strain plot as a function of fiber pre-heat temperature.

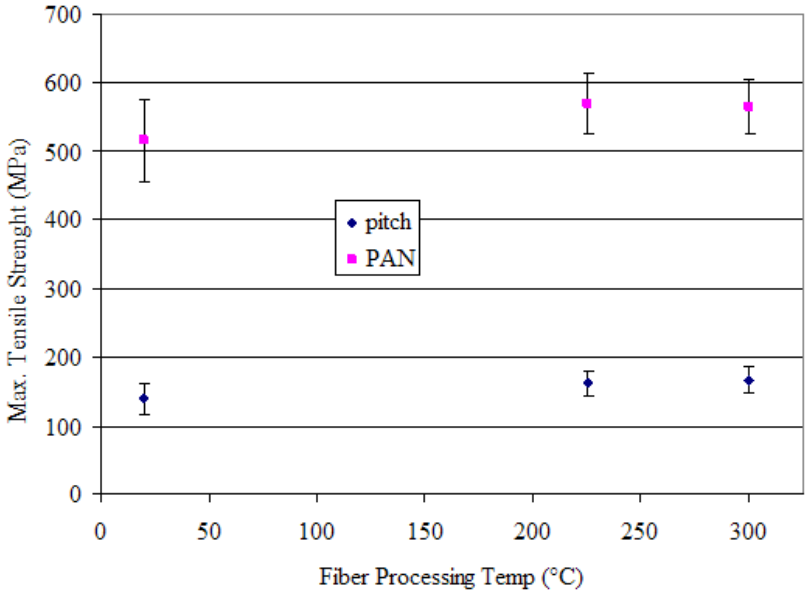

Figure 9. Maximum tensile strength for each sample set as a function of fiber pre-heat temperature.

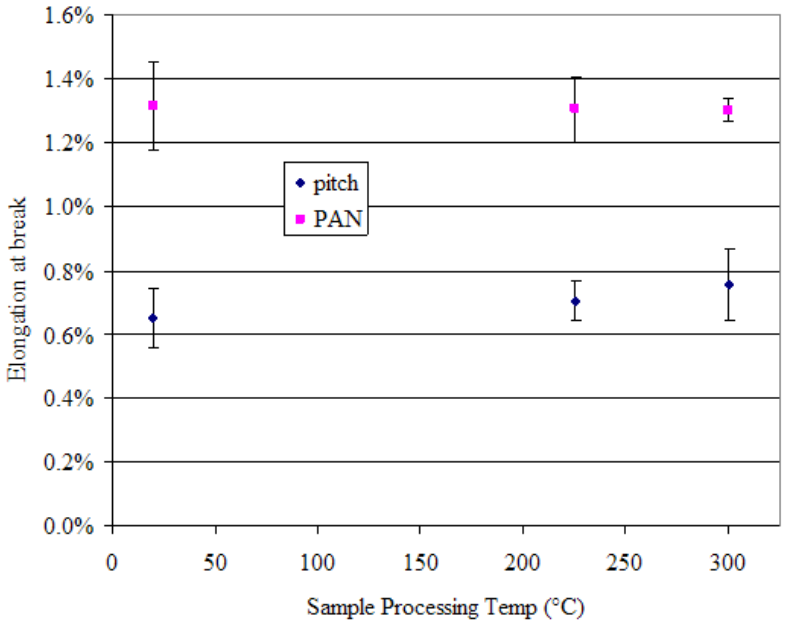

Figure 10. Elongation at break as a function of fiber pre-heat temperature.

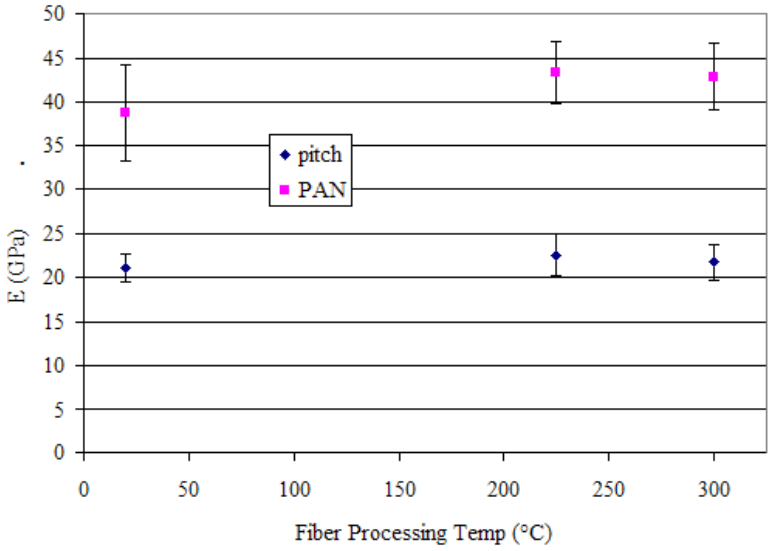

Figure 11. Elastic modulus as a function of fiber pre-heat temperature.

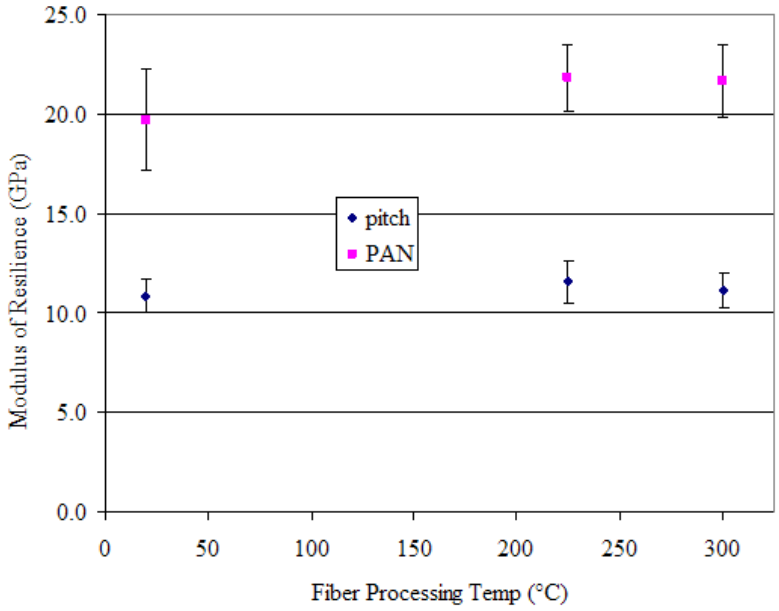

Figure 12. Modulus of resilience as a function of fiber pre-heat temperature.

Optical Microscopy

Next, tape samples were embedded in an epoxy matrix, sectioned, polished to 0.3 μm with alumina polishing compound, then viewed with a VanGuard microscope having 4x, 10x, 40x, and 80x lenses using a Steindorff digital camera having 10x magnification yielding magnifications between 40x and 800x. The overall fiber dispersion of tapes of each type (pitch and PAN) and fiber pre-heating (25, 250, 300 ºC) was determined by optical microscopy at 40x. Full descriptions of all images are given in Reference 1. Figure 13 shows a typical tape with pitch fibers, Figure 14 for PAN fibers. All tapes showed that the edges had more fibers than the center region, as can be seen in Figures 13 and 14. In addition, the center regions had large regions of nearly pure matrix. These pure matrix regions were usually above/below a row of fibers, and in some cases between concentrations of fiber. Higher magnifications were used to examine the wetting and dispersion more closely. Figures 15 (100x) and 16 (400x) show examples of the optical micrographs collected. In Figure 15, the pitch fibers are observed to be larger in diameter than the PAN fibers. Also, a few extremely large diameter pitch fibers can be seen, as can fibers that are similar to pies with a missing piece. In both composite systems, the fibers appear reasonably well wet by the polymer, although some of the pitch fiber composites show more voids in the polymer matrix. The PAN fiber composites were also examined at high magnification, 800x (Figure 17). The PAN fibers appear to be well dispersed and wet. In addition, the PAN fibers are observed to have a very consistent diameter.

The observations from these samples highlight the need for more investigation into the mechanisms involved in dispersing the fibers in the matrix in order to create a more uniform composite.

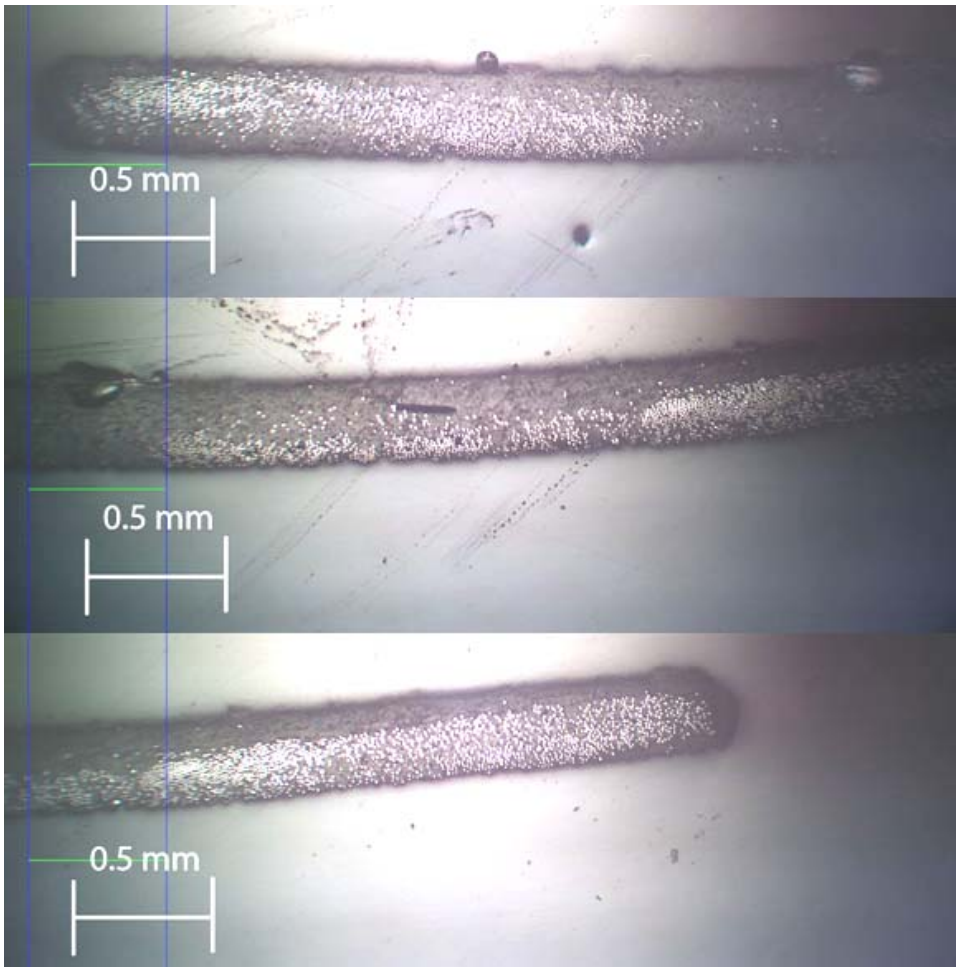

Figure 13. Images showing full width of room temperature preheat pitch sample (40x).

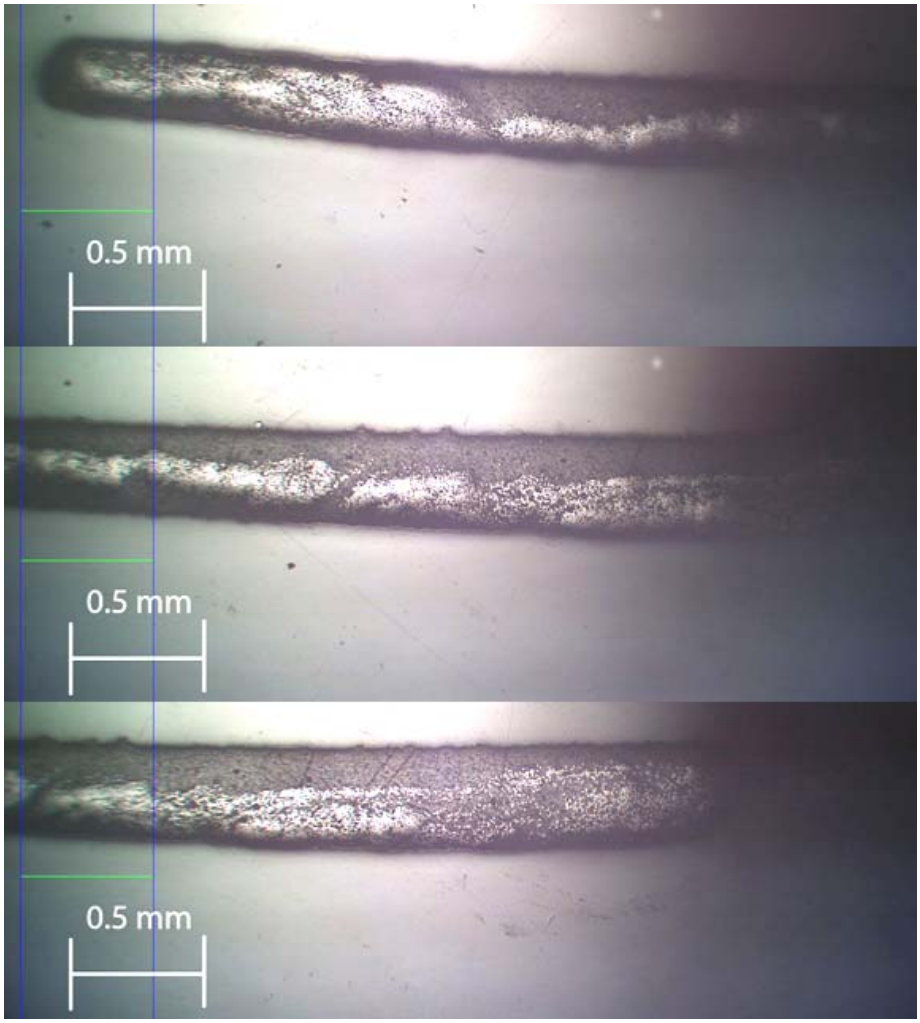

Figure 14. Images showing full width of room temperature preheat PAN sample (40x).

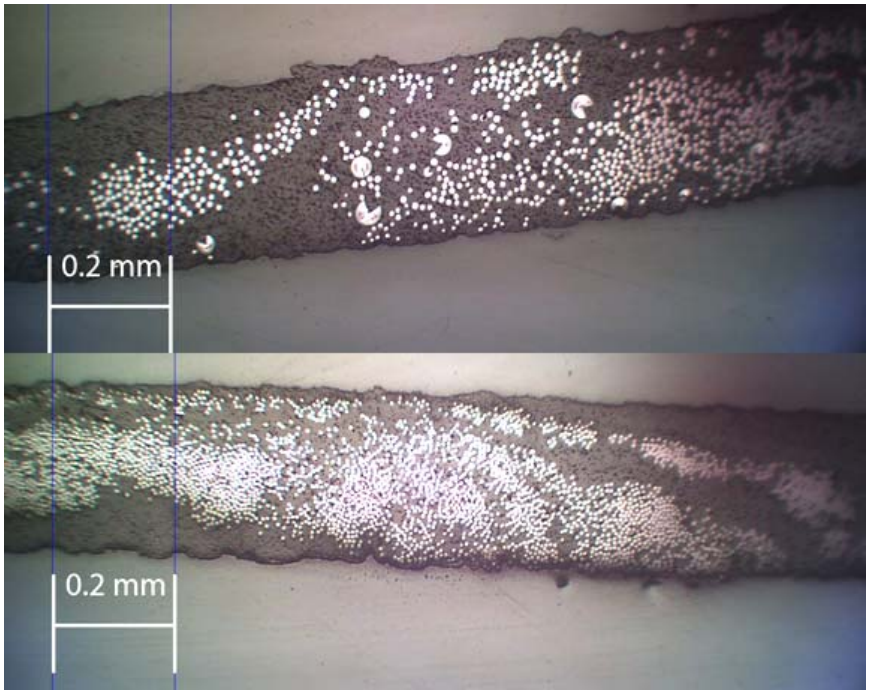

Figure 15. Comparison of pitch (top) and PAN (bottom) fiber composites at 100x.

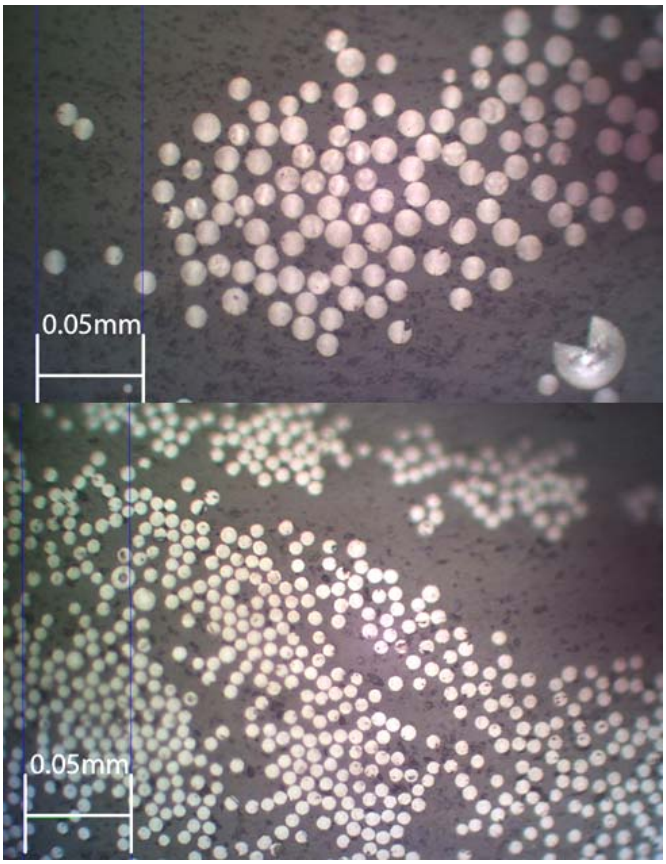

Figure 16. Comparison of pitch (top) and PAN (bottom) fiber composites at 400x.

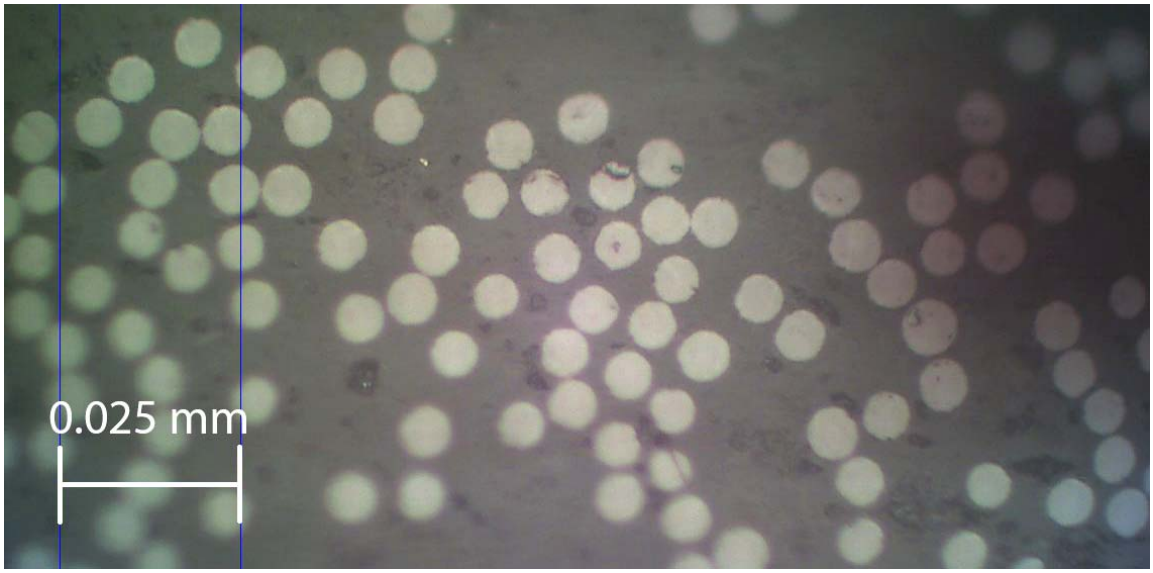

Figure 17. PAN fiber composite at 800x.

Scanning Electron Microscopy

Fractured tensile samples were viewed on the scanning electron microscope (SEM). The SEM used was a Carl Zeiss Supra 40VP field emission scanning electron microscope. Samples were gold coated to give images a greater depth of focus. All images were taken at 10 kV excitation energy. SEM images were taken of the fractured surface of tested tensile samples. In many cases, the SEM images confirmed what was observed by optical microscopy. Full description of all images is given in Reference 1. From Figure 18 it can be noted that the room temperature preheat fibers are concentrated towards the top of the sample while the 225 ºC preheat fibers were more evenly distributed through the thickness. Fiber pullout is also shown by the holes in the matrices. A higher magnification image of an area showing a block of matrix with fibers is shown in Figure 19. The fibers appear to be well wet by the matrix.

By comparison PAN fiber composites exhibited much longer fiber pullout lengths as shown in Figure 20. Because of this, examining the regions between the fibers was more difficult. However, Figure 21 shows a close-up of one region exhibiting considerable matrix existing between the pulled-out fibers.

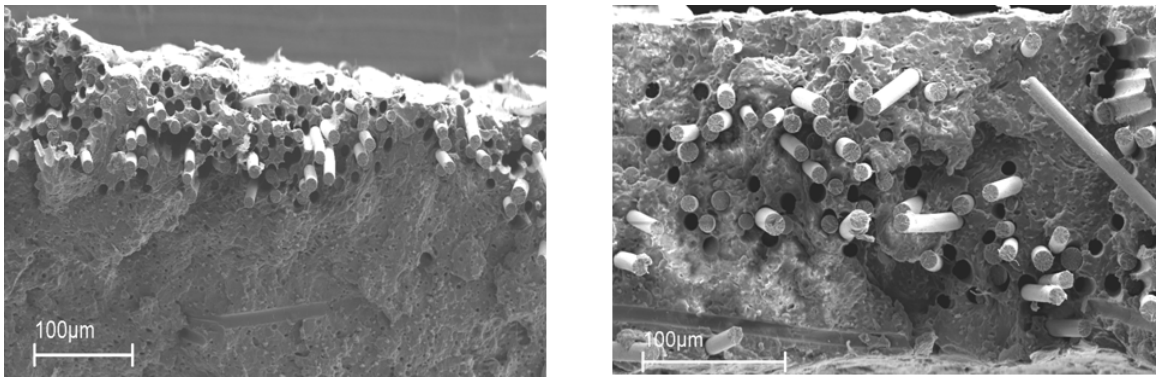

(a) (b)

Figure 18. Fracture surface SEM micrographs of through thickness of pitch fiber composites with room temperature (a) and 225 ºC (b) preheat.

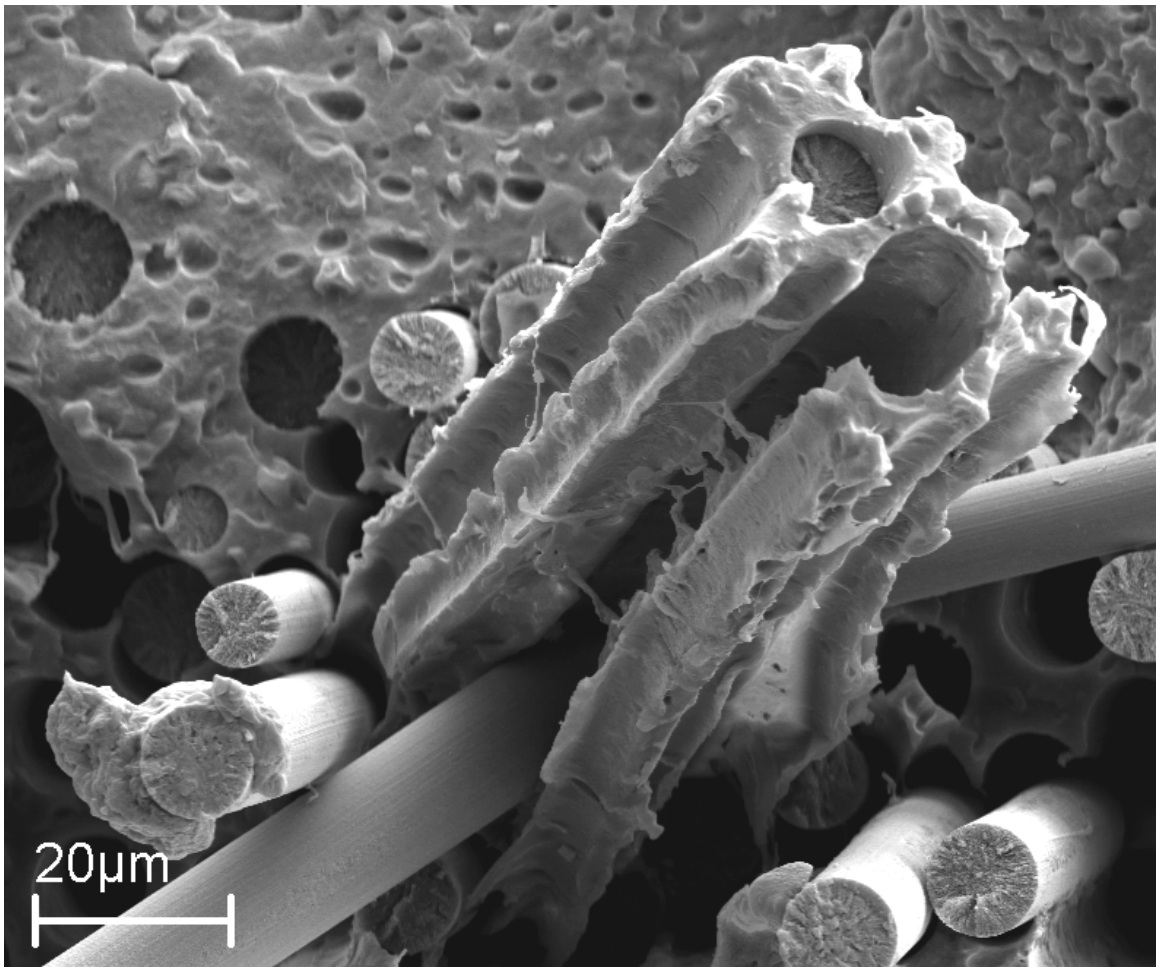

Figure 19. Close-up of fiber pullout on the fracture surface of a pitch composite.

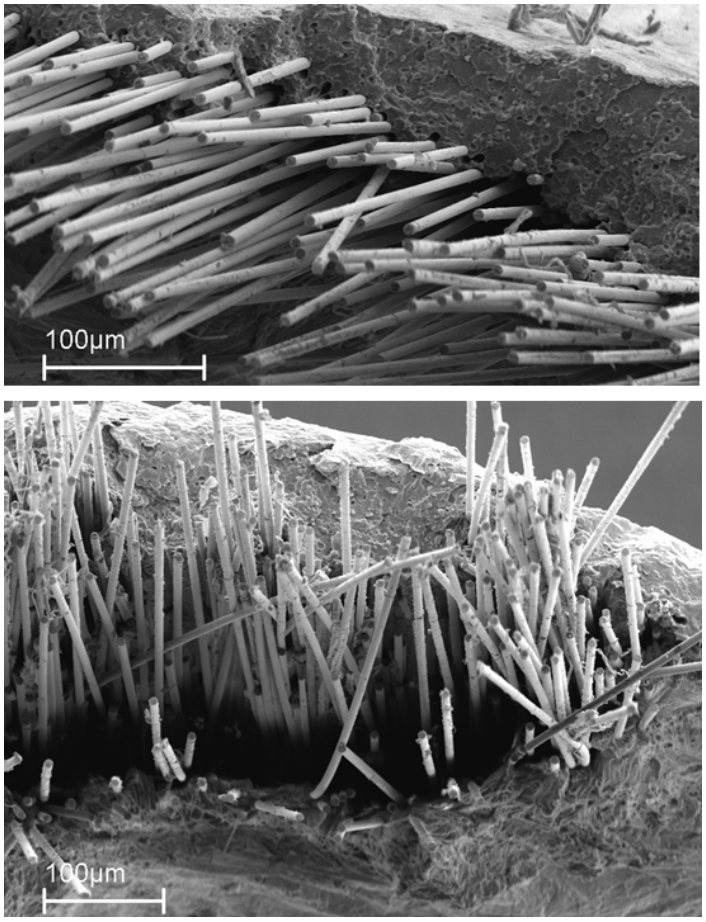

Figure 20. Fracture surface of PAN fiber composites with 225 ºC (top) and 300 ºC (bottom) fiber preheat.

Figure 21. Close-up of fiber pullout on the fracture surface of a PAN composite.

Conclusions

Highlights of the 2007-8 research include:

1. Finished design and manufacture of a miniature-DRIFT process laminate machine, including a detailed manual.
2. Experimentally tested the laminates resulting from conclusion 1 via tensile testing
3. Optical microscopy revealed good fiber wetting for both types of fibers tested with polypropylene.
4. Optical microscopy revealed that, especially in the center, fibers tended to clump together and were not evenly distributed throughout the thickness of the tape.
5. Scanning electron microscopy revealed that the fracture surfaces showed fiber pull-out and good wetting of the fibers.

Reference

1. McGlothlen, R. G., "Design and Testing of a Compact DRIFT Machine for Manufacturing of Continuous Fiber Thermoplastic Composites", Masters of Science Thesis, South Dakota School of Mines and Technology, 2008.

Presentations/Publications/Patents

1. McGlothlen, R. G., "Design and Testing of a Compact DRIFT Machine for Manufacturing of Continuous Fiber Thermoplastic Composites", Masters of Science Thesis, South Dakota School of Mines and Technology, 2008.
2. Robinson, L., Cross, W.M., Kjerengtroen, L. and Kellar, J., "Thermoplastic Melting and Wetting Behavior on Carbon Fibers", Joint ND/SD EPSCoR Conference, Sept. 2007, Fargo, ND.

I. Composite Crash-Energy Management (ACC 100[i])

Principal Investigator: Mark E. Botkin
General Motors Corporation
30500 Mound Rd
Warren, MI 48090
(586) 986-0510; fax: (586) 986-0446, e-mail:mark.e.botkin@gm.com

Technology Area Development Manager: Joseph A. Carpenter
(202) 586-1022; fax: (202) 586-1600; e-mail: joseph.carpenter@ee.doe.gov

Field Project Officer: Aaron D. Yocum
(304) 285-4852; fax: (304) 285-4403; e-mail: aaron.yocum@netl.doe.gov

Expert Technical Monitor: Philip S. Sklad
(865) 574-5069; fax: (865) 576-4963; e-mail: skladps@ornl.gov

---

Contractor: United States Automotive Materials Partnership (USAMP)
Contract No.: DE-FC05-02OR22910 through the DOE National Energy Technology Laboratory

---

Objective

- Experimentally determine the effects of material, design, environment, and loading on macroscopic crash performance to guide the design and the development of predictive tools.
- Determine the key mechanisms responsible for crash-energy absorption and examine microstructural behavior during crash to direct the development of material models.
- Develop analytical methods for predicting energy absorption and crash behavior of components and structures.
- Conduct experiments to validate analytical tools and design practices.
- Develop and demonstrate crash design guidelines and practices.
- Develop and support design concepts for application in demonstration projects.

Approach

- Conduct experimental projects to increase understanding of the global and macro influences of major variables on crash performance.
- Use the data from these experiments to create crash intuition, guidelines, and rules-of-thumb and data for the validation of analysis developments.
- Conduct microscopic experimental characterization to define the mechanisms that occur during and as a result of the crash process.
- Develop and validate analytical design tools to predict structural crash performance based on both phenomenological and micro-mechanical approaches to material and crash-mechanism modeling.

Accomplishments

- Development of a new random-fiber composite (RaFC) geometry-generation algorithm (High Fiber Volume Fraction Sequential Inclusion - HFVFSI) capable of achieving high fiber volume fractions comparable with those envisioned for practical applications (~35%).

- Generation of an automated finite-element modeling (FEM) analysis procedure using the commercial software package ABAQUS®, to statistically investigate the influence of the representative volume element (RVE) size on the elastic properties of the homogeneous random carbon-fiber (CF) material.
- Validation of the FEM results through comparison with analytical and semi-analytical approaches for random CF material.
- A first-level, multi-scale, crush-prediction software tool has been completed and delivered to the Automotive Composites Consortium (ACC). Quasi-static test results for both round and square tubes of 30^o, 45^o, and 60^o tubes have been compared to analysis simulations.

Future Direction

- Continue the development of geometry-generation algorithms and software implementation to achieve high fiber volume fractions. A user-friendly, completely-automated, software environment is necessary for rapid geometry generation for material design and analysis.
- Perform FEM-based analysis to evaluate the equivalent homogeneous material elastic properties, in conjunction with determination of minimum RVE size, for carbon-fiber RaFCs and elliptical fiber cross-sections.
- Conduct micro-scale experimental work and develop the corresponding internal state variables (ISVs) for the developed RVE.
- Develop specific material modeling subroutine for ABAQUS® for RVE implementation and consequent macro-structure damage analysis of random CF.
- Account for the rate-sensitivity effects, and calibrate the rate sensitivity model to the available test data in multi-scale modeling of braids.
- Study the effects on damage & failure characteristics of "size" of specimen/structural dimensions relative to the size of the damage zone and/or microstructure.
- Study the effects of temperature during processing on resin properties.
- Test random CF tubes for the purpose of validation of the random CF crush prediction project.

Introduction

The purpose of the Composite Crash-Energy Management project is to develop and demonstrate the technologies required to apply production-feasible structural composites in automotive crash and energy-management applications. Efforts within the project are intended to understand the mechanisms of polymer-composite crash, develop analytical tools for use in vehicle design, and build a knowledge base for the vehicular application of lightweight polymer composites. The efforts relate to materials, molding and assembly processes and design configurations that are useful in realistic applications. Design-analysis methods will be developed that can be used at several different steps in the design process. These steps require different levels of precision and speed-of-use, and the appropriate tools are expected to include both micro-mechanical and phenomenological approaches.

Crashworthiness Assessment of Tubular RaFC Structures Based on Micro and Interfacial Mechanics

The goal of this work is to create a novel Hierarchical, Micro Experimental and Computational Characterization (HiMECC) algorithm for RaFCs. This will be realized through the following deliverables: (1) Develop computational tools for RaFC micro-scale material characterization and damage modeling;
(2) Conduct experimental work to determine required material parameters and validate numerical analysis tools; (3) Determine key mechanisms responsible for macro-scale failure; and (4) Develop and demonstrate crash design guidelines and practices.
To date, the following tasks have been completed:
1. Development of a random-geometry-generation algorithm and software implementation based on the Random Sequential Adsorption (RSA) approach.
2. Generation of RaFC geometries for materials with up to 20% volume fraction using the RSA algorithm.
3. Development of a procedure for numerical determination of the elastic constants for the equivalent homogeneous material.
4. Generation of an automated FEM analysis procedure using the commercial software package ABAQUS®, to statistically investigate the influence of the RVE size on the elastic properties of the homogeneous material.

5. Validation of the FEM results through comparison with analytical and semi-analytical approaches.
6. Development of a new RaFC geometry-generation algorithm (High Fiber Volume Fraction Sequential Inclusion - HFVFSI) capable of achieving high fiber volume fractions comparable with those envisioned for practical applications (~35%). The new algorithm accounts for fiber bundle curvatures occurring during the manufacturing process, as well as for arbitrary bundle cross-sections. The curved bundle geometry is implemented using spline modeling, with three-dimensional (3D) bundle-intersection checks carried out by employing convex optimization algorithms.
7. Optical investigation of E-glass and carbon-fiber RaFC samples for geometry characterization (Figures 1 and 2).
8. Generation of RaFC geometries for materials with up to 36.7% volume fraction (Figure 3). Validation of the FEM results for large fiber volume fractions through comparison with analytical and semi-analytical approaches.

Figure 1. Optical characterization of RaFC samples – in-plane view.
Left: E-Glass-fiber sample; Right: Carbon-fiber sample.

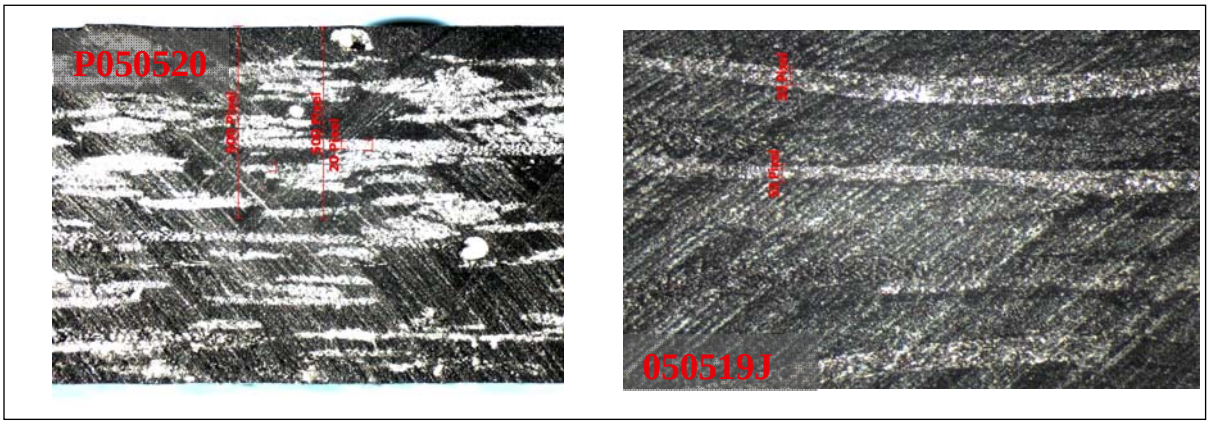

Figure 2. Optical characterization of RaFC samples – through thickness view.
Left: E-Glass fiber sample; Right: Carbon-fiber sample.

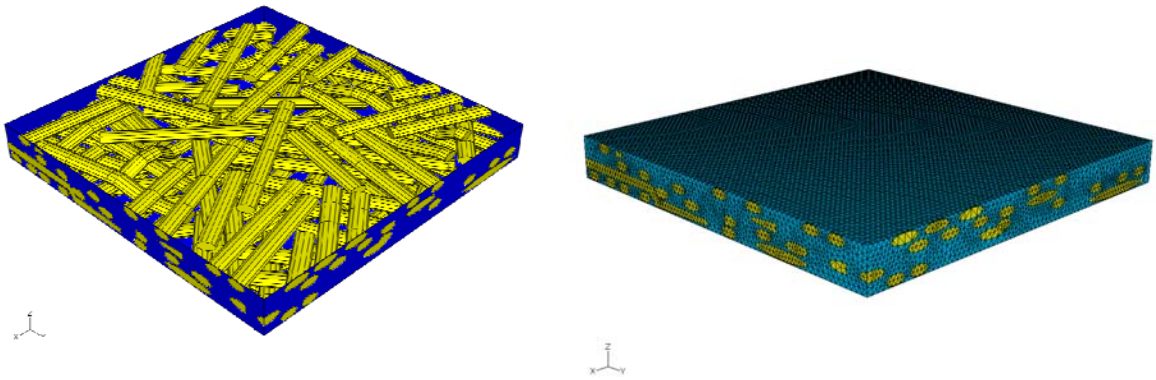

Figure 3. HFVFSI-algorithm-generated RVE of 36.7% volume fraction random composite (eliptical cross-section bundles).

Multi-scale Design System

Over the past year, we developed a Multi-scale Design System (MDS) and validated it on circular and square tube crush simulation with different (30^o, 45^o, 60^o) braid angles. Size effects and the influence of tow buckling were studied and implemented into the model. A multi-step calibration (parameter identification) scheme was developed and implemented. A comprehensive user manual for multiscale design system and a complete set of demonstration movies have been developed for the MDS.

The MDS consists of the state-of-the-art, multi-scale analysis tools integrated with the commercial finite-element analysis (FEA) engine (ABAQUS) and optimization package for model calibration (or parameter identification) and validation. The MDS, schematically illustrated in Figure 4, consists of:

a. Mathematical upscaling: derivation of coarse-scale equations from fine-scale equations. This is accomplished using mathematical homogenization theory.

b. Computational upscaling: reducing the complexity of solving a fine-scale problem to a manageable size for available computational resources.

c. Parameter identification: solving an inverse problem for constitutive parameters (interfaces, fibers/tows, matrix) by minimizing the error between experimental data at coupon and fine-scale levels hosted in the Experimental Depository.

d. Graphic User Interface (GUI) based on ABAQUS/CAE. The GUI, which serves as the front-end for the analysis, is implemented via Python codes taking advantage of ABAQUS/GUI toolkit.

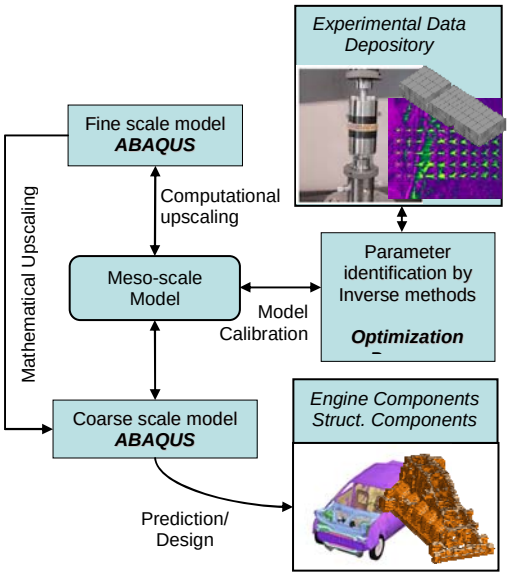

Figure 4. MDS developed at Rensselaer.

Figure 5 depicts braid architectures considered in our studies.

For all tube-crush simulations we considered quasistatic loading (load rate = 0.5 in/min), initiator plug with 5/16-inch fillet radius, two layers of braided composite, and quarter-tube

models. For circular tubes, the inner diameter is 2.35 in. as illustrated in Figure 6.
Figure 7 compares the multi-scale simulations and experimental results for the 45^o braid architecture shown in Figure 5. An excellent agreement with the experiment can be observed.

Figure 8 compares the multi-scale simulations and experimental results for the 30^o braid architecture shown in Figure 5. This time, the agreement with experiment is not as good. Possibly, this can be attributed to the fact that, so far, we have not incorporated rate effects and interface failure into the model. This is also true for the calibration phase.

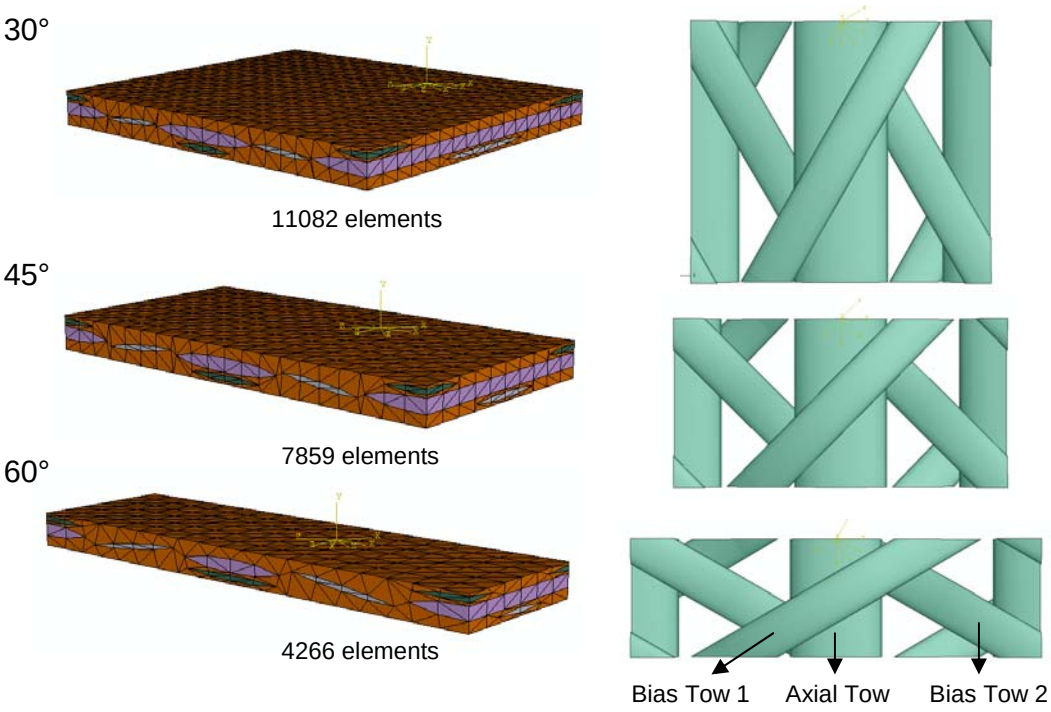

Figure 5. Braid architectures considered in simulations.

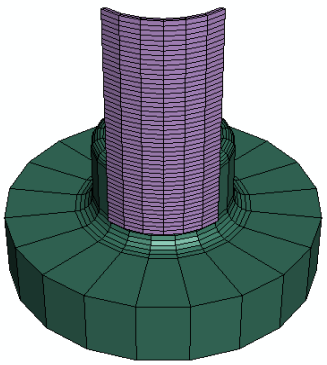

Figure 6. Circular tube model.

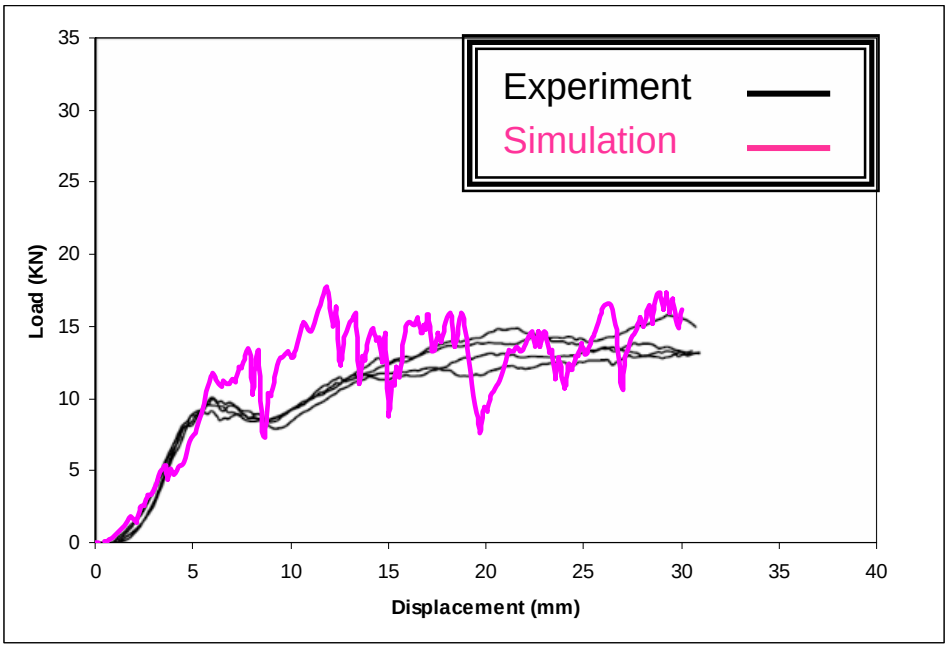

Figure 7. Comparison of the multi-scale simulation and experimental results for circular tube made of 45^{o} braid architecture in quasistatic loading.

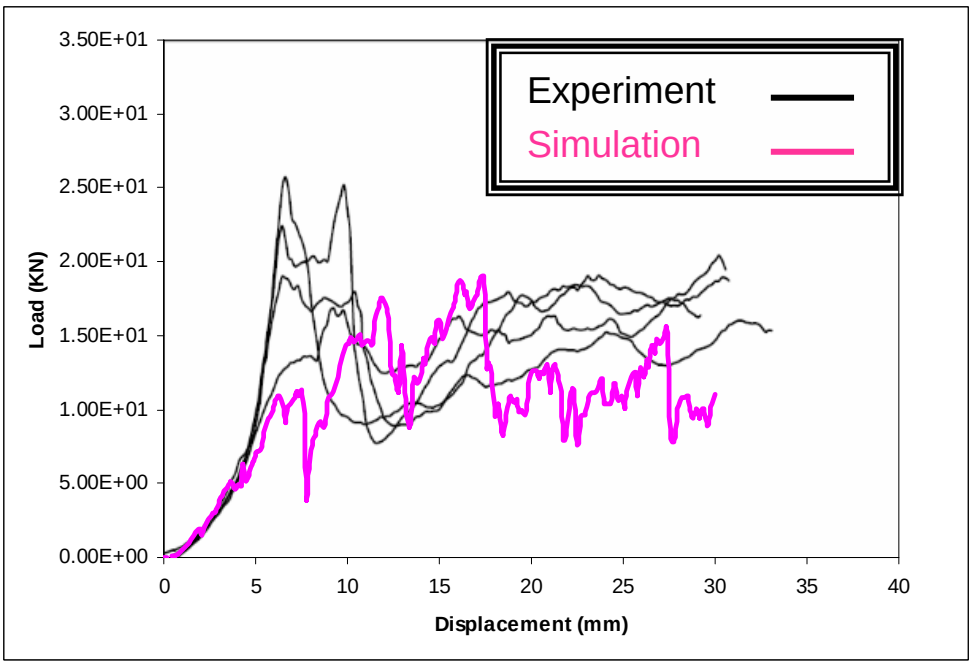

Figure 8. Comparison of the multi-scale simulation and experimental results for circular tube made of 30^{o} braid architecture in quasistatic loading.

Figure 9 compares the multi-scale simulations and experimental results for the 60° braid architecture shown in Figure 5. Again, an excellent agreement with the experiment can be observed.

Next, we studied the mesh-size effect, that is, the influence of mesh size on simulation results.

Figure 10 summarizes the findings of these studies. Interestingly, the model shows very little if any influence to the mesh size. For coarser meshes, the oscillations are higher, which is due to the fact that when element is removed, the load is reduced. The larger element is eroded, the larger jump is expected.

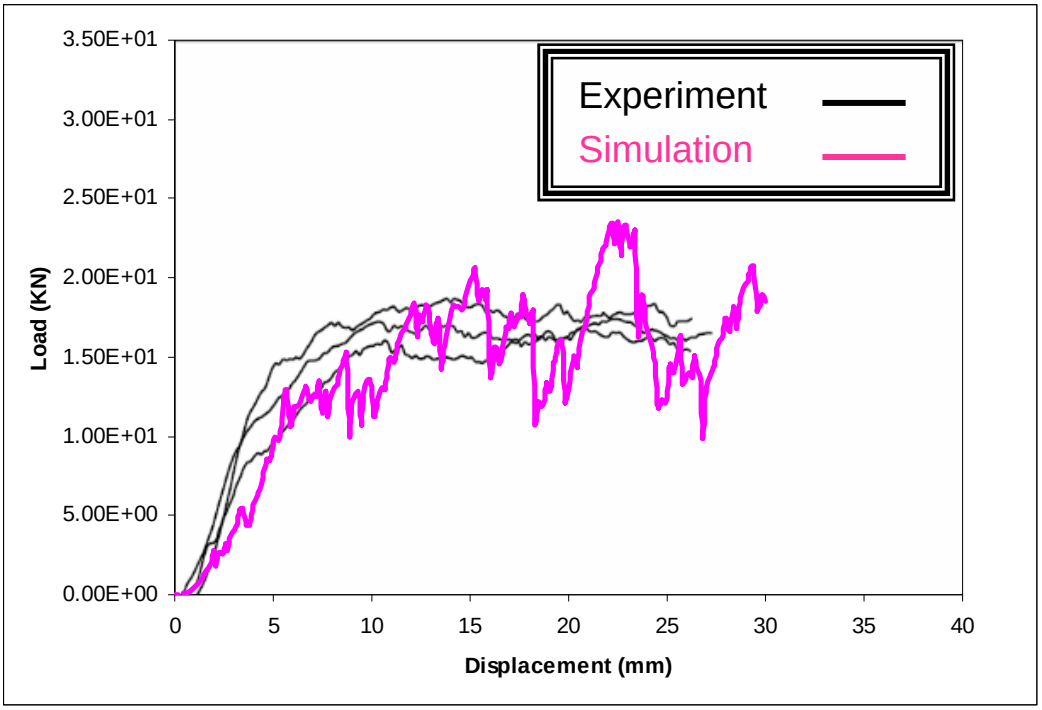

Figure 9. Comparison of the multi-scale simulation and experimental results for circular tube made of 60° braid architecture in quasistatic loading.

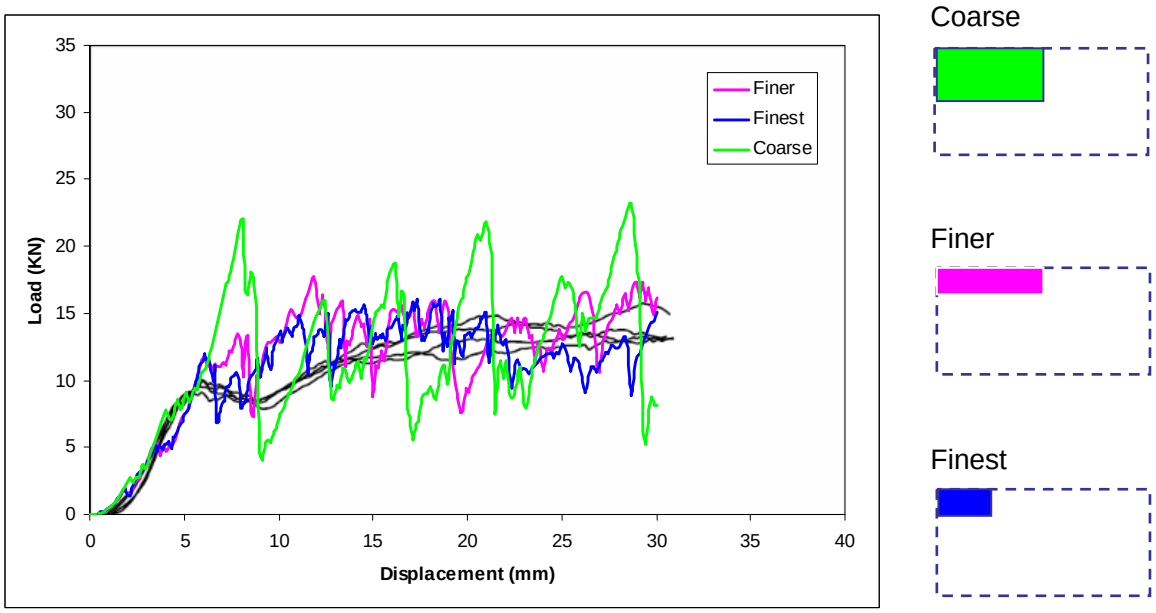

Figure 10. Size effect studies for three different mesh sizes shown on the right.

Next, we conducted crush simulations of square tube as shown in Figure 11. The inner dimensions of the tube were 2 in. x 2 in. and inner corner radius of 0.33 in. An initiator plug with ¼-inch fillet radius was considered.

Figure 12 compares the multi-scale simulation and experimental results for the 45° braid architecture shown in Figure 5.

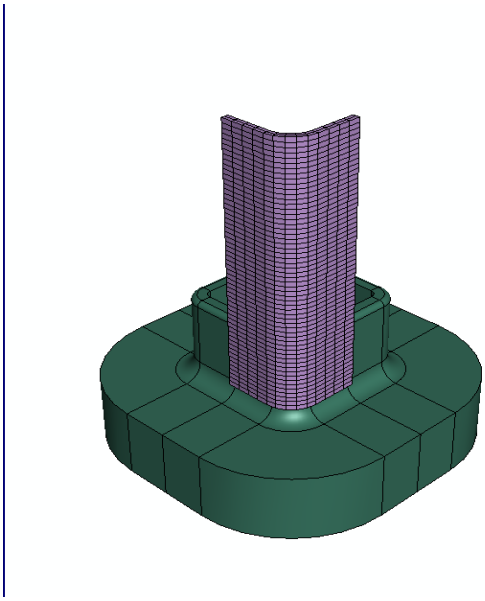

Figure 11. Square tube model.

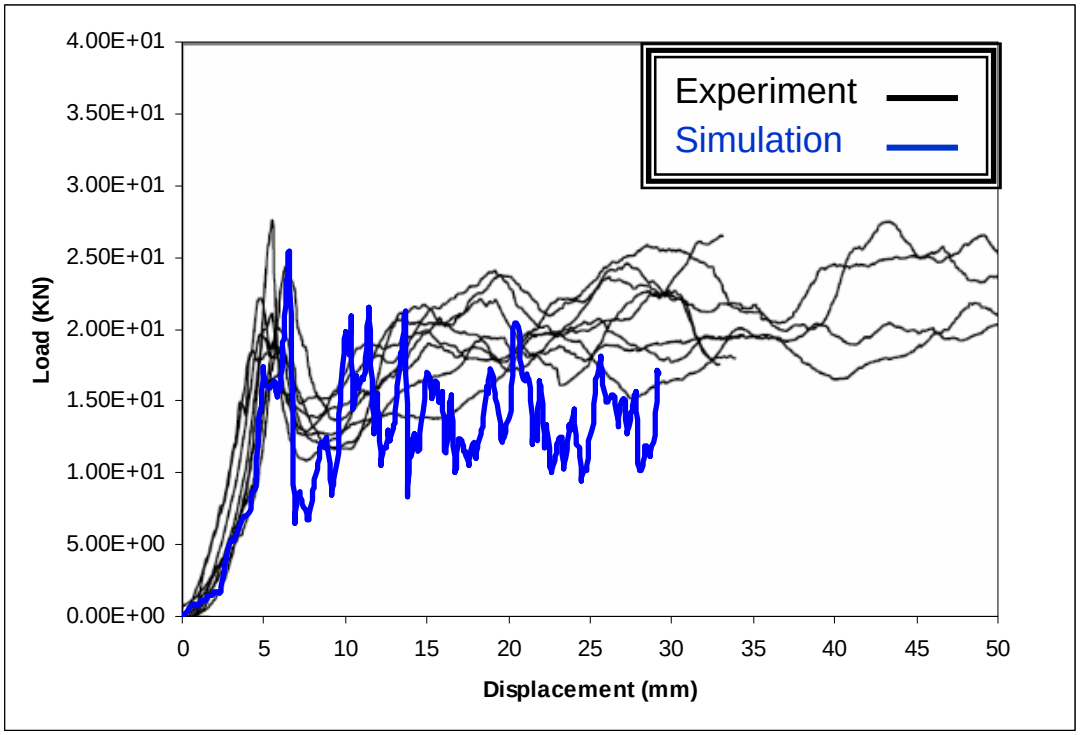

Figure 12. Comparison of multi-scale simulation and experimental results for square tube made of 45° braid architecture in quasistatic loading.

Figure 13 compares the multi-scale simulation and experimental results for the 30° braid architecture shown in Figure 5.

Figure 14 compares the multi-scale simulation and experimental results for the 60° braid architecture shown in Figure 5.

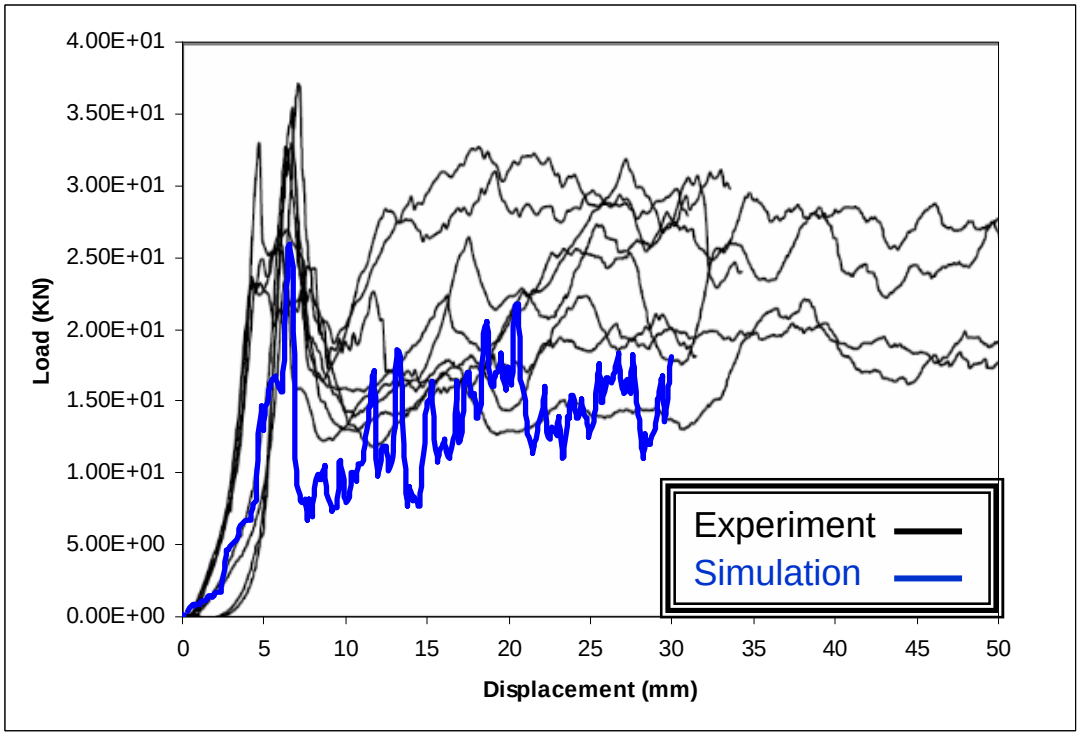

Figure 13. Comparison of multi-scale simulation and experimental results for square tube made of 30° braid architecture in quasistatic loading.

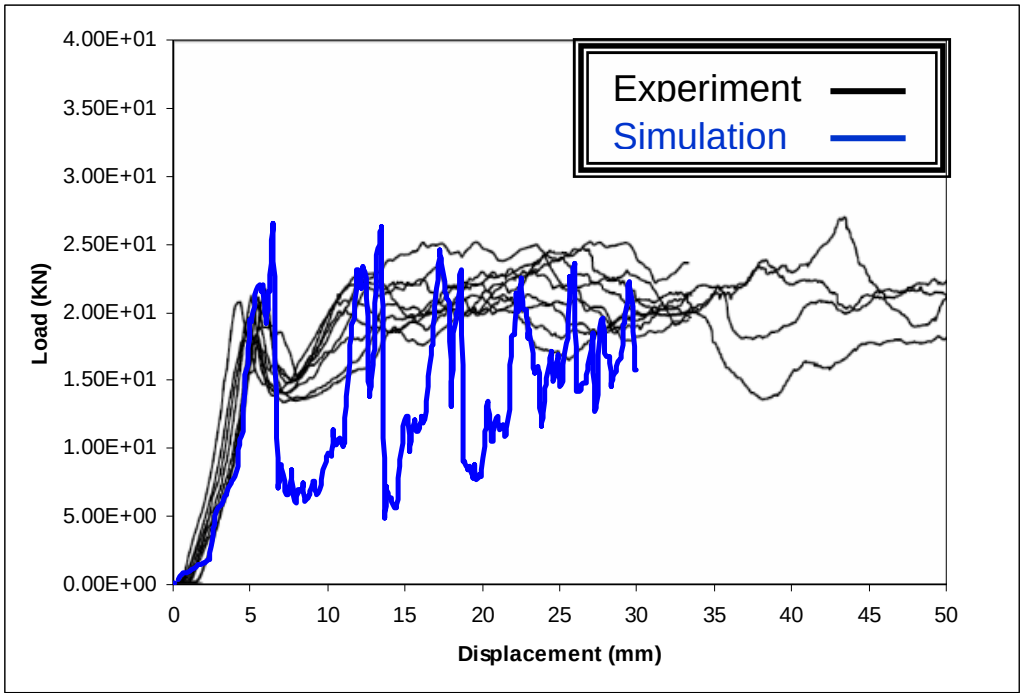

Figure 14. Comparison of multiscale simulation and experimental results for square tube made of 60 braid architecture in quasistatic loading.

These results demonstrate the need for considering interface failure. Note that implementation of interface failure will affect the calibrated properties of microconstituents. This is because the failure properties of microconstituents were calibrated to fit the coupon data.

Size Effects in Textile Composites

This new effort is focused on developing a qualitative and quantitative understanding of the important topic of meso-to-macro size effects in structures made of textile-composite, quasi-brittle materials. Such an understanding plays a role in the accurate modeling and characterization of structural crashworthiness and energy absorption in components made of lightweight, quasi-brittle materials (such as textile composites). Obtaining an understanding and useful insights of size effects, along with verifiable experimental evidence and clarification of the implications of the size effects for computational FEM of structures made of two-dimensionally triaxially-braided composites (2DTBC), is the major goal of the project.

It is important at this point to clarify what is meant by "size" and what are the "effects". "Size" refers to the size of specimen/structural dimensions relative to the size of the damage zone and/or micro-structure. "Effects" refer to those effects on damage and failure characteristics, nominal strength, and post-peak regime in materials exhibiting such strength–size dependence.

This new effort is motivated by the following fundamental question: What is the relationship between the measurements of energy released and dissipated (i.e., fracture properties and material nonlinearities) carried out in the laboratory at the coupon level of a 2DTBC, and their manifestations at the structural level in a real crash setting of a structure made of the same 2DTBC. That is, do the measured overall material/ structural properties change when different size specimens are tested? It is important to note that the issue of concern in this topic (i.e., specimen-size effects on measured material properties) does not stem from the well-known statistical distribution of micro-flaws in a material based on Weibull theory, but rather from an energetic consideration driven by the relatively-recent findings that quasi-brittle materials exhibit size effects because their fracture process-zone is not negligible (in size) compared with structural dimensions.

This new effort is divided into two parts and led by two collaborating universities. The work involves extensive experimental testing (including the design and construction of a new resign transfer molding (RTM) tool to test large braided-carbon plaques) and advanced state-of-the-art computational modeling and validation. The work is focused on one matrix/resin system and three carbon-fiber-braid architectures. At the end of this two-year effort, the sponsor will receive all information related to tests, material characterizations, and results, as well as all modeling assumptions, FEMs and external/user modules, validation results and recommendations according to the detailed deliverable and requirements stated in the detailed proposal.

Presentations/Publications/Patents

1. Pan, Y., A.A. Pelegri, L. Iorga (2007), Analysis of 3D random chopped fiber reinforced composite using the finite element method, Journal of Computational Material Science (under review.)
2. Iorga, L., Y. Pan, A. A. Pelegri (2007), Comparison of stiffness prediction approaches for random fiber composites, ASME Applied Mechanics and Materials Conference, McMAT 2007, June 3-7, 2007.
3. Pan, Y., A.A. Pelegri, L. Iorga (2007), The Elastic Properties of 3-D Random Chopped-Fiber Reinforced Composite, ASME Applied Mechanics and Materials Conference, McMAT 2007, June 3-7, 2007.
4. Pan, Y., L. Iorga, A. A. Pelegri (2007), Modeling of 3-D Random Chopped Fiber Composites with Curved Non-Circular Fibers, ASME International Mechanical Engineering Congress and Exhibition, IMECE 2007, November 11-15, 2007
5. Iorga, L., Y. Pan, A. A. Pelegri (2007), Material characterization of random fiber composites in the elastic domain, ASME International Mechanical Engineering Congress and Exhibition, IMECE 2007, November 11-15, 2007.

[i] Denotes project 100 of the Automotive Composites Consortium (ACC), one of the formal consortia of the United States Council for Automotive Research (USCAR, www.uscar.org) set up by Chrysler, Ford and General Motors to conduct joint, pre-competitive research and development.

J. Engineering Property Prediction Tools for Tailored Polymer Composite Structures

Principal Investigator: Ba Nghiep Nguyen
Pacific Northwest National Laboratory (PNNL)
902 Battelle Boulevard, P.O. Box 999, MS: K5-22, Richland, WA 99354
(509) 375 3634; fax: 509-375 6736; e-mail: Ba.Nguyen@pnl.gov

Co-Principal Investigator: Vlastimil Kunc
Oak Ridge National Laboratory (ORNL)
P.O. Box 2009, Oak Ridge, TN 37831
(86) 574 8010; fax: 865-574-0740; e-mail: kuncv@ornl.gov

Technology Area Development Manager: Joseph A. Carpenter
(202) 586-1022; fax: (202) 586-1600; e-mail: joseph.carpenter@ee.doe.gov

Expert Technical Monitor: Philip S. Sklad
(865) 574-5069; fax: (865) 574-6098; e-mail: skladps@ornl.gov

---

Contractor: PNNL, ORNL
Contract No.: DE-AC06-76RL01830, DE-AC05-00OR22725

Objective

- Enable the optimum design of lightweight automotive structural components using long-fiber-reinforced injection-molded thermoplastic composites (LFTs).

Approach

Phase I: Technical feasibility assessment

- Perform a technical assessment of current process models and computational methods for short-fiber polymer injection-molded composites in order to determine their accuracy, limitations and potential applications to LFTs.
- Identify the research directions needed to develop process and constitutive models for LFTs.
- Understand and examine the LFT emerging microstructure, characterization techniques and material processing.
- Characterize fiber orientation in LFT samples.
- Examine the molding behaviors of glass and carbon fibers.

Phase II: Research and development

Develop an integrated approach that links process to structural modeling allowing the optimum design of LFT composite structures. This work includes:

- development of process models for LFTs that allow simulations of LFT structures in order to predict flow-induced fiber orientation and other microstructural features,
- development and implementation of LFT constitutive models for structural finite-element analyses that make use of the composite microstructure predicted by process modeling. These constitutive models will predict the composite thermoelastic properties and its nonlinear behaviors due to damage, fatigue, creep and impact,
- development of characterization methods for LFT materials,
- injection-molding of larger samples and complex geometries,
- experimental testing to determine the model parameters and to validate the process and constitutive models.

Accomplishments

- A fiber-orientation model for LFTs was developed. This model is defined as the *anisotropic rotary diffusion* (ARD) model that extends the Folgar-Tucker model to LFTs.
- Computational models developed in fiscal year (FY) 2006 were applied to compute the elastic properties and coefficients of thermal expansion (CTEs) of LFT samples.
- Models were developed to predict the reduction of the elastic moduli as a function of fiber curvature and fiber/matrix debonding.
- A homogenized elastic-plastic model for LFTs was developed and implemented into ABAQUS.
- A failure criterion was implemented in the homogenized elastic-plastic model to predict strength of LFTs.
- A method for correcting the raw fiber-length distribution (FLD) was developed, and the Weibull's distribution was used to represent the corrected FLD. FLD effect on the elastic properties was studied.
- A cooperative research and development agreement (CRADA) with Moldflow, Inc. was signed which has brought Moldflow, Inc. to the project.
- PNNL built the tooling for injection-molding glass/polypropylene (PP) ISO-plaques using the same molding parameters as Delphi, and also optimized parameters.
- Experimental methods for measuring fiber length in LFTs were developed at ORNL and successfully applied to characterize FLD in LFT samples.
- FLDs and elastic moduli were measured for all material configurations.
- Mechanical tests were performed to obtain stress-strain responses of LFT samples.
- Procedure for obtaining high-quality tomography reconstruction of glass-fiber LFTs was developed, enabling measurement of orientation and curvature of individual filaments.
- Matched individual filaments from optical microscopy and tomography reconstruction for samples.
- Testing equipment capable of operating within the X-ray micro-tomography unit was developed.
- LFT specimens were tested and progressive damage was observed using coupled testing tomography.

Future Direction

- Further develop process and property prediction models for LFTs. Collaborate with Moldflow to analyze simple and larger injection-molded geometries.
- Develop a creep model for LFTs and enhance the homogenized elastic-plastic model to include progressive damage.
- Utilize previously-developed measurement techniques to determine fiber orientation and fiber length in newly-molded parts. Generate extensive set of experimental results supporting development of non-linear and time-dependent material models.
- Further develop advanced material microstructure characterization tools to establish fiber curvature and other fiber-network parameters. Advance understanding of processes active in LFTs subjected to load by observing deformations and damage in loaded samples in three dimensions.
- Procure materials and subsequently mold test samples with selected Tier 1 molder.

Introduction

During fiscal year (FY) 2007, we focused our modeling efforts on validating the thermoelastic property predictions for LFTs against the experimental results. In parallel, a fiber-orientation model for these materials was developed that incorporates an ARD term to capture fiber orientation in LFTs. Preliminary predictions by the ARD model agreed with the experimental results for LFTs. Concentrated long fibers induce fiber curvature that reduces the composite properties. A micromechanical model based on the Eshelby-Mori-Tanaka (EMT) approach was then developed to compute the composite elastic properties as a function of fiber curvature. Fiber/matrix debonding was also investigated. This problem was modeled by a modified EMT formulation that accounts for imperfect fiber/matrix interfaces. Finally, a homogenized elastic-plastic model for LFTs and a failure criterion were developed and implemented in ABAQUS allowing the simulations of LFT stress-strain responses until failure.

Property prediction requires fiber-orientation- and length-distribution data. By manual measurement, it was verified that the Leeds' system [1] could be used to measure fiber orientation in LFTs. Therefore, fiber orientation results determined by

the Leeds' system were used in the computation. In the meantime, measurement methods were developed to systematically characterize fiber-length distributions (FLDs) in LFTs. Also, a method was developed to correct the raw FLD data. A tensile-testing machine within a tomography unit was designed and developed allowing us to observe the LFT microstructure and its evolution during loading. Finally, mechanical testing was performed to determine the material stress-strain responses until failure allowing the validation of the elastic-plastic model and strength prediction.

Prediction of the LFT Thermoelastic Properties

Computation of the LFT Thermoelastic Properties

These computations contain three steps [2-3]. First, the elastic stiffness and CTEs of a reference unidirectional (UD) composite are determined using the EMT model [4-5]. The reference composite contains the same fiber-volume fraction and length distribution as the actual composite. Next, the stiffness and CTEs of the actual composite are determined from the solutions for the reference composite that are averaged over all possible orientations using the orientation averaging method [6-7]. Finally, the overall stiffness and CTEs of the composite specimen can be determined considering the specimen as being formed by a stacking sequence of composite layers. The lamination theory is then applied to calculate the composite overall properties formed by this stacking sequence.

Figure 1 presents the corrected FLD expressed in terms of weight of fibers versus fiber length for an LFT glass/PP ISO-plaque, while Figure 2 shows the measured and predicted fiber-orientation tensor components, A_{11} and A_{22}. These distributions were used in the computation of the through-thickness elastic properties and CTEs for this specimen (Figures 3, 4 and 5). The *z*-coordinates normalized by the specimen thickness, *h* are used in Figs 2-5. Table 1 presents the longitudinal ($\overline{E}_{11}$) and in-plane transverse ($\overline{E}_{22}$) moduli for this plaque. The moduli predicted based on both the experimental fiber-orientation distribution (FOD) and corrected FLD agree well with the experimental results. However, the computation using the FOD predicted by the current fiber orientation model (*reduced strain closure* (RSC) model [8]) under-predicts the modulus $\overline{E}_{22}$. This is because the RSC model under-predicts A_{22}. The use of the Weibull's FLD and experimental FOD also has provided good predictions (Table 1).

Effect of fiber curvature

The effect of fiber curvature on the elastic properties was studied using a unit-cell homogenization approach and micromechanical modeling [9]. The first approach used a unit cell with a fiber or fiber bundle. Appropriate boundary conditions were prescribed to extract the elastic stiffness components. The second approach made use of the EMT model in which fiber curvature was accounted for through the variation of fiber orientation within a prescribed range that corresponds to a given degree of fiber curvature. Figure 6 presents the predicted variations of the normalized elastic moduli as a function of the fiber curvature represented by the end-angle θ. These results show that curved fibers significantly affect the composite properties since they lead to a significant reduction of modulus E_{11} while relatively small increase in E_{22} is achieved. The 1-direction is parallel to the segment joining the fiber ends. The 2-direction is in the plane containing the curved fiber.

	Prediction (1) MPa	Prediction (2) MPa	Prediction (3) MPa	Experiment MPa
$\overline{E}_{11}$	6017	5361	6001	6063
$\overline{E}_{22}$	6935	6377	6916	7211

Table 1. Predicted and measured elastic moduli $\overline{E}_{11}$ and $\overline{E}_{22}$ for an LFT glass/PP ISO-plaque – Use of (1) experimental FOD and corrected FLD – (2) predicted FOD (RSC model) and corrected FLD – (3) experimental FOD and Weibull's FLD.

Effect of Fiber/Matrix Debonding

It has been observed that in some of our tested specimens, the modulus values were significantly lower than expected. One of the reasons for lower properties is fiber/matrix debonding. This defect was modeled using the modified EMT formulation

proposed in [10]. To include some initial fiber/matrix debonding due to processing, it was assumed that debonding manifests as fiber/matrix sliding without separation. This assumption leads to the following expression for the fiber/matrix interface compliance tensor, η_{ij} :

$$\eta_{ij} = \beta(\delta_{ij} - n_i n_j) \qquad (1)$$

where β is a parameter that expresses the debonding intensity, and δ_{ij} is the identity tensor. n_i and n_j are the components of the unit normal vector at the fiber/matrix interface. $\beta = 0$ represents the perfect fiber/matrix interface while $\beta \to \infty$ corresponds to free fiber/matrix sliding. Eq. (1) was then introduced into the modified EMT formulation to compute the stiffness matrix of the reference UD composite. Finally, the stiffness matrix of the as-formed composite containing debonded fiber/matrix interfaces is obtained from the solution for the reference composite that is averaged over all possible orientations using the orientation averaging method [6-7]. The elastic properties predicted for an LFT glass/PP center-gated disk are shown in Table 2. Accounting for fiber/matrix debonding has improved the elastic property prediction for this material.

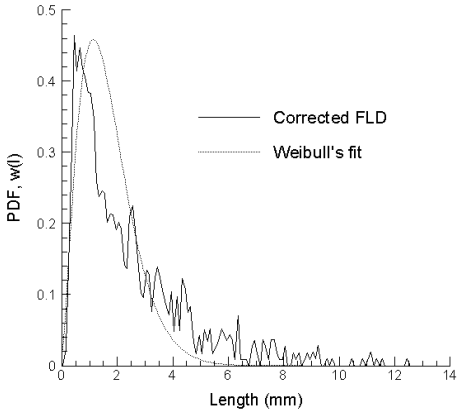

Figure 1. Corrected FLD in terms of probability density function (PDF) for weight of fibers for a glass/PP ISO-plaque - Weibull's distribution was used to fit the corrected FLD data.

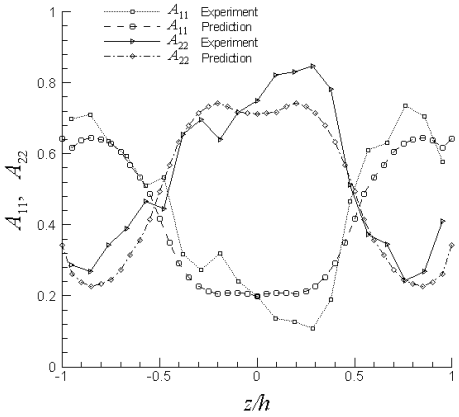

Figure 2. Predicted and measured fiber orientation tensor components A_{11} and A_{22} for a glass/PP ISO-plaque. The prediction was achieved by the RSC model.

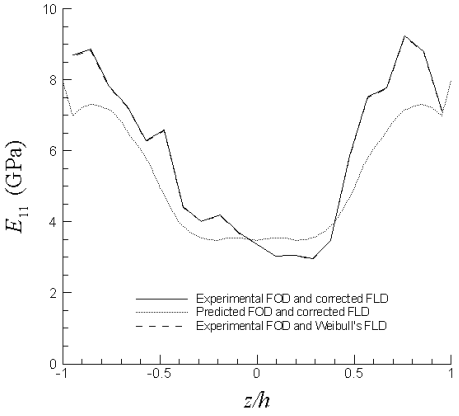

Figure 3. Predicted thru-thickness variations of the elastic modulus E_{11} for a glass/PP ISO-plaque. The 1-direction is the plaque longitudinal direction.

	Prediction (no debonding) MPa	Prediction (debonding, β=20) MPa	Experiment MPa
$\overline{E}_{11}$	5543	4833	4737
$\overline{E}_{22}$	7703	7246	6840

Table 2. Predicted and measured elastic moduli $\overline{E}_{11}$ and $\overline{E}_{22}$ for an LFT glass/PP center-gated disk.

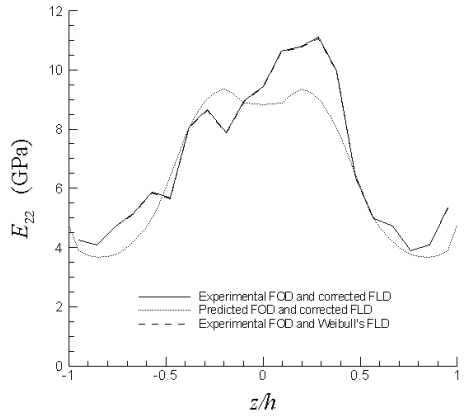

Figure 4. Predicted thru-thickness variations of the elastic modulus E_{22} for a glass/PP ISO-plaque. The 2-direction is the plaque in-plane transverse direction.

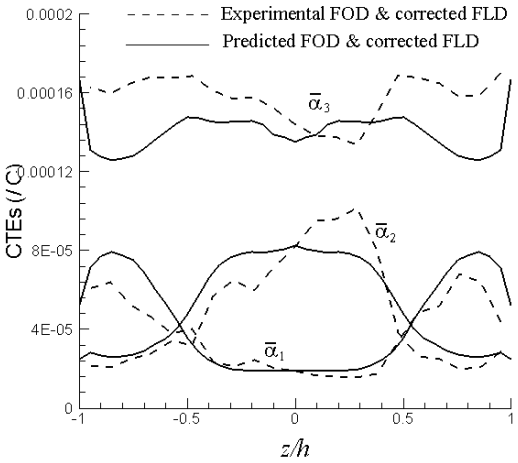

Figure 5. Predicted CTEs ($\bar{\alpha}_1, \bar{\alpha}_2$, and $\bar{\alpha}_3$) for a glass/PP ISO-plaque.

An Elastic-Plastic and Strength-Prediction Model for LFTs

Thermoplastic composites exhibit nonlinear stress-strain responses that are caused by the elastic-plastic behavior of the thermoplastic resin and progressive damage due to matrix cracking, fiber/matrix debonding, fiber pull-out and fiber breakage. An elastic-plastic model for LFTs was developed that accounts for *elastic fibers* embedded in an *isotropic elastic-plastic matrix* obeying the deformation theory of plasticity [11] and the Ramberg-Osgood relation given by [12]:

$$\varepsilon_{\mathrm{m}}^{\mathrm{eq}} = \frac{\sigma_{\mathrm{m}}^{\mathrm{eq}}}{E_{\mathrm{m}}} + \left(\frac{\sigma_0}{E_{\mathrm{m}}}\right)\left(\frac{\sigma_{\mathrm{m}}^{\mathrm{eq}}}{\sigma_0}\right)^n \qquad (2)$$

where $\sigma_{\mathrm{m}}^{\mathrm{eq}}$ and $\varepsilon_{\mathrm{m}}^{\mathrm{eq}}$ are the matrix equivalent stress and strain. E_{m} is the matrix elastic modulus, and σ_0 and n are the reference stress and hardening exponent, respectively. An *incremental* EMT approach was formulated to compute the composite (overall) stress increment resulting from the composite strain increment and the material nonlinearity. The composite overall response is computed incrementally. The incremental EMT procedure is as follows. First, the matrix tangent modulus is computed from the matrix elastic and plastic moduli using the Ramberg-Osgood relation. This allows the computation of the composite instantaneous stiffness tensor by the standard EMT model and fiber-orientation averaging technique. Next, the matrix-strain increment resulting from the overall strain increment is calculated (using the fiber and matrix-strain-concentration tensors) to compute the matrix stress increment. The matrix-stress is then updated to calculate the matrix equivalent stress using the deformation theory of plasticity.

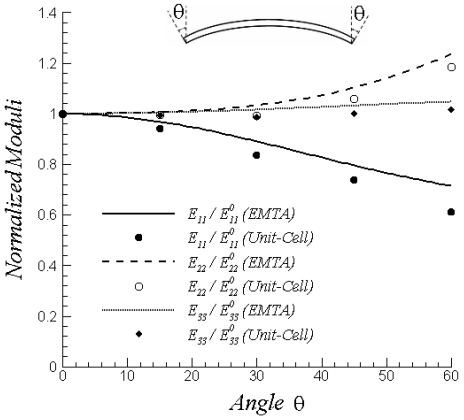

Figure 6. Variation of the normalized moduli with the end-angle θ representing fiber curvature. The values of the moduli for straight fibers (θ =0) were used for the normalization. EMTA stands for the Eshelby-Mori-Tanaka approach.

Finally, the matrix equivalent plastic strain is updated using Eq. (2) and is saved to start the next increment. Also, the composite overall stress is updated. At each increment, potential failure of the composite is predicted using the Van Hattum-Bernado model [13]. This model expresses the Tsai-Wu failure criterion in terms of matrix and fiber strengths based on the Kelly-Tyson model [14] and fiber-orientation tensors to account for the fiber-orientation effect on the composite strength.

The elastic-plastic and strength-prediction model was implemented into the ABAQUS finite-element code by means of user subroutines. Fiber-orientation data from process modeling or measurement were imported into an ABAQUS analysis via a utility subroutine of this code. In addition, FOD is represented by the Weibull's distribution in terms of weight of fibers versus fiber length. Figures 7 and 8 show the tensile longitudinal and in-plane transverse responses predicted by this model for a LFT glass/PP ISO-plaque. Measured FOD was used in the computation. On these figures are also presented the experimental results for this specimen. It has been found that the model predicts well the longitudinal stress-strain behavior up to a certain loading level (about 2/3 of the experimental strength). After that, the experimental curves become more nonlinear than the predicted one. In fact, progressive damage became more and more important about the end of the loading leading to pronounced nonlinearity observed in the experimental curves. Progressive damage is being studied, and the effect on the composite response will be discussed in our next report.

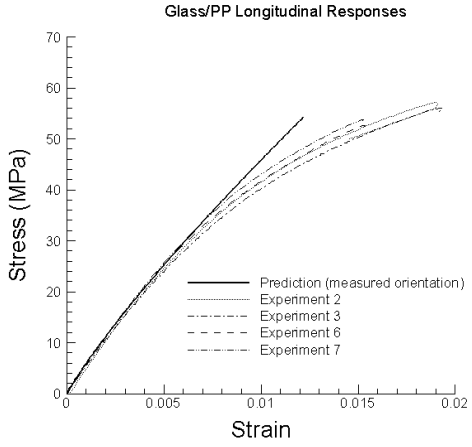

Figure 7. Predicted and experimental longitudinal stress/strain responses for a glass/PP ISO-plaque.

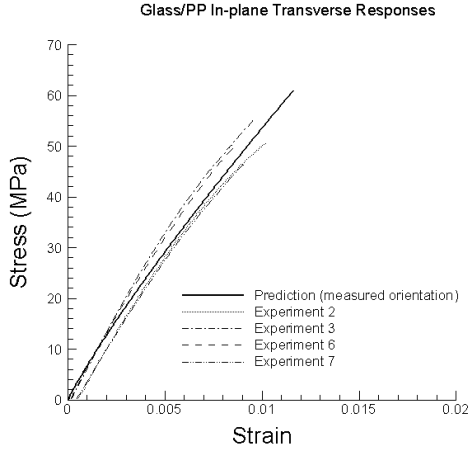

Figure 8. Predicted and experimental in-plane transverse stress/strain responses for a glass/PP ISO-plaque.

A Fiber Orientation Model for LFTs

Previously, an assessment of process models showed that using a large value of the interaction coefficient C_I in the RSC model allowed a correct prediction of the flow-direction component, A_{11} of the second-order fiber-orientation tensor [2, 15]. However, the thickness-direction component A_{33} was then over-predicted, resulting in the under-prediction of the cross-flow component A_{22}. Thus, it was necessary to develop a better fiber-orientation model for LFTs. The Folgar-Tucker model accounted for fiber-fiber interactions through the isotropic rotary diffusion governed by C_I [16-17]. It was hypothesized that accounting for such interactions with ARD would allow us to better capture the FOD in LFTs. Such a model then replaces the scalar C_I with a tensorial description **C** for the fiber-fiber interactions.

Phan-Thien and Fan [18] proposed a fiber-orientation model using ARD. However, the Phan-Thien/Fan model's diffusion term failed to return the fibers to an isotropic orientation at steady state, a necessary condition of any diffusion model. To correct the Phan-Thien/Fan model, an expression for rotary diffusion was developed that was defined on the surface of the unit sphere traced by all orientations of the unit vector **p** [19]. The expression for the ARD model to properly match the LFT fiber orientation data is:

$$\begin{aligned}\dot{\mathbf{A}} &= (\mathbf{W}.\mathbf{A} - \mathbf{A}.\mathbf{W}) + \xi(\mathbf{D}.\mathbf{A} + \mathbf{A}.\mathbf{D} - 2\overline{\overline{\mathbf{A}}}:\mathbf{D}) \\ &+ \dot{\gamma}(2\mathbf{C} - 2(\mathrm{tr}\mathbf{C})\mathbf{A} - 5(\mathbf{C}.\mathbf{A} + \mathbf{A}.\mathbf{C}) + 10\overline{\overline{\mathbf{A}}}:\mathbf{C})\end{aligned} \quad (3)$$

where **A** and $\overline{\overline{\mathbf{A}}}$ are the second- and fourth-order orientation tensors, respectively. $\dot{\mathbf{A}} = D\mathbf{A}/Dt$ with t being the time. **W** is the vorticity tensor, and **D** is

the rate of the deformation tensor. $\dot{\gamma}$ is the scalar magnitude of **D**, and ξ is the shape parameter (ξ=1 for any fiber). Tensor **C** is constructed from the **A** and **D** tensors as:

$$\mathbf{C} = b_1\mathbf{I} + b_2\mathbf{A} + b_3\mathbf{A}^2 + b_4\frac{\mathbf{D}}{\dot{\gamma}} + b_5\frac{\mathbf{D}^2}{\dot{\gamma}^2} \qquad (4)$$

where b_i (i=1,..,5) are the scalar constants. A systematic method of selecting b_i was developed in [18] to ensure stable and valid orientation solutions. To properly match experimental orientation data, one may need to slow the predicted orientation dynamics of a given model. For instance, the RSC model [8] can objectively slow the orientation dynamics of the Folgar-Tucker model. Treating the ARD model similarly, the ARD-RSC model is obtained as:

$$\begin{aligned}\dot{\mathbf{A}}^{\mathrm{ARD-RSC}} &= (\mathbf{W}.\mathbf{A} - \mathbf{A}.\mathbf{W}) \\ &+ \xi(\mathbf{D}.\mathbf{A} + \mathbf{A}.\mathbf{D} - 2[\overline{\overline{\mathbf{A}}} + (1-\kappa)(\overline{\overline{\mathbf{L}}} - \overline{\overline{\mathbf{M}}} : \overline{\overline{\mathbf{A}}})] : \mathbf{D}) \\ &+ \dot{\gamma}(2[\mathbf{C} - (1-\kappa)\overline{\overline{\mathbf{M}}} : \mathbf{C}] - 2\kappa(\mathrm{tr}\mathbf{C})\mathbf{A} \\ &- 5(\mathbf{C}.\mathbf{A} + \mathbf{A}.\mathbf{C}) + 10[\overline{\overline{\mathbf{A}}} + (1-\kappa)(\overline{\overline{\mathbf{L}}} - \overline{\overline{\mathbf{M}}} : \overline{\overline{\mathbf{A}}})] : \mathbf{C})\end{aligned} \qquad (5)$$

where **C** is given by Eq. (4). $\overline{\overline{\mathbf{L}}}$ and $\overline{\overline{\mathbf{M}}}$ are the fourth-order tensors that are defined in terms of the eigenvalues and eigenvectors of **A**. κ (<1) is a scalar parameter which controls the rate of orientation dynamics. With κ = 1/30 and b_1 = 7.848×10^{-4}, $b_2 = 2.357 \times 10^{-2}$, $b_3 = 1.0 \times 10^{-2}$, $b_4 = 1.168 \times 10^{-5}$, and b_5=-3.0×10^{-3}], an excellent fit to all the experimental orientation data was obtained for the LFT glass/PP ISO-plaque (Figs 9 and 10).

Experimental Characterization of Fiber Length Distribution

Techniques developed for sample and fiber separation for FLD measurement were described in our previous reports. Figure 11 shows FLD measurement results for the glass/PP and carbon/PP center-gated disks. Results for slow and fast cavity mold filling speeds are presented. The results indicate that slow cavity-filling speed results in greater retention of longer fibers, whereas fast mold-filling speed induces greater fiber-length attrition. This result was expected.

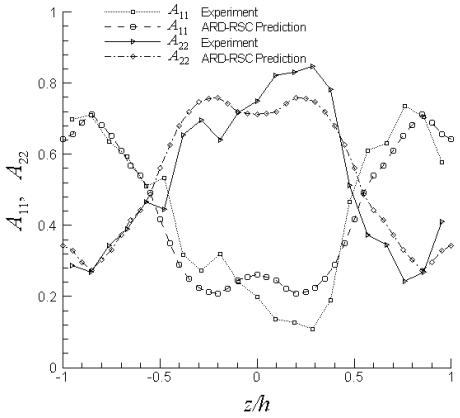

Figure 9. Predicted (by the ARD-RSC model) and measured fiber-orientation tensor components A_{11} and A_{22} for a glass/PP ISO-plaque.

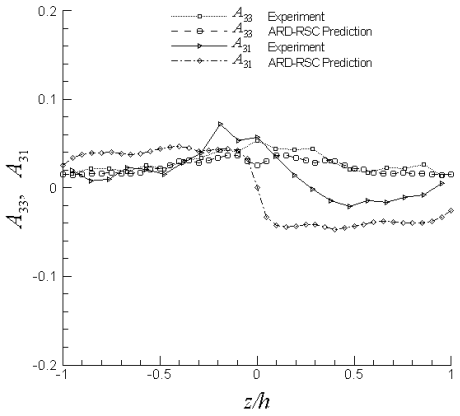

Figure 10. Predicted (by the ARD-RSC model) and measured fiber-orientation tensor components A_{33} and A_{31} for a glass/PP ISO-plaque.

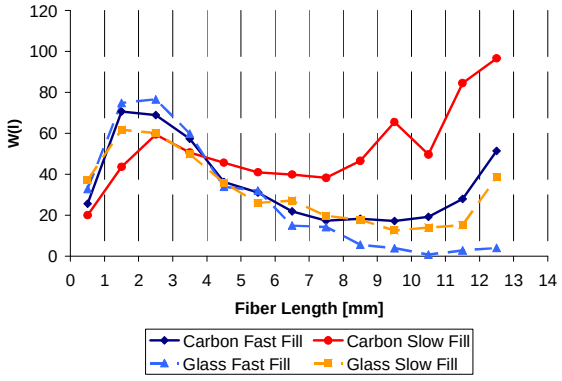

Figure 11. Measured weighted FLDs for disk specimens.

Figure 11 also indicates greater retention of long fibers in carbon/PP samples. This result was not expected due to the perceived brittleness of carbon

fibers. Greater retention of fiber length can be caused by higher strength of carbon filaments used in the material and/or by smaller diameter of carbon fibers in comparison with glass fibers. If one assumes that screw action, shear flow and fiber-fiber interactions subject filaments to bending, fibers with smaller diameter would experience lower stress compared to fibers with larger diameter at identical displacement.

Results presented in Figure 11 were measured manually using ImageJ [20] software and the sample population was 2000 fibers. The number of fragments below 0.3 mm in size was estimated, and correction for preferential selection of longer fibers was applied before using these measurements in calculations referenced above. Measurements on a limited number of identical samples were performed separately by ORNL and PNNL to validate the measurement techniques and the results matched each other very closely. Development of automated software, which would measure most of the fiber lengths automatically and which would separate problematic regions for manual measurement, yielded mixed results due to very short fragments being present in realistic samples. While the software measured a large number of fiber lengths, the number of fibers left over for manual measurement was still too large for a realistic sample size.

Mechanical Testing

Mechanical tests were performed to determine elastic properties in flow and cross-flow directions. Most of the tests were performed to increase the number of replicate data points for samples molded at Delphi. A limited number of carbon/PP ISO plaques molded at PNNL were also evaluated. Measurement averages performed on three or more replicates are presented in Table 3. Carbon/PP samples molded at PNNL exhibited poor fiber/matrix adhesion resulting in soft failure at lower than expected loads. This behavior was previously observed in the carbon/PP center-gated disks molded by Delphi and indicates the need to optimize carbon-fiber sizing for the given thermoplastic matrix. Neat PP samples exhibited strong strain-rate dependency indicated in Figure 12.

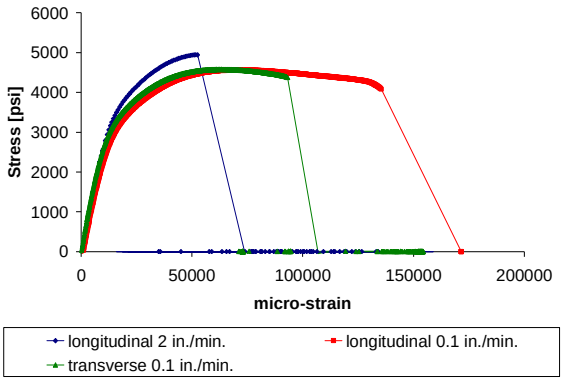

Figure 12. Stress-strain behavior of samples obtained from neat PP ISO plaques indicating strain-rate dependence.

These results were obtained from dog-bone specimens designed to eliminate grip failures and to accommodate existing plaque sizes. Identical specimen dimensions were subsequently used to obtain stress-strain behavior of LFT glass/PP samples. These tests provided consistent stress-strain curves as indicated in Figure 13. Measurements were performed for the entire set of glass-filled ISO plaques and for comparison with the elastic-plastic predictions (see Figures 7-8).

	AS3D	**AF3D**	**AS3I**	**AF3I**
$\bar{E}_{11}$ (MPa)	5305	4905	6370	6063
$\bar{E}_{22}$ (MPa)	7521	7698	7213	7211
	BS3D	**BF3D**	**PP31C**	
$\bar{E}_{11}$ (MPa)	7821	7256	10070	
$\bar{E}_{22}$ (MPa)	12031	10161	9486	

Table 3. Experimentally-measured stiffness values for glass/PP and carbon/PP disk and ISO specimens.

AS3D: 3-mm slow-fill glass/PP center-gated disk
AF3D: 3-mm fast-fill glass/PP center-gated disk
AS3I: 3-mm slow-fill glass/PP ISO-plaque
AF3I: 3-mm fast-fill glass/PP ISO-plaque
BS3D: 3-mm slow-fill carbon/PP center-gated disk
BF3D: 3-mm fast-fill carbon/PP center-gated disk
PP31C: 3-mm fast-fill carbon/PP ISO-plaque

Advanced Characterization of Fiber Architecture

Description of fiber architecture was so far confined to FODs and FLDs. Properties of LFTs

are strongly influenced by these distributions; however, it became apparent through observation and through analytical work that these measures do not describe fiber architecture of LFTs with the same fidelity as for short-fiber-reinforced thermoplastics. Fiber curvature and the nature of fiber entanglement appear to have significant influence on properties of LFTs. X-ray micro-tomography can be used to evaluate the fiber network inside a small LFT sample. Tomography reconstruction must be of high quality for fiber surface and fiber ends to be clearly distinguishable. This required reduction of specimen size to approximately 0.5 mm x 0.5 mm and long exposure time. After reducing the size of the specimens used for fiber-orientation measurement by the Leeds' system, it was possible to match individual filaments in the micrograph of Leeds' samples and in the tomography reconstruction. Filaments identified on the polished surface were subsequently tracked below the surface to establish their curvature and depth below the surface. Figure 14 shows section of a micrograph of an AS3D Leeds' sample and corresponding section of tomography reconstruction showing behavior of filaments below the polished surface. Tracking of filaments has been performed manually; however, techniques to accomplish this using software are being investigated.

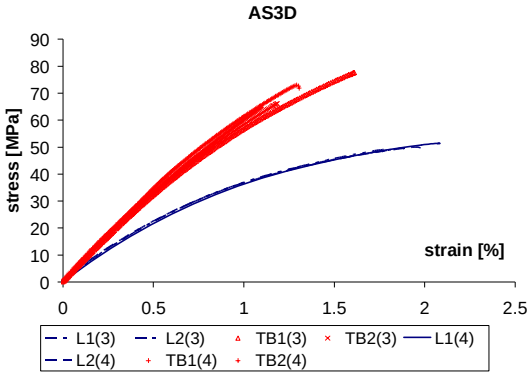

Figure 13. Four replicates of stress-strain curves for longitudinal (L) and transverse (TB) specimens show consistent measurements of material properties obtained from dog-bone specimens.

Design of Testing Equipment for X-Ray Micro-Tomography Unit

The micro-tomography unit located at ORNL is being used to evaluate the microstructure of LFTs. These investigations have shown significant fiber curvature being present in the samples. Fiber curvature may influence elastic properties, as discussed in the previous section, and it likely influences non-linear and ultimate properties of the material. A testing machine capable of operating within the tomography unit was designed in order to evaluate the effect of fiber curvature as well as the presence of short fiber fragments and non-uniform fiber distribution on the strain state of a sample subjected to mechanical loading. Solid modeling and finite-element analysis were used to ensure load capacity of 300 lbf and 150° of unobstructed view necessary for full three-dimensional (3D) reconstruction of fiber-reinforced sample loaded to failure (Figure 15).

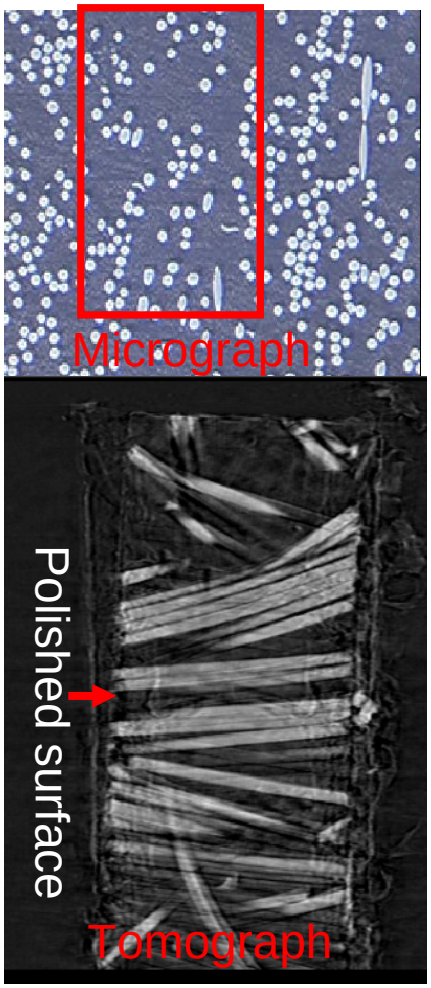

Figure 14. AS3D micrograph and corresponding section of tomography reconstruction.

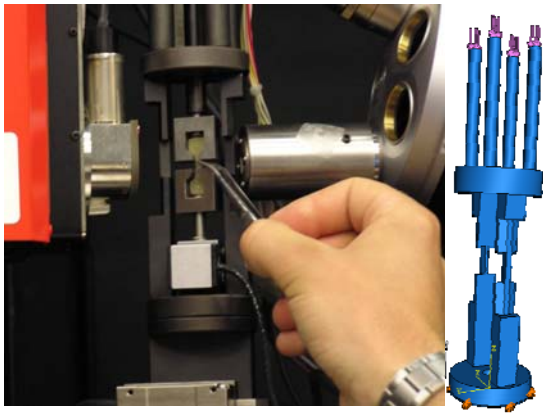

Figure 15. Testing machine within X-ray micro-tomography unit and corresponding solid model.

First, it has been proven that it was possible to obtain 3-D reconstruction of LFT sample subjected to load. Even though the specimen may relax significantly during imaging necessary for full reconstruction, individual filaments can be clearly distinguished. Post-failure investigations confirm previous observations of fiber bridging across initial crack opening. Figure 16 shows reconstruction of fiber architecture after failure and its section showing a region in which fibers still bridge from one crack surface to another.

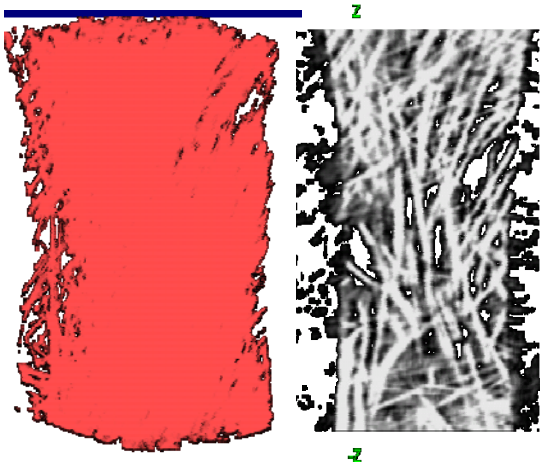

Figure 16. Tomography reconstruction and its section showing fiber bridging in LFTs after initial failure.

It was still necessary to apply load, albeit low in magnitude, to pull out or break these remaining fibers. Observations performed with this new tool should allow better identification of damage processes active within material under load. Understanding these processes will enable us to develop better predictive tools for LFTs.

Conclusions

Computational tools were developed to successfully predict the thermoelastic properties of LFTs. In addition, fiber curvature and fiber/matrix debonding were modeled and their effects on the LFT elastic properties were determined. An elastic-plastic model associated with a failure criterion was developed and implemented in ABAQUS to predict the stress-strain responses of LFTs until failure. The elastic-plastic responses agreed fairly well with the experimental results.

A fiber-orientation model for LFTs was developed that replaces the isotropic rotary diffusion term in the Folgar-Tucker model by an anisotropic rotary tensorial expression. The ARD model can provide more accurate predictions of fiber orientation in LFTs.

Methods have been established to efficiently measure fiber-length distributions in LFTs for property predictions. These methods have been applied to obtain FLDs in LFT samples. Also, it has been found that the correction of the FLD raw data is necessary for more accurate property predictions. The Weibull's distribution can accurately represent the actual distribution for weight of fiber lengths. Fiber curvature has been observed in LFT samples using X-ray micro-tomography, and the effect of fiber curvature on the composite elastic properties has been investigated and modeled.

Finally, testing equipment for the X-ray micro-tomography unit has been designed to allow observing the microstructure of LFT samples. The developed methodology is very promising for characterizing the composite microstructure that is needed in the analysis of the LFT nonlinear behavior due to damage.

References

[1] P.J. Hine, N. Davidson, R. A. Duckett, A. R. Clarke, I. M. Ward (1996). "Hydrostatically Extruded Glass-Fiber-Reinforced Polyoxy-methylene. I: The development of Fiber and Matrix Orientation." *Polym. Compo.*, 17:720-729.

[2] B.N. Nguyen, J.D. Holbery, V. Kunc (2006). "Engineering Property Prediction Tools for Tailored Polymer Composite Structures." In:

Automotive Lightweighting Materials, DOE Office of FreedomCAR and Vehicle Technologies, *FY 2006 Progress Report*.

[3] B.N. Nguyen, V. Kunc, B.J. Frame, J.H. Phelps, C.L. Tucker III, S.K. Bapanapalli, J.D. Holbery, M.T. Smith (2007). "Fiber Length and Orientation in Long-Fiber Injection-Molded Thermoplastics – Part I: Modeling of Microstructure and Elastic Properties." *J. Comp. Mater.* (submitted).

[4] J.D. Eshelby (1957). "The Determination of The Elastic Field of An Ellipsoidal Inclusion and Related Problems." *Proc. Royal Soc. London*, A 241:376-396.

[5] T. Mori, K. Tanaka (1973). "Average Stress in Matrix and Average Elastic Energy of Materials with Misfitting Inclusions." *Acta Metall.*, 21:571-574.

[6] S.G. Advani and C.L. Tucker III (1987). "The Use of Tensors to Describe and Predict Fiber Orientation in Short-Fiber Composites." *J. Rheol.*, 31 (8):751-784.

[7] C. Camacho, C.L. Tucker III, S. Yalvac, R.L. McGee (1990). "Stiffness and Thermal Expansion Predictions for Hybrid Short-Fiber Composites." *Polym. Compos.*, 11:229-239.

[8] C.L. Tucker III, J. Wang, and J.F. O'Gara (2007). "Method and Article of Manufacture for Determining a Rate of Change of Orientation of A Plurality of Fibers Disposed in A Fluid. U. S. Patent No. 7,266,469. See also Wang J., O'Gara J. F., and Tucker III, C. L. (2007). "An Objective Model for Slow Orientation Kinetics in Concentrated Fiber Suspensions: Theory and Rheological Evidence." *J. Rheol.* (submitted).

[9] S.K. Bapanapalli, B.N. Nguyen (2007). "Prediction of Elastic Properties for Curved Fiber Polymer Composites." *Polym. Compos. (in press).*

[10] J. Qu (1993). "The Effect of Slightly Weakened Interfaces on the Overall Elastic Properties of Composite Materials," *Mech. Mater*." 14:269-281.

[11] A.S. Khan, S. Huang (1995). "Continuum Theory of Plasticity." Wiley InterScience, New York.

[12] J. Aboudi (1991). "Mechanics of Composite Materials." Elsevier Science Publishers, Amtersdam, The Netherlands.

[13] F.W.J. Van Hattum, C.A. Bernado (1999). "A Model to Predict the Strength of Short Fiber Composites." *Polym. Compos.*, 20(4):524-533.

[14] A. Kelly, W.R. Tysons (1965). "Tensile Properties of Fibre-Reinforced Metals: Copper/Tungsten and Copper/Molybdenum." *J. Mech. Phys. Solids*, 13:329-350.

[15] J.H. Phelps and C.L. Tucker III (2006). "Assessing Fiber Orientation Prediction Capability for Long-Fiber Thermoplastic Composites." Technical Report submitted to PNNL, University of Illinois at Urbana-Champaign, IL 61801.

[16] R.S. Bay, C.L. Tucker III (1992). "Fiber Orientation in Simple Injection Moldings. Part I: Theory and Numerical Methods." *Polym. Compos.*, 13: 317-331.

[17] F. Folgar, C.L. Tucker III (1984). "Orientation Behavior of Fibers in Concentrated Suspensions."*J. Reinf. Plast. Comp.*, 3: 98-119.

[18] N. Phan-Thien, X.-J. Fan, R. I. Tanner, and R. Zheng (2002). "Folgar-Tucker Constant for A Fibre Suspension in A Newtonian Fluid. *J. Non-Newt. Fluid Mech.*, 103:251-260.

[19] Phelps, J.H., Tucker III, C.L. (2006). "The Anisotropic Rotary Diffusion Model for Fiber Orientation." Technical Report submitted to PNNL, University of Illinois at Urbana-Champaign, Urbana, IL 61801.

[20] Rasband, W.S., ImageJ, U. S. National Institutes of Health, Bethesda, Maryland, USA, http://rsb.info.nih.gov/ij/, 1997-2005.

Presentations/Publications/Patents

[1] G. Velez-Garcia, V. Kunc (2006). "Experimental Methods to Evaluate Fiber Length and Orientation Distribution of Long Glass Fibers in Injection Molded Thermoplastics." Presented at Fiber Society Conference, Knoxville, TN, October 10-12, 2006.

[2] S.K. Bapanapalli, B.N. Nguyen (2007). "Prediction of Elastic Properties for Curved Fiber Polymer Composites." *Polym. Compos.* (*in press*).

[3] B.N. Nguyen, V. Kunc, B.J. Frame, J.H. Phelps, C.L. Tucker III, S.K. Bapanapalli, J.D. Holbery, M.T. Smith (2007). "Fiber Length and Orientation in Long-Fiber Injection-Molded Thermoplastics - Part I: Modeling of Microstructure and Elastic Properties." *J. Comp. Mater*. (submitted).

[4] B.N. Nguyen, V. Kunc, B.J. Frame, J.H. Phelps, C.L. Tucker III, S.K. Bapanapalli, J.D. Holbery, M.T. Smith (2007). "From Process Modeling to Elastic Property Prediction for Long-Fiber Injection-Molded Thermoplastics." Proc. 7th Annual SPE Automotive Composites Conference & Exposition, Detroit, Sep. 11-13, 2007

[5] V. Kunc V, B.J. Frame, B.N. Nguyen, C.L. Tucker III, G. Velez-Garcia (2007). "Fiber Length Distribution Measurement for Long Glass and Carbon Fiber Reinforced Injection Molded Thermoplastics." Proc. 7th Annual SPE Automotive Composites Conference & Exposition, Detroit, 11-13, 2007.

[6] B.N. Nguyen, V. Kunc, M.T. Smith (2007). "Prediction of Elastic Properties for Long-Fiber Thermoplastic Injection-Molded Composites." Presented at the 2007 ASME Applied Mechanics and Materials Conference (McMat 2007), Austin, TX, June 3-7, 2007.

K. Predictive Modeling of the Structure and Properties of Polymer-Matrix Composites: NSF/DOE Grant Projects

Principal Investigator: BN Nguyen
Pacific Northwest National Laboratory (PNNL)
P.O. Box 999, Richland, WA 99352
(509) 375-3634, e-mail: ba.nguyen@pnl.gov

Principal Investigator: Vlastimil Kunc
Oak Ridge National Laboratory (ORNL)
One Bethel Valley Road, Oak Ridge, TN 37831-6053
(865) 574-8010, e-mail: kuncv@ornl.gov

DOE Technology Area Development Manager: Joseph A. Carpenter
(202) 586-1022; fax: (202) 586-1600; e-mail: joseph.carpenter@ee.doe.gov

National Science Foundation (NSF) Grant Monitor: Joycelyn S. Harrison
(703) 292-7088; e-mail: j-harris@nsf.gov

Contractor: PNNL
Contract No.: DE-AC06-76RL01830

Objective

- The objective of these six projects, jointly funded by NSF and DOE and administered by NSF as grants, is to perform fundamental development of modeling, simulation and processing of polymer composite materials. These projects support the DOE-funded "Engineering Property Prediction Tools for Tailored Polymer Composite Structures" project being conducted jointly by ORNL and PNNL (see 8.J). The NSF/DOE-funded projects are intended to investigate alternate modeling and processing approaches that can contribute to more fundamental understanding of the mathematical and physical behavior of fiber-reinforced polymer composites. The following sections provide a high-level summary of the grant objectives and work progress during 2007. Each of the projects was extensively outlined in the Automotive Lightweighting Materials annual progress report for fiscal year (FY) 2006 and detailed reports providing significantly higher levels of detail for the work accomplished during FY 2007 are available through NSF. The publications listed at the end of each section also provide more details.

Comparative Determinations of Orientation in Injection-Molded Thermotropic Liquid-Crystalline Copolyester (TLCP) Plaques

Wesley R. Burghardt, Ph.D.
Department of Chemical & Biological Engineering
Northwestern University
2145 Sheridan Road, Room E136
Evanston, IL 60208
(847) 467-1401; fax: (847) 491-3728;
e-mail: w-burghardt@northwestern.edu

NSF Award ID: 0521823

Research and Education Activities

During 9/1/06 thru 8/31/07, we made considerable progress on both experimental and simulations aspects of this project.

On the experimental side, the new graduate student working on this project (Mr. Fang) led a synchrotron run at the Advanced Photon Source to implement refinements in our *in situ* injection-molding experiment. New capabilities were added to monitor time-dependent changes in the pressure of the molding machine, pneumatic supply, and temperature within the mold. Acquisition of these

signals was coordinated with collection of x-ray scattering data, in order to allow closer coordination between the time-resolved structural data and the actual stages of mold filling. In addition, a second mold geometry (T-shaped plaque) was fabricated and tested, in order to see how variations of mold geometry influence orientation development. A second synchrotron run was performed in summer 2007 in order to obtain high quality *ex situ* scattering data on the same plaques produced during the time-resolved *in situ* experiments. Analysis of these data is still pending; this is a necessary step to fully interpret the *in situ* data. Dr. Bubeck (collaborator from Michigan Molecular Institute (MMI)) participated in each of these experiments. Finally, Mr. Fang has continued involvement with the surface orientation studies led by MMI.

Significant progress has also been made in adapting process-simulation software to simulate orientation distributions in complex processing flows of thermotropic liquid-crystal polymers (TLCPs). This approach relies on a strong analogy between the Larson-Doi polydomain model for liquid crystalline polymers, and the Folgar-Tucker fiber-orientation model that is widely used in composites processing. Mr. Fang has nearly completed an extensive set of simulations of isothermal, complex-channel flows, allowing detailed testing of the performance of this modeling approach against extensive x-ray scattering data previously collected in our flow experiments using x-ray scattering in a unique channel-flow extrusion die. Future efforts will concentrate on extending the simulation effort to *ex situ* and *in situ* data from injection molding.

Beyond the primary purpose of the project as the focal point in Mr. Fang's graduate education, results were also disseminated to the broader community via two conference presentations during 2006-07 (Society of Rheology and American Institute of Chemical Engineers), both focusing on our new *in situ* injection-molding capabilities.

Findings

Refinements to the *in situ* molding apparatus will allow for more meaningful analysis and presentation of data relative to events during the injection-molding cycle. Detailed conclusions from the latest experiments are still pending, awaiting completion of analysis of data from our most recent experiments.

Our first extensive series of simulations have demonstrated that the Larson-Doi polydomain model (and the simulation strategy drawing upon the Folgar-Tucker analogy) are quite capable of predicting many subtle details of how orientation develops in complex flows of liquid-crystalline polymers. This is the first time such simulations have been performed.

Journal Publications

- Rendon, S.; Burghardt, W. R.; Bubeck, R.A., "Orientation Dynamics in Commercial Thermotropic Liquid Crystalline Polymers in Transient Shear Flows", Rheologica Acta, (2007).
- Rendon, S.; Bubeck, R. A.; Thomas, L. S.; Burghardt, W.R.; Hexemer, A.; Fischer, D. A., "Interrogation of 'Surface', 'Skin' and 'Core' Orientation in Thermotropic Liquid Crystalline Copolyester Moldings by Near-Edge X-ray Absorption Fine Structure and Wide-Angle X-ray Scattering", Journal of Applied Polymer Science, (2007).

A Hierarchical, Structure-Oriented and Stochastic Approach to Model Liquid Molding Processes

Thanasis D. Papathanasiou
Department of Chemical Engineering
University of South Carolina
Columbia, SC 29208
(803) 777-7219; fax: (803) 777-6245;
e-mail: papathan@engr.sc.edu

NSF Award ID: 0522221

Research and Education Activities

Our research activities in the previous year were focused on the following:

(1) Continued to develop microstructure-generation codes and to test/propose metrics that quantify microstructural features such as fiber clustering. A Monte-Carlo method was implemented using a Lennard-Jones inter-fiber potential and microstructures exhibiting various degrees of clustering were generated.

(2) Continued to investigate the effects of microstructure on the permeability of unidirectional fibrous media, using in-house two-dimensional (2D) and parallel-boundary-element codes. Specifically, the effects of non-uniform inter-tow and intra-tow fiber packing and random fiber clustering were studied.

(3) Started to implement a parallel-boundary-element code for solving three-dimensional Stokes flow problems.

(4) Started to implement the Fast Multipole Boundary Element Method (FMBEM). The FMBEM for solving 2D potential flow problems has been applied to study the barrier-improvement factor in flake-filled membranes.

In the same period we attended:

(1) A Workshop titled 'A short course on the Fast Multipole Boundary Element Method', Los Angeles, California, USA. July 22, 2006.

(2) The annual SPE Conference ANTEC 2007, Cincinnati, Ohio, USA. May 7-11, 2007.

Findings

Further details on our activities are included in the full NSF report. Principal technical focus and findings include:

(1) Computation of the effects of microstructure on the permeability of unidirectional fibrous media was performed. Specifically, the effects of non-uniform inter-tow and intra-tow fiber packing and random fiber clustering were studied.

(2) Quantification of fiber clustering was performed using a metric derived from Ripley's K-function.

(3) Benchmarking of the performance of a parallel-boundary-element code for solving three-dimensional Stokes flow problems was completed using two different matrix assembly parallelization strategies.
(4) Use of a Fast Multipole Boundary Element Method code to investigate the effect of internal structure on the mass flux across random arrays of impermeable flakes was completed.

Journal Publications

1. Chen X. and T.D. Papathanasiou, 'The transverse permeability of disordered fiber arrays: A statistical correlation in terms of the mean interfiber spacing', Transport in Porous Media, accepted, 3/2007.
2. Chen X. and T.D. Papathanasiou, 'Micro-Scale Modeling of Axial Flow through Unidirectional Disordered Fiber Arrays', Composites Science and Technology, 67 (2007) 1286-1293
3. Xiaoming Chen and T.D. Papathanasiou, "The transverse permeability of disordered fiber arrays: A statistical correlation in terms of the mean interfiber spacing", Transport in Porous Media, accepted 3/2007
4. X.Chen and T.D.Papathanasiou, "Permeability of Flake-filled Barrier Membranes: A Numerical Evaluation", SPE ANTEC-2007 Proceedings, paper # 0621, p. 621, (2007). Published.

Linking Process-Induced Properties to Thermoplastic-Matrix Woven-Fabric Composites

Principal Investigator: James A. Sherwood
Department of Mechanical Engineering
University of Massachusetts Lowell
One University Avenue
Lowell, MA 01854
(978) 934-3313; fax: (978) 945-5701;
e-mail: James_Sherwood@uml.edu

NSF Award ID: 033126

Research and Education Activities

The major research activities have been in the area of studying the friction between a woven, commingled glass-polypropylene fabric and the steel tool for thermoforming processes. Additional research has been conducted in the area of material modeling techniques using classical mechanics of materials approaches and the finite-element method (FEM).

Findings

According to a parametric study conducted using a finite-element model of the thermostamping process with the empirical friction model developed in this research, increasing the velocity of the punch increased the reaction force on the punch more than increasing the binder force. Thus, it is important to incorporate a friction model based on changing processing parameters into predictive

numerical simulations. Otherwise, the reaction force on the punch could be greatly over-predicted or under-predicted.

A normalization method was proposed for the picture-frame tests. It was found that using this normalization method, the test data obtained using different sizes of picture frames and specimens could be normalized so that they were comparable.

A finite-element model composed of a combination of shell and truss elements could be used to build a model for woven-fabric composites. The shell elements can represent the interactions among tows and the truss elements can represent the tows. The hybrid finite-element model could be used to simulate the picture-frame test, bias-extension test and the thermostamping process. The results, including the reaction force and the distributions of stress and strain in the stamped part, could be used to predict and to optimize the real manufacturing process.

A user-defined subroutine containing the friction model resulting from this research was developed for use with ABAQUS implicit finite-element modeling software. This friction model is for use with glass-polypropylene woven-fabric composites in contact with a steel tool during thermoforming processes. Two user-defined subroutines containing the material models resulting from this research were developed for use with ABAQUS implicit finite-element modeling software. These material models are for use with glass-polypropylene woven-fabric composites during thermoforming processes. Currently, these numerical tools are being shared with our research partners at Northwestern University to advance the research supported by this grant. ABAQUS, Inc. has expressed interest in incorporating this friction subroutine into future releases of their finite element package. It will be available on the website (http://m-5.uml.edu/acmtrl).

Related Journal Publications

There were no publications on this project to-date. The following references are provided for information:

1. Gorczyca, J., Sherwood, J. and Chen, J., "Friction between the Tool and the Fabric During the Thermostamping of Woven Co-Mingled Glass-Polypropylene Composite Fabrics", Proceedings for the 18th Annual American Society for Composites Conference, p. 1, vol. CD, (2003).
2. Gorczyca, J., Sherwood, J., Lu, L. and Chen, J., "Friction and Shear in Thermostamping of Composites - Part I", Journal of Composite Materials, p. 1911, vol. 38, (2004).
3. Gorczyca, J., Sherwood, J. and Chen, J., "Friction Model for use with a Commingled Fiberglass-Polypropylene Plain-Weave Fabric and the Metal Tool during Thermostamping", European Finite Element Revue, p. 729, vol. 14, (2005).
4. Composite Fabrics: FEA with User-Defined Subroutines in ABAQUS/Standard", Proceedings for the 19th Annual American Society for Composites Conference, p. 1, vol. CD, (2004).
5. Li, X., Sherwood, J., Liu, L. and Chen, J., "A material model for woven commingled glass-polypropylene composite fabrics using a hybrid finite element approach", International Journal of Material Product & Technology, p. 59, vol. 21, (2004).
6. Li, X., Sherwood, J. Lu, L., Chen, J., "Material Model and Finite Element Model for Woven Commingled Glass-Polypropylene Composite Fabrics", Proceedings for the 18th Annual American Society for Composites Conference, p. 1, vol. CD, (2003). Published,
7. Lu Liu, Julie Chen, Xiang Li, James Sherwood, "Two-Dimensional Macro-Mechanics Shear Models of Woven Fabrics", Composites Part A, p. 105, vol. 36, (2005). Published,
8. Lu Liu, Julie Chen, Jennifer Gorczyca, James Sherwood, "Modeling of Friction and shear in thermo-stamping process - Part II", Journal of Composite Materials, p. 1931, vol. 38, (2004).
9. Lu Liu, Julie Chen, James Sherwood, "Material Modeling and Benchmark Testing of Woven-Fabric Composites in the Thermo-Stamping Process", 7th ESAForm Conference paper, p. 357, vol. 7, (2004).
10. Lu Liu, Julie Chen, James Sherwood, "Analytical Model of Shear of 4-harness Satin Weave Fabrics", 8th Numiform Conference paper, p. 338, vol. CP712, (2004).
11. Lu Liu, Julie Chen, James Sherwood, "Parametric Study of Commingled Glass/Polypropylene Woven Fabrics during Shear", Proceedings of the 19th annual

American Society for Composites conference, p. 1, vol. CD, (2004).
12. Peng XQ, Cao J, Chen J, Xue P, Lussier D, Liu L, "Experimental and numerical analysis on normalization of picture frame tests for composite materials", Composites Science Technology, p. 11, vol. 64, (2004).
13. Li, X., Sherwood, J., Liu, L., and Chen, J., "Hybrid Finite Element Model of Woven-Fabric Composite", Proceedings of the 19th Annual American Society for Composites, p. 1, vol. CD, (2004).
14. J.L. Gorczyca, J.A. Sherwood, J. Chen, "Friction at the Tool-Fabric Interface during the Thermostamping of Woven Commingled Glass-Polypropylrnr Composite Fabrics", Proceedings of the 7th Esaform Conference on Material Forming, p. 337, vol. 7, (2004).
15. X. Li, J.A. Sherwood, L.Liu, J. Chen, "Simulation of Double-Dome Stamping of Twill Woven Fabric Composites", Proceedings of the 8th Esaform Conference on Material Forming, p. 1003, vol. II, (2005).
16. X. Li, J. Sherwood, J. Gorczyca, J. Chen, L. Liu, "A Study of the Thermostamping Process for a Woven-Fabric Composite", Third M.I.T. Conference on Computational Fluid and Solid Mechanics, p. 229, (2005).
17. L. Liu, J. Chen, "A solid mechanics shear model of commiingled glass/polypropylene woven fabrics", Third M.I.T. Conference on Computational Fluid and Solid Mechanics, p. 237, (2005).
18. Gorczyca, J., Sherwood, J. and Chen, J., "Development of a Friction Model for Use in the Thermostamping of Commingled Glass-Polypropylene Woven Fabrics", Composites Part A, p. 393, vol. 38, (2007).
19. Xiang Li, James A. Sherwood, Lu Liu, and Julie Chen, "Simulation of Double Dome Stamping of Twill Woven Fabric Composites", Proceedings of the 8th ESAForm Conference on Material Forming, Cluj, Romania, p. 1, vol. 8th, (2005).

Incorporating Higher Order Tensors in the Computation of Polymer Composite Mechanical Properties

Principal Investigator (PI): Douglas E. Smith
University of Missouri at Columbia
E2411 Lafferre Hall/MAE Dept., Columbia, MO 65211
(573) 884-6552; fax: (573) 884-5090; e-mail: smithdoug@missouri.edu

NSF Award ID: 0522694

Research and Education Activities

The objective of this research is to develop a predictive capability that evaluates the mechanical properties of short- and long-fiber-reinforced polymer composites from higher-order orientation tensors. The approach is to develop an automated three-dimensional finite-element procedure for predicting the effective mechanical properties of a fiber suspension from its orientation distribution and the mechanical properties of the constituent materials. The work also includes measuring fiber orientations with micro-computerized tomography (CT) imaging techniques and developing a computational approach for generating fiber samples numerically from polymer melt flow simulation results. As part of this research, a Monte-Carlo simulation procedure will be used to assess the statistical nature of the predicted properties and the simulation methodology will be demonstrated on industrially-relevant products.

Fiber-reinforced polymer composites are the material of choice in numerous engineering applications due, in part, to their superior strength-to-weight ratio. This is especially true for long- and short-fiber composite products, which also benefit from extremely versatile manufacturing methods such as injection molding. As a result, there continues to be a major effort to incorporate more fiber-reinforced polymers in commercial products, particularly in the US automotive industry where future vehicles must have reduced weight, emissions, and fuel consumption. Indeed, a specific objective of the FreedomCAR program at the US Department of Energy, a co-sponsor and collaborator of this research, is to reduce the weight of an automotive structure by 50% for the same cost and durability as seen in today's products. The research also includes the development of educational visualization tools that will provide a clearer understanding of fiber suspension mechanics for future engineering students.

Previous work in the areas of numerical methods, composite mechanics, and fiber-orientation analysis will serve as a basis for further development. The focus here is to:

1) Develop a model for predicting mechanical properties from higher-order orientation tensors derived from flow simulations or measurements that is not limited by the material symmetry requirements imposed by current models.

2) Develop an automated, three-dimensional voxel-based, finite-element modeling technique that may be used to predict the effective mechanical properties of a fiber suspension.

3) Integrate micro-CT-derived fiber-orientation states to illustrate the applicability of the proposed approach on production hardware to be obtained from Visteon Corporation.

4) Statistically assess mechanical-property calculations to address sampling issues associated with using the proposed averaging techniques.

5) Demonstrate the proposed methodology on an industrially-relevant polymer composite product where flow-simulation software is to be provided from Moldflow Corporation.

6) Develop techniques for visualizing discrete fibers and fiber suspensions in reinforced polymer composites to provide students at the graduate and undergraduate levels, as well as other composite materials researchers, insight into the microstructure of polymer composites.

Project activities that have been performed to date are as follows (note that this project is in year 2 having started September 2005):

1) Literature review and collection of related information and theory.

2) Development of a Monte-Carlo simulation method for evaluating the statistical nature of elastic mechanical properties of short-fiber composites that is based on sample fiber sets defined by orientation-distribution functions in homogeneous and non-homogeneous flow fields.

3) Derivation of elastic mechanical properties from fiber-orientation tensors that is based on the expected values of the compliance tensor for random individual fibers.

4) Derivation of the statistical nature, including the mean and standard deviation, of the elastic mechanical properties from fiber-orientation tensors and fiber-distribution functions.

5) Development of a voxel-based, finite-element procedure for evaluating the mechanical properties of a set of short fibers in a polymer matrix. This includes the development of a representative volume element and the appropriate boundary conditions.

6) Verification of voxel-based, finite-element approach for single fibers within a polymer matrix.

7) Development of a program for defining the spatial location and orientation of a set of fibers from fiber size and aspect ratio, and a fiber-orientation distribution function.

8) Development of a new fiber-interaction model that simulates fiber/fiber collisions in a manner that is suitable for use in an injection-molding simulation program.

9) Development of a composite materials-based model for the fibrous annulus of the human intervetral disk.

Findings

The most significant finding in the research conducted to date under this award deals with the relationship between fiber-orientation tensors and the resulting elastic mechanical properties of short-fiber composites. Nearly two decades ago, Advani and Tucker presented an equation for computing a stiffness (or compliance) tensor from a 4^{th}-order fiber-orientation tensor and the constitutive properties of the fiber and matrix. This earlier work used the unidirectional elastic properties of several single fibers, each having a pre-selected orientation, to arrive at the final result which was given with little derivation. In our work, a rigorous derivation has been developed to evaluate the same results from the statistical expectation of single-fiber mechanical properties where the distribution of fibers is defined by the fiber-orientation distribution function. Unidirectional properties of single fibers are rotated into a

common reference frame where the rotation tensor is defined by directions that follow the orientation distribution function itself. As a result, we are now able to compute mechanical properties from either orientation tensors or fiber-orientation distribution functions. We have also been able to show that orientation tensors having an order higher than four do not contribute to the expectation value when the commonly used Fourier basis functions are employed. This derivation reduces to the Advani and Tucker form when it is assumed that fibers do not interact under stress and strain in the final composite.

Using a similar derivation technique, we have also derived, for the first time, a means to quantify the statistical variability in the elastic properties of a short-fiber composite. This work provides the variance of a characteristic volume of fibers from the fiber-orientation distribution function or higher-order tensors. It is shown that the variance requires orientation tensors through 8th order when orientation tensors are used in place of an actual distribution function.

In addition, a Monte-Carlo simulation method has been developed to assess the statistical nature of short-fiber composites that may be described by fiber-orientation distribution functions. In this work, sample sets of fibers are defined by a representative cell size, fiber size, and volume fraction. For each sample set, elastic mechanical properties are computed from the calculations described above. The results of numerous sample sets are then combined to obtain the mean and standard deviation of the predicted elastic properties. The calculations have been performed for selected fiber-orientation distribution functions, as well as those that are computed from simple homogeneous and non-homogeneous flows. Results have validated those derived from the orientation function expectation described above. We have also compared the results of these calculations when various closure approximations are employed.

Work continues on the development of a voxel-based, finite-element implementation to compute the elastic mechanical properties for both short- and long-fiber composites. The current approach divides a representative volume element into cube-shaped finite elements. The number of elements and number of degrees of freedom are significantly reduced by increasing the element size while adding additional integration points to capture the spatial variation in mechanical properties. The model is being developed in the general purpose finite-element program ABAQUS where the user-defined element subroutine is employed to add this additional capability. The representative volume element includes the appropriate periodic boundary conditions so that the results are representative of a larger domain. Verification simulations are underway at this time where preliminary results show that we can reproduce elastic moduli consistent with classical theories for isotropic materials. Numerous 2D and three-dimensional (3D) examples from the literature are being used to validate this new modeling approach. Anisotropic results suggest a modification of the multi-Gauss point approach will be required to obtain the correct properties.

The Monte-Carlo simulation program described above is being enhanced for use with our voxel-based, finite element model. A molecular-dynamics simulation is being used to adjust the position of fibers so that they do not overlap in space and maintaining a predefined orientation distribution function. Preliminary results look positive; however, development continues in order to use this approach to fulfill the objectives of this research project.

Our new fiber-interaction model has been implemented in a program that evaluates fiber-orientation tensors for fiber distributions in an arbitrary flow. Limits on the parameters contained in the model have been established and limitations of the approach have been identified. Fiber-orientation predictions have been compared with test data obtained from PNNL. Results show a significant improvement in elongational flows, but much less effect in shear-dominated flows. Further development is needed to obtain an improved accuracy in shear flows.

As part of the REU supplement to this grant, an undergraduate student is developing a finite- element modeling approach for representing the fibrous annulus as a long-fiber composite material. All previous approaches 'stitch' in bar elements within a matrix of solid bricks to represent the fibers. This earlier approach is tedious and is only

appropriate for simple geometries. Our approach rotates a transversely-isotropic elasticity tensor defined by the matrix and fiber properties into the direction of the disk fibers. As a result, each element has its own fiber orientation and elastic properties. This approach will make it possible to model the actual disk geometry which is far more complex than that used in earlier analyses. Our approach is made possible by leveraging the short- and long-fiber composites work described above.

The US Department of Energy FreedomCAR program is providing partial support for this project through NSF DMI. They are also making available computational resources and data from their testing that is related the goals and tasks of this research. A project kick-off meeting was held in August 2005 to initiate the collaborative effort.

As part of this collaboration, information on research progress is exchanged between the PI and personnel at PNNL, which includes reports, journal articles, test data and PowerPoint presentations. PNNL has also made available computer facilities where future Monte Carlo simulations will be run.

Journal Publications

1. D.A. Jack and D.E. Smith, "Material Property Predictions for Short-Fiber Polymer Composites: Part 1, Analytical Forms for Expectation and Variance from Orientation Tensors", Journal of Composite Materials, Submitted.
2. D.A. Jack and D.E. Smith, "Material Property Predictions for Short-Fiber Polymer Composites: Part 2, Validation of Analytical Expectation and Variance with the Method of Monte Carlo", Journal of Composite Materials, Submitted
3. David A. Jack and Douglas E. Smith, "The Effect of Fiber Orientation Closure Approximation on Mechanical Property Prediction", Composites Part A., p. 975, vol. 38, (2007).

Simulation of Compression-Resin Transfer-Molding Process for Manufacturing Net-Shape Structures.

Principal Investigator: Suresh G. Advani

Department of Mechanical Engineering
University of Delaware
Newark, DE 19716
(302) 831-8975; fax: (302)-831-8525;
e-mail: advani@me.udel.edu

NSF Award ID: 0521789

All liquid composite molding (LCM) processes require one to place a fibrous preform inside the mold. The mold is sealed and a liquid resin is injected to saturate the preform. The fibers in the preform and the preform itself are usually stationary but in some variations they may undergo small (and slow) deformation during the injection process. Next, the resin is allowed to cure and the part is removed. Two commonly used techniques in this process are resin-transfer molding (RTM) and vacuum-assisted resin-transfer molding (VARTM).

The subject of this work, compression resin-transfer molding (CRTM) differs from the other LCM processes by injecting the resin before the mold is fully closed and preform compacted. The gap between preform and mold surface serves for uniform resin distribution over the part surface. Following mold closure and preform compaction then distributes the resin through the preform thickness.

This process offers the potential to manufacture moderately-sized structures in a few minutes while preserving the advantages of RTM, net-shape manufacturing of complex curvatures with Class A surface finish.

In all LCM variations, the flow of the resin through the preform is important. If particular sections of the preform remain dry after the injection is complete, the resulting void will seriously compromise the part properties. The cost of trial-and-error part design created a need for the simulation of the filling process using science-based process model. For conventional RTM processes, many reliable computer simulation tools have been established and validated with experiments. However, for the other LCM variations the modeling tools are scarce and RTM tools are usually adapted, though the results are sometimes not quite satisfactory.

The resin flow in CRTM process is more complex than in any other LCM variation. It exhibits three distinct stages. All of the phases can be modeled as flow through porous media under different boundary and initial conditions. The three stages are

1. Resin injection into the narrow gap between the mold platen and the fiber preform in the mold.
2. Closing of the gap while squeezing the resin into preform without direct contact between movable tool part and the perform.
3. Compaction of the preform by the mold platen along with continuing resin impregnation.

Research and Education Activities

We extended, streamlined and analyzed the existing approach to model CRTM and enhanced its capabilities by fully modeling preform deformation. The scheme was successfully utilized to analyze the process and to identify significant process parameters. However, low computational performance continues to be an issue. To address this concern, extended problem descriptions which include fiber tow saturation and preform deformation were developed. As the material description necessary to utilize either of these models far exceeds the usual level of characterization in LCM, preform materials of suitable types were characterized. On the educational side, the process model was introduced in an undergraduate course on Introduction to Principles of Composites Manufacturing (MEEG 655).

Findings

The current approach that combined the RTM governing equation with an iterative process clearly showed that the resulting pressure was very different. An existing RTM simulation package was utilized to model the CRTM process with limited success and some parametric studies were performed. The preform displacement was added into the model and a 2D version, more suitable for process study, was developed. This model provided tools for extensive analysis of parameters influencing the process. New governing relations for the general LCM was implemented in a full, finite-element-based numerical scheme. The scheme is currently being tested. Methodology was developed to test preform materials in order to obtain the full set of material data necessary for modeling. Several materials, including the programmable powdered perform process (P4, see 8.C) preform, were characterized to obtain wet and dry deformation behavior and permeability/deformation relations.

Journal Publications

None.

Simulation of Injection Molding of Thermoplastics Reinforced with Short and Long Fibers

Principal Investigator: Donald G. Baird
Department of Chemical Engineering
Virginia Polytechnic Inst & St U
Blacksburg, VA 24061
(540) 231-5998; fax: (540) 231-2732;
email:dbaird@vt.edu

NSF Award ID: 0521918

A procedure for identifying the appropriate rheological experiments to determine a unique set of rheological parameters in a constitutive equation for polymers, containing long glass fibers was developed. Furthermore, the equations of motion coupled, with this constitutive equation, have been used to formulate a simulation of injection molding in which flow and fiber orientation are coupled. This has been done initially assuming Hele-Shaw flow but is presently being extended to general flow including the advancing front. Appropriate rheological tests were developed which provide the necessary material parameters needed in the numerical simulation.

Research and Education Activities

The goal of this work is to improve on current predictions of fiber orientation in polymer matrices using a constitutive relation in which fiber orientation is coupled with the flow and not post-calculated. The major research and education activities are:

1. To develop rheological techniques for handling fluids containing high aspect-ratio fibers and to connect the rheological behavior to fiber orientation. Studies have been carried out to determine the impact of fiber concentration, aspect ratio, orientation distribution and suspending medium viscoelasticity on the rheology of short- and long-glass-fiber composite fluids.

2. To teach numerical methods suitable for handling the flow of complex fluids. A finite-element simulation was developed as discussed below.
3. Numerical schemes which give conversion at high Deborah numbers were addressed. A code for a discontinuous Galerkin finite-element method has been written that can handle multiple viscoelastic constitutive equations. Simulations have been carried out for shear/extensional rheometrical flows and 2D injection-molding flows with the Hele-Shaw approximation.
4. Rheometry in conventional rheometers is difficult especially for long-fiber systems. A sliding-plate rheometer was designed and built for studying the rheology and flow of long-glass fiber composites.
5. Methods for investigating fiber orientation during flow were investigated. Center-gated samples were injection molded and analyzed for fiber orientation at ORNL.

Findings

1. Rheological Characterization Technique (short fibers): Developed a novel rheological technique that addresses problems associated with the non-homogeneous shear field found in parallel-plate rotational rheometers and boundary interactions in cone-and-plate rheometers.
2. Rheological Characterization Technique (long fibers): The mechanical components (currently unable to purchase the electrical components) of a sliding-plate rheometer have been designed and fabricated primarily for the purpose of performing unbiased and reproducible rheological experiments on long-glass-fiber-filled polymeric fluids that are otherwise impossible to perform on rotational rheometers. In addition, the rheometer will be used in tracking the transient evolution of long-fiber orientation upon startup and cessation of shear flow.
3. Rheology: Rheological characterization of the short-glass-fiber composites was performed, including intermittent stress growth/relaxation tests to elucidate the stress contribution of the fiber, matrix, and flow field on the transient evolution of fiber orientation. Rheological characterization of the long-glass-fiber composite has been deemed impossible without the completion of the sliding-plate rheometer.
4. Model (short fibers): A constitutive relation has been developed that incorporates stress contributions from the fiber and the viscoelastic suspending medium and includes the ideas of non-affine motion. Model predictions show good agreement compared to rheological experiments and preliminary results for the experimentally-determined fiber orientation.
5. Fiber-Orientation Measurements: We have determined an approach to characterizing the 3D fiber orientation within composite parts using confocal laser microscopy. We have initiated the characterization of fiber orientation in both rheometrical flows and complex flow geometries.
6. Model (long fibers): Various approaches to modeling flexible fibers have been investigated. These approaches include modifying current theory for rigid fibers to include a 'flexibility parameter', track individual fibers using Hinch's infinitely- flexible fiber theory or constitutive equations resulting from bead-rod theory.
7. Simulations: Developed a Galerkin/discontinuous Galerkin finite-element simulation package to simulate the filling stage of injection molding. The features of this simulation package are: use of multiple constitutive equations, compare with Hele-Shaw approximation for end-gate plaque and cetergated disk, and combined front tracking/ALE technique for advancing front simulations.

Training and Development

The students involved in this project are learning:

1) how constitutive relations for polymers containing high aspect-ratio fibers are developed; 2) how to design rheological tests for assessing the parameters in the models; 3) how to develop finite-element code for complex fluids in which structure and flow are coupled; 4) the importance of coupling simulations with the measurement of fiber orientation.

Journal Publications

1. PR. Eberle, D. G Baird, and P Wapperom, "Modeling the Transient Rheology of a Polypropylene Melt Reinforced with Long

and Short Glass Fibers", SPE Technical Papers, p. 1257, vol. 52, (2006). Published.
2. D. Baird and A. Eberle, "Modeling The Rheology And Orientation Distribution Of Short Glass Fibers Suspended In Polymeric Fluids: Simple Shear Flow", Proceedings of the 65th Annual Technical Conference, p. 2823, vol. 65, (2007). Published.
3. P. E. Eberle, D. G. Baird, and P. Wapperom, "The Rheological Properties of Non-Newtonian Fluids Containing Glass Fibers: A Review of Literature", Ind. Eng. Chem. Res. Submitted.

L. Structural Nanocomposite Design

Co-Principal Investigator: Thomas E. Lacy
Associate Professor, Aerospace Engineering
Mississippi State University (MSST)
316c Walker Bldg., P.O. Box A
Mississippi State, MS 39762
(662) 325-2754; fax: (662) 325-7730; e-mail: lacy@ae.msstate.edu

Co-Principal Investigator: Yuanxin Zhou
Assistant Professor, Tuskegee Center for Advanced Materials (T-CAM), Department of Mechanical Engineering
Tuskegee University (TU)
Tuskegee AL 36088
(334) 724-4222; fax: 334-727-8801; e-mail: yzhou@tuskegee.edu

Co-Principal Investigator: Shaik Jeelani
Director, Center for Advanced Materials (CAVS)
Vice President, Research and Sponsored Programs
Tuskegee University (TU)
Tuskegee AL 36088
(334) 727-8970; fax: (334) 724-4224; e-mail: jeelanis@tuskegee.edu

Technology Area Development Manager: Joseph A. Carpenter
(202) 586-1022; fax: (202) 586-1600; e-mail: joseph.carpenter@ee.doe.gov

Contract Monitor: Aaron Yocum
(304) 285-4852; fax: (304) 285-4403; e-mail: aaron.yocum@netl.doe.gov

---

Contractor: MSST
Contract No.: 4000054701

Objective

- Design low-cost nanoreinforced composite systems for automotive structural applications.

Approach

A multiscale design methodology is being employed to investigate the effects of nanoreinforcements on the mechanical properties of fiber-reinforced composites for automotive structural applications. Critical issues being addressed include: selection of key combinations of fibers (glass, carbon, natural, etc.), matrix materials (thermoset, thermoplastic), and relatively cost-effective nanoreinforcements (vapor-grown carbon nanofibers, nanoclay particles, etc.); fabrication of fine-scale and coupon-scale material samples for static and dynamic testing; and development of a multiscale materials modeling strategy for assessing high-performance nanocomposites that accounts for the influence of material-processing parameters on mechanical properties of the material under static and dynamic loads. This effort involves completion of five primary objectives.

- Determine appropriate composite fiber-matrix systems and identify and prioritize candidate nanoreinforcements for evaluation.
- Investigate the effects of different mixtures of nanoreinforced fibers/polymer matrices from a manufacturing and cost perspective.
- Quantify nanoreinforced structure-property relations experimentally.
- Study material failure modes and energy-absorption characteristics under different loading conditions.

- Development of a multiscale materials model based upon micromechanics models and experiments for nanocomposites.

Accomplishments

- Selected readily-available, low-cost thermoset (polyester) and thermoplastic (polypropylene) resins as the primary matrix materials in this investigation; other polymer resins (*e.g.*, epoxy) may be considered as part of supplemental investigations associated with this work.
- Selected Applied Science, Inc. PR-24 carbon nanofibers (CNFs) as the primary nanoreinforcement for use in the initial examination.
- Selected E-glass unidirectional- and woven-fabric plies as the primary traditional continuous-fiber reinforcement phase in this investigation because of their widespread use in automotive applications.
- Fabricated nanophased resin test specimens comprised of a thermoset polyester resin and varying weight fractions of CNFs using a combination of mechanical mixing, sonication, addition of catalyst, dessication and cure.
- Evaluated the dispersion of nanoreinforcements within polymer resins using scanning electron microscopy (SEM).
- Established a method for functionalizing CNFs in order to enhance dispersion in and interaction with the polyester matrix, as well as to minimize CNF agglomeration.
- Established vacuum-assisted resin transfer molding (VARTM) as a viable, inexpensive technique to fabricate continuous-fiber E-glass laminates with nanophased thermoset resins.
- Fabricated nanophased thermoplastic resins (*e.g.*, CNF/ polypropylene) using well-established extruding, grinding and hot-press techniques.
- Performed three-point bend experiments for two-phase (nanoreinforced) resin test specimens comprised of polyester reinforcement with varying weight fractions of CNFs (0.0%, 0.5%, 1.0%, 1.5%, 2.0%, 3.0%).
- Established a student exchange between MSST and T-CAM, where two MSST minority undergraduate students fabricated CNF/polyester three-point bend test specimens and compression-test specimens using T-CAM experimental facilities.
- Used SEM to assess damage morphology and failure mechanisms for nanophased resins.
- Initiated development of a multiscale materials modeling strategy that employs a combination of micromechanics models, three-dimensional (3D) finite elements (ABAQUS, GENOA), and validation experiments for nanocomposites.
- Established a partnership with AlphaStar, Inc. for the modeling of nanocomposites using the finite-element code GENOA.
- Submitted and published one refereed journal article.
- Submitted one conference paper for presentation.

Future Direction

- Continue ongoing dynamic mechanical analysis (DMA) and thermo-gravimetric analysis (TGA) testing of CNF/ polyester resins to assess the thermal properties of nanophased polymer resins.
- Conduct structure-property tests for three-phase composite systems (nanophased resin, E-glass plies) in order to assess the mechanical behavior and failure of the structural nanocomposites.
- Determine weight fractions of nanoreinforcements that lead to optimal nanophased resin and structural nanocomposite properties.
- Determine material failure modes and energy-absorption characteristics for structural nanocomposites subjected to static and dynamic loading conditions. Perform flexure, tension, fatigue, fracture, and dynamic tests of structural nanocomposites.
- Validate micromechanical model for determining effective properties of nanophased resins using structure-property data.
- Incorporate effective nanophased resin properties from micromechanical models into 3D finite-element models of three-phase composites. Validate numerical models using structure-property data.

Introduction

A multiscale design methodology is being employed to investigate the effects of nanoreinforcements on the mechanical properties of fiber-reinforced composites for automotive structural applications. Critical issues being addressed include: selection of key combinations of fibers (glass, carbon, natural, etc.), matrix materials (thermoset, thermoplastic), and relatively cost-effective nanoreinforcements (vapor-grown carbon nanofibers, nanoclay particles, etc.); fabrication of fine-scale and coupon-scale material samples for static and dynamic testing; and development of a multiscale materials modeling strategy for assessing high-performance nanocomposites that accounts for the influence of material processing parameters on mechanical properties of the material under static and dynamic loads. A literature review of recent experimental and modeling activities related to nanoreinforced composites, particularly those involving glass fibers coupled with thermoset resins (e.g., vinyl ester, polyester, as well as epoxy), was performed (cf., Odegard, et al., 2001; Ghoniem, et al, 2003; Thostenson, et al., 2004; Buryachenko, et al., 2005; Gates, et al., 2005; Odegard, et al., 2005; Valavala and Odegard, 2005; Hussein, et al., 2006; Liu and Brinson, 2006; Fischer, et al., 2007). Such material systems are of particular interest to the Automobile Composites Consortium (ACC). A dialogue has been initiated with the ACC in order to solicit guidance and feedback on relevant aspects of the research, including identification of additional industry partners to participate in cost-share relationships with MSST, T-CAM, and the Department of Energy (DOE). A summary of year one accomplishments is included in the following discussion.

Determination of Composite Fiber-Matrix Systems and Nanoreinforcements

Because of their widespread use and relatively low cost, one commercially-available thermoset resin (U.S. Composites, Inc. polyester) and one thermoplastic resin (polypropylene) were selected as the primary matrix materials in this investigation; other polymer resins (e.g., epoxy) are being considered as part of supplemental investigations associated with this work (*cf.*, Zhou, *et al.*, 2007). Applied Science, Inc. PR-24 carbon nanofibers (CNFs) (typical diameters, 60-200 *nm*; typical lengths, 20-100 μ*m*) were selected as the primary nanoreinforcement for use in this examination. CNFs are relatively inexpensive and possess excellent mechanical properties. Because of prevalent use in automotive applications, E-glass unidirectional- and woven-fabric plies are being used as the primary traditional continuous-fiber reinforcement phase in this investigation.

Investigation of the Effects of Different Mixtures of Nanoreinforced Fibers/Polymer Matrices on Manufacturing

In year one, nanophased resin test specimens comprised of a thermoset polyester resin and varying weight fractions of CNFs were fabricated using a combination of mechanical mixing, sonication, addition of catalyst, dessication, and cure; Figure 1 shows a flowchart of the fabrication process used to develop the two-phase resin system. The resin used in this study is commercially-available stand polyester from US Composite, Inc. The weight fractions of CNFs were varied between 0-4% in order to identify an optimal combination that gives the best thermal and mechanical properties. In general, precalculated amounts of carbon nanofibers and liquid polyester (Part A) were mixed together in a beaker using high-intensity ultrasonic irradiation (Ti-horn, 20 kHz Sonics Vibra Cell, Sonics Mandmaterials, Inc., USA) for 30 minutes on pulse mode (50 seconds on/25 seconds off). The beaker containing a given mixture was submerged in an ice bath to avoid a temperature rise during the sonication process. Once the irradiation was complete, a catalyst (part B in Figure 1) was mixed with the modified polyester using a high-speed mechanical stirrer for roughly 10 minutes. The ratio of part A to part B was 100:1. The rigorous mixing of part A and part B typically produces highly reactive, volatile vapor bubbles at initial stages of the reaction, which could lead to detrimental void formation in the final product (two-phase resin). A high vacuum was applied for 30 minutes to the solution using a Brand Tech Vacuum system to completely remove any bubbles; the mixture was then transferred into plastic- and Teflon-coated metal molds and kept for 24 hours at room temperature. The cured material was demolded and trimmed and test samples were

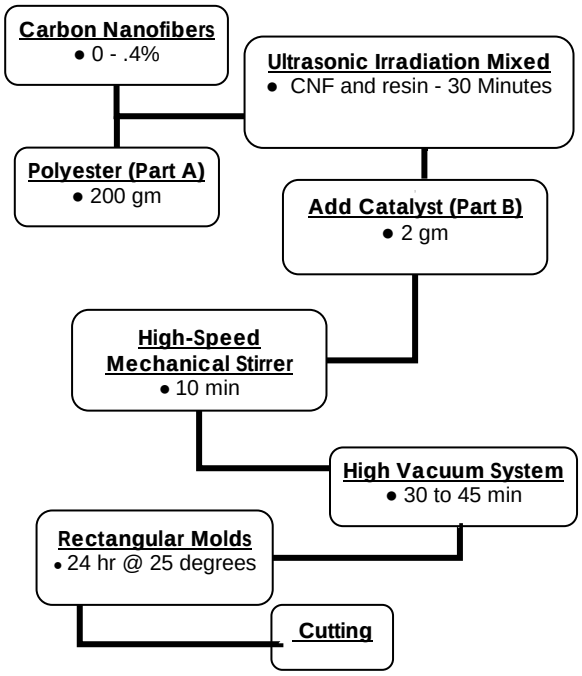

Figure 1. Manufacturing of nanophased resin samples.

machined for thermal and mechanical characterization.

The dispersion of nanoreinforcements within the polyester resin was evaluated using scanning electron microscopy (SEM). SEM images of the failure surfaces associated with three-point bend specimens suggest that agglomeration of CNFs during fabrication and processing is a concern. As a consequence, current efforts are aimed at functionalizing CNFs in order to enhance dispersion in and interaction with the polyester matrix.

Nanophased thermoplastic resins (e.g., CNF/polypropylene) have been fabricated using well-established extruding, grinding, and hot-press techniques (*cf.*, Zhou, *et al.*, TBD). Supplemental investigations of low-cost fabrication/ processing techniques will continue into year two of the project.

VARTM has been established as a viable technique to fabricate continuous-fiber E-glass laminates with nanophased thermoset resins involving a variety of different nanoreinforcements (*cf.*, Chisholm, *et al.*, 2005; Chowdhury, *et al.*, 2006, Zhou, *et al.*, 2006). VARTM may be used to produce high-quality composite parts and is an attractive alternative to autoclave processing.

Experimental Structure-Property Relations for Nanoreinforced Materials

In accordance with American Society for Testing and Materials (ASTM) D790-86, three-point bend experiments were performed for two-phase (nanoreinforced) resin test specimens comprised of polyester reinforced with vapor-grown CNFs. Test samples were cut from larger panels using a Felker diamond-coated steel saw. Six different weight fractions of CNFs (0.0%, 0.5%, 1.0%, 1.5%, 2.0%, 3.0%) were initially considered in order to identify an optimal combination that gives the best thermal and mechanical properties. Three replicates were tested for each weight fraction, for a total of 18 flexural tests. As part of a student exchange associated with this work, two MSST minority undergraduate students fabricated CNF/polyester three-point bend test specimens and compression test specimens using T-CAM experimental facilities.

Preliminary flexural data from these tests contained some surprising results: both the flexural modulus and strength for the three-point bend specimens generally *decreased* with increasing CNF content. This is in contrast to earlier results obtained by T-CAM for CNF-reinforced epoxy, where the inclusion of CNFs resulted in an increase in mechanical properties. Additional experimental investigations will be performed in order to more fully assess the mechanical and thermal performance of CNF/polyester resins. These include an ongoing assessment of the dispersion/agglomeration of CNFs in the resin, consideration of lower weight fractions of CNF reinforcement (*e.g.*, 0.1%, 0.2%, 0.3%, 0.4%), as well as functionalization of the CNFs. In order to enhance the adhesion between the CNFs and polyester resin, MSST will chemically treat CNFs to induce an oxide layer on the fiber surface. Such modified fibers will be used in upcoming mechanical and thermal tests performed at T-CAM. In addition, a lower-viscosity polyester resin is also being considered for use in this study.

Figure 2 contains SEM images of the fracture surface from a three-point bend specimen comprised

of neat polyester (0% weight fraction CNFs) at different magnifications. As seen in Figure 2a, the neat resin exhibits a relatively smooth fracture surface; an initial crack occurred the near the tensile edge of specimen. The higher magnification fractographic image shown in Figure 2b shows striated features typical of brittle fracture behavior, thus accounting for the generally low fracture toughness of the unfilled polyester.

Figure 3 contains SEM images of the fracture surface from a three-point bend specimen comprised of 0.5% CNF/polyester at different magnifications. In contrast with results obtained for the neat resin, the initial crack did not occur at the tensile edge of the specimen. As can be seen in Figure 3a, failure initiation occurred in the interior of the specimen in the vicinity of a large particle that appears to be an agglomeration of several CNFs. Apparently, the crack initiation was caused by the stress concentration due to the agglomerated particle. Figure 3b shows a higher-magnification SEM image of the fracture surface somewhat removed from the agglomerated particle. Note that the fracture surface is substantially rougher than that for the neat polyester (*cf.*, Figure 2b). This suggests that *well distributed* CNFs have the potential to inhibit crack propagation and increase fracture toughness of the resin. Figure 2c contains a high-resolution SEM image that clearly shows a number of dispersed individual CNFs emanating from the fracture surface. Of course, in order to fully realize the potential of nanoreinforced resins, the CNFs must be processed in manner that will minimize agglomeration and the associated stress concentrations. CNF functionalization and surface treatment are being investigated in order to optimize surface chemistry, enhance interaction/bonding between the polymer matrices (*e.g.*, polypropylene, polyester) and CNFs, and to ensure proper dispersion during mixing/ sonication of nanophased materials. This issue will be addressed in upcoming experimental activities associated with this work.

Based upon flexural stiffness/strength data, in conjunction with SEM images of the failure surfaces (*cf.*, Figures 2-3), proper dispersion of CNFs is a crucial aspect in the development of nanophased resins with superior mechanical properties. Initial test results suggest that improper dispersion of the nanophase can result in a decrease in mechanical test results suggest that improper dispersion of the strength. Of course, in order to fully realize the potential of nanoreinforced resins, the CNFs must be processed in a manner that will minimize agglomeration and the associated stress concentrations. As mentioned previously, functionalization of CNFs is being performed in order to address this issue. Initial experimental results suggest that *well distributed* CNFs have the potential to inhibit crack propagation and increase fracture toughness of the resin. Dynamic mechanical analysis (DMA) and thermo-gravimetric analysis (TGA) testing of CNF/polyester resins are currently being performed to assess the thermal properties of nanophased thermoset resins. Similar tests will be performed for nanophased thermoplastics.

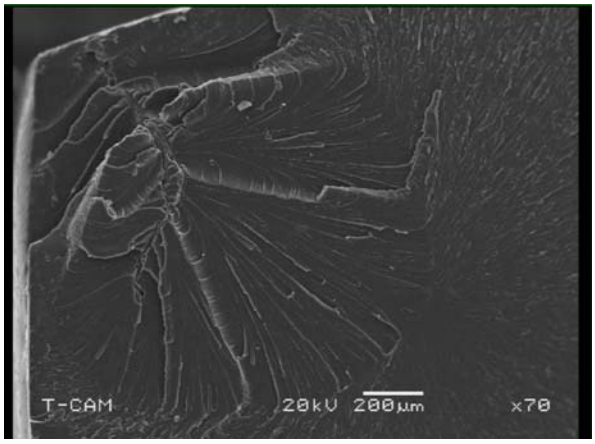

a)

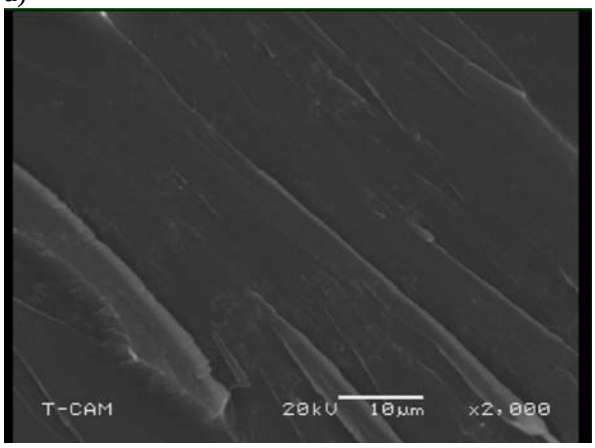

b)

Figure 2. SEM images of fracture surface for three-point bend specimen comprised of neat polyester. a) Crack near free surface of specimen and b) higher resolution image of fracture surface typical of brittle fracture.

Structure-property tests are being developed for three-phase composite systems (nanophased resin, E-glass plies) in order to assess the mechanical behavior and failure of the structural nanocomposites. These activities will continue into year two of the project.

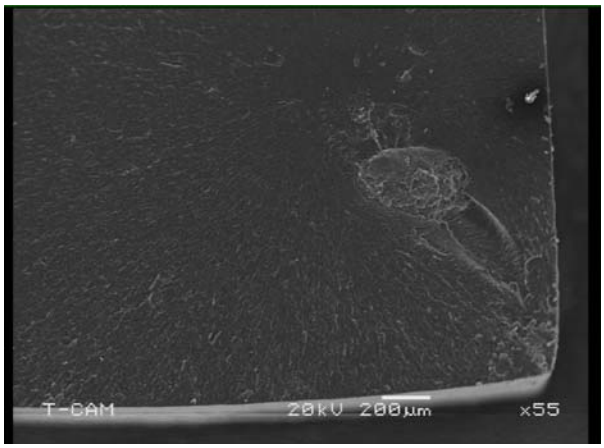

a)

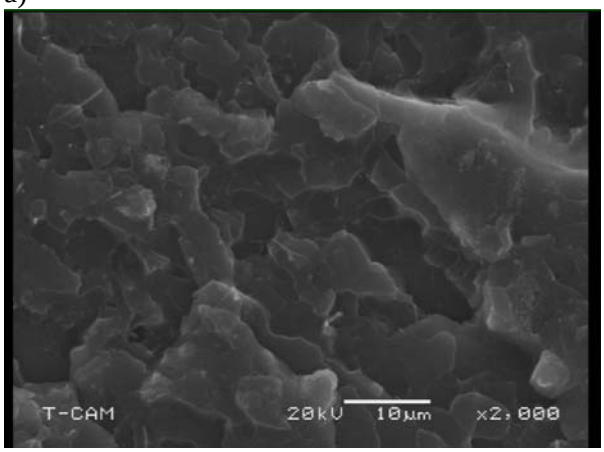

b)

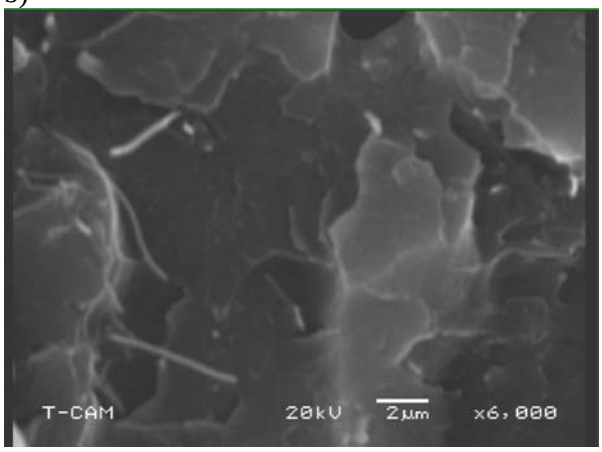

c)

Figure 3. SEM image of fracture surface for 0.5% CNF/polyester three-point bend specimen. a) Crack near agglomerated particle, b) typical fracture surface and c) CNFs bridging the fracture surface.

Assessment of Nanocomposite Material Failure Modes and Energy-Absorption Characteristics under Different Loading Conditions

Once optimal levels of CNFs have been determined for the candidate thermoset and thermoplastic resins, the static and dynamic failure behavior of test specimens comprised of three-phase composites will be investigated using a number of standard tests, with emphasis on energy absorption/crash applications. The goal of this work is to establish relationships between composite processing, constituent morphology, properties and macroscale performance. The effects of nanoreinforcements on macroscale physical properties (stiffness, toughness, energy absorption, *etc.*) will be examined using a combination of three-point bend tests (ASTM D790), tensile tests D3039), fatigue tests, crush tests, fracture tests, Hopkinson bar tests, and other experiments involving specimen geometries and lay-ups of interest to the ACC. A combination of visual inspection, light microscopy, SEM and transmission electron microscopy (TEM) will be used to assess damage development and failure of structural nanocomposite specimens.

Similar studies of carbon fiber/CNF-reinforced epoxy composite systems suggested that inclusion of relatively small amounts of CNFs can lead to a marked improvement in macroscale performance (*cf.*, Zhou, *et al.*, 2006). For example, Figures 4a and 4b contain SEM images of the tensile failure surfaces for continuous carbon fibers reinforced with neat epoxy and CNF-reinforced epoxy, respectively. As can be seen from the figure, use of a nanophased resin appears to dramatically improve the quality of the fiber/matrix interface. The motivation for this work is to fabricate cost-effective nanoreinforced composite materials suitable for automobile primary structural applications. The majority of these activities will be performed in year two of this project.

Development of Multiscale Materials Model Based upon Micromechanics and Experiments for Nanocomposites

Materials property data obtained from structure-property tests are being used in the development and validation of representative volume element (RVE)-based micromechanical models of the two-phase (nanoreinforced) resins. The multiscale modeling methodology developed in this work involves both nanoscale and mesoscale homogenizations. The former is required to establish effective properties of the nanoreinforced matrix (here the characteristic size of a typical nanoreinforcement may be several orders of magnitude smaller than a typical glass-fiber diameter). One key issue is the establishment of an empirically-validated material model (and appropriate homogenization technique) for predicting effective properties of the two-phase matrix; a variety of methods (molecular dynamics, finite elements, etc.) are currently being considered.

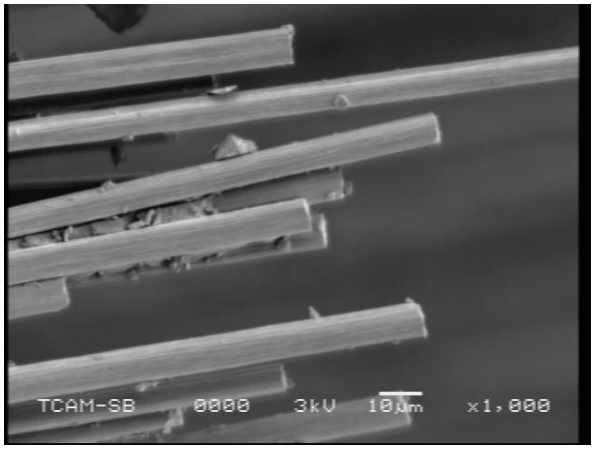

a)

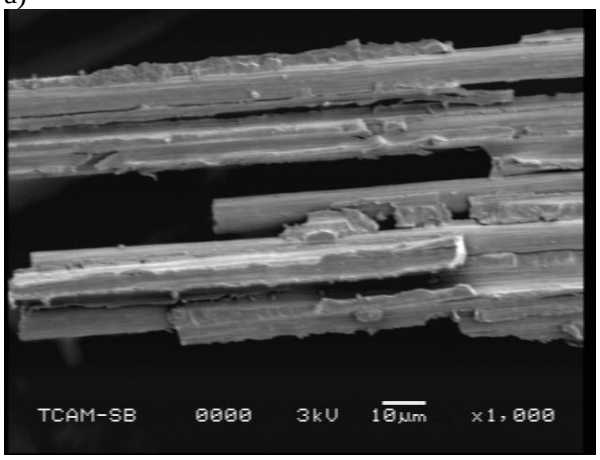

b)

Figure 4. SEM image of continuous-carbon-fiber composite with a) neat epoxy resin and b) CNF/epoxy resin.

Three-dimensional finite-element (FE) models of two-phase resin systems are being developed to establish effective properties of the nanoreinforced matrix. Effective nanophase resin properties obtained from FE simulations are being compared to those obtained using analytic micromechanics solutions (e.g., Mori-Tanaka method and similar effective medium idealizations; *cf.*, Mura, 1991; Nemat-Nasser and Hori, 1993). Effective property data from these simulations, as well as from bulk structure property tests performed by T-CAM, will be employed in a RVE-based FE model of the fiber system/ enhanced resin subjected to both load control and displacement control boundary conditions. Standard homogenization techniques (*cf.*, Mura, 1991; Nemat-Nasser and Hori, 1993) will be employed to determine the effective properties of the three-phase composite systems (i.e., nanophased polymer matrix, traditional continuous-fiber system architectures), with an initial focus on E-glass plain-weave woven-fabric laminates. Modeling and simulation activities will continue into the second year of the project.

Conclusions

The goal of this investigation is to exploit expertise in polymer chemistry, composite materials processing, and computational solid mechanics to design, synthesize, test and analyze cost-effective multiscale engineered nanocomposites for automobile primary structural applications. One key challenge is to establish empirically-validated, multiscale methodologies, based on the morphologies and geometries of real heterogeneous materials, to obtain structure-property relationships over a wide range of length scales.

A crucial aspect of the work is that structure-property relations will be experimentally validated using a combination of fine-scale and macroscale tests. This study should facilitate the development of engineered multiscale materials design by providing insight into relationships between nanomaterial fabrication/processing, chemical and physical characteristics, and interaction and evolution of structure across disparate spatial scales that leads to improved macroscale performance

Presentations/Publications/Patents

1. Zhou, Y., Akanda, S.R., Jeelani, S., and Lacy, T.E., "Nonlinear Constitutive Equation for Vapor-Grown Carbon Nanofiber-Reinforced SC-15 Epoxy at Different Strain Rate," accepted for publication in *Materials Science & Engineering A*, 2007.
2. Zhou, Y., Jeelani, S., and Lacy, T.E., "Strain Rate Dependent Behavior of Carbon Nanofibers Filled Polypropylene," abstract submitted for presentation at the 49th AIAA/ ASME/ ASCE/ AHS/ ASC Structures, Structural Dynamics, and Materials Conference, Schaumberg, IL, April 7-10, 2008.

References

1. Buryachenko, V.A., Roy, A., Lafdi, K., Anderson, K.L., and Chellapilla, S., 2005, "Multi-scale mechanics of nanocomposites including interface: Experimental and numerical investigation," *Composites Science and Technology*, **65**, 2435–2465.
2. Chisholm, N., Mahfuz, H., Rangari, V.K., Ashfaq, A., Jeelani, S., 2005, “Fabrication and mechanical characterization of carbon/SiC-epoxy nanocomposites,” *Composite Structures*, 67, 115–124.
3. Chowdhury, F.H., Hosur, M.V., Jeelani, S., 2006, “Studies on the flexural and thermomechanical properties of woven carbon/nanoclay-epoxy laminates,” *Materials Science and Engineering A*, 421, 298–306.
4. Fisher, F.T., Bradshaw, R.D., and Brinson, L.C., “Fiber waviness in nanotube-reinforced polymer composites: I. Modulus predictions using effective nanotube properties,” submitted to *Composites Science and Technology*, 2007.
5. Gates, T.S., Odegard, G.M., Frankland, S.J.V., and Clancy, T.C., 2005, " Computational materials: Multi-scale modeling and simulation of nanostructured materials, *Composites Science and Technology*, **65**, 2416-2434.
6. Ghoniem, N.M., Busso, E.P., Kioussis, N., Huang, H., 2003, "Multiscale modelling of nanomechanics and micromechanics: an over-

view," *Philosophical Magazine*, **83(31–34)**, 3475–3528.
7. Hussain, A., Hojjati, M., Okamoto, M., and Gorga, R.E., 2006, "Review Article: Polymer-Matrix Nanocomposites, Processing, Manufacturing, and Application: An Overview," *Journal of Composite Materials*, **40(17)**, 1511-1575.
8. Liu, H., and Brinson, L.C., 2006, "A hybrid numerical-analytical method for modeling the viscoelastic properties of polymer nanocomposites," *Journal of Applied Mechanics*, **73,** 758-768.
9. Mura, T., 1991, Micromechanics of Defects in Solids, Second Edition, M. Nijhoff Publ., The Hague.
10. Nemat-Nasser, S., and Hori, M., 1993, Micromechanics: Overall Properties of Heterogeneous Materials, North-Holland, Amsterdam.
11. Odegard, G.M., Gates, T.S., Nicholson, L.M., and Wise, K.E., 2001, "Equivalent-Continuum Modeling of Nano-Structured Materials," **NASA/TM 210863**, 1-30.
12. Odegard, G.M., Clancy, T.C., and Gates, T.S., 2005, "Modeling of the mechanical properties of nanoparticle/polymer composites," *Polymer*, **46**, 553–562.
13. Thostenson, E.T., Li, C., and Chou, T.-W., 2004, "Nanocomposites in context," *Composites Science and Technology*, **65**, 491–516.
14. Valavala, P.K., and Odegard, G.M., 2005, "Modeling techniques for determination of mechanical of polymer nanocomposites," *Review Advance Material Science*, **9**, 34-44.
15. Zhou, Y., Pervin, F., Rangari, V., Jeelani, S., 2006, "Fabrication and evaluation of carbon nano fiber filled carbon/epoxy composite," *Materials Science and Engineering A*, 426, 221–228.
16. Zhou, Y., Akanda, S.R., Jeelani, S., and Lacy, T.E., "Nonlinear Constitutive Equation for Vapor-Grown Carbon Nanofiber-Reinforced SC-15 Epoxy at Different Strain Rate," accepted for publication in *Materials Science & Engineering A*, 2007.
17. Zhou, Y., S.R., Jeelani, S., and Lacy, T.E., "Strain Rate Dependent Behavior of Carbon Nanofibers Filled Polypropylene," abstract submitted for presentation at the 49th AIAA/ ASME/ ASCE/ AHS/ ASC Structures, Structural Dynamics, and Materials Conference, Schaumberg, IL, April 7-10, 2008.